THE UNIVERSITY
of EDINBURGH

Probing mechanisms by which cerebral vascular disease may influence cognitive impairment and dementia

Mosi Li

MBBS, MSC

Doctor of Philosophy

The University of Edinburgh

2019

THE UNIVERSITY *of* EDINBURGH

Abstract

Introduction

Vascular cognitive impairment (VCI) describes a full spectrum of cognitive deficits caused by underlying cerebral vascular alterations, regardless of the specific mechanisms involved. Several factors such as ageing, stroke, hypertension and cerebral hypoperfusion are associated with an increased risk of developing VCI. Vascular dementia (VaD) is the second most common cause of dementia after Alzheimer's disease (AD). It is now recognised that considerable overlaps exist between the features of VaD and AD. Key pathological and neuroimaging features including cerebral amyloid angiopathy (CAA), white matter lesions (WML), microinfarcts and microbleeds are evident in both VaD and AD. Furthermore, brain infarction has been reported to influence the presence and severity of clinical expressions such as cognitive performance of AD, suggesting a common pathophysiological mechanism that contributes to the development of cognitive deficits. However, gaps remain in understanding the exact mechanisms by which vascular risk factors contribute to cognitive decline and neurodegenerative processes leading to dementia. Given the importance of blood supply to the brain for maintaining its structural and functional integrity, it has been proposed that vascular risk factors may affect the cerebral haemodynamic and alter the vascular function resulting in damages to the brain. These changes may involve altered neurovascular coupling that is a critical mechanism for regulating the dynamic changes of local cerebral circulation. Further, impaired vascular function, amyloid-β (Aβ) accumulation in the cerebral vasculature and disrupted neurovascular unit are found in VCI. The glymphatic pathway, a clearance route for removing soluble waste from the brain to periphery, has been proposed to play a role in the pathogenesis of VCI.

Mounting evidence has suggested that cerebral hypoperfusion, by large vessel occlusion and stenosis, is emerging as a major contributor to cognitive impairment. This has led to the development of mouse models of bilateral common carotid stenosis (BCAS), a model

narrowing both common carotid arteries by placing microcoils. The BCAS model has been reported to produce many features of VCI, including white matter damage, microglial activation, gliovascular disruption, increased oxidative stress (by increased NADPH oxidase 2 (NOX2) levels) as well as memory impairment. To investigate whether there is an interaction between cerebral hypoperfusion and microvascular Aβ accumulation, a mixed model that demonstrates both microvascular amyloid (Tg-SwDI mouse model) and BCAS has been developed. In this thesis, it is hypothesized that the complex interaction of Aβ and BCAS leads to cognitive impairment via an impaired glymphatic function in addition to perfusion deficits that promote vascular related lesions and neurodegenerative changes. Second to this, given clear links between NOX2, hypoperfusion and amyloid accumulation, it was further hypothesised that NOX2 is a central mechanism leading to VCI.

Methods

Mice were given BCAS surgery to mimic cerebral hypoperfusion for a period of 3 months. *In vivo* laser speckle imaging was performed to evaluate the changes in cortical blood flow. This was followed by additional CBF measurements using arterial spin labelling (ASL)-based magnetic resonance imaging (MRI), which gave a non-invasive access to CBF information in the cerebral cortex, hippocampus and thalamus. Neurovascular coupling was assessed by performing whisker stimulation. Barnes maze was used to assess the spatial learning and memory function at 3 months following BCAS or sham surgery. For the examination of glymphatic function, *in vivo* intracisternal injection and *ex vivo* imaging of CSF fluorescent tracers were performed. Histological assessment and immunohistochemistry were used to examine vascular related pathology, Aβ burden, astrogliosis and basement membrane changes following BCAS.

Results

Part 1: To examine the effect of BCAS on cerebral perfusion deficits, glymphatic function and cognition in Tg-SwDI mice compared to wild-type mice.

The first studies in the thesis sought to examine the effect of BCAS and microvascular amyloid on the extent of cerebral perfusion deficits and cognitive impairment. The first step was to validate whether the BCAS model has an effect on cerebral perfusion. Cortical cerebral blood flow (CBF) was examined by laser speckle imaging. This revealed sustained reductions of CBF at 24 hours, 1 and 3 months following the establishment of BCAS ($p<0.001$) but no effect of the microvascular Aβ was found to affect cortical perfusion ($p>0.05$). To further explore the CBF changes in other brain regions following BCAS, Arterial spin labelling (ASL), a technique widely used in clinical imaging, was performed. A significant effect of BCAS was confirmed in the dorsolateral cortex and hippocampus ($p<0.001$, respectively) but no genotype effect of the microvascular Aβ or any interaction was found ($p>0.05$, respectively). In order to investigate whether long-term carotid stenosis has a further effect on cognitive function in the experimental animals, assessment of Barnes maze demonstrated that BCAS mice spent longer escape latency than the sham mice in both wild-type and Tg-SwDI animals ($p<0.05$, respectively) indicating visuo-spatial learning was significantly impaired at 3 months following BCAS. To determine the effect of BCAS and Aβ on long-term memory, a probe test was taken to examine whether mice remember the previous training target after a period of time. This test revealed that all groups spent a significantly higher percentage of time than chance (25%). Exclusively in wild-type BCAS mice, the percentage of time spent in the target quadrant was significantly lower than by chance ($p<0.05$). In addition, there was no significant effect of BCAS or Aβ on the percentage of time spent in the correct quadrant ($p>0.05$, respectively). These results suggested long-term memory was not impaired in BCAS and the presence of amyloid. Further to enhance the detection of spatial learning and memory impairment, reversal trials were taken to evaluate the ability of experimental animals to learn a new location. Compared to wild-type mice that still learned the new tests showing significantly improved performance over time ($p<0.05$), both the Tg-SwDI sham and BCAS mice no longer learned the task ($p>0.05$). The long-term memory tested in reversal tests showed impairment in both wild-type and Tg-SwDI BCAS as well as in the presence of amyloid after increasing the

difficulties in reversal probe tests. The results indicated the only mice from wild-type sham (37.40 ± 12.63) ($p<0.05$) spent a significantly higher percentage of time by 12.40 (95%CI, 1.84 to 22.96) than by chance, $t(7)=2.8$, $p=0.027$ and a significantly higher percentage of time than Tg-SwDI BCAS mice ($p<0.05$) with all the other groups spending a lower percentage of time than chance (wild-type BCAS: 27.57 ± 11.12%, Tg-SwDI sham: 20.36 ± 15.50%, Tg-SwDI BCAS: 26.79 ± 16.79%).

To further explore the potential mechanisms by which BCAS causes cognitive impairment, the glymphatic entry was further assessed. This revealed that the global influx of CSF tracers was different across the anatomical levels ($p<0.001$) but unaltered post-BCAS in wild-type and Tg-SwDI mice ($p>0.05$, respectively). To explore whether BCAS influences CSF glymphatic influx, *ex vivo* images of the CSF tracer influx in the dorsolateral cortex (DL CTX) and hippocampus (CA1-DG molecular layer) on the D-3 tracer were measured. The results showed in both regions, altered CSF influx was found in the BCAS and Tg-SwDI mice due to the main effect of BCAS ($p=0.037$ and $p=0.011$, DL CTX and CA-DG regions respectively) but not Aβ ($p>0.05$, respectively). Taken together, these first studies support the original hypothesis that BCAS causes cognitive impairment via reduced cerebral perfusion and impaired glymphatic function. However, there was no exacerbation of these effects in Tg-SwDI mice.

Part 2: To examine the effect of BCAS on neurovascular function, degenerative changes and amyloid accumulation in Tg-SwDI mice compared to wild-type mice.

To begin with, responses of cortical blood vessels to whisker stimulation were recorded and quantified as the mean CBF percentage increase from the baseline. There was a significant effect of BCAS ($p<0.001$), whereby impaired neurovascular coupling was observed in the BCAS mice from both wild-type and Tg-SwDI mice. However, there was no significant effect of Aβ in these mice ($p>0.05$). Vascular related lesions including microinfarcts and microbleeds were compared by measuring the frequency in experimental animals. No vascular lesions were detectable in wild-type and Tg-SwDI sham mice. 4/10 mice were

found to have vascular lesions in the wild-type BCAS mice following 3 months of surgery. 6/10 mice were identified with vascular lesions in the Tg-SwDI mice. No significant difference in proportions ($p>0.05$) was found between Tg-SwDI BCAS and wild-type BCAS mice. To discern the mechanisms by which BCAS and microvascular amyloid may impact on the glymphatic function, the extent of astrogliosis was further studied. GFAP immunostaining was undertaken to investigate the extent of reactive gliosis post-BCAS. Increased astrogliosis following BCAS was found ($p<0.05$), but no effect of Aβ or interaction was found in the dorsolateral cortex. The hippocampal CA1-DG molecular layer was further analysed, and this showed a significant effect of Aβ ($p=0.002$) but no effect of BCAS ($p>0.05$) and interactions ($p>0.05$) on astrogliosis. Further, Aβ load was evaluated in the cortex and co-labelled with collagen 4 (COL4) (a marker of the basement membrane of blood vessels) to enable the assessment of microvascular amyloid in the Tg-SwDI mouse model. A significant increase in the total amount of amyloid as well as the percentage of vascular amyloid was detected post-stenosis ($p<0.05$, respectively). No changes of COL4 levels were found in the mice post-BCAS ($p>0.05$). In summary, these results demonstrated that BCAS impaired neurovascular coupling and promoted amyloid accumulation in the cerebral microvasculature.

Part 3: To determine whether targeting NOX2 has an effect on cerebral perfusion, degenerative changes and cognitive impairment in Tg-SwDI mice compared to wild-type mice.

The third aim of the thesis was to determine the effect of NOX inhibitor (apocynin) on the previously reported cerebral hypoperfusion, impaired neurovascular coupling, development of neurodegenerative pathologies and cognitive deficits caused by BCAS in the Tg-SwDI mice. Following BCAS surgery, mice were immediately fed with either apocynin or vehicle in their drinking water for 3 months. Cortical CBF changes after the treatment of apocynin were assessed using laser speckle imaging, in apocynin treated mice, a recovery of CBF from the BCAS apocynin group after 3 months of treatment was found. The further investigation of

neurovascular coupling revealed that apocynin restored vascular function following carotid stenosis. A significant interaction between BCAS surgery and apocynin treatment ($p<0.05$) was found after 3 months of treatment. The mice that received 3 months of apocynin treatment showed a robust response during the stimulation. The frequency of vascular lesions was counted to compare whether inhibiting NOX activity could provide any beneficial effect on the development of vascular pathology. However, there was no significant difference in proportions between the mice treated with vehicle and apocynin ($p>0.05$). The cortical amyloid load was assessed by double labelling of COL4 and 6E10. The results revealed no effect of treatment on the Aβ burden and vessel densities compared to vehicle treated group ($p>0.05$). Finally, the cognitive function was assessed using Barnes maze. It demonstrated that apocynin did not improve spatial learning and memory in the behavioural tests ($p>0.05$, respectively).

Conclusions

The findings in this thesis demonstrate novel evidence of how carotid stenosis damages the cerebral microcirculation and structure, contributing to the pathogenesis of cognitive impairment. Specifically, long-term BCAS caused chronic cerebral hypoperfusion and impaired glymphatic function, which is likely to contribute to the accumulation of Aβ in the microvasculature. Additionally, carotid stenosis caused sustained cerebral hypoperfusion and led to impaired neurovascular coupling, neurodegenerative changes and cognitive deficits. However, despite evidence supporting a basis for targeting NADPH oxidase, there was only a modest beneficial effect of the NOX inhibitor on neurovascular function.

Collectively, this thesis provides evidence that following the carotid stenosis, while reducing cerebral perfusion, the glymphatic drainage pathway may be affected, leading to cognitive impairment. This new data adds credence to a growing body of human studies that alternate mechanisms may exist in addition to cerebral hypoperfusion leading to VCI. The treatment with non-selective NOX inhibitor successfully restored blood perfusion and vascular function with no ultimate improvement in cognitive function, suggesting a limited role by targeting

NOX to restore the full pathological processes in VCI. Thus, further studies using more specific method targeting post-carotid stenosis events will help to understand the proposed mechanisms and provide a therapeutic strategy.

Lay summary

Vascular cognitive impairment (VCI) refers to the full spectrum of cognitive impairment (e.g. failure in memorising and reasoning, etc.) caused by damage to the brain blood vessels. Multiple vascular risk factors are associated with such vascular damage leading to the insufficient blood supply for delivering oxygen and nutrients to the brain. These affected vessels are either blocked by a clot or burst. Therefore, once the blood supply is cut off, and surrounding brain cells die. Damage to the brain blood vessels are also common in Alzheimer's disease (AD), which is the most common type of dementia affecting memory, thinking skills and mental abilities. There are considerable overlaps between dementia caused by vascular damages and AD, suggesting a common mechanism may contribute to the development and pathogenesis of cognitive impairment.

Brain hypoperfusion, a term used to describe the reductions in the brain blood flow due to the occlusion or narrowing of vessels, is emerging as a key mechanism leading to the decline of brain functioning. So far, significant gaps remain in our understanding and knowledge about VCI forming the basis of the studies within this thesis. It is yet not fully understood whether cerebral hypoperfusion interacts with vascular amyloid accumulation that is the pathological hallmark of AD and exacerbates the disease outcomes. Moreover, whether reductions in blood flow causes damage to the brain waste clearance system (glymphatic pathway) resulting in amyloid accumulation is not defined. It is also not clear whether targeting oxidative stress would prevent cognitive decline in response to reductions in blood flow. Multiple imaging techniques, tissue staining, and learning/memory tests were performed on mouse models to investigate the brain structural and functional changes following brain hypoperfusion. A surgery-induced mouse model of hypoperfusion and a transgenic mouse model of AD (Tg-SwDI) were used in the studies within the thesis. Collectively, the results suggest that sustained reductions in brain blood flow led to impaired vessel function, tissue damages and memory impairment. Impaired brain waste clearance function (glymphatic system) was observed in addition to brain hypoperfusion, and this might

contribute to the accumulation of amyloid in the blood vessel walls. The application of a safe and natural compound (apocynin) to inhibit the oxidative stress successfully improved brain blood supply, vascular function but did not prevent tissue damages and cognitive impairment. Thus, further studies using more specific method targeting hypoperfusion events will help to understand the proposed mechanisms and provide a therapeutic strategy.

Declaration

I declare that this thesis was composed by myself, that the work contained herein is my own except where explicitly stated otherwise in the text, and that this work has not been submitted for any other degree or professional qualification.

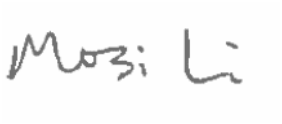

Mosi Li

November 2019

Acknowledgements

Foremost, I would like to express my sincere gratitude to my supervisor Professor Karen Horsburgh for her guidance and persistent support throughout my PhD study. Her encouragement and immense knowledge have greatly assisted the progress of the studies written in this thesis.

Second, I would like to acknowledge my committee member, Dr Paul Skehel, for his valuable guidance and insightful comments on my PhD study and advice on my thesis writing.

I would also like to thank all my colleagues in Horsburgh lab, for their wonderful collaboration and all the helps I have received to overcome difficulties during my experiments. I want to thank you all for making the lab such a lovely place for sharing happiness and knowledge. I would like to thank Dr Akihiro Kitamura, with who I have spent a lot of time working on challenging experiments together. I also need to thank Dr Jessica Duncombe, who has taught me lots of knowledge during my PhD especially the works on the animal experiments. I also want to thank Dr Emma Sigfridsson and Dr Jemma Pilcher who have been working and studying with me in the lab throughout my PhD. I also want to thank Duncan and Jon who work in the LF2 unit and are always friendly and know everything about the LF2 facility.

List of Abbreviations

AD	Alzheimer's disease
APP	Amyloid precursor protein
Aβ	Amyloid-β
ACA	Anterior cerebral artery
AChA	Anterior choroidal artery
ASK1	Apoptosis signal-regulating kinase 1
AQP4	Aquaporin-4
ASL	Arterial spin labelling
BA	Basilar artery
BCCAo	Bilateral common carotid artery occlusion
BCAS	Bilateral common carotid stenosis
BBB	Blood-brain barrier
CAA	Cerebral amyloid angiopathy
CADASIL	Cerebral autosomal dominant arteriopathy with subcortical infarcts and leukoencephalopathy
CARASIL	Cerebral autosomal recessive arteriopathy with subcortical infarcts
CMI	Cerebral microinfarcts
CVD	Cerebral vascular disease
CSF	Cerebrospinal fluid
CSF	Cerebrospinal fluid
CM	Cisterna magna
COL4	Collagen 4
CCA	Common carotid arteries
CBF	Cortical cerebral blood flow
DTI	Diffusion tensor imaging
DMSO	Dimethylsulfoxide
DPI	Diphenyleneiodonium
DL CTX	Dorsolateral cortex
DUOX1	Dual oxidase 1
DUOX2	Dual oxidase 2
ECs	Endothelial cells
FAD	Flavin adenine dinucleotide
GFAP	Glial fibrillary acidic protein
H&E	Haematoxylin and eosin

ICA	Internal carotid arteries
ISF	Interstitial fluid
ICP	Intracranial pressure
MRI	Magnetic resonance imaging
MAP	Mean arterial pressure
MCA	Middle cerebral artery
MCAO	Middle cerebral artery occlusion
MCI	Mild cognitive impairment
DIR	MRI Double Inversion Recovery
NOX2	NADPH oxidase 2
NVU	Neurovascular unit
NADPH oxidase	Nicotinamide adenine dinucleotide phosphate oxidase
NO	Nitric oxide
O^2	Oxygen
PFA	Paraformaldehyde
PU	Perfusion units
PVMs	Perivascular macrophages
PVS	Perivascular space
PET	Positron emission tomography
PComA	Posterior communicating artery
ROS	Reactive oxygen species
ROI	Region of interest
SPECT	Single photon emission computed tomography
SMCs	Smooth muscle cells
SHRSP	Spontaneously Hypertensive Stroke Prone Rat
SAS	Subarachnoid space
O^{2-}	Superoxide
TCD	Transcranial Doppler
UCCAO	Unilateral common carotid artery occlusion
VCI	Vascular cognitive impairment
VCING	Vascular cognitive impairment neuropathology guidelines
VaD	Vascular dementia
VA	Vertebral arteries
WMH	White matter hyperintensities
WML	White matter lesions

Table of Contents

Table of Figures

Table of Tables

Chapter 1. Introduction

1. Overview

The brain is an organ of high metabolic demand relying on the persistent supply of blood to maintain normal function. Several mechanisms, such as cerebral autoregulation and neurovascular coupling are responsible for regulating the dynamic changes of cerebral circulation. There is emerging evidence suggesting that vascular risk factors contribute to the functional and structural alterations in the cerebral vascular system leading to vascular damage. Cerebral vascular disease (CVD) is a significant factor associated with cognitive impairment and dementia, such as Alzheimer's disease (AD). Key pathological and neuroimaging features including white matter lesions (WML), microbleeds, lacunes and enlarged perivascular space (PVS), which are evident in both Alzheimer's disease (AD) and vascular dementia (VaD) (Dichgans and Leys, 2017). The considerable overlap between AD and VaD, representing the two most common causes of vascular cognitive impairment (VCI), suggest that a common pathophysiological mechanism involving cerebral vascular alterations, may contribute to the development of cognitive impairment.

Cerebral hypoperfusion, induced by large vessel occlusion and stenosis is an early marker that can be detected before the onset of dementia symptoms (Iadecola, 2013). Mouse models of cerebral hypoperfusion, induced by bilateral common carotid stenosis (BCAS), have been reported to disrupt the gliovascular integrity and cause cognitive deficits (Holland et al., 2015). Furthermore, cerebral hypoperfusion causes accumulation of Aβ, leading to the formation of cerebral amyloid angiopathy, microinfarcts and microbleeds via a potential mechanism of oxidative stress (Holland et al., 2015, Salvadores et al., 2017). However, gaps remain in our

understanding about VCI as to whether there are alterations in vascular function following long-term perfusion deficits, cognitive impairment, and whether there is impaired Aβ clearance via the glymphatic pathway. It is also unclear whether there are further impacts upon vascular function, neurodegenerative changes following carotid stenosis and the variation in the presence of Aβ. The impact of blocking NADPH oxidase (NOX) by apocynin and possible improvement of perfusion deficits, neurovascular coupling and neurodegenerative changes remain to be investigated.

2. Cerebral blood flow and related control mechanisms

2.1 Fundamentals of CBF

Cerebral blood flow (CBF) is defined as blood supply to the brain in a given period of time (Fantini et al., 2016). CBF levels are maintained within critical thresholds by homeostatic mechanisms to support healthy brain function. The brain is an energy-demanding organ. While the brain is only 2% of the total body weight of a healthy adult human, it receives as much as 15-20% of the cardiac output and accounts for approximately 20% of the total energy consumption of a healthy adult at rest (Peters et al., 2004). Cerebral blood perfusion is responsible for delivering oxygen, an essential substrate for the neuronal oxidative metabolism of substrates, including glucose, ketone bodies and lactate. (Belanger et al., 2011).

Cerebral circulation originates from two primary sources of blood perfusion: the anterior circulation and posterior or vertebrobasilar circulation. The anterior cerebral circulation is composed of branches of internal carotid arteries (ICA) that arise from common carotid arteries. Among these branches, anterior cerebral artery (ACA), middle cerebral artery (MCA), and the anterior choroidal artery (AChA) are arterial components with significant pathophysiological relevance. The function of the anterior portion of the cerebral circulation is to provide a requisite amount of blood to

the forebrain, including the frontal, temporal, and parietal lobes. The anterior circulation also supplies other brain regions such as diencephalon and internal capsule. The posterior cerebral circulation is formed by two vertebral arteries (VA) that emerge from subclavian arteries. The vertebral arteries then merge intracranially becoming the basilar artery (BA) and further branch into posterior cerebral arteries. The cerebral anterior and posterior arterial circulation meet as the circle of Willis (Figure 1-1), a prominent landmark of anatomic variability located within the brain's interpeduncular fossa surrounding the optic chiasm. The primary function of the circle of Willis is to form a collateral circulation to the brain. The circle of Willis is a network of cerebral blood vessels that provides connections between the vertebral and carotid circulations to ensure the brain does not lack blood and become affected by reduced blood flow when one system is occluded (Doyle et al., 2012). Compared to humans, the B6 mice do not always have a complete circle of Willis (Barone et al., 1993, Kitagawa et al., 1998). It has been reported about 10% of B6 mice were found to have a complete circle of Willis, 60% were lacking posterior communicating artery (PComA) on one side and 30% were missing both PComAs (McColl et al., 2004).

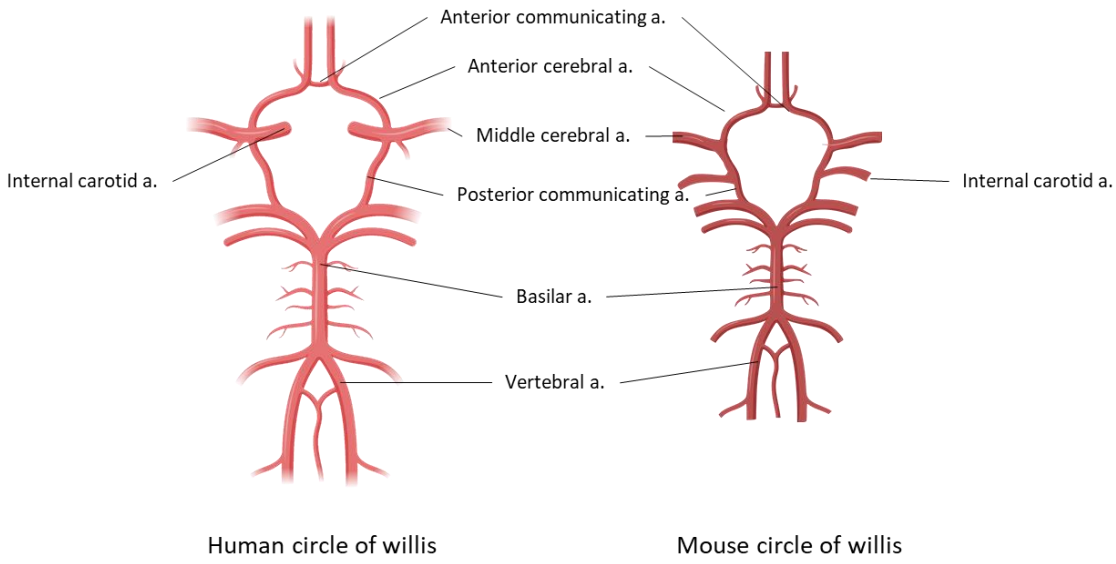

Figure 1-1 Circle of Willis in human and mouse.

Schematic diagrams show the human (left) and mouse (right) circle of Willis. The human circle of Willis consists of anterior cerebral arteries (ACA), anterior communicating artery (AComA), internal carotid arteries (ICA), posterior cerebral arteries (PCA) and posterior communicating arteries (PComA). In the C57Bl/6J mice, a deficient connection may occur between vertebral circulation and carotid circulation. Images were created in Biorender.com and edited in Inkscape.

2.2 Mechanisms that control CBF

2.2.1 Neurovascular coupling

Neurovascular coupling, also referred to as functional hyperaemia, is a mechanism of local cerebral blood flow (CBF) regulation that ensures the adequate delivery of oxygen and energy substrates to the localised brain areas following changes in neuronal activity. Neurovascular coupling requires the finely tuned coordination and communication of multiple cell types: neurons, glial cells (e.g., astrocytes, microglia and oligodendrocytes) as well as mural cells (e.g., endothelial cells (ECs), smooth muscle cells (SMCs) and pericytes). These cells constitute a functional unit which is named the neurovascular unit. They work together, both temporally and spatially, to generate, coordinate and transduce signalling molecules that underlie the increased

CBF (Iadecola, 2004, Iadecola and Nedergaard, 2007, Howarth, 2014, Iadecola, 2017). The components of the neurovascular unit vary at different levels of the cerebrovascular tree (Figure 1-2). Pial arterioles are covered by thick SMCs layers and surrounded by subarachnoid space and innervated by nerve fibres originating from cranial autonomic and sensory ganglia. Penetrating arterioles enter the brain tissue and are surrounded by perivascular space which contains cellular components such as perivascular macrophages (PVMs). As the penetrating arterioles go deeper in the parenchyma, the perivascular space disappears, and arterioles become wrapped with astrocytic endfeet. Arterioles at this level contain a single layer of SMCs lacking the perivascular nerves. Capillaries that lack SMCs are endowed with pericytes, which are embedded in the basement membrane of the endothelium. Due to the close contact and communication between the critical cellular components of the neurovascular unit, this mechanism enables the brain to have the capacity to increase CBF and oxygen that exceeds the metabolic demand and oxygen consumption (Kisler et al., 2017).

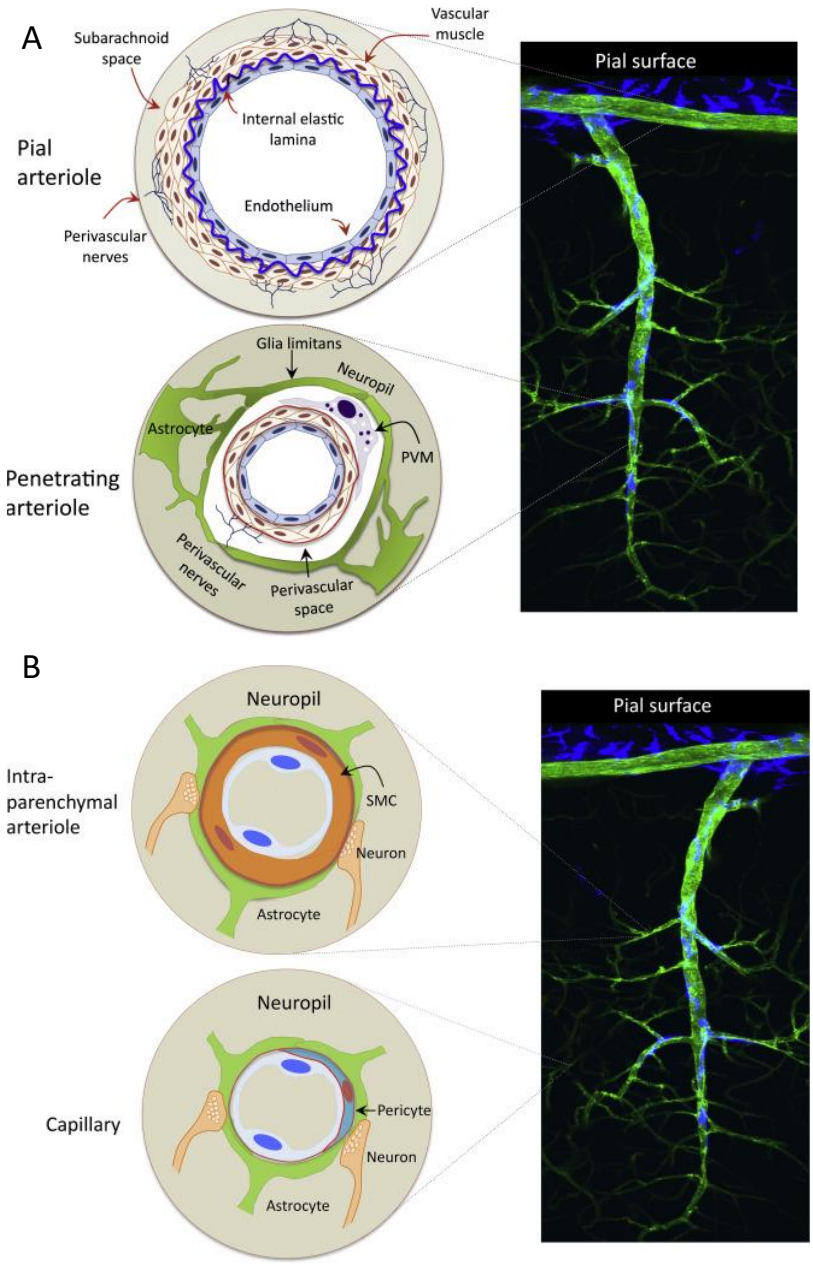

Figure 1-2 Structural diversity of neurovascular unit (NVU).

Schematic diagrams demonstrate the structural differences at different levels along the cerebral vascular tree. (A) Neurovascular associations at pial arteries and penetrating arterioles level. (B) Neurovascular associations at intraparenchymal arterioles and capillaries level. Cerebral vasculature (green) and PVMs and meningeal macrophages (blue). Images are taken from The Neurovascular Unit Coming of Age: A Journey through Neurovascular Coupling in Health and Disease, reused with permission (Iadecola, 2017).

The specific mechanism of neurovascular coupling is not yet fully understood. Recent evidence suggests different mechanisms may exist at capillary and arteriole levels (Iadecola, 2017): Capillaries are ideally positioned to receive neuronal and astroglial signals. Therefore, it has been proposed that neurovascular coupling could be initiated at the capillary level and conducted to upstream along the cerebral vascular tree (Iadecola, 2004). Synaptic activity leads to an increased level of extracellular K^+ and O^2 utilisation. K^+ activates inward rectifier potassium channels (Kir channels) located on the ECs and possibly pericytes, resulting in ECs hyperpolarisation. This hyperpolarisation propagates upstream via gap junctions on ECs and transmits to upstream penetrating arterioles. In the meantime, hypoxia causes increased deformability of red blood cells, leading to reduced viscosity and increased capillary blood flow. This causes shear stress on the capillary, which may cause hyperpolarisation of ECs to produce relaxation of SMCs by releasing endothelial vasodilators. At the level of intraparenchymal arterioles, the propagated response from capillaries is transferred to SMCs via myoendothelial junctions, leading to further relaxation and vasodilation. The vasodilation could be complemented by the vasoactive agents (nitric oxide (NO), adenosine, adenosine triphosphate (ATP), proteinoids, etc) released by nearby neurons and astrocytes during neural activity, which leads to sustain vasodilatory effects to upstream pial arterioles. Furthermore, the decrease in intravascular pressure and increased flow velocity induced by the downstream vasodilation may also lead to SMCs hyperpolarisation and relaxation by triggering myogenic response/flow-mediated vasodilation. At the level of pial arterioles, the haemodynamic response may not be driven directly by synaptic activity but depends on the retrograde propagation of vasodilation from the capillaries and arterioles at the activated site deep in the brain substance.

2.2.2 Alterations in neurovascular coupling

A growing body of evidence has shown the disrupted neurovascular function in ageing and neurodegenerative diseases, such as Alzheimer's disease (Duncombe et al., 2017b, Kisler et al., 2017). Most studies of the neurovascular alterations in AD have focused on the role of Aβ. Evidence from mouse models overexpressing APP provided evidence that Aβ can impair the neurovascular coupling leading to disruption in the cerebral microcirculation (Niwa et al., 2000, Iadecola et al., 1999, Tarantini et al., 2017). A common finding under these disease conditions is the mismatch between CBF, oxygen delivery, and local neuronal activity, suggesting compromised neurovascular unit integrity and functionality. Several mechanisms by which neurovascular coupling may be disrupted. A focus of this thesis is reactive oxygen species (ROS) that will be discussed in more detail in section 5 of this chapter. It is widely recognised that cells homeostasis is dependent on the well-regulated levels of ROS. Excessive production of ROS induced by Aβ has been shown to induce vascular oxidative stress leading to attenuation of neurovascular coupling in a mouse model overexpressing mutant APP (Tg2576) (Park et al., 2004a). Therefore, oxidative stress is believed to play a critical role in disruptions in neurovascular coupling (De Silva and Faraci, 2012, Takeda et al., 2009, Nicolakakis and Hamel, 2011, Chow et al., 2007, Zlokovic, 2005).

2.2.3 Cerebral autoregulation

Another mechanism that ensures the brain receives a constant blood supply is cerebral autoregulation. Cerebral autoregulation is a homeostatic process that protects the brain from fluctuations in arterial pressure. In a healthy human, when the mean arterial pressure (MAP) fluctuates between 50~60 and 160 mmHg, there is minimal or no change in CBF level (Lassen, 1959, Cipolla, 2007). The underlying mechanism of cerebral autoregulation may include multiple factors such as

myogenic response, neurogenic, and metabolic mechanisms (Yang and Liu, 2017). The myogenic activity is referred to as the constriction or dilation of the vascular smooth muscle cell in response to an increased or decreased intravascular pressure (Osol et al., 2002, Cipolla et al., 2009). It is a critical mechanism for the vascular smooth muscle to maintain proper vascular resistance under physiological conditions. The neurogenic control on cerebral autoregulation has been suggested to have limited influence under physiological conditions. However, under severe pathophysiological situations such as vasospasm following stroke with compromised myogenic regulation, the sympathetic control of CBF may become a more critical mechanism regulating CBF (ter Laan et al., 2013). Cerebral autoregulation is proposed to be mediated by the vasoactive factors that regulate vascular resistance to maintain a constant blood supply. Inadequate CBF can stimulate the release of vasoactive substances from the brain leading to arterial dilation. Examples of vasoactive substances include adenosine, a by-product from the ATP metabolism when the neuronal energy demand overrides blood supply (Winn et al., 1985).

2.2.4 Alterations in cerebral autoregulation

The main function of cerebral autoregulation is to stabilise blood supply to the brain during variations in perfusion pressure, thus defending the brain against risks caused by low or high systemic blood pressure (Claassen and Zhang, 2011). Impaired cerebral autoregulation has been seen in advancing ageing (Popa-Wagner et al., 2015). In animal models of AD producing Aβ protein, it has previously been reported that this vital mechanism is significantly affected. Work from Niwa et al. has shown that cerebral autoregulation was markedly disrupted in APP (+) mice and preserved in APP (-) mice. The disruption of autoregulation was paralleled by impairment in endothelium-dependent vascular responses. However, contrary to the discovery in animal models, cerebral autoregulation has been reported to be

preserved in humans. An earlier investigation in AD patients showed a preserved cerebral autoregulation during the disease by testing CBF responses to acute changes in arterial pressure (Simard et al., 1971). A recent study assessing cerebral autoregulation and baroreflex sensitivity in patients with dementia and mild cognitive impairment (MCI) showed no difference between these two mechanisms compared with controls (de Heus et al., 2018). Alterations in cerebral autoregulation may also occur in ischaemic brain injuries and lead to surviving brain tissue lacking protection against the potential damage subsequent to blood pressure changes. A review of transcranial Doppler (TCD) in combination with continuous blood pressure measurements has concluded impairment of cerebral autoregulation in several subtypes of ischemic stroke, and this is probably temporary and caused by stroke, or it may contribute to the stroke (e.g. in the case of chronic hypertension) (Aries et al., 2010).

3. Vascular cognitive impairment

Dementia is one of the most significant public health issues affecting approximate 35.6 million people worldwide with an estimated number increase to 66 million in the next decade and 115 million by the year of 2050 (Wortmann, 2012). Vascular dementia (VaD) is the second most common cause of dementia subtypes after Alzheimer's disease (AD) (Lobo et al., 2000). VaD and AD mechanisms and pathology commonly occur together in dementia subjects. For instance, brain infarction may influence the presence and severity of clinical expressions such as cognitive performance of AD (Snowdon et al., 1997, Esiri et al., 1999). Furthermore, a large proportion of elderly dementia subjects present pathological evidence of neuritic plaques or neurofibrillary tangles alongside vascular pathology (Schneider et al., 2007). Recent multifactorial data-driven analysis from Alzheimer's Disease Neuroimaging Initiative (ADNI) datasets suggest that cerebral vascular dysfunction

is the earliest pathological feature in AD (Iturria-Medina et al., 2016). Although there are common overlaps between VaD and AD, these two dementias have been studied separately for many years. The medical terminology to describe the cerebral vascular disease (CVD) associated cognitive deficits has evolved. The current consensus is using the term of vascular cognitive impairment (VCI), which refers to all types of cognitive impairment that are associated with CVD (Skrobot et al., 2017). VCI encompasses a full spectrum of cognitive changes from mild cognitive impairment (MCI) to VaD, regardless of the specific mechanisms involved (Dichgans and Leys, 2017).

3.1 Pathogenesis underlying VCI

The pathomechanisms underlying VCI are diverse. Theoretically, all causes of clinical stroke can result in brain damage and VCI (Figure 1-3). Given the importance of blood supply to the brain for maintaining its structural and functional integrity, it is evident that damage to the cerebral vascular system can influence brain function. Alterations in large and small blood vessels which cause perfusion deficits have been shown to have a significant impact on cognitive function. Dichgans et al. reported common mechanisms related to stroke aetiologies based on neuroimaging manifestations and pathological conditions including multiple infarcts, strategic infarcts, white matter lesion (WML) and lacunes, brain haemorrhages (including microbleeds), cerebral hypoperfusion, mixed vascular and Alzheimer's disease, cerebral amyloid angiopathy (CAA) and CADASIL. (see (Dichgans and Leys, 2017) and (Jellinger, 2013) for complete information).

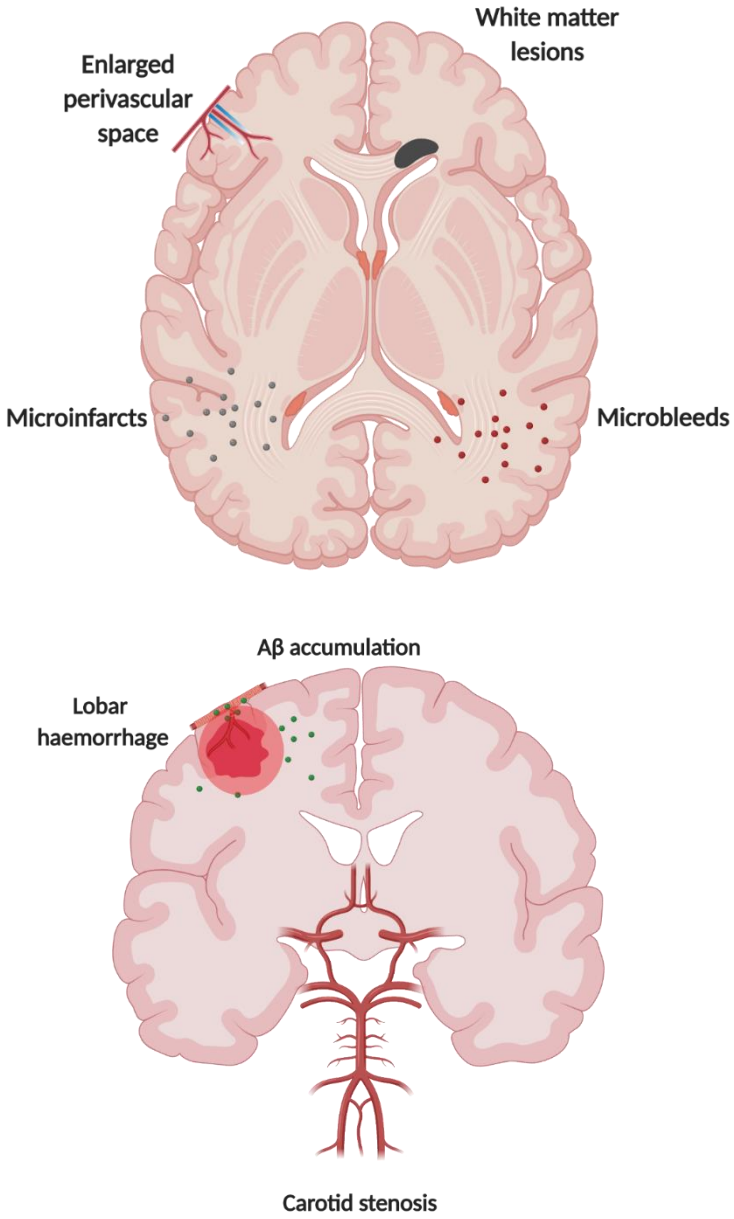

Figure 1-3 Common mechanisms underlying VCI.

Common pathogenesis underlying VCI includes all the aetiologies that can cause strokes, such as large artery occlusion and small vessel disease. In specific, white matter lesions (WML), microinfarcts, microbleeds, enlarged perivascular space (PVS), carotid stenosis, CAA and lobar haemorrhages. Images created with Biorender.com.

3.2 Risk factors for VCI

Evidence derived from several epidemiologic studies suggests that vascular risk factors are related to cognitive function (Li et al., 2011). Studies have identified several risk factors that increase the likelihood of developing cognitive impairment and dementia. Advanced age, poor diet, hypertension, atherosclerosis, hypoperfusion, amongst others, are known risk factors for the development of VCI. Gorelick et al. summarised a classification of risk factors according to their demographic, genetic, atherosclerotic and stroke-related features (Gorelick, 2004). Kalaria et al. also reviewed these risk factors and highlighted those modifiable or treatable risk factors for dementia with stroke-related injury (Kalaria et al., 2016). The demographic risk factors include older age, female sex and low education levels. In rare familial forms of the disease, such as cerebral autosomal dominant arteriopathy with subcortical infarcts and leukoencephalopathy (CADASIL), cerebral autosomal recessive arteriopathy with subcortical infarcts (CARASIL) and *COL4A1/COL4A2*, gene mutations *NOTCH3*, *HTRA1* and *COL4A1/A2* are causal for the disease. However, more recently, it has been found that missense variants in these genes can be found in the general common population and increase risk (Giau et al., 2019). A summarised list of reported risk factors is shown below (Table 1-1):

Table 1-1 Risk factors of VCI.

Risk factors	**Modifiable? (Yes/No)**	**Pre-clinical marker?**	**References**
Advanced age	No	-	(Pendlebury and Rothwell, 2009, Leys et al., 2005)
Female sex	No	-	(Lobo et al., 2000)
Genetic factors	No	Yes	**APOE and MTHFR (Dwyer et al., 2013)** CADASIL (NOTCH3), CARASIL (*HTRA1),* COL4-related angiopathies (*COL4A1*, *COL4A2), details in (Haffner et al., 2016)*
Hypertension	Yes	Yes	(Iadecola et al., 2016, Bucur and Madden, 2010, Knopman et al., 2001)
Diabetes mellitus	Yes	Yes (Type 2DM)	(Luchsinger et al., 2001, Saczynski et al., 2008, Peila et al., 2002, Knopman et al., 2001)

Stroke	Yes	Yes	(Sahathevan et al., 2012, Gorelick, 1997)
Hypoperfusion	Yes	Yes	(Ruitenberg et al., 2005), (Wolters et al., 2017), (Gregg et al., 2015)
Cardiac and carotid arterial diseases	Yes	Yes	(Johnston et al., 2004b, Romero et al., 2009, Arntzen et al., 2012, Hajjar et al., 2011, Flicker, 2010, Knopman et al., 2001)
Cigarette smoking	Yes	Yes	(Anstey et al., 2007)

Data derived from several references: (Kalaria et al., 2016, Dichgans and Leys, 2017).

3.3 Neuroimaging in VCI

Neuroimaging techniques have been developed as powerful tools for the diagnosis of VCI. The visualisation of ischaemic and haemorrhagic brain injury of grey and white matter in VCI is constructive in the clinical evaluation when lacking the brain samples for definite pathological diagnosis. Current neuroimaging techniques provide essential information such as neuroanatomical alteration of the disease and add to the prediction of subsequent cognitive impairment. Different brain imaging methods allow the *in vivo* examination of the structure, function, metabolic state and biochemistry of the brain, which are expected to improve the diagnosis and to stage disease progression and therapeutic strategies.

3.3.1 Structural neuroimaging

VCI manifests as white matter hyperintensities (WMH), lacunar infarcts, cerebral microbleeds and perivascular spaces (PVSs) identified by a neuroimaging modality (e.g. MRI) (Shi and Wardlaw, 2016, Wardlaw et al., 2013) (Figure 1-4). Findings of cerebral microinfarcts (CMI) on 3T MRI are particularly common in patients diagnosed with VaD (62%), AD (43%) and subjects with mixed AD vascular pathology (33%) (Brundel et al., 2012). Moreover, the frequent detection of CMI on MRI is observable after 12-month follow-up and therefore regarded as an MRI marker of CAA (van den Brink et al., 2018). A recent study using an MRI Double Inversion Recovery (DIR) sequence showed cortical ischaemic lesion burden is associated with carotid disease severity (Landi et al., 2015). The application of high-resolution 7T MRI allows the detection of cortical microinfarcts *in vivo* for the neuropathological investigation of vascular lesions (van Veluw et al., 2013). PVS, also known as Virchow-Robin space, is a unique anatomical structure surrounding blood vessels filled with CSF/ISF. It is increasingly recognised as a vital marker associated with cognition and may have important clinical implications (see more information (Charidimou et al., 2013, Potter et al., 2015b, Riba-Llena et al., 2018, Ding et al., 2017, Kwee and Kwee, 2007)). The high-field 7T MRI also improved PVS detection, providing novel insights into the critical pathophysiological structure of VCI (Bouvy et al., 2016, Chen et al., 2011). Other MRI methods such as Diffusion tensor imaging (DTI) provide a unique sequence to characterise the location, orientation, and anisotropy of the brain white matter tracts. It enables the evaluation of specific WM integrity, revealing the microstructural changes that may not be visible on other neuroimaging scans.

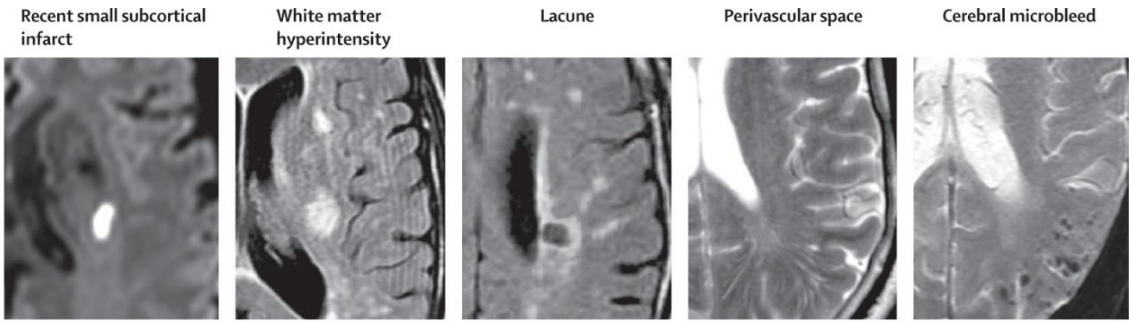

Figure 1-4 Examples of images from MRI findings for lesions related to VCI.

Example images of related lesions on human MRI scans. Subcortical infarcts, white matter hyperintensity (WMH), lacune, perivascular space (PVS) and microbleeds are features of VCI. Images adapted from (Wardlaw et al., 2013).

3.3.2 Arterial spin labelling in neuroimaging

Cerebral vascular alterations are common pathological findings in aged and dementia subjects. Cerebral hypoperfusion as a result of the disrupted cerebral vascular system can be detected by arterial spin labelling (ASL)-based MR imaging techniques. ASL is an MR technique that is non-ionizing and completely non-invasive for measuring tissue blood perfusion (Wolf and Detre, 2007). It utilises magnetically labelled arterial blood protons as an endogenous tracer. It provides a reliable and quantitative method suitable for measuring perfusion in healthy individuals and the population restricted by the exogenous contrast agents or radioactive agents. Clinical studies have demonstrated that ASL-based MRI detects hypoperfusion that is predictive of future functional and cognitive decline and the progression from MCI to dementia (Chao et al., 2010). Cerebral hypoperfusion and neurovascular uncoupling have been suggested to contribute to the pathogenesis of AD (Zlokovic, 2011). The presence of hypoperfusion occurs several years before the onset of clinical symptoms of AD. Therefore, CBF, as measured by ASL-based MRI, is considered a promising biomarker of AD, potentially even before the Aβ accumulation (Wierenga et al., 2014).

3.4 Neuropathological diagnosis of VCI

VCI is generally recognised as a net result of heterogeneous vascular lesions that cause impaired brain function. The pathological manifestations of vascular lesions are widely variable, and until the last few years, there has been no generally accepted protocol for post-mortem analysis for suspected VaD and VCI subjects. Cerebral vascular pathology, including microinfarcts, lacunes, brain haemorrhages and WML, is associated with cognitive decline (Snowdon et al., 1997, Launer et al., 2011, Vermeer et al., 2003). Efforts have been made to develop a consensus of criteria for the diagnosis of VaD and VCI. Neuropathologists and other scientists from across the UK have collaborated to develop Vascular cognitive impairment neuropathology guidelines (VCING), that provide a validated consensus approach to the pathological assessment and scoring criteria of VCI. Seven pathologies are the most potent predictors of cognitive impairment: leptomeningeal CAA, large infarcts, lacunar infarcts, microinfarcts, arteriolosclerosis, perivascular space dilation and myelin loss (Figure 1-5) (Skrobot et al., 2016). These neuropathologies are focal, multifocal or diffuse vascular lesions and can coexist. The VCING demonstrates major progress in assessing the contribution of vascular pathology to cognitive impairment and to determine which best predicts cognitive impairment.

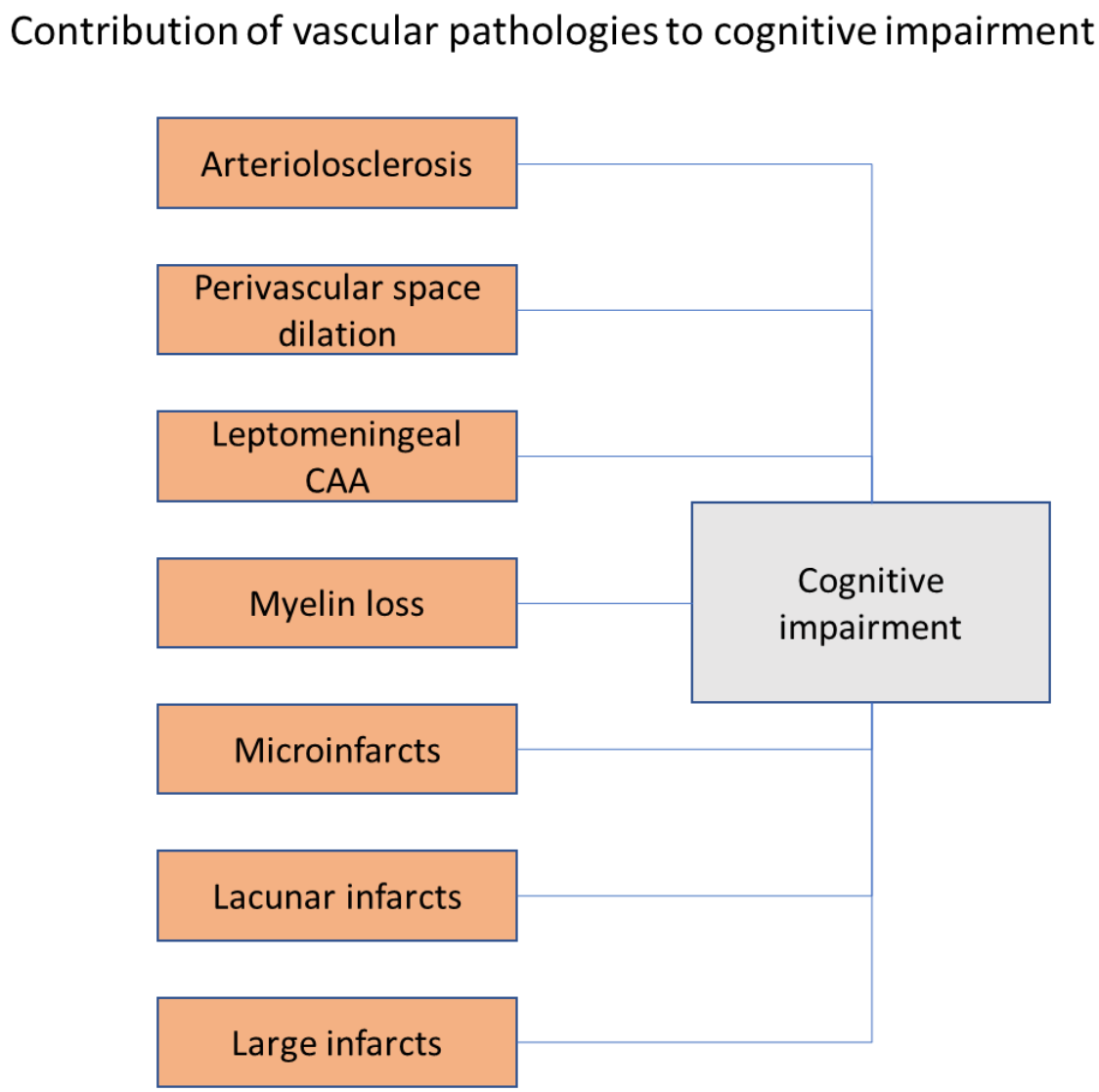

Figure 1-5 Key pathologies confirmed in VCING that are predictive of cognitive impairment.

In the VCING, univariable regression analysis shows that seven pathologies are significantly associated with cognitive impairment. Age, gender, APOE, and Braak stage were not associated with cognitive impairment (Skrobot et al., 2016).

3.5 Cerebral amyloid angiopathy, vascular dysfunction and VCI

Cerebral vascular deposition of amyloid-β protein (Aβ) is a neuropathological hallmark of VCI and is a common finding in older adults. The Aβ deposits in the walls of small and large blood vessels in the cortex and leptomeningeal vessels in

the form of cerebral amyloid angiopathy (CAA) (Figure 1-6) (Weller et al., 1998). Rare forms of familial CAA caused by specific mutations within the Aβ coding domain have amyloid deposition in the cerebral basement membrane and microvasculature (Levy et al., 1990, van den Boom et al., 2005). CAA is a risk factor in VCI that contributes to cognitive decline by promoting pathological consequences such as neuroinflammation, intracerebral haemorrhages, hypoperfusion and ischaemia associated with white matter hyperintensities and microinfarcts (Holland et al., 2008, Haglund et al., 2006, Dichgans and Leys, 2017, Chung et al., 2009, Okamoto et al., 2012, Rozemuller et al., 2005). There may be an interplay between Aβ accumulation and hypoperfusion/ischaemia, whereby perfusion deficits may also contribute to further Aβ accumulation as we have demonstrated previously in our group (Salvadores et al., 2017) and others (Kitaguchi et al., 2009, Huang et al., 2012). As part of my thesis, I have aimed to investigate interactions between cerebral hypoperfusion and Aβ accumulation. There are also new emerging links between Aβ accumulation and impaired glymphatic function (Mestre et al., 2017), which form a central part of this thesis and will be discussed below. The potential role of cerebral hypoperfusion in the pathogenesis of VCI has been described in the figure below (Figure 1-7).

The existing body of research on Aβ accumulation in the vasculature suggests that (Charidimou et al., 2012):

1. Aβ is predominantly generated by neurons and subsequently aggregated in the cerebral vasculature (Herzig et al., 2006). The neuronal overexpression of mutant amyloid precursor protein (APP) leads to the formation of CAA (Calhoun et al., 1999).

2. In contrast to Aβ plaques, which are insoluble Aβ42 deposition in the parenchyma, the predominant species of CAA is more soluble Aβ40 peptide in the

walls of cerebral vessels. Therefore, an increased Aβ40:42 ratio may indicate the shifts of amyloid from parenchymal to the perivascular compartment (Herzig et al., 2006).

3. Vascular deposition of Aβ results from the impaired perivascular clearance rather than overproduction of amyloid. (Attems et al., 2011, Herzig et al., 2006, Bu, 2009). Emerging evidence suggests CVD may affect the drainage of Aβ along the perivascular routes, promoting the development of CAA.

Aβ may cause brain injury through its complex effects on vascular function. Soluble Aβ can directly affect the endothelium-dependent vasomotor regulation of blood vessels (Dietrich et al., 2010). Reductions in cerebral blood flow are observed in transgenic mice overexpressing APP, preceding the formation of Aβ plaques (Niwa et al., 2002b). The Aβ disrupts the critical homeostatic mechanisms of cerebral blood flow; both cerebral autoregulation and neurovascular coupling were found markedly disrupted in transgenic mice studies (Niwa et al., 2002a, Niwa et al., 2000). These effects involve endothelial dysfunction included by NADPH oxidase-dependent oxidative stress (Thomas et al., 1996, Park et al., 2008).

The histological examination of CAA requires staining methods such as Thioflavin-S, Congo red or immunohistochemical staining. Prussian blue (Perl's) staining is useful to identify haemosiderin-laden macrophages related to CAA, suggesting chronic microbleeds (Figure 1-6F) (Serrano-Pozo et al., 2011). The characteristic histological alterations in CAA include the infiltration of Aβ in the media and adventitia, with smooth muscle cells replaced by Aβ deposition and acellular thickening of cerebral vessel walls (Kimbrough et al., 2015). The microvasculature becomes disrupted, demonstrating a "vessel-within-vessel" or "double-barrel" appearance (Figure 1-6F). Microaneurysm formation, perivascular

microhaemorrhages, fibrinoid necrosis may also be seen (Auriel and Greenberg, 2012).

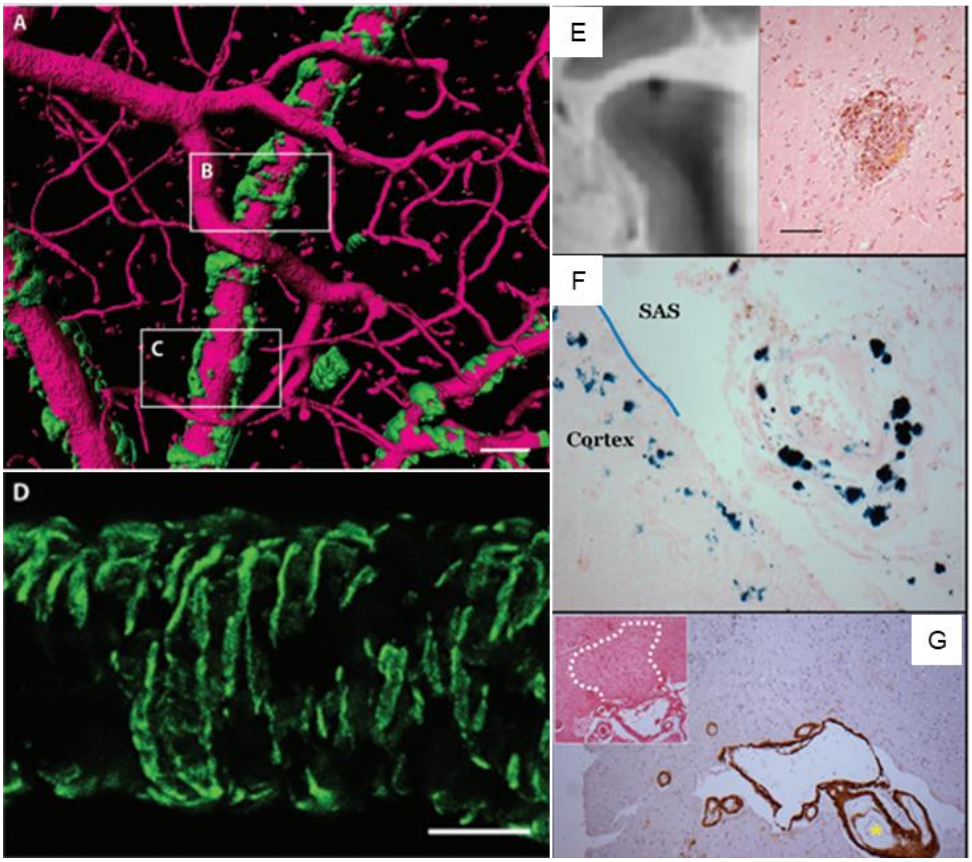

Figure 1-6 Amyloid accumulation in blood vessels in hAPPJ20 mouse and human post-mortem tissue.

(A) High-resolution 3D rendering created from in vivo multi-photon imaging of a hAPPJ20 mouse (15-months-old), where blood vessels are labelled with TRITC-Dextran (magenta) and vascular amyloid is labelled with methoxy-XO4 (green). Scale bar = 40 µm. (B and C) Regions partially covered or wrapped with vascular amyloid. (D) Image created from high-resolution confocal z-projection shows vascular amyloid in ring-like structures surrounding a vessel (subtracted from image) in an older hAPPJ20 mouse (27-month-old). Scale bar = 40 µm. (E) Post-mortem 7T MRI manifests a microbleed in the brain tissue of a patient diagnosed with dementia (81-year-old male) showing severe CAA on pathology. Corresponding haematoxylin and eosin (H&E) staining shows brown (haemosiderin) and yellow (haematoidin) deposits, indicating that this haemorrhage was not chronic but subacute. (F) Perl's Prussian blue staining shows a cortical superficial siderosis of a patient with CAA. Blue deposits (haemosiderin) label microbleeds in the subarachnoid space (SAS) surrounding a leptomeningeal arteriole and in the superficial layers of the cortex. (G) Histopathological manifestation of a cortical microinfarct. Vascular amyloid accumulation is seen in the leptomeningeal vessels and cortical arterioles. Images are reused with permissions (Charidimou et al., 2017, Kimbrough et al., 2015).

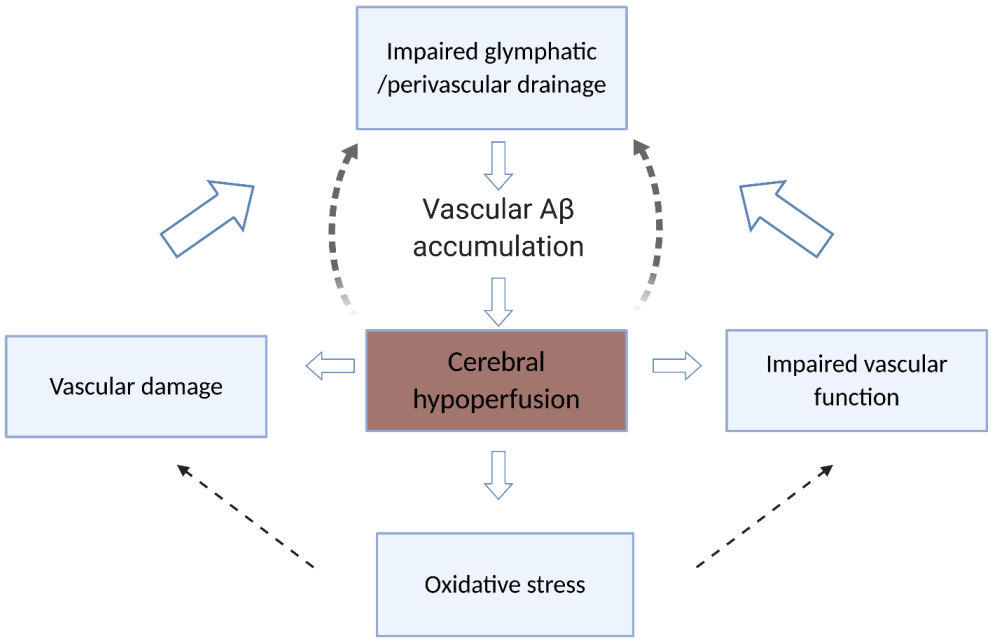

Figure 1-7 Potential pathways through which cerebral hypoperfusion causes accumulation of Aβ, vascular related damages and impaired vascular function.

Possible mechanisms of cerebral hypoperfusion resulting in vascular cognitive impairment (VCI) include damage to the cerebral vasculature and disruption in the vascular function. As alterations in the blood vessels and their functional integrity may affect the glymphatic and perivascular drainage pathway, failure of the Aβ clearance may lead to its accumulation in the vascular walls. Oxidative stress, induced by cerebral hypoperfusion, may in turn promote the vascular damage and vascular dysfunction. Together, these processes may form a destructive combination responsible for accelerating the effects initiated by cerebral hypoperfusion and vascular Aβ accumulation may exacerbate the effects induced by cerebral hypoperfusion.

3.6 Experimental models relevant to VCI

3.6.1 Mouse cerebral hypoperfusion model

The pathogenesis of VCI is still not fully understood this is in part due to the heterogeneity of the disease. Thus, animal models that recapitulate key pathological and behavioural features of human disease are critical to elucidate underlying molecular pathology. To date, there is no singular animal model that accurately

reflects all of the features of the disease process of VCI. However, there are models that have been developed that are useful for investigating key aspects of the disease, as outlined below, and which have been studied as part of this thesis.

Chronic cerebral hypoperfusion is closely associated with white matter pathology in VCI. As a result, models that mimic the reductions in perfusion were developed. Now a mouse model of Bilateral common carotid artery stenosis (BCAS) is the most promising for studying VCI (Venkat et al., 2015, Duncombe et al., 2017a). The BCAS model is induced by placing microcoils on both common carotid arteries (CCA) (Shibata et al., 2004). The selection of inner diameter for the microcoils is crucial since microcoils with varying inner diameters (from 0.16 to 0.22 mm) influence the degree of brain vascular injuries. A high mortality rate of 75% has been observed in mice when placing 0.16 mm microcoils after 14 days of BCAS surgery (Shibata et al., 2004). The 0.18 mm coil is the most acceptable setting as it provides expected pathological outcomes and an acceptable mortality rate. Extensive studies from our group and others have reported the pathophysiology identified in this model (Duncombe et al., 2017a). A common characteristic of this model is a modest reduction of mean cortical CBF of approximately 30-50% following BCAS surgery at 24 hours (Hattori et al., 2016, Shibata et al., 2004, McQueen et al., 2014). Diffuse white matter pathology is detectable from 14 days in the corpus callosum, caudoputamen, capsule and optic tract. Diffuse white matter pathology is found throughout the brain, including damage to myelin integrity, degraded myelin, axons and microglia in the absence of grey matter damage (Coltman et al., 2011). Proliferation and activation of microglia in white matter have been repeatedly reported, indicating a pronounced inflammatory response following chronic cerebral hypoperfusion (McQueen et al., 2014, Shibata et al., 2004, Coltman et al., 2011, Wakita et al., 1994). The BBB is also found to be disrupted following cerebral

hypoperfusion, contributing to WM lesions (Holland et al., 2015, Nakaji et al., 2006). Furthermore, impaired cognitive function is a common finding in the short term and chronically hypoperfused animals. Selective working memory deficits are observed via 8-arm radial arm maze at 30 days following BCAS (Shibata et al., 2007). In longer-term (approximately 6 months old) hypoperfused mice spatial working memory, reference learning and memory were shown to be impaired using behavioural tests in a radial arm and Morris water maze (Nishio et al., 2010).

There are several vessel occlusion models that produce cerebral hypoperfusion via permanent occlusion of common carotid arteries. The Bilateral common carotid artery occlusion (BCCAo) model was developed to mimic chronic cerebral hypoperfusion that is a common feature in human ageing and subjects with dementia. Extensive white matter damage, activation of microglia and astrogliosis were reported preferentially in the white matter (Farkas et al., 2004, Wakita et al., 1994). Cognitive impairment and anxiety-related responses were seen in this model, tested by Morris water maze, open field test and elevated plus maze (Soares et al., 2013). In BCCAo rats showing cognitive deficits, phosphodiesterase III inhibitor (cilostazol) was reported to promote differentiation and survival of oligodendrocytes and improve white matter damages (Miyamoto et al., 2010). Furthermore, permanent occlusion of a single common carotid artery (unilateral common carotid artery occlusion, UCCAO) in mice was reported to cause cognitive impairment following hypoperfusion with markedly increased pro-inflammatory cytokine interleukin-1 beta and interleukin-6 and decreased anti-inflammatory cytokines in the brain (Yoshizaki et al., 2008).

3.6.2 Spontaneously hypertensive stroke prone rats (SHRSP)

Hypertension is a major vascular risk factor associated with pathophysiological changes leading to cognitive impairment (Iadecola, 2013). The Spontaneously

Hypertensive Stroke Prone Rat (SHRSP) is a genetic rat model of severe hypertension and stroke with a genetic variant. It develops progressive hypertension from 8-9 weeks and severe hypertension with systolic pressure reaching 200 mmHg at about 12 weeks (Yamori, 1991). The SHRSP rat presents many features of VCI, such as cerebral infarction, haemorrhage and white matter damages. Since it is a genetic model altering the renin-angiotensin system, kidney and heart were also found to be affected (Kim et al., 1992). Gender differences have been reported and female rats appear to be less altered in endothelial cell dysfunction and inflammation (Ballerio et al., 2007). A recent study demonstrated that endothelial cell dysfunction is associated with white matter vulnerability via the secretion of shock protein 90α that affects the process of myelination (Rajani et al., 2018). It also showed that treatment with endothelial cell stabilising drugs reversed the observed pathologies and may be relevant to human VCI.

3.7 Animal models of amyloid accumulation

Increased accumulation of vascular amyloid and cerebral amyloid angiopathy (CAA), are neuropathological hallmarks of VCI and closely linked to AD. Animal models have been developed as tools for elucidating the mechanisms and therapeutic approaches for vascular amyloid accumulation. In the past decade, several transgenic mouse models have been developed to express human amyloid precursor protein (APP) with mutations associated with familial forms of the disease. Many of these mouse models demonstrate accumulated vascular Aβ including CAA in addition to the extracellular accumulation of Aβ (Hsiao et al., 1996, Davis et al., 2004, Sturchler-Pierrat et al., 1997).

3.7.1 Tg2576 mice

The Tg2576 mouse model is now one of the most well-characterised and commonly used models for AD preclinical studies (Hsiao et al., 1996). It expresses APP with the Swedish mutation KM670/671NL under a hamster prion protein cosmid vector. The hemizygous mice develop parenchymal Aβ plaques along with some amyloid accumulation in vessels by 11-13 months old. The Tg2576 mice exhibit many pathological features and cognitive impairment of AD, including increased Aβ production, Aβ42/Aβ40 ratio, plaque formation with associated age-dependent learning and memory deficits (Hsiao et al., 1996). The mouse model demonstrates a correlation between hippocampal dysfunction and the increased burden of extracellular Aβ42. Decreased dendritic spine density, impaired long-term potentiation and behavioural deficits occur months prior to the Aβ plaque deposition, and significant increases in astrogliosis and microglial activation could be observed in later stage at the 18 months of age (Jacobsen et al., 2006). Synapse loss may not be observed at an early age, but an increase of synaptophysin immunoreactivity can be detected and associated with the acquisition and spatial reference memory. This model has been used to examine the role of reactive oxygen species in behavioural dysfunction. This was reported that 12-15 months old Tg2576 mice lacking the catalytic subunit of NADPH oxidase 2 did not develop oxidative stress or behavioural deficits (Park et al., 2008).

3.7.2 Tg-SwDI mice

Tg-SwDI mouse model is primarily designed to study microvascular accumulation of Aβ. The Tg-SwDI expresses human neuronal amyloid precursor protein (APP), containing the transgenic Swedish K670N/M671L, Dutch (E693Q), and Iowa (D694N) mutations under the control of Thy1 promoter (Davis et al., 2004). In the model, the expression of human APP only exists in the brain, at lower levels than

those of endogenous mouse APP (Davis et al., 2004). Tg-SwDI mice demonstrate striking perivascular or vascular Aβ deposits closely associated with increased age (Davis et al., 2004). Tg-SwDI mice develop amyloid deposition with the high cerebral vascular association at an early stage starting at approximately 6 months of age. The amyloid depositions in the parenchyma are mostly deposited in the form of diffuse plaques that occur at about 3 months of age. Progressive and extensive Aβ deposits can be detected in the subiculum by 3 months, in the olfactory bulb, cortex, thalamus and basal forebrain by 6 months, and throughout the forebrain by 12 months (Davis et al., 2004). Additionally abundant astrogliosis and activated microglia associated with vascular amyloid deposits were reported predominantly in the regions of thalamus and subiculum (Miao et al., 2005). The temporal and regional profile of the Aβ immunoreactive vessels showed a notable level of microvascular amyloid by 6 months old in the thalamus and subiculum. A significant increase of microvascular amyloid can be detected with increasing age in all investigated regions, including forebrain, thalamus and subiculum (Miao et al., 2005). Occasionally, cerebral microhaemorrhages are observed in 12 month old mice and estimated to become more frequent as the mice age (Davis et al., 2004).

ELISA analysis of tissue fractions from isolated vessels and microvascular-depleted parenchyma taken from Tg-SwDI mice revealed higher levels of Aβ40 than Aβ42 in both fractions (Davis et al., 2004). In response to cerebral hypoperfusion, a key risk factor of VCI, Tg-SwDI mice show significantly increased soluble Aβ levels (Aβ40/42) at 1 month that precede insoluble Aβ at 3 months (Salvadores et al., 2017). Chronic cerebral hypoperfusion may increase the load of vascular Aβ, APP levels and processing through the mechanisms of pro-inflammatory and oxidative stress, leading to exacerbated cerebral microinfarcts and microhaemorrhages (Salvadores et al., 2017). Impaired spatial learning and memory performance have

been reported in mice completing the Barnes maze task at 3, 9 and 12 months of age, tests/factors that are associated with the microvascular amyloid accumulation and neuroinflammation (Xu et al., 2007). Tg-SwDI is a unique mouse model well placed for studying microvascular amyloid. The model develops microvascular amyloid at an early stage of the mouse's lifespan, exhibiting microvascular amyloid associated cognitive impairment, and a robust neuroinflammatory response.

4. Modulation of Aβ levels and accumulation and its implications for VCI

Abnormal Aβ accumulation in the brain begins decades before the expected symptom onset, suggested to be mainly owing to the insufficient clearance of the deleterious peptide (Bateman et al., 2012, Panza et al., 2019). As indicated previously, there is substantive evidence showing Aβ has powerful detrimental effects on the vasculature. Soluble Aβ is a potent vasoconstrictor and increased vascular amyloid may contribute to localised microvascular inflammation, and degenerative changes such as haemorrhages and microinfarcts (Niwa et al., 2001b, Paris et al., 2000, Salvadores et al., 2017). Understanding how Aβ levels are modulated through increased accumulation and clearance out of the brain becomes extremely important since it might eventually provide strategies to remove excessive Aβ peptides and protect the brain.

Aβ is removed from the brain by various mechanisms including enzymatic degradation, macrophage degradation, efficient clearance across the blood-brain barrier (BBB), ISF bulk flow, and CSF absorption into lymphatic systems (Figure 1-8) (Tarasoff-Conway et al., 2015). Among these mechanisms, the perivascular or glymphatic clearance of soluble Aβ has been gaining surprising interest and progress since the failure of Aβ clearance is recognised as a critical mechanism related to CVD and AD leading to cognitive decline.

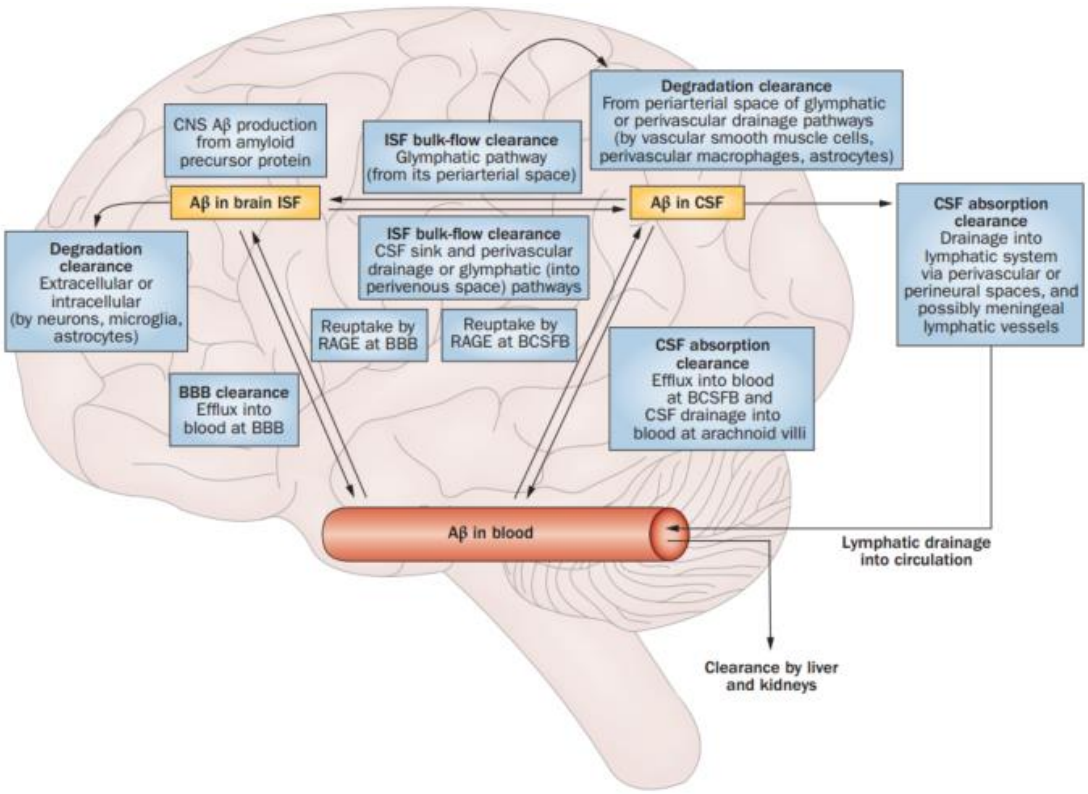

Figure 1-8 Schematic diagram shows proposed pathways for Aβ clearance.

Major pathways for the clearance of Aβ in the brain. Image is taken from Clearance systems in the brain-implications for Alzheimer disease, with permission of right holder (Tarasoff-Conway et al., 2015).

4.1 The glymphatic system

One primary functional clearance mechanism involved in waste elimination and its drainage from the CNS is the glymphatic system. The glymphatic system is described as a macroscopic waste clearance pathway that relies on CSF movement via the perivascular tunnels, mainly comprised of astrocytes, to promote the clearance of solutes and metabolites from the CNS (Figure 1-9). The glymphatic system may also facilitate the brain-wide distribution of many compounds in the CNS, including glucose, amino acids and neuromodulators (Jessen et al., 2015). This recently discovered clearance mechanism is termed the glymphatic system

owing to its dependence on the glial water flux as well as the lack of conventional lymphatic vessels in the brain.

4.1.1 Anatomy of the glymphatic system

In 2012, Iliff et al. reported the glymphatic system using advanced intravital two-photon imaging that confirmed Rennels's previous work (Rennels et al., 1990, Rennels et al., 1985). In the Iliff study, fluorescently labelled CSF tracer appeared in the perivascular space (PVS) of surface arteries within 5 minutes of administration in cisterna magna (CM), then subsequently moved deeper into the parenchyma within the PVS and basement membrane of penetrating arteries (Iliff et al., 2012). The spatial distribution of the CSF was validated using Tie2-GFP: NG2-DsRed double reporter mice that showed fluorescent ovalbumin flowed into the brain specifically within the arterial PVS between the smooth muscle and the astrocyte end-feet of the glial limitans (Iliff et al., 2012). Over the subsequent 3 hours, fluorescent ovalbumin was found within the basement membranes of capillaries and in the PVS of large draining veins (Iliff et al., 2012). Besides perivenous conduits, more recent studies reported exit routes of CSF clearance from the brain, perineural routes and meningeal lymphatic vessels were exit pathways potentially serving the glymphatic system (Eide et al., 2018, Ma et al., 2017b).

The cerebral vasculature plays a unique role in the glymphatic system. As reviewed in previous sections, the cerebral anterior and posterior circulation unite via communicating arteries at the basal circle of Willis. The anterior circulation supplies the neocortex of cerebral hemispheres, while the posterior circulation mainly supplies the brain stem and cerebellum (Prince and Ahn, 2013). Jessen et al. have reviewed the specific anatomy involved in the glymphatic system (Jessen et al., 2015). Cerebral arteries on the brain surface give rise to pial arteries running within subarachnoid space and subpial space. Pial arteries penetrate into brain

parenchyma and become penetrating arteries that form a PVS. The PVS is also termed Virchow-Robin spaces, filled with CSF and covered with leptomeningeal cells between the outmost layer of a blood vessel and astrocytic endfeet. A characteristic of the cerebral vasculature is that almost all arterioles, capillaries and venules within parenchyma are covered by astrocytic endfeet, forming a donut shaped tunnel surrounding vessels. The PVS gradually becomes continuous with the basal lamina as the arterioles penetrate deeply into parenchyma. The basal lamina, also known as basement membrane, is a specific type of extracellular matrix comprised of a mixture of laminin, COL4, nidogen, and heparan sulfate proteoglycans (Thomsen et al., 2017). In the brain, endothelial cells, astrocytes and pericytes reside within the three-dimensional protein network and interact with neurons and smooth muscle cells. The low resistance of basal lamina enables the CSF influx from the PVS to flow deep into the brain parenchyma, enter the basal lamina surrounding capillaries, and leave along with the perivenous space.

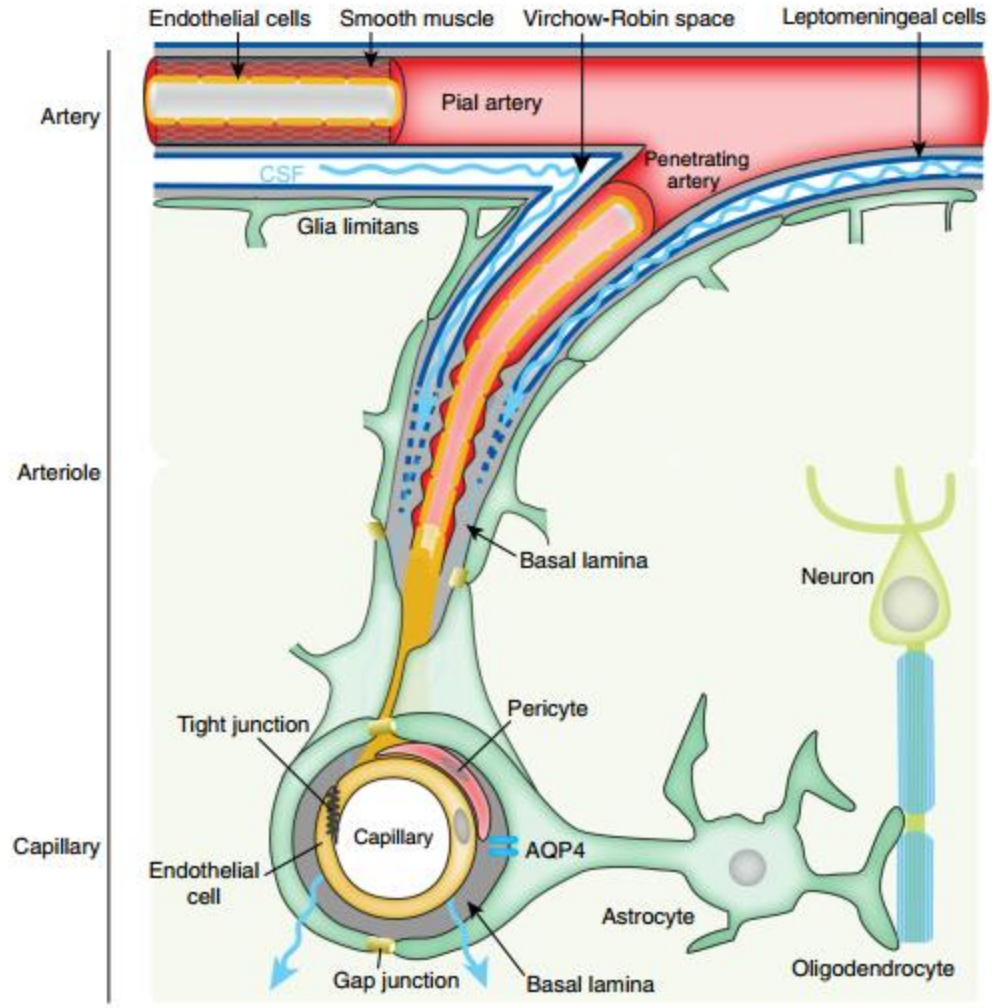

Figure 1-9 Proposed glymphatic CSF influx route.

CSF moves from the subarachnoid space into perivascular space, penetrating artery branch into arteriole and capillary level the perivascular space narrows and merged with basal lamina (Jessen et al., 2015). Image is taken from The Glymphatic System: A Beginner's Guide, with permission of the right holder.

4.1.2 Driving forces in the glymphatic pathway

The primary role of the glymphatic pathway has been reported as performing a waste clearance pathway in the neurophysiology. Therefore, it becomes critical to understand the factors that drive the glymphatic influx. Since the concept of glymphatic system depends on the neuro-glial-vascular network and extracellular

matrix, it is believed that any conditions influencing the integrity of the cellular and functional components within the system will direct the transport of CSF in the brain.

Benveniste et al. have summarized several factors which drive the glymphatic transport: 1. Arterial pulsation; 2. CSF transport and production; 3. State of arousal; 4. AQP4 water channels. Iliff et al. first demonstrated that unilateral ligation of internal carotid artery reduced arterial pulsation leading to the reduced rate of CSF-ISF exchange, while increased pulsatility of penetrating arteries resulted in enhanced CSF-ISF exchange (Iliff et al., 2013b). In late 2018, Mestre et al. used adapted *in vivo* two-photon imaging quantitatively measured CSF speed within the PVS/basement membrane simultaneously with cardiac and respiratory cycles, providing direct evidence that arterial pulsation drives CSF flow, at the same frequency as the cardiac cycles and the same direction of blood flow (Mestre et al., 2018b). While there were other claims that diffusion, a mechanism dependent on a solute's MW, govern the glymphatic fluid transport (Smith et al., 2017, Asgari et al., 2016). It is now likely the transport of glymphatic flow is governed by a mixed process of "convection" that includes both advection and diffusion, and each may have a variable contribution in different regions across the brain. Constant CSF production by the choroid plexus in the lateral ventricles and CSF reabsorption creates a pressure that drives the fluid flow through the ventricular system to the subarachnoid space. The normal production and transport of CSF may influence the glymphatic flow via a mechanism involving intracranial pressure (ICP) (Plog et al., 2015). The state of arousal has been reported to affect the glymphatic influx. In a study, Xie and colleagues reported natural sleep or anaesthesia led to a 60% increase in the interstitial space, subsequently causing a striking increase in CSF-ISF exchange, that improved clearance of Aβ (Xie et al., 2013). There is a debate regarding the role of astrocytic aquaporin-4 (AQP4) water channels in the

glymphatic system. AQP4 water channels are expressed in astrocytic endfeet that ensheathe the cerebral vasculature. In the healthy brain, the transport of convective bulk fluid is facilitated by AQP4 water channels, and reactive astrogliosis induced by disease conditions are thought to cause mislocalization of AQP4 from the astrocytic endfeet to its soma (Iliff and Nedergaard, 2013). Mice lacking the AQP4 in astrocytes demonstrated reduced CSF influx and a significant reduction in the clearance of ISF solutes, including mannitol and Aβ (Iliff et al., 2012). Thus, the reduced CSF solutes influx and clearance in AQP4$^{-/-}$ mice supported the concept that AQP4 is necessary for the transport of glymphatic flow.

The main issue is the proposed role of AQP4 in the transport of soluble solutes. Smith et al. re-examined the role of AQP4 in the solute movement in mouse brain following administration of tracer into the brain or parenchyma (Smith et al., 2017). First, they reported a size-dependent manner of CSF trace transport supporting a diffusion mechanism. This finding has been recently questioned by the evidence provided by Mestre and colleagues that clearly showed the *in vivo* pulsatile manner of CSF tracer transport in the PVS/basement membrane (Mestre et al., 2018b). Second, the transport of fluorescent tracer was reported not to be affected after cardiorespiratory arrest, whereas this conclusion has been challenged by the simultaneously measured cardiac and respiratory frequency, showing the CSF flow driven by cardiac cycle and reduced in hypertension. Third, Smith and colleagues also claimed that AQP4 gene deletion did not impair the CSF influx in both mice and rat models. Followed by a multicentre validation of AQP4 knock-out lines that CSF influx was shown to be higher in wild-type mice than AQP4 KO lines (Mestre et al., 2018a). Accordingly, hydraulic forces associated with arterial pulsation, AQP4 water channels, and physiological CSF production absorption as well as sleep are currently viewed as driving forces in the glymphatic system.

4.1.3 Imaging the glymphatic pathway

There have been several approaches developed to visualise the glymphatic system. *Ex vivo* imaging is a commonly used method for the analysis of glymphatic system. It is performed by *ex vivo* imaging with thick brain sections following *in vivo* administration of CSF tracers (Iliff et al., 2012). It provides the high spatial resolution that enables the investigation of glymphatic function from the cellular to the brain-wide level depending on the scale of the selected region of interests. This method is advantageous when assessing multiple markers in relation to glymphatic flow. It allows the use of immunohistochemical staining and transgenic reporter animals for labelling astrocytes, endothelial cells, and other cellular components within the NVU.

In vivo two-photon imaging is a powerful tool in animal studies investigating the glymphatic system. A craniotomy is required to implant a glass window that allows an optimal depth of a few hundred micrometres for imaging. This method provides high spatial resolution, real-time monitoring of the fluorescent tracer's transport. It can be used on transgenic reporter mice (Tie2-GFP: NG2-DsRed) to study the features of glymphatic influx, enabling the arteries and veins to be distinguished (Iliff et al., 2012).

Transcranial macroscopic imaging is another *in vivo* imaging technique providing global information of the glymphatic pathway. It is less invasive than two-photon imaging but provides relatively lower spatial resolution. Other modalities for imaging glymphatic system include MRI and PET scans. MRI and PET scans are used in both clinical settings and basic research due to their least invasive feature compared to other imaging methods. For instance, contrast-enhanced MR has been used to demonstrate the CSF-ISF exchange in rodents following intrathecal paramagnetic contrast agent injection (Iliff et al., 2013a). In a recent study, intrathecal administration of gadobutrol into idiopathic normal pressure hydrocephalus patients

followed by multiple MRI exams showed the promise of assessing human glymphatic function (Ringstad et al., 2017).

4.1.4 Implications of the glymphatic system in AD and CVD

Impaired glymphatic clearance has emerged as an essential mechanism in CVD and dementia. This conceptualised pathway allows the CSF-ISF exchange and downstream outflow of ISF and solute like Aβ to drain out of the brain. There is increasing evidence suggesting advanced age, acute ischaemic stroke and multiple infarcts impact on the glymphatic drainage (Gaberel et al., 2014, Kress et al., 2014, Wang et al., 2017). The glymphatic system also has important implications for understanding CAA, the primary Aβ40 deposition in the walls of penetrating and leptomeningeal arteries clinically associated with lobar haemorrhages (Attems et al., 2011). The movement of CSF containing Aβ peptides along the periarterial spaces is a critical process for downstream drainage and disturbance to this pathway may contribute to the Aβ accumulation in the vessel walls. Importantly, in the settings of ageing and AD, vascular abnormalities, reactive astrogliosis, enlarged perivascular spaces and altered extracellular matrix are common findings that may directly affect the glymphatic system.

5. Oxidative stress is a link between vascular risk factors and CVD

5.1 Oxidative stress

Oxidative stress is considered to play a significant role in the ageing process and neurodegenerative diseases. It is defined as an imbalance between the levels of free radicals and antioxidants in a biological system. Although the exact mechanisms behind the alterations of the cerebral vascular system and brain cells in the CVD remain largely unclear, increasing evidence has suggested chronic

oxidative damage caused by excess reactive oxygen species (ROS) is one of the most convincing theories. ROS includes radical species (e.g. superoxide anions and hydroxyl radicals) as well as non-radical oxidant (e.g. hydrogen peroxide). ROS can be produced by a variety of biomedical processes such as mitochondria, NADPH oxidase, nitric oxide (NO) synthase and xanthine oxidase (Starkov, 2008, Dworakowski et al., 2006, Porasuphatana et al., 2003, Kelley et al., 2010). Low levels of ROS demonstrate a physiological role modulating normal cellular function and redox signalling (Remacle et al., 1995, Schieber and Chandel, 2014). ROS are short-lived and readily react with a variety of substrates such as proteins and lipids to initiate neuronal cell death and neurodegeneration through different downstream pathways (Barnham et al., 2004).

5.2 Targeting NADPH oxidase mechanisms

Although there are multiple enzymes and metabolic processes that can produce ROS, the key producers of ROS in brain cells are NADPH oxidase (NOX) family, including seven multisubunit enzymes with various tissue and cell distributions (Panday et al., 2015). The NOX isoforms consist of NOX1-NOX5, dual oxidase 1 (DUOX1) and DUOX2, all of which produce superoxide except NOX4 producing hydrogen peroxide. NOX2, formerly known as gp91phox, is expressed in various cell types in the brain, including neurons, endothelial cells, and microglia (Chrissobolis et al., 2012, Brandes, 2003, Surace and Block, 2012). NOX2 is widely distributed in various tissues such as cerebral endothelium. The cerebral vasculature is a major target of oxidative damage, and emerging evidence indicates a direct link between cerebral vascular injuries and cognitive impairment.

The activation of NOX2 is a critical source of the neurovascular oxidative stress associated with cerebral vascular disruption (Park et al., 2007). NOX2 is comprised

of six different subunits that assemble to form an active enzymatic complex for the generation of superoxide (Figure 1-10) (Drummond et al., 2011). Two subunits gp91phox and p22phox are integral membrane-bounding proteins that form the heterodimeric flavocytochrome b558 (cyt b558) complex. Unstimulated subunits p67phox, p47phox, p40phox and GTPase RAC bind together as a complex in the cytosol, while upon stimulation the p47phox becomes phosphorylated and subsequently, this complex translocates to the membrane and interacts with cyt b558 to generate active oxidase. Activated gp91phox interacts with NADPH then convert molecular oxygen (O_2) to superoxide (O_2^-), which participates in various harmful processes. Released superoxide (O_2^-) is highly reactive. It quickly reacts with iron to generate reactive hydroxyl radical, or in the presence of nitric oxide (NO) to future produce neurotoxic peroxynitrite.

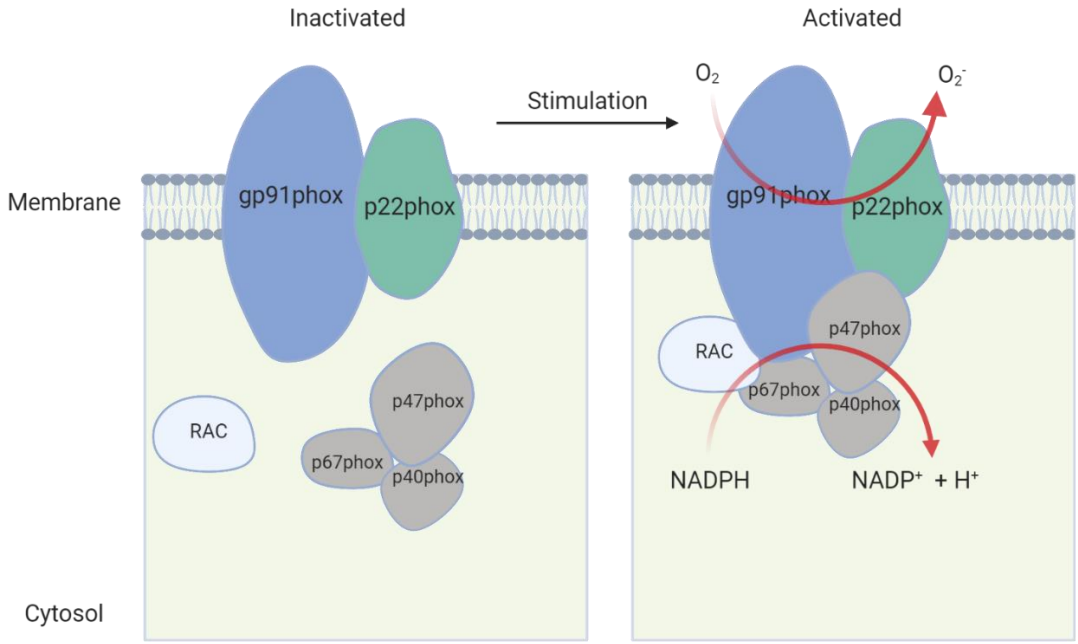

Figure 1-10 Schematic diagram shows the inactivated and activated forms of NADPH oxidase 2 (NOX2).

The NOX2 consists of six different subunits that assemble to form an active enzymatic complex for the generation of superoxide (O_2^-). The catalytic subunit gp91phox combines with p22phox forming the membrane-bounding complex (cyt b558). In the cytosol, p67phox, p47phox, p40phox form a cytosolic complex and bind with GTPase RAC then translocate to membrane docking with cyt b558 complex. Upon the activation, NADPH is processed by activated NOX2 and generate superoxide (O_2^-).

6. NOX in cerebral vascular disease

NOX isoforms, including NOX1, NOX2, NOX4 and NOX5 in the blood vessel walls are described by Drummond et al.(Drummond et al., 2011). NADPH oxidase-dependent oxidative stress has been implicated in many vascular pathological conditions such as hypertension, diabetes, cerebral haemorrhagic and ischaemic brain injuries (Rajagopalan et al., 1996, Gill and Wilcox, 2006, Ayer and Zhang, 2008, Tang et al., 2012). Increased NOX activity is associated with CVDs and their risk factors. Specifically, NOX1 and NOX2 are considered to play harmful roles, and

the absence of these oxidases demonstrated protective effects against vascular injuries (Matsuno et al., 2005, Walder et al., 1997).

Recent studies have shown that increased activation of NOX1, NOX2 and NOX4 are associated with ROS production and pathological processes after cerebral ischaemia (Choi et al., 2015, Yoshioka et al., 2011, Kleinschnitz et al., 2010). In particular, NOX1 expression was increased and associated with oxidative damage to DNA in vulnerable brain regions following experimental stroke (Choi et al., 2015). In mice subjected to middle cerebral artery occlusion (MCAO) followed by reperfusion, increased NOX2 activity resulted in oxidative stress and vascular dysfunction (De Silva et al., 2011). Upon acute stroke, NOX4 has been reported as a significant source of oxidative stress in human and mouse brains and proposed as a novel drug target for stroke therapy (Kleinschnitz et al., 2010). Furthermore, in cerebrovascular disease models such as global cerebral hypoperfusion, an increase of NOXs activity and expression lead to cognitive impairment via oxidative stress-apoptosis signal-regulating kinase 1 (ASK1) pathway. Pharmaceutical inhibition of NOX enzymes by NOX inhibitor apocynin improved cognitive function in mice subjected to BCAS surgery (Toyama et al., 2014). Ansari et al. have studied the various protein components of NOX2 in the post-mortem human brain samples and demonstrated increased levels of cytosolic subunits p67phox, p47phox and p40phox, but membrane-bound subunits (gp91phox) and p22phox) remained stable with the progression of AD (Ansari and Scheff, 2011). Clinical data also demonstrated that NOX isoforms (p47phox and gp91phox) expression and activity significantly increased in the mild cognitive impairment (MCI) patients suggesting NOX-associated redox in the early stage of AD (Bruce-Keller et al., 2010).

7. NOX inhibitors

Mounting evidence suggests that NOX inhibition is neuroprotective against various brain pathological processes such as ischaemic damage. Several pharmacological compounds have been discovered to target NOX enzymes. Of all these compounds, apocynin and diphenyleneiodonium (DPI) are the most widely studied. Although these compounds have demonstrated a promising future for the therapeutic purpose, inhibitors with higher specificity and selectivity are still highly sought after to ensure the clinical application.

7.1 Diphenyleneiodonium (DPI)

DPI was demonstrated to protect the brain by inhibiting the flavoprotein from preventing the production of superoxide. In the experimental rat model of stroke followed by reperfusion (MCAO/R), a combination of DPI and dimethylsulfoxide (DMSO) reduced infarct sizes and BBB damage and improved neurological outcome (Nagel et al., 2007). DPI also protected the brain by not only suppressing oxidative stress induced by transient focal cerebral ischaemia but also limiting leukocytes migration and infiltration (Nagel et al., 2012). However, DPI shows poor selectivity of all NOX isoforms and reacts with flavin adenine dinucleotide (FAD)-containing enzymes that play a role in many metabolic pathways (Kahles et al., 2007).

7.2 Apocynin

Apocynin, also known as acetovanillone, is an oxidase assembly inhibitor that prevents the p47phox subunits binding with membrane-bound heterodimer (Drummond et al., 2011). It is derived initially from Apocynum species that has been used by Chinese and South Asian people to manage inflammatory diseases (Simonyi et al., 2012). Apocynin has demonstrated high effectiveness and excellent

safety profile in a variety of studies (Yu et al., 2008). The intraperitoneal administration of apocynin in mice models of global cerebral ischaemia showed a neuroprotective effect on spatial learning and memory (Shen et al., 2011). CAA is a pathological hallmark in AD and characteristic finding in CVD. Han et al. reported ROS contributed to the formation of CAA, vascular function and microhaemorrhages in a mouse model of AD (Han et al., 2015). NOX-derived ROS is shown to mediate CAA-induced cerebral vascular injuries. The inhibition of NOX by apocynin successfully reduced oxidative stress that improved vascular reactivity in Tg2576 mice. The improved vascular function is potentially attributed to reduced CAA. Interestingly, apocynin is reported to down-regulate the expression of ApoE that is a crucial factor in promoting CAA formation.

8. Summary

Multiple vascular risk factors cause damage to the cerebral vascular network contributing to neurodegenerative changes (such as WMH, microbleeds and microinfarcts) leading to VCI. These types of vascular related changes are also present in AD (Skrobot et al., 2016). The considerable overlap between the pathology of AD and VaD suggest a common pathophysiological mechanism that contributes to cognitive impairment and neurodegeneration, resulting in dementia. Further, increased microvascular amyloid deposition and CAA increases the risk of stroke lesions (Okamoto et al., 2012, Soontornniyomkij et al., 2010) suggesting a vicious cycle of events.

As outlined previously, sustained reductions in blood flow are emerging as a critical contributor to VCI promoting brain microvascular pathology, leading to cognitive deficits and dementia. In order to investigate the underlying mechanism, the BCAS animal model has been established. Furthermore, to understand the role of vascular

amyloid deposition in pathomechanisms, a transgenic mouse model of microvascular amyloid has been developed. These models additionally allow interactions between carotid stenosis and amyloid accumulation to be investigated. Related to this work impaired glymphatic function is emerging as a key player in vascular disease and dementia and regulator of amyloid clearance. However, whether glymphatic function is altered with carotid stenosis remains to be determined. These gaps in pre-existing knowledge form the basis of the studies within the thesis.

9. Hypothesis

It is hypothesized that the complex interaction of AD and carotid stenosis leads to cognitive impairment via impaired glymphatic function in addition to perfusion deficits that promote vascular amyloid accumulation. Moreover, given clear links between NOX2, hypoperfusion and amyloid, it was further hypothesised that NOX2 is a central mechanism leading to VCI.

10. Study aims

In this thesis, CBF changes following BCAS was the primary outcome of interest and glymphatic function, cognition, vascular function, vascular related pathology, neurodegenerative changes, and amyloid burden as well as the effect of NOX2 inhibitor treatment were considered as secondary outcome of interest. These following study aims were investigated in chapter 3, 4 and 5:

Aim 1: To examine the effect of BCAS on cerebral perfusion deficits, glymphatic function and cognition in Tg-SwDI mice compared to wild-type mice.

Aim 2: To examine the effect of BCAS on neurovascular function, degenerative changes and amyloid accumulation in Tg-SwDI mice compared to wild-type mice.

Aim 3: To determine whether targeting NOX2 has an effect on cerebral perfusion, degenerative changes and cognitive impairment in Tg-SwDI mice compared to wild-type mice.

Chapter 2. Material and methods

1. Animals

All experimental animals used in the present thesis were conducted following the UK Home Office Animals (Scientific Procedures) Act 1986 and additional local ethical and veterinary approval (Biomedical Research Resources, University of Edinburgh). Mice were group held in standard cages with bedding, food, water and nestles under 12 h dark/light cycles. Male Tg-SwDI mice and wild-type C57Bl/6J littermates were bred in-house (a number of wild-type C57Bl/6J mice were imported from Charles River Laboratories Inc, UK). Tg-SwDI mice were used as an AD model to study microvascular amyloid accumulation. Tg-SwDI mice are known to express human neuronal amyloid precursor protein (APP), containing the transgenic Swedish K670N/M671L, Dutch (E693Q), and Iowa (D694N) mutations under the control of Thy1.2 promoter (Figure 2-1) (Davis et al., 2004). Surgeries including both sham and bilateral common carotid stenosis (BCAS) surgery were performed by an independent researcher. The mice were coded to ensure the surgery they received, and their genotypes were blinded from the researcher who completed the rest of the experiment. The detailed information regarding the age, gender, genotype and number of animals used in each study are described in the corresponding methods sections in Chapters 3, 4 and 5.

The group size was decided based on power calculation of previous CBF data from arterial spin labelling (ASL), since CBF changes were considered as the primary outcome measure. A minimum group size of n=8 was required to achieve a significance value of $p<0.05$ at a power of 0.8.

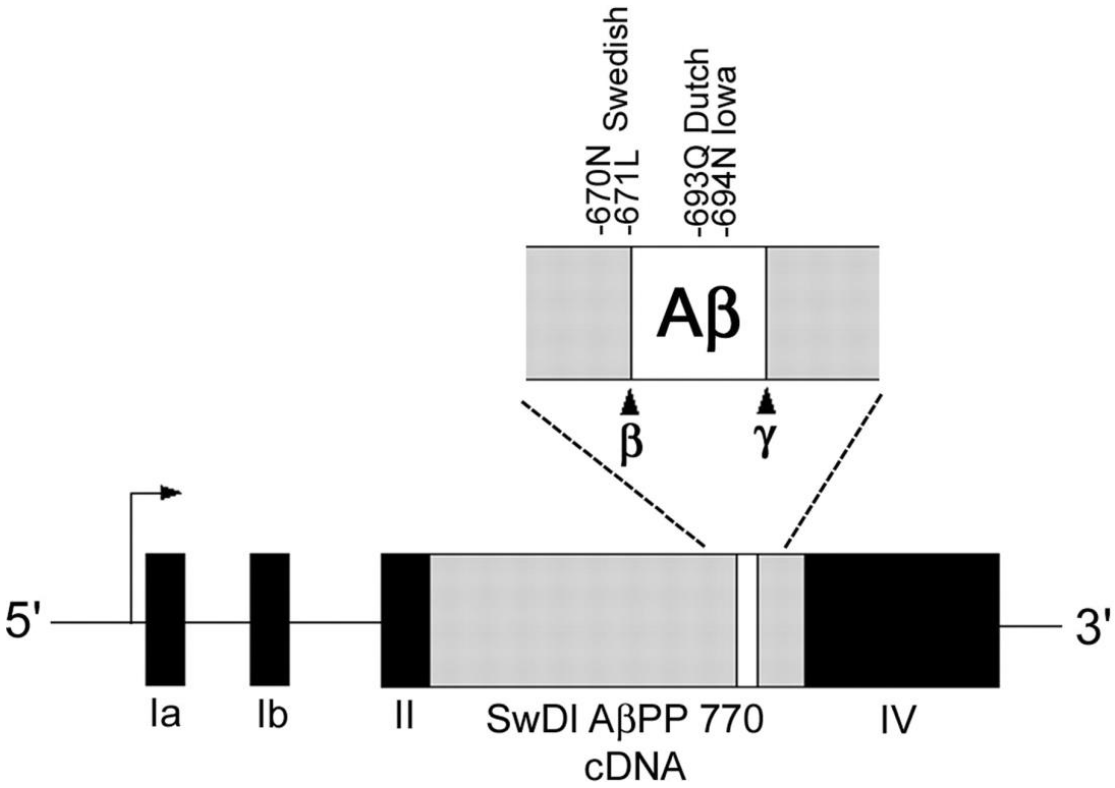

Figure 2-1 Schematic diagram shows Thy1.2 promoter-transgenic human SwDI mutant APP construct.

The Tg-SwDI mice express human APP gene, isoform 770, containing the Swedish 670N/671 L, Dutch (639Q) and Iowa (694N) mutations under the control of Thy1.2 promoter.

2. Bilateral common carotid stenosis (BCAS) surgery

Mice were anaesthetised initially by 5% isoflurane in oxygen and then maintained under 1.5% isoflurane/oxygen mix. After the incision area was shaved and cleaned with iodine, a midline incision is made and tissues dissected to reveal the common carotid arteries. These were isolated using silk threads (size: 4/0) and microcoils applied (0.18mm internal diameter, Sawane Spring Co, Shizuoka, Japan) permanently to both common carotid arteries (Figure 2-2). Details of surgical methods have been outlined in previous studies (Shibata et al., 2004, Coltman et al., 2011, Reimer et al., 2011a, Holland et al., 2011b). A 30 minutes interval was given between the application of the two microcoils to minimise the effects of acute CBF reduction caused by the placement of microcoils. Sham-operated animals

underwent the identical procedure except for the application of microcoils to both arteries. Surgery was conducted by Prof. Karen Horsburgh.

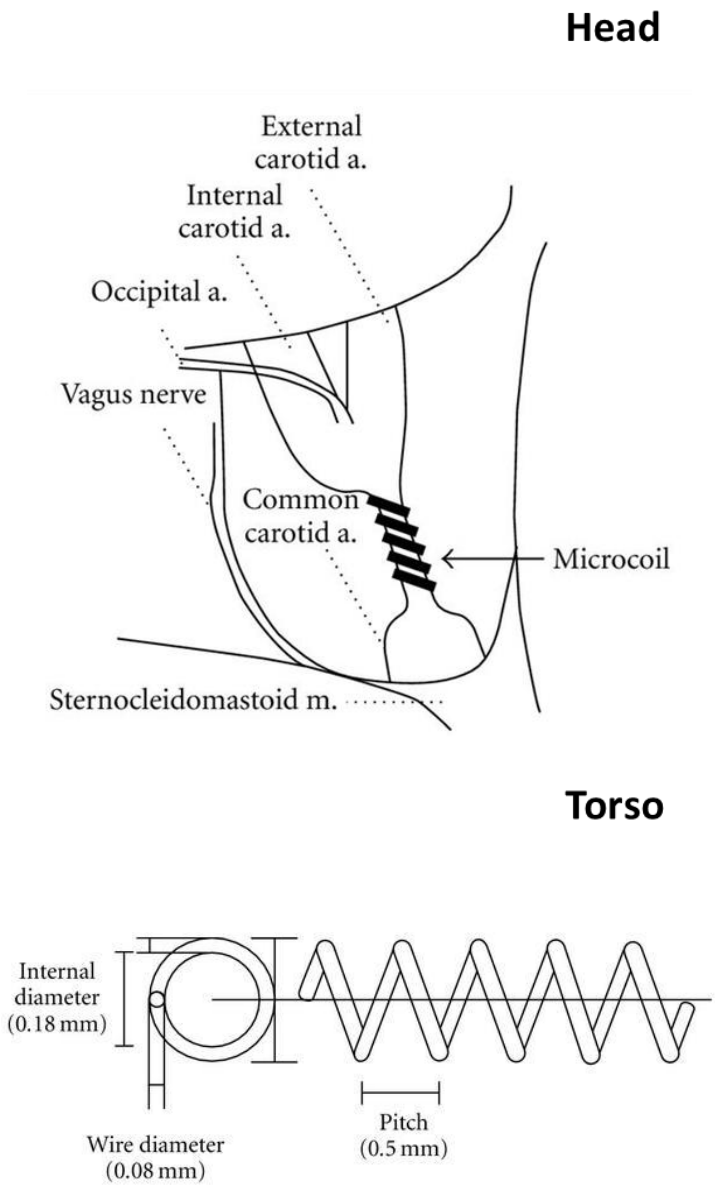

Figure 2-2 Demonstration of bilateral common carotid stenosis induced by placing microcoils.

The microcoils are placed on the common carotid artery of a C57BL/6J mouse by surgical procedure (only one side is shown as an example). The microcoils used in the current thesis was made from piano wire with a wire diameter of 0.08 mm and inner diameter 0.18 mm, which has been used in the previous study (Ihara and Tomimoto, 2011).

3. Administration of NOX inhibitor apocynin

Apocynin is a non-specific NADPH oxidase assembly inhibitor that prevents the p47phox subunits binding with membrane-bound heterodimer (Drummond et al., 2011). Following the establishment of hypoperfusion, mice were given either via vehicle or apocynin (Sigma, UK) ain their drinking water at a dose of 30 mg/kg/day. A stock of apocynin was prepared and stored at -20 °C and deforested with light protection before the administration. Apocynin and vehicle were changed three times a week with maximal duration less than three days to maintain freshness. The consumption of apocynin and water were monitored throughout the study.

4. Cerebral blood flow measured by MR arterial spin labelling (ASL)

A 7.0T Agilen (Varian) preclinical MRI system was used to collect T1-weighted and arterial spin labelling (ASL) data (Figure 2-3). Experimental animals were anaesthetised under 5% isoflurane in oxygen for induction then placed in an MRI compatible holder (Rapid Biomedical, Wurzburg, Germany). Isoflurane was maintained at 1.5% in oxygen during scanning. Rectal temperature was monitored and regulated at around 37 ºC by an airflow heating system. Respiratory rate was maintained at 70-100 breaths per minute. The T1-weighted images were acquired at 1.7 mm posterior to Bregma in stereotactic coordinates of Mouse Brain Atlas (Paxinos and Franklin, 2001). Resting cerebral blood flow was measured using ASL at the level corresponding to T1-weighted scans with a Look-Locker FAIR single gradient echo (LLFAIRGE) sequence (Kober et al., 2008). Maps of cerebral blood flow were constructed from ASL data in Matlab using in-house scripts. Cerebral blood flow maps were analysed in ImageJ (v1.46, NIH, Bethesda, MD, USA) using unbiased regions of interest from T1-weighted images acquired with the ASL sequence. Imaging studies were conducted with the support of Dr Jessica Duncombe, Dr Maurits Jansen and Dr Ross Lennen.

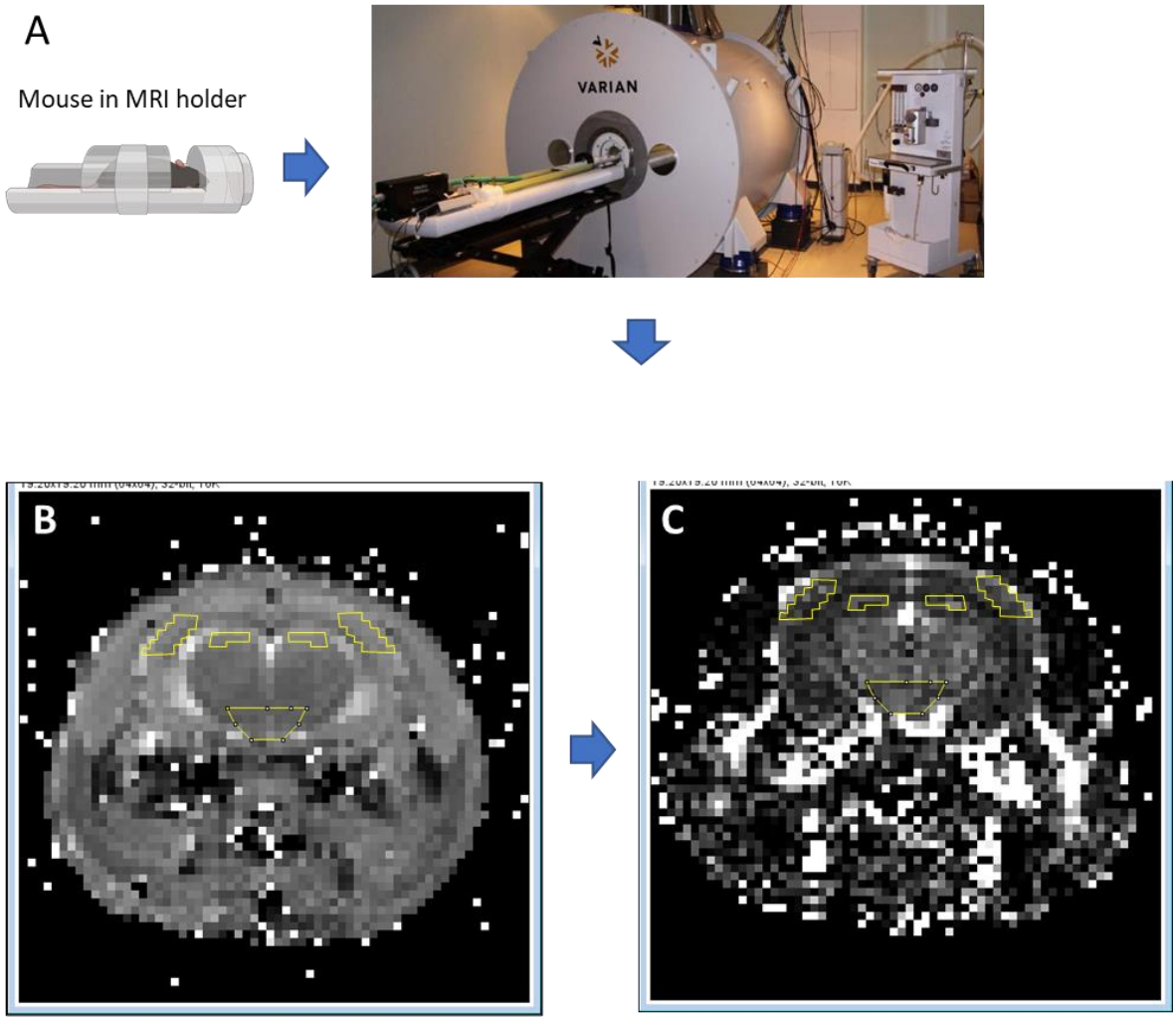

Figure 2-3 Cerebral blood flow measured by MR arterial spin labelling (ASL).

A mouse was placed on a compatible holder to be placed in an MRI scanner. (A) Vital signs including body temperature and respiratory rate were monitored. (B and C) Regions of interests was drawn on T1 (B) then transferred to ASL sequence (C) and further analysed in ImageJ.

5. Assessment of cortical blood flow using laser speckle contrast imaging

Laser speckle contrast imaging was applied for measuring *in vivo* cortical blood flow using a method reported previously (McQueen et al., 2014). Mice were given 5% isoflurane in oxygen in an anaesthetic chamber for induction. Then mice were placed on a stereotaxic frame with their head fixed into position. Isoflurane was maintained at 2-2.5% in oxygen-enriched air via a nose cone, and rectal temperature was monitored and maintained at

around 37 ºC. An incision was made along the midline to expose the skull then properly covered with gel to keep the surface moisturised. Laser speckle contrast imager (moorFLPI-2, Moor Instruments, UK) was positioned 20 cm above the incision. Image resolution was set at 752 x 580 pixels and the frequency at 1 frame/second (20 ms/frame). Two minutes of perfusion data was recorded after the stabilisation of reading. For repeated measures, laser speckle imaging was taken at baseline (before surgery), 24h, 1 month and 3 months following BCAS and the surgical incision was sutured, and mice were allowed to recover at the end of each imaging session except the endpoint experiment.

Raw images from laser speckle imaging were analysed using moorFLPI2 Review software (v4.0). Two uniformed squares were drawn on barrel cortex on both left and right hemisphere and made to avoid any artefacts on the skull. The regions of interest were consistent over time and between each mouse. Data from both left and right barrel cortex were collected to obtain a mean value of CBF. The CBF data is presented in perfusion units (PU) and calculated as the percentage change to baseline blood flow. CBF laser speckle imaging study was conducted with the support of Dr Jessica Duncombe.

6. Assessment of neurovascular coupling by performing whisker stimulation

Repeated whisker stimulation was used to evoke neurovascular coupling in the barrel cortex following the procedure described in (Figure 2-4). Mice were anaesthetised by intraperitoneal injection with α-chloralose (50 mg/kg) and urethane (750 mg/kg) to preserve physiological vascular responses. Whiskers on the right side were trimmed at approximate 1 cm for stimulation and were cut on the left to avoid any unwanted disturbances. Mice were positioned on the stereotaxic frame with their head fixed into position. Oxygen was supplied via a nose cone, and rectal temperature was monitored and maintained at around 37 ºC. Laser speckle imager (moorFLPI-2, Moor Instruments, UK) was set up according to the methods described in the above section. Stable cortical blood flow in the Barrel cortex was recorded for 2 minutes as the baseline recording (Figure 2-5). During stimulation, the

whiskers were deflected by rapid back-and-forth movements using an electric stimulator for 30 seconds to evoke the neuronal activity in the contralateral Barrel cortex. CBF was set to return to baseline before the next stimulation. Three successful recordings were recorded for data processing. Raw images from laser speckle imaging were analysed using moorFLPI2 Review software (v4.0). The mean response amplitude was collected and calculated as the result of the percentage increase from baseline. Neurovascular coupling study was conducted with the support of Dr Jessica Duncombe.

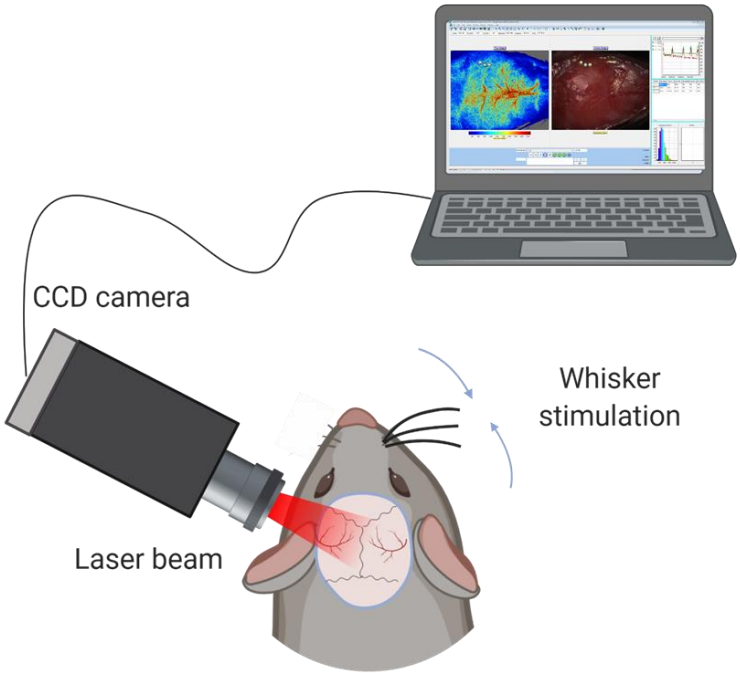

Figure 2-4 Neurovascular coupling assessed by whisker stimulation.

The schematic diagram shows neurovascular coupling assessed by measuring the blood flow changes in the Barrel cortex after whisker stimulation. The stimulation was given on the right side of whiskers and reading was recorded from Barrel cortex on the contralateral side. Three successful recordings, including both before and after stimulation, were collected for data processing.

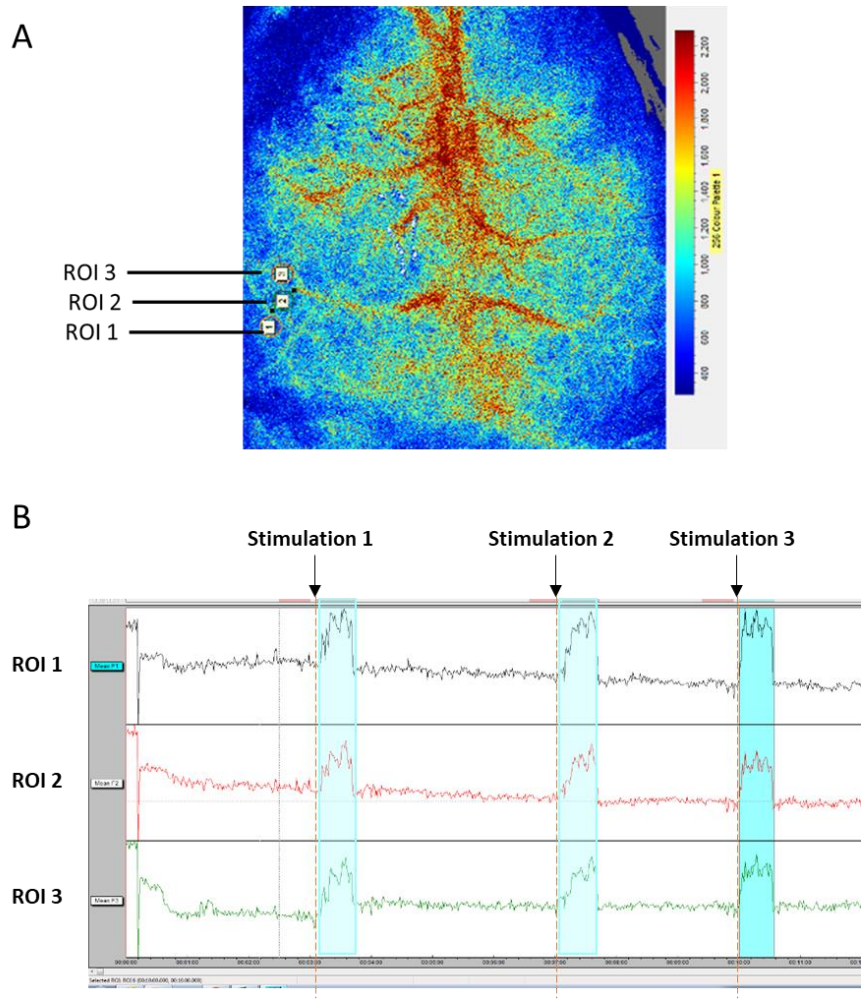

Figure 2-5 Examples of ROIs drawn for neurovascular coupling assessment using whisker stimulation.

(A) Three ROIs were placed on the Barrel cortex that was on the contralateral side of whisker stimulation. (B) Stable cortical blood flow in the Barrel cortex was recorded for 2 minutes for each stimulation as the baseline recording. All measurements of CBF data from baseline and stimulation phases were performed in triplicate (30 seconds/stimulation, highlighted in green boxes) for each region to calculate the mean response amplitude.

7. Assessment of cognitive function using the Barnes maze

The Barnes maze was used to assess the spatial learning and memory function at 3 months after the mice received BCAS or sham surgery. The Barnes maze used in the present thesis was comprised of one white circular platform and 20 circular holes around the outside edge of the platform, with 91.5 cm diameter and 115 cm height (Figure 2-6) (San Diego Instruments). There is one dark escape chamber attached to one of the holes allocated to each experimental animal. Visual cues were prepared using different colour and shaped

objects and placed on the curtains and walls around the maze. There was one white cylinder with 10.5 cm diameter for retaining animals at the beginning of each trial. All the tests were recorded by a camera attached to a computer directly above the centre of the platform. Movements of the animals were recorded by using software ANY-maze v 4.99. All the tests were performed in the behaviour testing room where the room temperature can be controlled at a constant 20 ºC. A summarised schedule of Barnes maze used in this thesis is described below (Figure 2-7). Experimenters performing the tests were blinded throughout the experiments and mice were randomly allocated into a running order generated in Excel on a daily basis. Barnes maze was conducted with the support of Dr Jessica Duncombe.

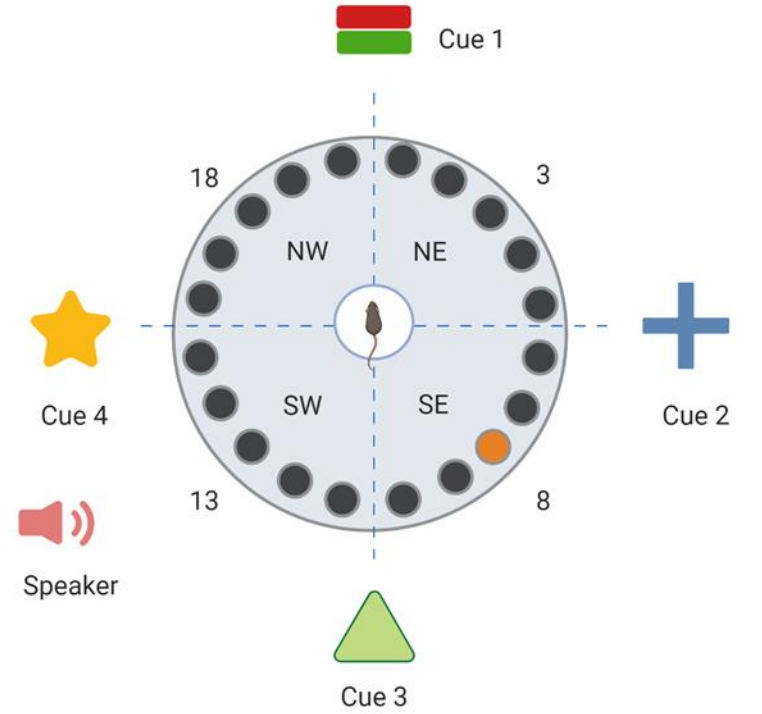

Figure 2-6 Barnes maze for testing spatial learning and memory.

(Top) The schematic diagram demonstrates the maze consisted of four defined quadrants (northeast: NE, southeast: SE, southwest: SW and northwest: NW) and one central area, visual cues mounted on the walls and a speaker for generating white noise. A target hole in orange colour is shown as an example. In the acquisition tests, hole "3, 8, 13 and 18" were randomly allocated to each mouse as a target hole, then it was switched 180° in reversal tests. (Bottom) Image of Barnes maze in the behavioural testing room.

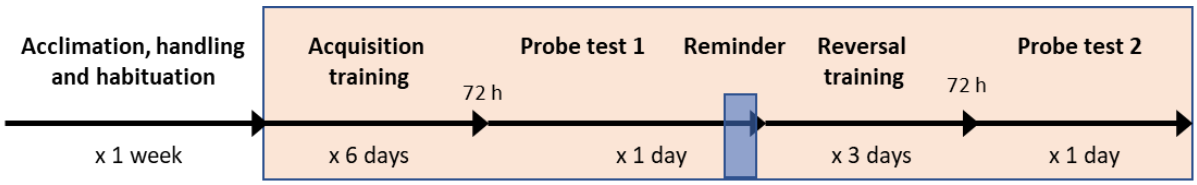

Figure 2-7 A summarised schedule of Barnes maze.

A summarised schedule shows the working flow of Barnes maze used in this thesis.

7.1 Acclimation, handling and habituation

Animals were brought into the behavioural testing room and placed in the holding cylinder to acclimate to the testing environment for 10 seconds for two days before habituation. One week before the training session, mice were handled by experimenter and habituated to the maze and escape the cage. Each mouse was placed in the holding cylinder for 10 seconds then allowed to explore the arena for 3 minutes under low-stress conditions after removal of the cylinder, without aversive white noise stimulation. Then mice were guided to the escape cage and allowed inside for 2 minutes. All the animals were allocated one fixed number for the cage during the behaviour test. The maze and the escape cage were cleaned with ethanol to avoid any olfactory cues between each trial.

7.2 Visuo-spatial learning and working memory test (Acquisition training)

During the training session, mice were trained to find the escape chamber over 6 days, with 2 trials per day (60-minute inter-trial interval). The platform consists of 20 escape holes, and the location of escape chamber remained constant to each mouse but was shifted clockwise 90 degrees between mice to avoid any olfactory cues. The mouse was placed in the holding cylinder for 10 seconds. The aversive white noise was given once the test started and switched off once the mouse entered the escape chamber. If the mouse failed to enter the target hole, the experimenter should guide the mouse to the escape cage; then the aversive stimulus stopped as soon as the mouse entered the chamber.

7.3 Acquisition 72 h probe test

The acquisition 72 h probe trial was performed 72 hours after the acquisition probe, and all the elements remained the same. The acquisition probe and probe trials aimed to test the acquisition short and long-term memory of the mice.

7.4 Reminder training

Following the final acquisition probe trials, retraining was carried out under the same condition as the acquisition training phase. The reminder training day was aimed to ensure no extinction of hole location memory occurred in the probe test.

7.5 Reversal training

During the reversal training session, mice were trained to find the escape cage following same procedure as the acquisition training phase, but with the allocated escape cage shifted 180 degrees to the opposite side of the stage. The mice were trained over 3 days, with 2 trials per day (60-minute inter-trial interval) in reversal training to evaluate the spatial learning ability in the increased difficulty of the task.

7.6 Reversal 72 h probe test

The reversal probe trial was performed 72 hours after the final reversal training. Animals were given 90 seconds to explore the maze with the escape cage removed. All the elements in the reversal probe remained same as reversal training test.

7.7 Measurements

Trials were recorded by a recording system above the arena and measured using tracking software Any-maze version 4.99. Spatial learning was assessed by the total time to enter the escape cage (escape latency). Similarly, the time of animals to first encounter the target hole

was recorded as primary latency as well as the total time and path length spent in the trials recorded as total latency and total distance, respectively.

8. Assessment of glymphatic function

8.1 Intracisternal injection of CSF tracers

Mice were initially anaesthetised with isoflurane (5% in oxygen), then positioned in a stereotaxic frame and anaesthetic maintained at approximately 1.5% (in oxygen). The respiration was regulated using a ventilator. The posterior atlanto-occipital membrane was surgically exposed, and a 32GA needle attached to a Hamilton syringe was inserted into cisterna magna (Figure 2-8). Alexa Fluor 488 fluorescein labelled 3 kDa soluble lysine fixable dextran D-3 (green) (D7156, Invitrogen) and Alexa Fluor 594 ovalbumin conjugate OA-45 (Red) (O34783, Invitrogen) were mixed at 1:1 ratio and infused at a concentration of 5 µg/µl, at a rate of 0.5 µl/min over 20 minutes (10 µl total volume) through a syringe pump (Harvard Apparatus). The needle was held in place for 10 minutes and then removed, and atlantooccipital membrane was sealed to avoid any reflux of CSF. For fast observation of CSF glymphatic entry, 1% Evans blue dye in PBS was injected into cisterna magna using the same methods described above.

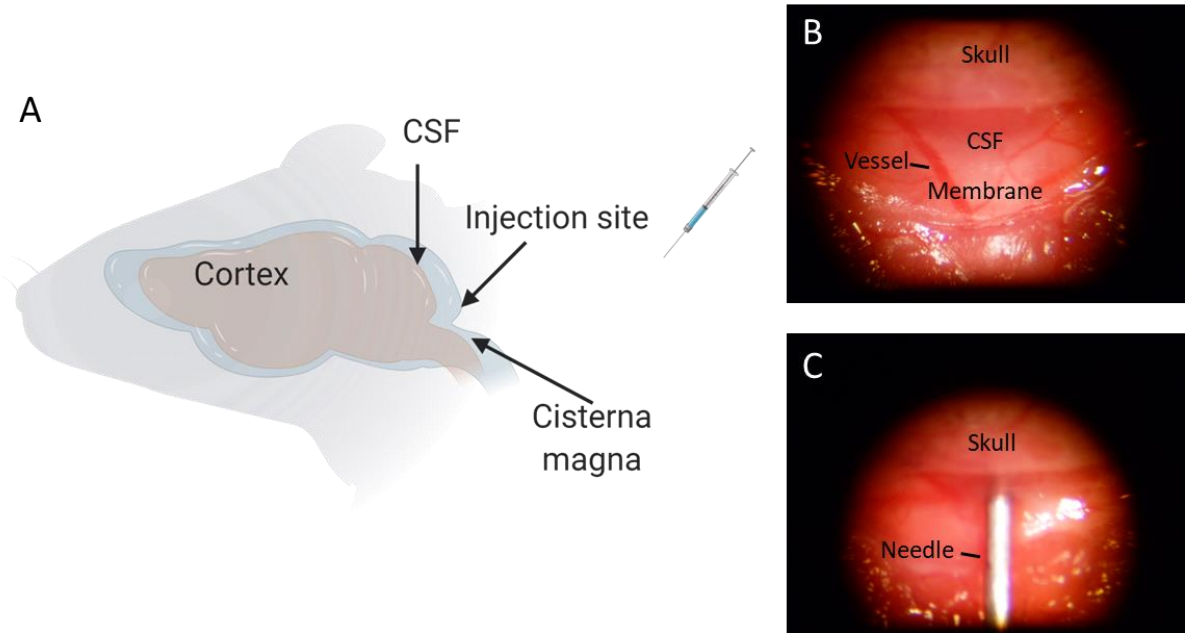

Figure 2-8 Intracisternal injection of fluorescent tracers.

Fluorescent tracers were injected into cisterna magna under a microscope. (A) The schematic diagram shows the injection site and the location of cisterna magna of a mouse head. (B) Image taken before the injection shows the skull, atalanto-occipital membrane and CSF and a blood vessel underneath the membrane. (C) The needle was inserted into the membrane with no damage to the blood vessel and reflux of CSF. Image A was created from Biorender.com.

9. *Ex vivo* imaging of CSF fluorescent tracer

Tracer movement from the subarachnoid space of the cisterna magna into the brain was imaged using a slide scanner (ZEISS Axio Scan.Z1). Multi-channel whole-slice images of each animal at eight sequential levels (1.18, 0.74, 0.14, -0.34, -1.06, -1.82, -2.46 and -2.70 mm to bregma, Mouse Brain Atlas) were generated at 20x magnification. This included separate DAPI, Alexa Fluor® 488 fluorescein labelled 3 kDa soluble lysine fixable dextran D-3 (green) and Alexa Fluor® 594 ovalbumin conjugate OA-45 (Red).

All images were scanned using constant exposure time for each channel by the slide scanner. For the quantification of tracer movement into the brain, scanned images were analysed in ImageJ software (v1.46, NIH, Bethesda, MD, USA) as described previously. Raw images were obtained for further analysis. Region of interest (ROI) was defined using

the DAPI channel to identify anatomical regions. Fluorescent intensity measure was used for comparing global glymphatic influx and % area measure was used for regional tracer influx quantification.

10. Perfusion fixation

Mice were transcardially perfused with 30 ml phosphate-buffered saline (PBS) then whole brains were fixed in 4% paraformaldehyde in PBS for 24 hours. Tissues for further cryostat sectioning were transferred into 30% sucrose solution in PBS for 72 hours. Brains were placed in pre-cool isopentane -42 ºC for 5 minutes then stored in -80 ºC freezer and coronal sections (12 µm) were cut using a cryostat. Brain tissues for further vibratome were sectioned into coronal planes (100 µm) on a vibratome then stored in the cryoprotective medium in a -20 ºC freezer.

11. Histological assessment of vascular related lesions

11.1 Haematoxylin and eosin (H&E) staining

To determine the vascular related lesions, such as microinfarcts, sections were stained with H&E method using standard protocols to visualise the presence of ischaemic tissue damage. 6 stereotactic levels of brain sections (0.86 mm, 0.14 mm, -0.46 mm, -1.34 mm, -1.70 mm and -2.30 mm to Bregma) were examined for the presence of these vascular related changes. Sections were removed from the freezer and allowed to air dry. Sections were rinsed in running tap water and through a series of steps for delipidising. Staining was performed using filtered haematoxylin (Thermo Fisher, UK) for 3 minutes. Sections were rinsed in running tap water and added to 1% Acid Alcohol for maximum 10 seconds before being placed in running tap water for 2 minutes. Sections were then transferred to Scott's tap water for 2 minutes until the tissue sections turn blue, washed in running tap water for 2 minutes and placed in EosinY Alcoholic (Thermo Fisher, UK) for 2 minutes. Finally, sections

were rinsed in running tap water, dehydrated through serial alcohols (70%, 90%, 100%) and placed in xylene for 15 minutes then mounted with DPX.

11.2 Perl's Prussian blue staining

Perl's Prussian blue staining was used to detect the haemorrhagic tissue damage by examining the presence of iron using a standard kit (HT20, Sigma, UK). Frozen sections were removed from the freezer and allowed to air dry. Sections were rehydrated to distilled water, then placed in a 1:1 mix solution of potassium ferrocyanide and hydrochloric acid for 10 minutes. Sections were then placed in distilled water and incubated in DAB/Metal concentrate diluted in peroxide buffer (Metal Enhanced DAB Substrate Kit, Thermo Fisher, UK) for 15 minutes. Finally, sections were rinsed in running tap water, dehydrated through serial alcohols (70%, 90%, and 100%) and placed in xylene for 10 minutes then mounted with DPX.

11.3 Immunohistochemistry

Immunostaining was carried out according to standard protocols (Table 2-1). Frozen (12 μm) sections were removed from the freezer and allowed to air dry for 30 minutes. Slides were washed in PBS followed by a series of ethanol (70%, 90% and 100%) for dehydration then placed in xylene for 10 minutes. Sections were rehydrated through serial ethanol (100%, 90% and 70%) then rinsed in water. Antigen retrieval was performed using 10mM citric buffer (PH 6.0) at 100 ºC under pressure for 10 minutes then covered with proteinase K working solution for 10 minutes at room temperature. Sections were rinsed in PBS and incubated in blocking buffer (10% normal serum, 0.5% BSA) for 1 hour at room temperature. Subsequently, sections were incubated in primary antibody solution (amyloid 6E10, 1:1000, Covance, SIG-39320, mouse monoclonal antibody; COL4, 1:400, Fitzgerald, 70R-CR013X, rabbit polyclonal antibody) overnight at 4 ºC. Sections were then rinsed in PBS and incubated in secondary antibody (anti-rabbit Alexa Fluor 546, 1:500, Invitrogen A-11010; anti-mouse Alexa Fluor 488 1:500, Invitrogen A-11001) for 1 hour at room temperature.

Vibratome sections, generated for evaluation of glymphatic function, were rinsed in PBS and mounted onto superfrost plus slides (VWR international) followed by serial ethanol (70%, 90% and 100%) and then placed in xylene for 10 minutes. Sections were rehydrated through serial ethanol (100%, 90% and 70%) then rinsed in running water. Antigen retrieval was performed using 10mM citric buffer (PH 6.0) at 100 ºC under pressure for 10 minutes. Then sections were incubated in primary antibody solution (GFAP, 1:1000, Life technologies, 13-0300, Rat monoclonal antibody) overnight at 4 ºC. Sections were rinsed in PBS and incubated in non-fluorescent biotinylated secondary antibody (anti-rat, 1:100, Vector Laboratories, YO809) for 1 hour at room temperature followed by 1 hour incubation with Vector ABC Elite kit (Vector Laboratories). Finally, sections were visualised with the DAB peroxidase substrate kit (Vector Laboratories).

Table 2-1 Antibodies used for immunohistochemical and immunofluorescent staining.

Primary antibody	Target	Dilution	Retrieval	Supplier	Secondary antibody	Dilution	Supplier
6E10	Aβ	1:750	Citrate/ 95 °C	Covance SIG-39320	Biotinylated anti-mouse	1:100	Vector BA2000
Anti-COL4	Basement membrane	1:100	Citrate/ 95 °C	Millipore AB769	Anti-goat Alexa Fluor 546	1:500	Life-tech A11056
Anti-COL4	Basement membrane	1:400	Citrate/ 95 °C	Fizgerald, 70R-CR013X	Anti-rabbit Alexa Fluor 546	1:500	Invitrogen A-11010
Anti-GFAP	Astrocytes	1:1000	Citrate/ 95 °C	Life-tech 13-0300	Biotinylated anti-rat	1:100	Vector YO809
AQP4	Aquaporin 4 (AQP4)	1:200	Citrate/ 95 °C	Millipore AB3594	Anti-rabbit 405	1:100	Ab175651

12. Analysis of immunohistochemistry

Immunostained 12 µm frozen sections were analysed using a laser scanning confocal microscope (ZEISS LSM 710, Germany). Cortical amyloid load and blood vessel density were determined by the percentage of areas of positive 6E10 and COL4 staining, respectively. The vascular amyloid load was determined by the JACoP colocalization plugin by calculating the Mander's coefficient, and data were shown as % vascular amyloid. Images were taken in the cortex of Tg-SwDI mice. Regions of interest were defined on DAPI channel covering the pial surface to approximate the depth of 250 µm. Astrogliosis was assessed using 100 µm vibratome cut sections by measuring the percentage of stained area occupied

by GFAP positive staining, images were obtained using the method described above using a slide scanner using auto thresholding (triangle method). All measurements were carried out using ImageJ (v1.46, NIH, Bethesda, MD, USA).

13. Statistical analysis

Data were analysed using a two-way ANOVA with surgery and genotype as two between subject factors followed by Bonferroni's multiple comparison test to compare ASL measured CBF levels, neurovascular coupling, regional glymphatic function, astrogliosis, and Barnes maze probe tests. Statistical comparison of cortical CBF, spatial learning, global glymphatic influx were carried out by repeated measures ANOVA with surgery and genotype as between subject factors followed by Bonferroni's multiple comparison test. One sample t-test was used to compare the performance of each group with the chance in the Barnes maze probe tests. Mann-Whitney U test was used to compare the amyloid burden and blood vessel density. Difference in proportions test was performed to compare vascular related lesions. Statistical analysis was performed using IBM SPSS Statistics 22. Unless otherwise stated, data are presented as mean ± standard error, $p<0.05$ is considered to be statistically significant.

Chapter 3. Effect of bilateral common carotid artery stenosis and amyloid on cerebral blood perfusion and glymphatic function and link to cognitive impairment

1. Introduction

Cerebral vascular disease (CVD) is a significant factor contributing to cognitive impairment and dementia, such as Alzheimer's disease (AD) (Gorelick et al., 2011). Extensive well-characterised cohort studies have highlighted the co-existence of vascular disease with AD (Esiri et al., 1999, Snowdon et al., 1997, Hachinski and Munoz, 1997, De Jong et al., 1997, de la Torre, 2000b, de la Torre, 2000a, de la Torre, 2000c). Key neuroimaging features (white matter lesions, microbleeds, lacunes and enlarged perivascular spaces) are found in both AD and CVD, and they share several vascular risk factors, such as hypertension, diabetes and atherosclerosis (Dichgans and Leys, 2017). Vascular risk factors in midlife are also associated with an increased burden of Alzheimer-related pathologies, such as amyloid protein, in the human brain suggesting a direct relationship (Gottesman et al., 2017).

Global reductions in cerebral blood flow are associated with increased risk of progression from mild cognitive impairment to dementia suggestive that perfusion plays a crucial role in disease progression (Alsop et al., 2010, Chao et al., 2010). Reduced cerebral perfusion has been linked to white matter attenuation, a key feature common to both AD and dementia associated with CVD (Barker et al., 2014, Schuff et al., 2009). Common artery stenosis of varying degrees is invariably associated with cognitive impairment (Johnston et al., 2004b, Cheng et al., 2012, Balestrini et al., 2013, Alosco et al., 2013) and carotid stenosis (>25%) has been linked to a greater burden of white matter hyperintensities (Romero et al., 2009). Large and small vessel disease is also linked to Alzheimer's disease dementia (Arvanitakis et al., 2016). Reduced cerebral perfusion, impaired cerebrovascular reactivity and haemodynamic responses are increasingly recognised in the early stages of AD (Hughes et al., 2014, de la Torre, 2012b). Our work and others using animal models have shown that

chronic cerebral hypoperfusion as a result of bilateral carotid stenosis leads to cognitive decline through mechanisms that involve hypoxia-induced white matter damage and gradual deterioration of the neuro-glial-vascular unit including endothelial dysfunction, microvascular inflammation and BBB leakage (Shibata et al., 2004, Holland et al., 2015, Fowler et al., 2017, Kitamura et al., 2017, Roberts et al., 2018). Although there is substantive evidence reduced blood flow contributes to vascular disease, a causal relationship remains a matter of controversy; primarily due to the cross-sectional nature of clinical studies and, in the few longitudinal studies conducted, reduced blood flow occurs after vascular disease burden (de la Torre, 2012a). Emerging data have highlighted alternative mechanisms that may also contribute to disease progression, and in particular, the impaired glymphatic function is emerging as a critical player in AD and VaD. The glymphatic pathway is a brain-wide clearance process that relies on the movement of CSF via the perivascular network facilitated by aquaporin-4 water channels on the astroglial endfeet to promote the elimination of waste out of the brain (Iliff et al., 2012). CSF flow within the perivascular space is regulated by cerebrovascular pulsatility, which is now considered to be a key factor regulating glymphatic function (Iliff et al., 2013b, Mestre et al., 2018b). Enlarged perivascular space (PVS) is a common feature of CVD and dementia linked to vascular risk factors and inflammation (Potter et al., 2015a, Ding et al., 2017, Wardlaw et al., 2013, Doubal et al., 2010, Aribisala et al., 2014b, Shi and Wardlaw, 2016). There is also evidence of impaired glymphatic function in pre-clinical models relevant to CVD. Notably advanced age, acute ischaemic stroke and multi-infarct stroke, diabetes and subarachnoid haemorrhage (SAH) have all been shown to have a significant impact on drainage function (Kress et al., 2014, Gaberel et al., 2014, Wang et al., 2017). Disturbances of the glymphatic function are also related to a build-up of amyloid, Aβ protein, in both human and rodent brain (Xu et al., 2015, Shokri-Kojori et al., 2018).

The first studies in the thesis sought to examine the effect of bilateral carotid stenosis (BCAS) and microvascular amyloid on the extent of cerebral perfusion deficits and cognitive

impairment. A well-characterised murine model of BCAS was used that has been studied extensively within our group and others (Medina and Avila, 2014, Shibata et al., 2004). Further, in light of the evidence that flow-limiting large-vessel stenosis contributes to vascular and AD pathophysiology (Gupta and Iadecola, 2015), and that impaired glymphatic function is a pivotal contributor to impaired Aβ clearance. The glymphatic function was then investigated in the BCAS model and Tg-SwDI mice.

2. Hypothesis

In the present study, it was hypothesised that bilateral common carotid stenosis (BCAS) and microvascular amyloid lead to cognitive impairment via cerebral perfusion deficits and impaired glymphatic drainage function.

3. Study aims

This study aimed to assess alterations in cerebral perfusion as primary outcome of interest and second to this to determine if glymphatic function was altered following BCAS. Cognitive impairment and interactions with microvascular amyloid were also determined by studying BCAS in Tg-SwDI mice.

4. Materials and Methods

4.1 Animals

Male heterozygous Tg-SwDI and wild-type mice were subjected to BCAS or sham surgeries. Mice were group caged in standard cages with bedding, food, water and nestle under 12 h dark/light cycles. The Tg-SwDI mice are primarily designed to study the microvascular accumulation of amyloid. The Tg-SwDI expresses human neuronal amyloid precursor protein (APP), containing the transgenic Swedish K670N/M671L, Dutch (E693Q), and Iowa (D694N) mutations under the control of Thy1 promoter (Davis et al., 2004). At the outset, a cohort of mice (n=42) (Tg-SwDI and wild-type littermates at 7-9 months old of age) were

recruited in experiments for the investigation of CBF including laser speckle contrast imaging and MR ASL, and behavioural tests (cohort 1). The second cohort of mice (total number=33, Tg-SwDI mice at 5-7 months and imported wild-type C57Bl/6J at 4-5 months old of age) were prepared for the investigation of glymphatic function (cohort 2). Mice were randomly assigned to experimental groups for all studies. In cohort 1, 1 mouse in Tg-SwDI BCAS was culled due to the severe bleeding during the surgery. 4 mice in Tg-SwDI and 2 mice in WT groups were culled due to the poor recovery following BCAS surgery. Therefore, these mice were excluded from the study. Final group size for cohort 1: n=8 WT sham, n=10 WT BCAS, n=6 Tg-SwDI sham, n=10 Tg-SwDI BCAS. In cohort 2, n=10 WT sham, n=8 WT BCAS, n=7 Tg-SwDI sham, n=8 Tg-SwDI BCAS. A summary of mice used in experiments has been described in Figure 3-1.

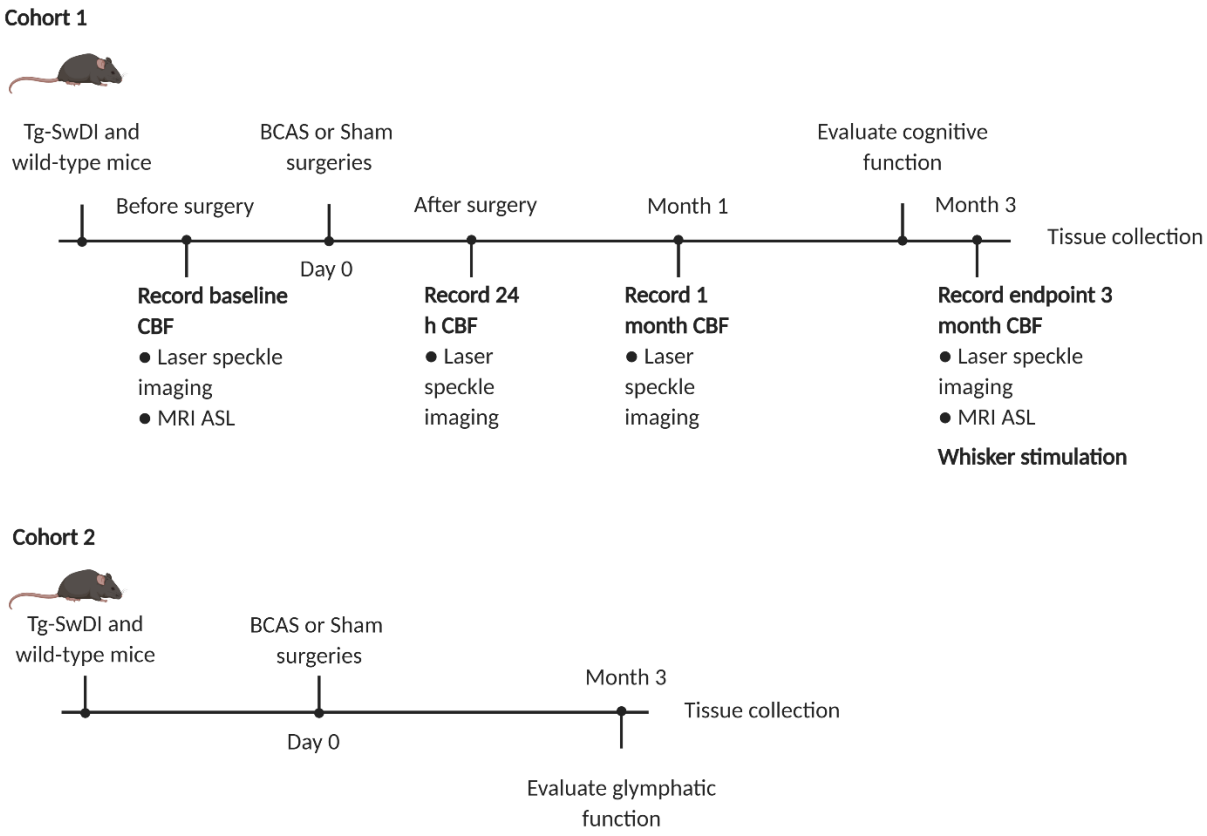

Figure 3-1 Summary of animals used in experiments.

A brief summary demonstrates that mice from cohort 1 were used in experiments including laser speckle imaging, MRI ASL, behavioural tests and whisker stimulation, as well as cohort 2 aimed to investigate the glymphatic function. Both cohorts underwent a period of 3 months following BCAS or sham surgeries.

4.2 Bilateral common carotid stenosis (BCAS) surgery

BCAS surgery was performed under isoflurane anaesthesia by applying microcoils (0.18mm internal diameter, Sawane Spring Co, Shizuoka, Japan) permanently to both common carotid arteries. Details of surgical methods have been described in previous studies (Shibata et al., 2004, Coltman et al., 2011, Reimer et al., 2011a, Holland et al., 2011b). A 30 minute interval was given between the application of the two microcoils to minimise the acute CBF changes caused by the placement of microcoils. Sham-operated animals underwent the identical procedure except for the application of microcoils to both arteries.

4.3 *In vivo* laser speckle contrast imaging

Laser speckle contrast imaging was used for measuring *in vivo* cortical blood flow using a method reported previously (McQueen et al., 2014). Mice were anaesthetised with Isoflurane in oxygen-enriched air, and an incision was made along the midline to expose the skull then properly covered with gel to keep the surface moisturised. Cortical CBF data was recorded at baseline (before surgery), 24h, 1 month and 3 months following BCAS and sham surgeries and then the surgical incision was sutured, and mice were fully recovered in an incubator at the end of each imaging session except the endpoint experiment at 3 months post-surgery. Raw images from laser speckle imaging were analysed using moorFLPI2 Review software (v4.0). Two uniformed squares were drawn on barrel cortex on both left and right hemisphere and made to avoid any artefacts on the skull. Regions of interest were consistent over time and between each mouse. Data were presented in perfusion units (PU) and calculated as the percentage change to baseline blood flow.

4.4 CBF measured by MR arterial spin labelling (ASL)

A 7.0T Agilen (Varian) preclinical MRI system was used to collect T1-weighted and arterial spin labelling (ASL) data, as described in Section Chapter 2. The T1-weighted images were acquired at 1.7 mm posterior to Bregma in stereotactic coordinates of Mouse Brain Atlas (Paxinos and Franklin, 2001). Resting CBF was measured using ASL at the level corresponding to T1-weighted scans with a Look-Locker FAIR single gradient echo (LLFAIRGE) sequence (Kober et al., 2008). Maps of CBF were constructed from ASL data in Matlab using in-house scripts. CBF maps were analysed in ImageJ (v1.46, NIH, Bethesda, MD, USA) using unbiased regions of interest from T1-weighted images acquired with the ASL sequence.

4.5 Assessment of spatial learning and memory using Barnes maze

The Barnes Maze was used to determine the differences in spatial learning and memory at 3 months after BCAS or sham surgery. The maze is comprised of one white circular platform and 20 circular holes around the outside edge of the platform, and an escape chamber was attached to one of the holes allocated to each experimental animal. Visual cues were specially designed and placed on the curtains and walls around the maze. All the tests were recorded using a camera connected with a tracking software ANY-maze v 4.99 (San Diego, California). The detailed information for the setting and testing schedule can be found in the general materials and methods section Chapter 2.

4.6 Assessment of glymphatic function by intracisternal injection of CSF tracers

Mice were anaesthetised with isoflurane and maintained with 1.5% isoflurane in oxygen enriched airflow. The respiration was regulated using a ventilator. The posterior atlantooccipital membrane was surgically exposed as described in Chapter 2, D-3 (green) and OA-45 (red) tracers were mixed at 1:1 ratio and infused at a concentration of 5 µg/µl, at a rate of 0.5 µl/min over 20 minutes through a syringe pump (Harvard Apparatus). The needle was held in place for 10 minutes after the completion of the injection, then removed, and the atlantooccipital membrane was sealed to avoid any reflux of CSF. For fast observation of CSF glymphatic entry, 1% Evans blue dye in PBS was injected into cisterna magna using the same methods described above.

4.7 Tissue processing

At the end of the experiments, mice from both cohort 1 and 2 were transcardially perfused with 30 ml PBS then whole brains were fixed in 4% paraformaldehyde in PBS for 24 hours. For cohort 1, brain tissues were further transferred into 30% sucrose solution in PBS for 72 hours. Brains were placed in precool isopentane -42 ºC for 5 minutes then stored in -80 ºC

freezer, and coronal sections (12 µm) were cut using a cryostat. For cohort 2, the brains were sectioned into coronal planes (100 µm) on a vibratome then stored in the cryoprotective medium in -20 ºC freezer.

Tracer movement from the subarachnoid space into the brain was imaged using a slide scanner (ZEISS Axio Scan.Z1). Multi-channel whole-slice images of each animal at hippocampal level (-1.82 mm to bregma) were generated at 20x magnification. This included separate DAPI, Alexa Fluor 488 and Alexa Fluor 594 channels. All images were scanned using constant exposure time for each channel by the slide scanner. For the quantification of tracer movement into the brain, scanned images were analysed in ImageJ software (v1.46, NIH, Bethesda, MD, USA) as described previously (Iliff et al., 2012). Region of interest (ROI) was defined using the DAPI channel to identify anatomical regions. Auto-thresholding (triangle method) was used to measure the % area of positive signal that is the glymphatic CSF influx.

4.8 Immunohistochemistry

To visualise the spatial location of fluorescent CSF tracers, basement membrane (COL4) and astrocytic endfeet marker (AQP4) were stained following standard protocols introduced in the Methods section (Chapter 2). Images were obtained using a laser scanning confocal microscope (ZEISS LSM 710, Germany).

4.9 Statistical analysis

Details of statistical analysis were summarised in Chapter 2. CBF results from ASL, regional CSF tracer influx, Barnes maze probe tests, were analysed by two-way ANOVA followed by Bonferroni’s multiple comparison test. Cortical CBF from laser speckle imaging, Barnes maze spatial learning and global CSF tracer influx were carried out by repeated measures ANOVA followed by Bonferroni's multiple comparisons. One sample t-test was used to compare the performance of each group with the chance. Statistical analysis was performed using IBM SPSS Statistics 22.

5. Results

5.1 CBF reductions at 24 hours, 1 month and 3 months after the establishment of carotid stenosis

At the outset of the studies, a key aim was to define the extent of CBF reductions post-BCAS and determine if there were differences between WT and Tg-SwDI mice. Laser speckle contrast imaging was used to investigate the effect of BCAS on cortical blood flow in WT and Tg-SwDI mice. Cortical CBF was recorded at baseline (CBF data collected at 24 hours before surgeries), 24 hours, 1 month and 3 months post-surgery, respectively (Figure 3-2). Data was quantified as percentage changes from baseline blood flow at each point post-surgery.

CBF was reduced post-BCAS and there was a significant effect of time ($F_{(2.4, 128.4)}$ =45.9, $p<0.001$) and BCAS surgery ($F_{(1, 53)}$ =180.1, $p<0.001$). However, there was no significant effect of genotype (Aβ) ($F_{(1, 53)}$ =0.001, $p>0.05$) (Figure 3-3). A significant interaction between time and surgery ($F_{(2.4, 128.4)}$ =47.3, $p<0.001$) was observed. Post-hoc tests showed significant reductions of CBF in both WT and Tg-SwDI mice when compared to their sham counterparts following hypoperfusion surgery at 24 hours ($p<0.001$), 1 month ($p<0.001$) and 3 months ($p<0.001$), respectively. Thus, the study demonstrated that BCAS results in sustained CBF reductions, but there were no differences between WT and Tg-SwDI mice.

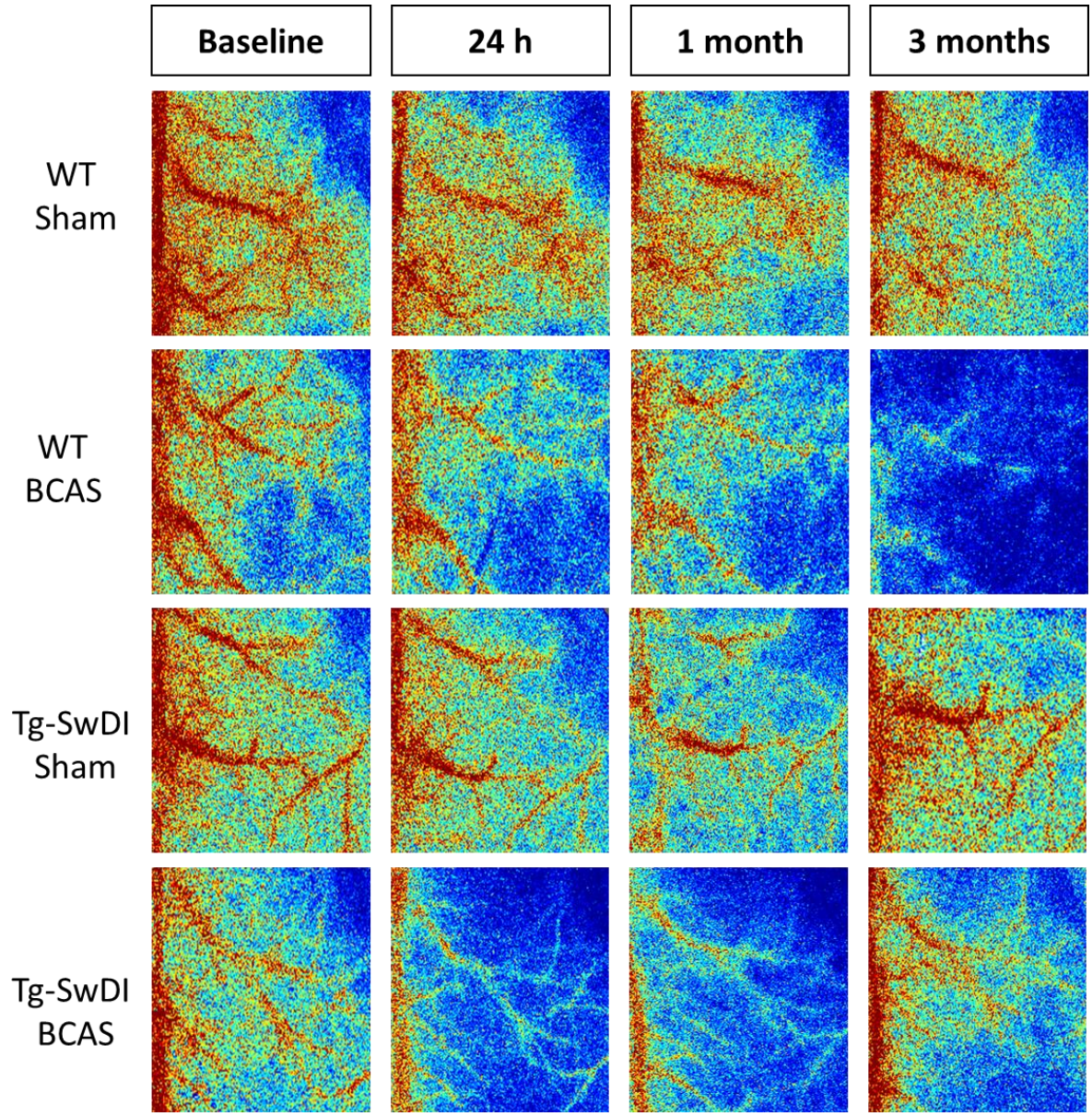

Figure 3-2 Representative images of cortical CBF measured by laser speckle imaging.

Laser speckle imaging was used to evaluate cortical CBF. Images taken at 24 hours before BCAS or sham surgeries were defined as baseline CBF, each animal was imaged at 24 hours, 1 month and 3 months after surgeries.

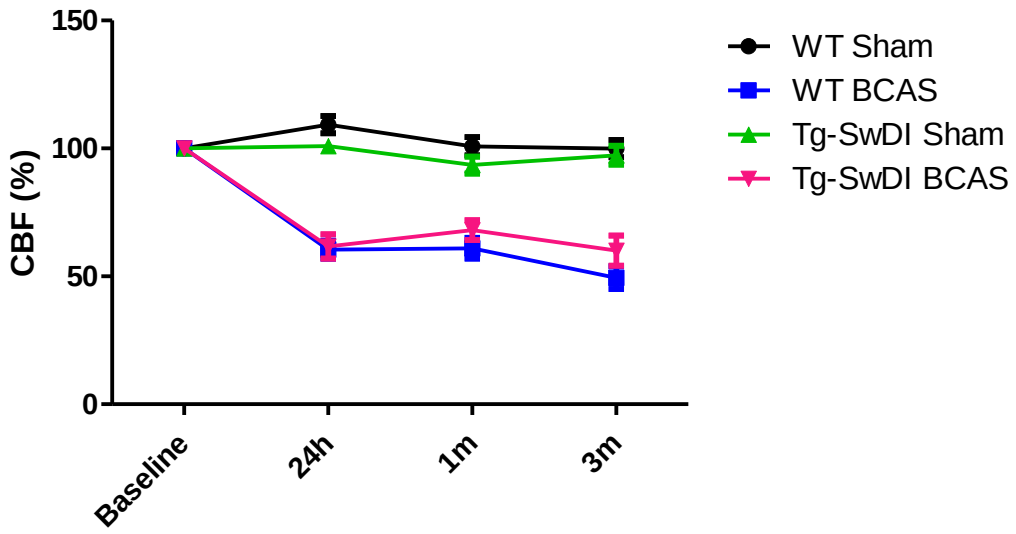

Figure 3-3 CBF reductions at 24h, 1 and 3 months following surgery.

Cortical CBF was assessed using laser speckle contrast imaging at baseline, 24 hours, 1 month and 3 months following BCAS surgery. BCAS surgery but not amyloid had a significant effect on CBF reduction. A significant interaction between time and surgery was observed. Post-hoc analysis showed significantly reduced CBF in both WT and Tg-SwDI mice when compared to their sham counterparts following hypoperfusion surgery at all three-time points after surgery: 24 hours, 1 month, and 3 months ($p<0.001$, respectively). Data presented as mean ± SEM.

5.2 Regional cerebral arterial perfusion is reduced post-BCAS in wild-type and Tg-SwDI mice

To verify the effect of BCAS surgery on the CBF and determine whether CBF was altered in deeper parts of the brain, the regional CBF was further assessed using MR arterial spin labelling (ASL). This advanced non-invasive technique was able to determine regional CBF changes throughout different brain regions. Previous studies have mainly used measures such as Laser Doppler flowmetry which only provide a measure of cortical CBF. The aim was to determine both the extent of reductions in regional CBF post-BCAS and whether this may differ between WT and Tg-SwDI mice impacting on the interpretation of further studies.

Regional alterations in CBF were measured in the dorsolateral cortex (DL CTX), hippocampus and hypothalamus.

Resting CBF (rCBF) at hippocampal level (Bregma -1.82mm) was collected at baseline and 3 months following BCAS or sham surgeries (Figure 3-4). In DL CTX, there was a significant main effect of surgery ($F_{(1, 26)} = 14.8$, $p<0.001$) but not genotype ($p>0.05$) and interaction ($p>0.05$) on rCBF (Figure 3-5A). Post-hoc analysis indicated that rCBF was significantly reduced in BCAS mice in both wild-type ($p=0.013$) and Tg-SwDI ($p=0.010$) groups. Furthermore, in the hippocampus CA1-DG molecular region, there was a main effect of surgery ($F_{(1, 26)} = 17.96$, $p<0.001$) but not genotype ($p>0.05$) and interaction ($p>0.05$) (Figure 3-5B). Post-hoc analysis showed significantly reduced CBF in BCAS mice from both wild-type ($p=0.022$) and Tg-SwDI ($p=0.002$) groups. Interestingly, in the basal hypothalamus region, BCAS did not lead to significantly reduced blood perfusion ($p>0.05$) and similarly there was no significant main effect of genotype ($p>0.05$) (Figure 3-5C).

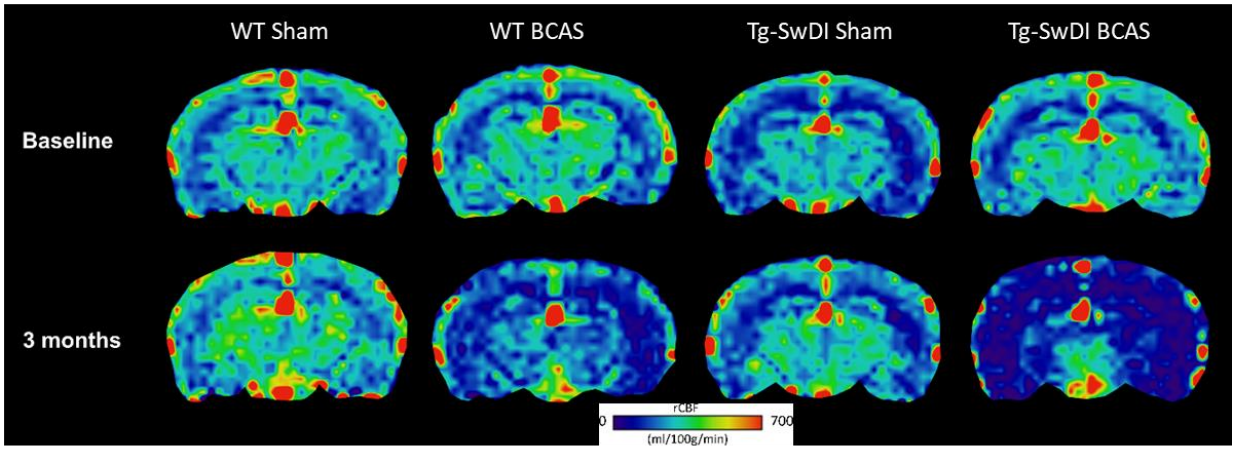

Figure 3-4 MR ASL imaging was used to measure rCBF at baseline and 3 months post-surgery.

MR ASL imaging was used to verify regional CBF levels. Representative images of baseline and 3 months from the WT or Tg-SwDI mice subjected to sham or BCAS surgeries have been collected at hippocampal level (Bregma -1.82mm). Three regions of interests including DL CTX, hippocampus and hypothalamus were selected to compare the effect of BCAS and amyloid on regional CBF.

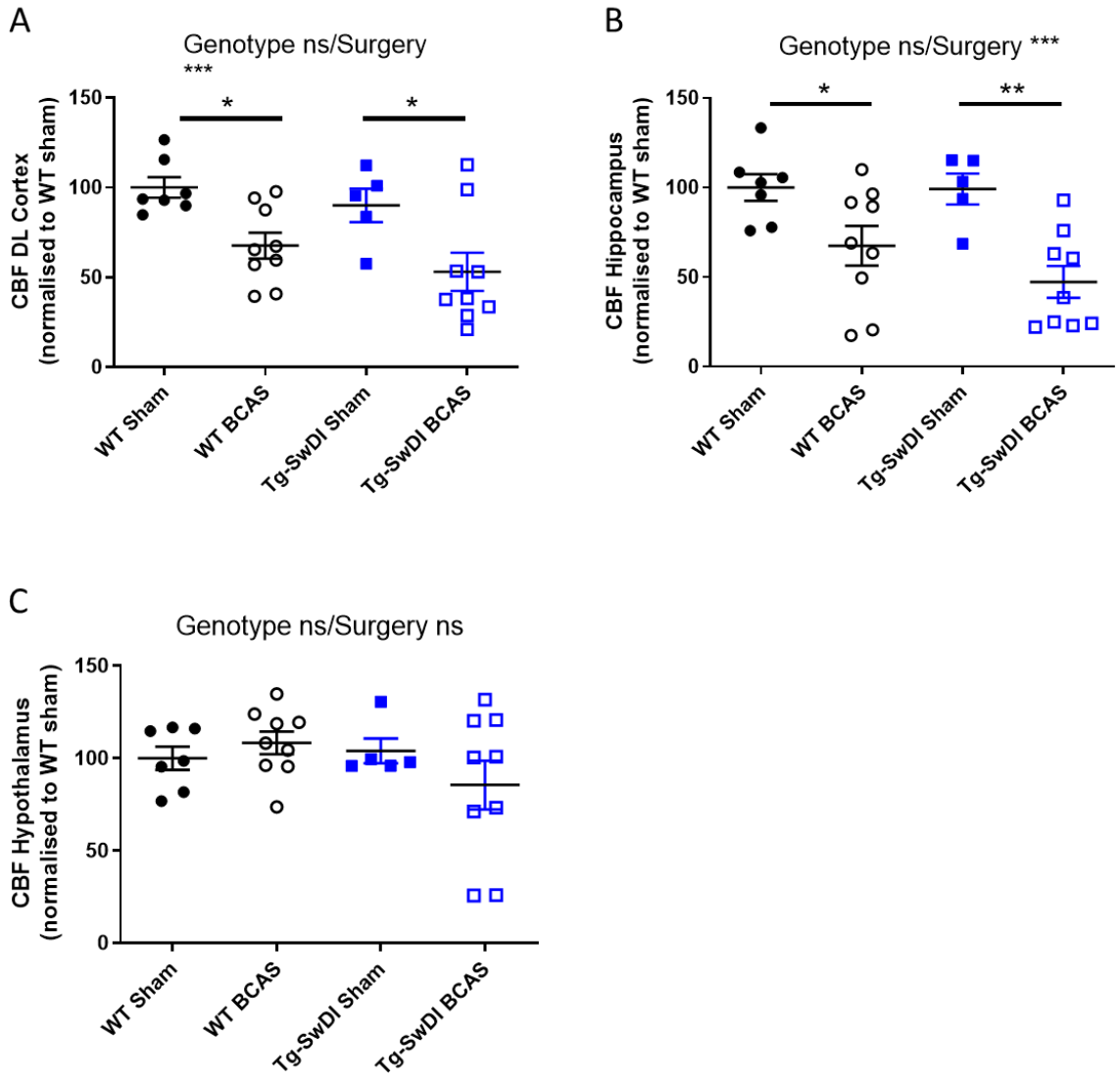

Figure 3-5 MR ASL imaging (7.0 T) shows decreased rCBF in the cerebral cortex, hippocampus and hypothalamus.

ASL measured the rCBF level in the dorsolateral cortex (DL CTX), hippocampus CA1-DG molecular region and hypothalamus. (A) The comparison of blood flow in the DL CTX. BCAS surgery but not genotype was found to have a significant effect on rCBF. Post-hoc analysis indicated that CBF was significantly reduced in BCAS mice in both wild-type and Tg-SwDI groups. (B) The comparison of rCBF between groups in the hippocampus. There was a main effect of surgery but not genotype and interaction. Post-hoc analysis showed significantly reduced blood flow in BCAS mice from both wild-type and Tg-SwDI groups. (C) In the hypothalamus region, there was no significant main effect of either BCAS surgery or genotype. Data are presented as mean ± SEM and analysed by two-way mixed ANOVA with post-hoc Bonferroni procedure; n=7 WT sham, n=9 WT BCAS, n=5 Tg-SwDI sham, n=9 Tg-SwDI BCAS.

5.3 Cognitive function was significantly impaired in BCAS mice at 3 months following surgery

In order to investigate whether long-term carotid stenosis has a further effect on cognitive function in our experimental animals, Barnes maze was performed to evaluate the visuo-spatial learning and memory at 3 months following surgery (Figure 3-6). Motor ability across groups was compared as a control measurement to determine whether the motor function was altered due to surgery (BCAS) or genotype (Aβ) effect.

There was a significant effect of genotype but not BCAS on the motor movement across groups ($F_{(1, 30)}$ =8.2, p<0.01) and time (Day) ($F_{(5,150)}$ =8.334, p<0.001) across groups (Figure 3-7A). Therefore, the measurement relying on motor ability cannot be used to compare the difference between different genotype groups. Escape latency was a velocity-dependent measure defined as the total time that mice spent to escape into the target chamber in each training test. This parameter was taken to evaluate the visuo-spatial learning of experimental animals. In WT groups (Figure 3-7B), there was a significant main effect of time ($F_{(5, 80)}$ =19.8, p<0.001) showing decreased escape latency with increasing training days, and surgery (F (1, 16) =4.6, p<0.05) showing BCAS mice spent more extended time than sham group to enter target chamber. In Tg-SwDI mice (Figure 3-7C), there was also a significant effect of time ($F_{(5, 70)}$ =13.9, p<0.001) showing decreased time to escape with increasing training days and surgery ($F_{(1, 14)}$ =5.4, p<0.05) showing BCAS mice spent significantly longer time to escape the maze than sham group. These results indicated that both BCAS and sham mice successfully learned the task with performance improving over time. Moreover, BCAS mice took significantly longer time to escape the maze in both WT, and transgenic mice, suggesting distinct impairment of visuo-spatial learning in mice following surgery regardless of genotype.

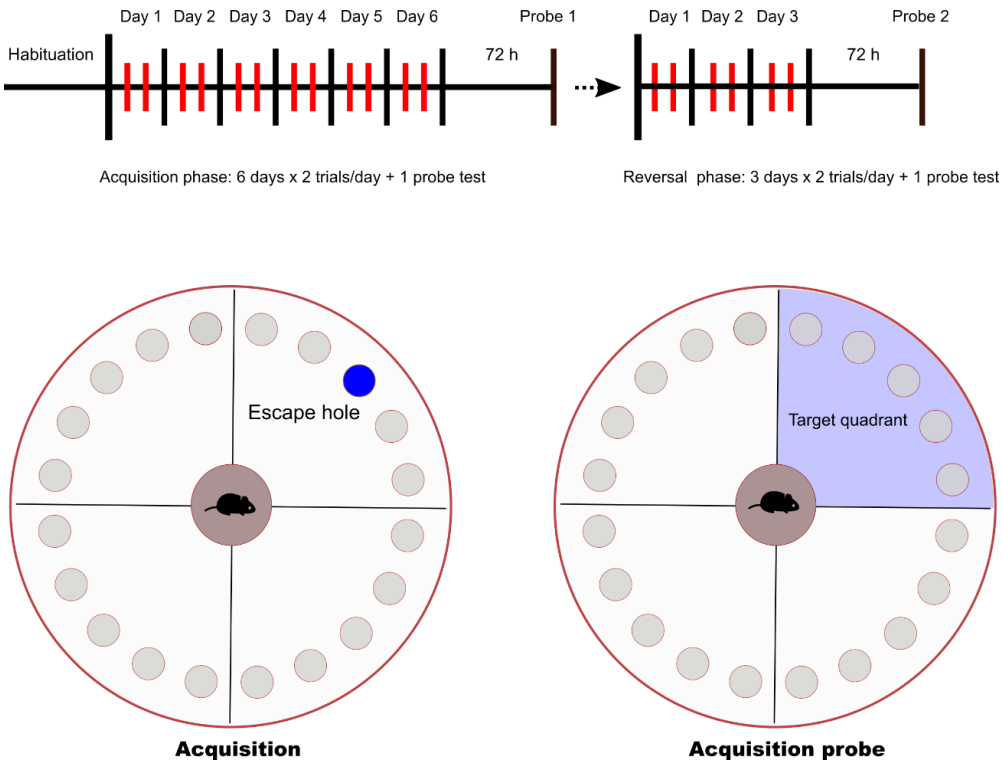

Figure 3-6 Barnes maze was performed to assess visuo-spatial learning and working memory.

Visuo-spatial learning and memory were assessed using Barnes maze consisting of training trials, 72 hours probe trial, reversal training and reversal 72 hours probe trials. Acquisition training sessions and probe trials were used to assess cognitive function. Test schedule was shown briefly to explain the 6 consecutive training days with 2 trials per day followed by a 72 h probe test (acquisition phase) and 3-day sessions of reversal tests followed by a 72 h probe test (reversal phase). Example images of escape hole and defined target quadrant are shown in diagram.

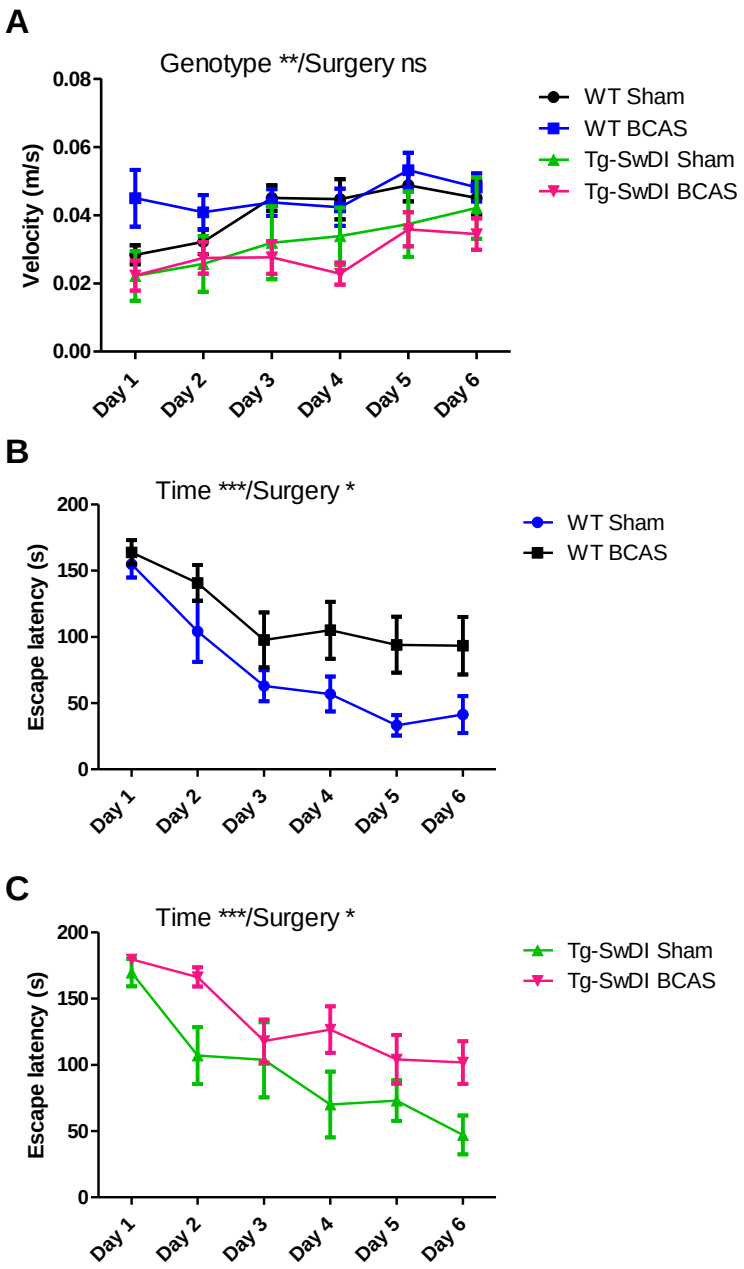

Figure 3-7 Visuo-spatial learning was significantly impaired at 3 months following BCAS surgery.

The velocity was taken as a control measure to assess whether the motor function was affected by the genotype or surgery across different groups. (A) A significant effect of amyloid ($p<0.01$) but not BCAS was found to influence the motor function across groups. (B) Escape latency in WT animals was measured to assess the visuo-spatial learning ability following 3 months Sham or BCAS surgery, a significant effect of time ($p<0.001$) showing a decreased latency to escape into target chamber with increasing training days, and BCAS surgery showing longer time for BCAS mice to escape the chamber. (C) Escape latency in Tg-SwDI mice showed a significant effect of time ($p<0.001$), showing decreased time to escape with increasing training days and surgery

*showing BCAS mice spent a significantly longer time to escape. *, **, *** and ns indicate p<0.05, 0.01, 0.001 and not significant, respectively. Data presented as mean ± SEM, n=8 WT sham, n=10 WT BCAS, n=6 Tg-SwDI sham, n=10 Tg-SwDI BCAS.*

To investigate the effect of chronic BCAS on long-term memory, a probe test was taken after 72 hours of the final training trial to examine whether experimental animals remembered the previous training target after removing the escape chamber. Data was quantified as percentage time spent in the target quadrant where the allocated chamber used to be. Results indicated that mice from WT sham (p=0.004), Tg-SwDI sham (p=0.021) and Tg-SwDI BCAS (p=0.025) all spent a significantly higher percentage of time than by chance (25%). Exclusively in WT BCAS mice, the percentage time spent in the target quadrant was significantly lower by 18.20 (95% CI, 2.97 to 39.37) than average by chance, t (9) =1.95, p=0.84 (Figure 3-8) There was no significant effect of surgery or genotype on the % time spent in the correct quadrant.

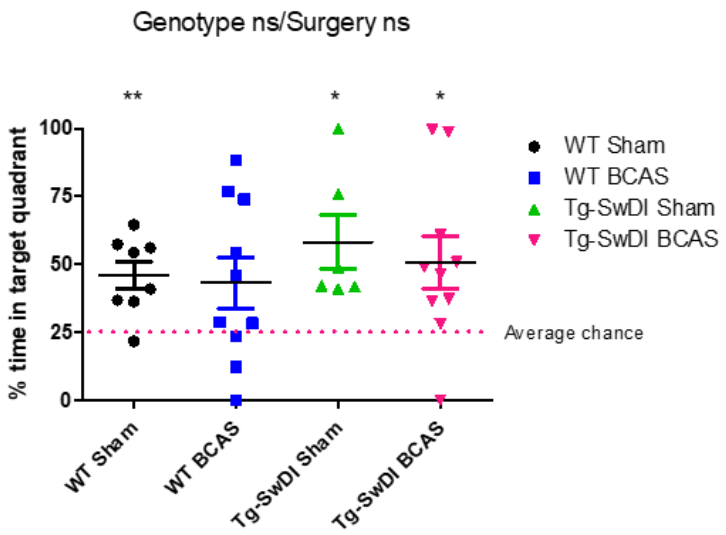

Figure 3-8 Long-term memory was not impaired in BCAS and the presence of amyloid.

*In the acquisition 72h probe test, all mice performed above chance (WT sham p=0.004, Tg-SwDI sham p=0.021 and Tg-SwDI BCAS p=0.025) except WT BCAS mice that did not spend significantly longer time than average by chance (p>0.05) (** indicates p<0.01, and * indicates p<0.05, one sample t-test compared to chance=25%). There was no significant effect of either genotype or surgery on the % time spent the correct quadrant (p>0.05, respectively) (Two-way ANOVA). n=8 WT sham, n=10 WT BCAS, n=6 Tg-SwDI sham, n=10 Tg-SwDI BCAS.*

5.3.1 Reversal test

To further enhance the detection of spatial learning and memory impairment, reversal trials were taken to evaluate the ability of experimental animals to learn a new location and testing the flexibility of executive function, escape hole location was switched 180° to the opposite side of maze (Figure 3-9). In the WT mice, there was a significant effect of time ($F_{(2, 32)} = 10.4$, $p<0.001$) showing decreased time to escape with increasing training trails but no significant effects of surgery ($p>0.05$) on escape latency were detected (Figure 3-10A). In Tg-SwDI mice, no significant effects of time ($p>0.05$) and surgery ($p>0.05$) were detectable in both sham and BCAS mice indicating transgenic mice failed to learn the new task and unsurprisingly no significant effects of time ($p>0.05$), and surgery ($p>0.05$) were observed (Figure 3-10B). These suggest WT mice subjected to BCAS surgery still learnt the enhanced task, but Tg-SwDI mice failed to learn the reversal task due to amyloid pathology.

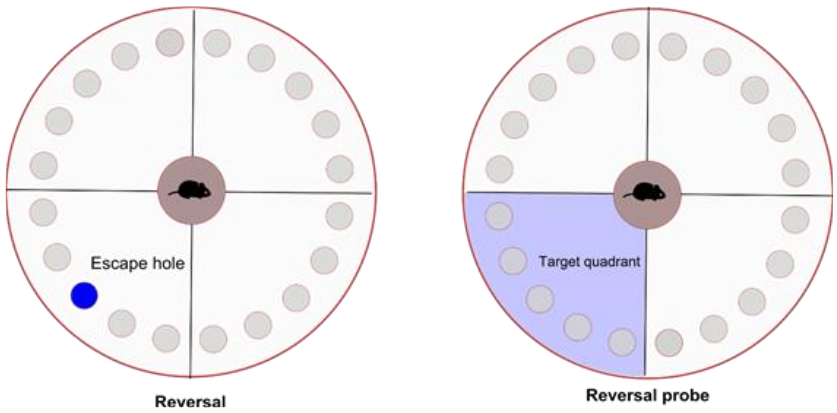

Figure 3-9 Reversal training trials and probe tests were performed to evaluate the cognitive function after enhancement of tests.

Reversal training and probe tests were performed to evaluate the cognitive function, representative images showing the mouse placed in the central area to begin a test and allocated escape hole and its corresponding target quadrant.

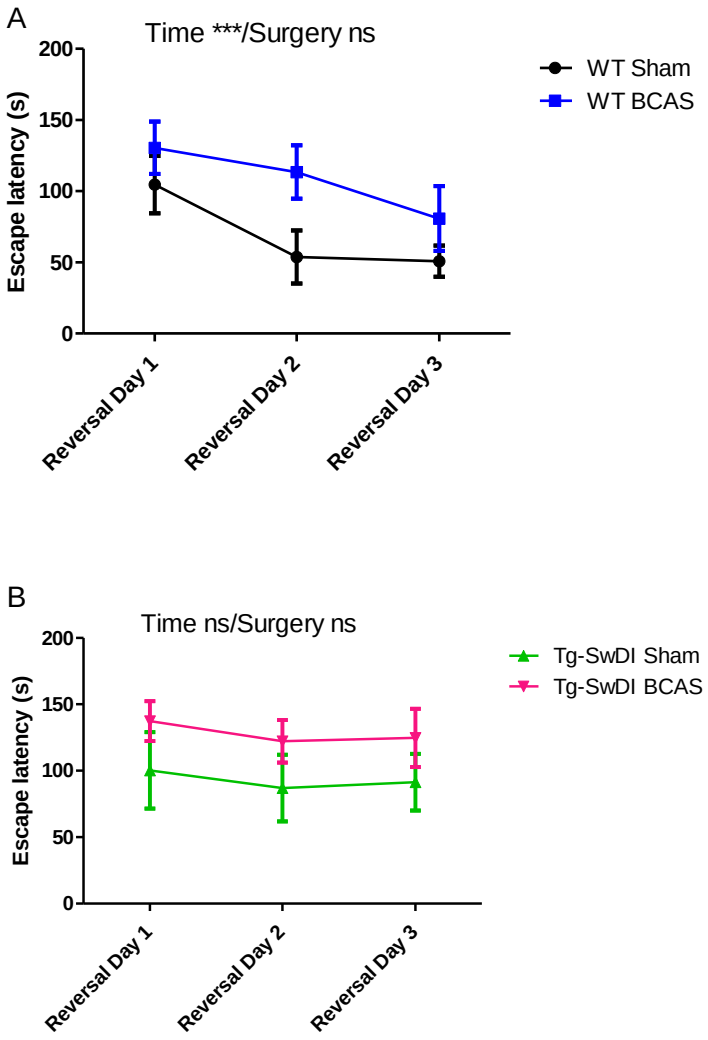

Figure 3-10 Tg-SwDI mice failed in spatial reversal learning.

*(A) In WT mice, a significant effect of time (p<0.001) shows decreased time to escape with increasing training trails but no significant effects of surgery on escape latency. (B) In Tg-SwDI mice, no significant effects of time and surgery were detectable in both sham and BCAS mice. *** and ns indicate p<0.001 and not significant, respectively. Data presented as mean ± SEM, n=8 WT sham, n=10 WT BCAS, n=6 Tg-SwDI sham, n=10 Tg-SwDI BCAS.*

The reversal probe test was performed following 72 hours of the final training trial (Figure 3-11). Results indicated only mice from WT sham (37.40 ± 12.63) ($p<0.05$) spent a significantly higher percentage of time by 12.40 (95%CI, 1.84 to 22.96) than by chance, $t(7)=2.8$, $p=0.027$ and a significantly higher percentage of time than Tg-SwDI BCAS mice ($p<0.05$) with all the other groups spending lower percentage of time than chance (WT

BCAS: 27.57 ± 11.12%, Tg-SwDI sham: 20.36 ± 15.50%, Tg-SwDI BCAS: 26.79 ± 16.79%) (Figure 3-11). There was no significant effect of surgery ($p>0.05$) or genotype ($p>0.05$) on % time spent in the correct quadrant (Figure 3-11).

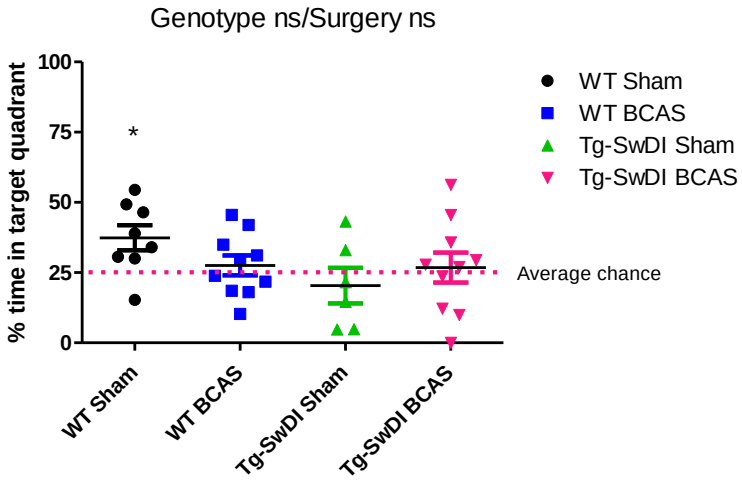

Figure 3-11 Long-term memory was impaired in both WT and Tg-SwDI BCAS as well as in the presence of amyloid.

*72 hours reversal probe test showed impaired long-term memory in BCAS and transgenic mice after enhanced detection of memory impairment. The reversal probe was performed following 72 hours of the final training trial. * and ns indicate $p<0.05$ and not significant, respectively. Data presented as mean ± SEM, n=8 WT sham, n=10 WT BCAS, n=6 Tg-SwDI sham, n=10 Tg-SwDI BCAS.*

5.4 Validation of CSF glymphatic influx/entry

Previously, our group has reported that BCAS altered Aβ peptide pools leading to increased Aβ accumulation in the cerebral vasculature (Salvadores et al., 2017). The current experiment aimed to interrogate whether the glymphatic function is modified following BCAS and whether amyloid interacts with BCAS leading to further changes on glymphatic pathway since this pathway has been proposed in relation to the progression of CAA (Iliff et al., 2012). To visualise glymphatic entry, Evans blue dye was used for *in vivo* injection into cisterna magna since this technique allows fast observation of the presence of CSF. Normal wild-type mice were injected then whole brain was carefully collected without perfusion to obtain an image of the CSF glymphatic entry on the surface of brain. Representative images

show the Evans blue dye distributed along the surface of brain vessels (e.g. Middle cerebral artery) (Figure 3-12A and B).

To understand the localisation of the CSF glymphatic influx, fluorescent tracers were further injected into the cisterna magna when mice were anaesthetised with isoflurane. The brain slices were immunostained with several markers to illustrate the spatial location of CSF tracer and other cellular components such as basement membrane and water channel AQP4. In the first place, the CSF glymphatic influx was imaged in *ex vivo* fixed brain slices, and collagen IV was stained as a marker of basement membranes. As shown in the representative images, the D-3 tracer was located in the perivascular domains that are perivascular space (PVS) (Figure 3-13A and C) or colocalised with the basement membrane marker COL4 (Figure 3-13B and D).

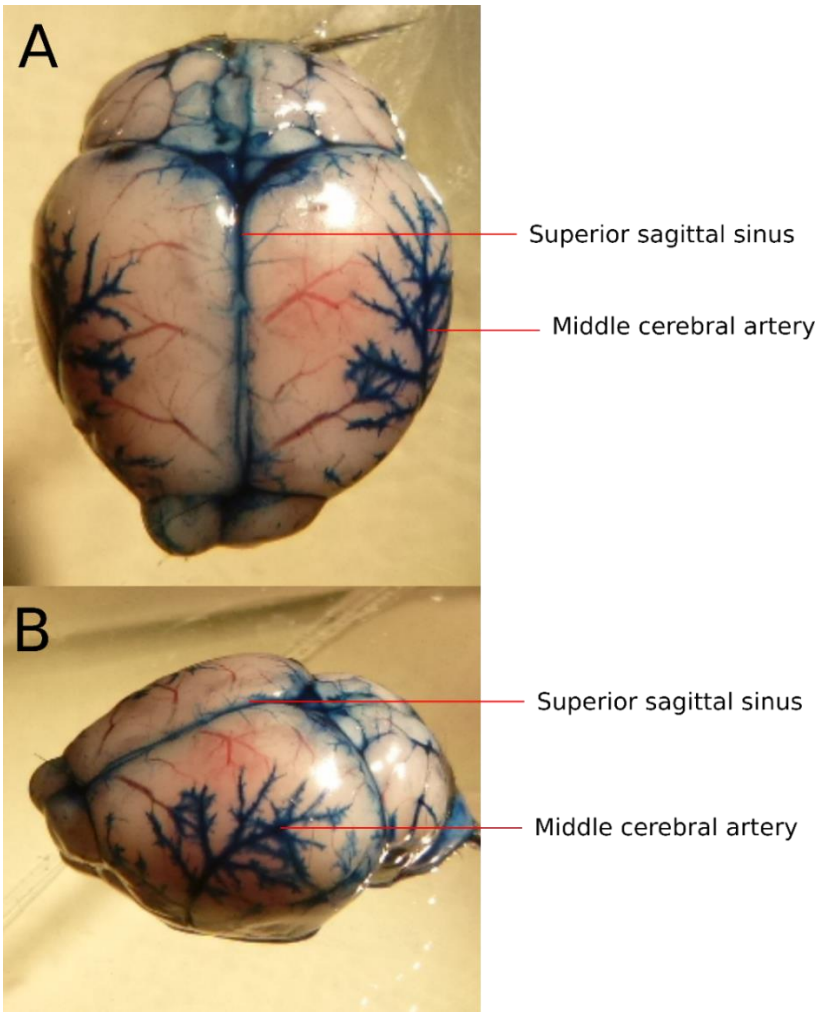

Figure 3-12 Evans blue dyes in CSF moved along perivascular domains in the middle cerebral artery (MCA) supplied cerebral cortex.

Evans blue dyes in aCSF were injected into cisterna magna of a normal mouse without transcardial perfusion. At the surface of the brain, dyes were found distributed along blood vessels, and the middle cerebral artery (MCA) and its branches, some of the dyes were also along the superior sagittal sinus, inferior cerebral vein, and transverse sinus.

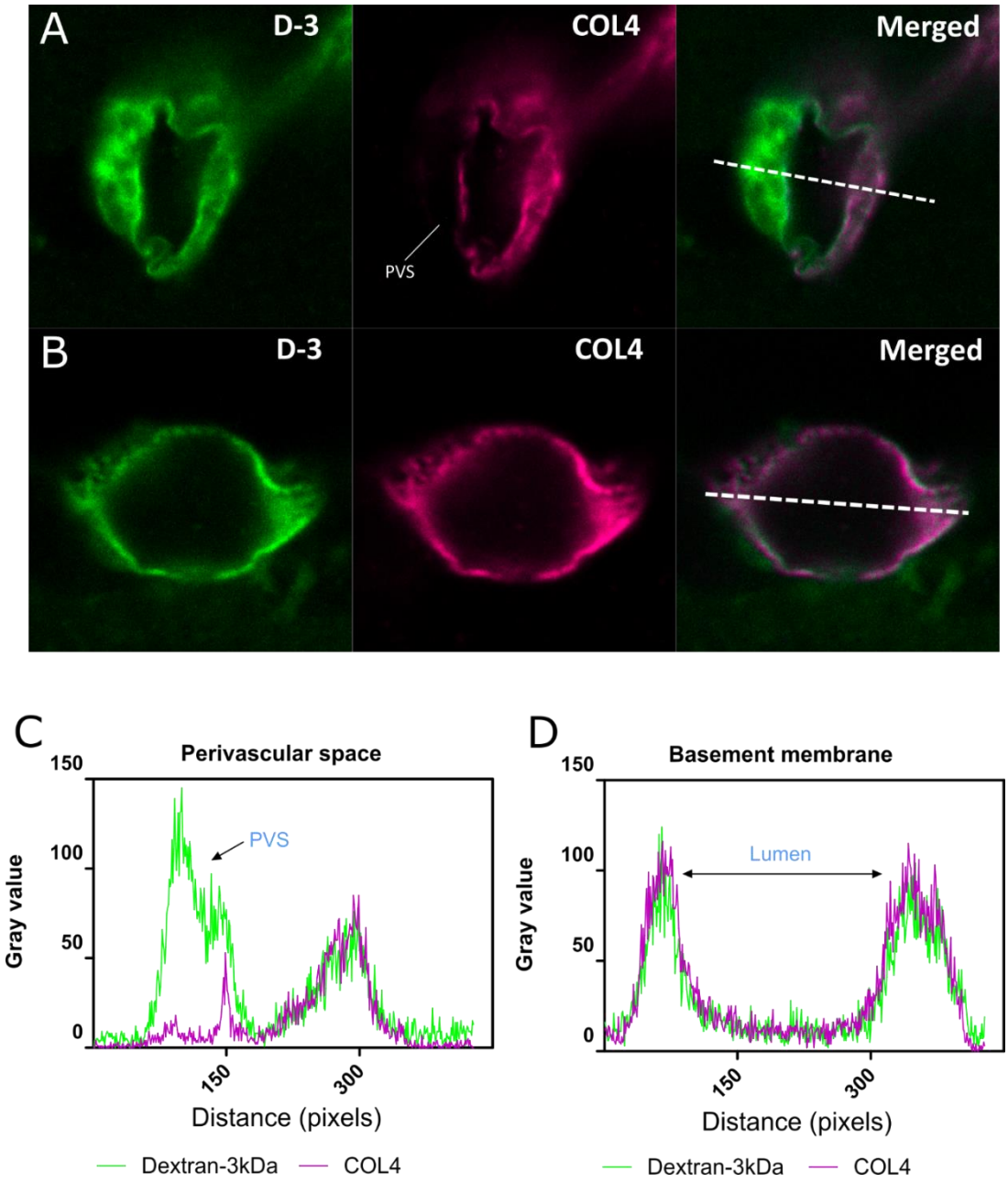

Figure 3-13 Representative images of CSF glymphatic influx in the cerebral cortex.

The immunostaining of vascular basement membrane marker COL4 (collagen 4, magenta) revealed the localisation of CSF fluorescent tracer (D-3, green) is inside the perivascular space (A and C) or colocalised with the basement membrane (B and D).

To determine the localisation between CSF tracers and astroglial compartment, I further investigated the CSF tracers and astrocytic endfeet marker AQP4. Representative images obtained after the immunostaining work of AQP4 with the CSF tracers at multiple areas of blood vessels are. In the representative images obtained at the penetrating artery level, the

D-3 tracer had a higher occupancy of the signal. By contrast the OA-45 tracer had very few glymphatic influx near the same penetrating artery (Figure 3-14A). In the images from the level of a superficial cortical blood vessel, both tracers were surrounded with the tissue expressing AQP4 (Figure 3-14B) showing a donut-shaped tunnel surrounding vasculature. The images obtained near the area between hippocampal CA3 and dorsal part of the lateral geniculate complex showed a consistent pattern of the CSF influx is along the vessel walls and wrapped with the tissue expressing AQP4 (Figure 3-14C).

In summary, the CSF glymphatic influx from our observation using the *ex vivo* imaging showed the localisation of CSF tracers, basement membrane and astroglial compartment. Thus, the following work aimed to address the initial questions regarding the BCAS, amyloid or their possible interactions on the glymphatic function.

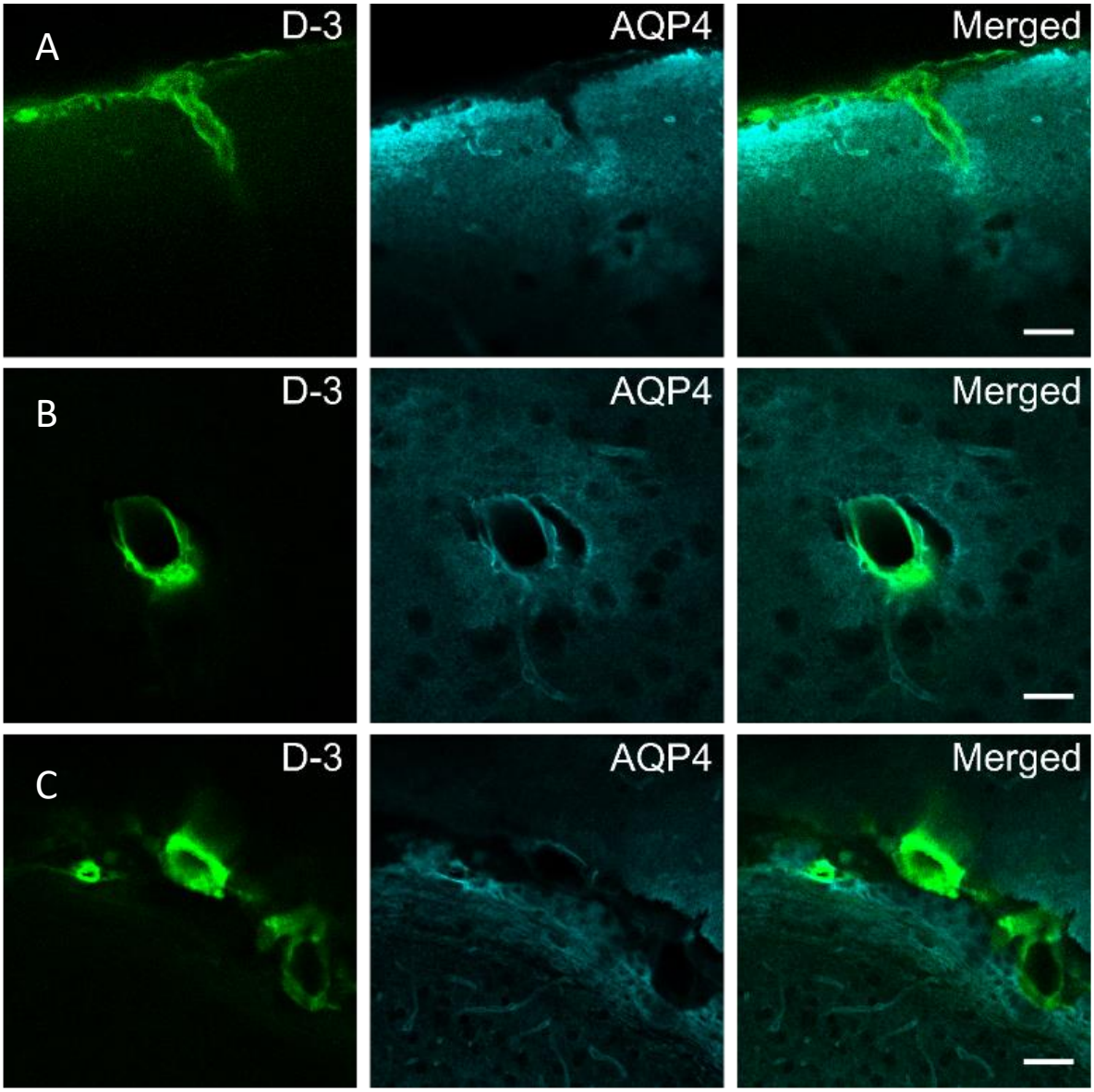

Figure 3-14 Representative images of CSF tracers in relation to astrocytic endfeet marker AQP4 and proposed glymphatic influx.

Representative images showing the spatial location of tracers D-3, fluorescein labelled 3 kDa soluble lysine fixable dextran (green). D-3 tracer is surrounded by the glial astrocytic endfeet expressing AQP4. (A) Surface artery penetrates cerebral cortex surrounded by AQP4 stained brain tissue; the D-3 tracer shows filling the space along the blood vessel at the surface of the brain. (B) Coronal image of a superficial blood vessel and spatial location with astrocytic endfeet. (C) Tracers and AQP4 immunostaining in the deep brain region at the area between hippocampus and thalamus. Scale bar= 50 µm.

5.5 The global influx of CSF tracers is different across the anatomical levels but unaltered post-BCAS in wild-type and Tg-SwDI mice

After verifying the cerebral blood perfusion changes after BCAS and localisation of the CSF glymphatic influx, the next aim was to examine whether BCAS affected the global glymphatic function. At the outset, global glymphatic tracer influx was evaluated in wild-type and Tg-SwDI mice and determined whether glymphatic influx was altered after BCAS. The global intensity of including Dextran-3 kDa (D-3) and Alexa Fluor Ovalbumin-45 kDa (OA-45) was measured in coronal sections sampled throughout the brain using a method previously described (Iliff et al., 2012) (Figure 3-15). In the first place, the total intensity of each group was measured. There was no significant effect of BCAS or amyloid when measuring D-3 and OA-45 occupancy at the whole brain level (surgery $p>0.05$, genotype $p>0.05$, respectively) (Figure 3-16A and B). Eight sequential levels of *ex vivo* brain sections from each animal were collected to evaluate the CSF tracer influx at 1.18, 0.74, 0.14, -0.34, -1.06, -1.82, -2.46 and -2.70 mm to bregma (Figure 3-15A). A significant effect of the anatomical level ($F_{(3.36, 90.71)} = 23.2$, $p<0.001$), and a trend of interaction between the anatomical level and BCAS ($F_{(3.36, 90.71)} = 2.4$, $p=0.068$) on the influx of the D-3 tracer were observed (Figure 3-16C). At the most rostral and caudal side of the brain, tracer influx was higher than other levels (Figure 3-16C). At the level of -1.06 mm to bregma, mean global tracer intensity (47.4 AU) was the lowest compared to other levels. However, there was no significant effect of genotype and surgery or interaction between these two factors ($p>0.05$). For the evaluation of OA-45 tracer influx, there was a significant effect of anatomical level ($F_{(4.21, 113.71)} = 20.3$, $p<0.001$) (Figure 3-16D). The highest intensity was observed at the most rostral and caudal levels similar to the D-3 tracer. There was no significant effect of surgery, genotype and interactions between these factors ($p>0.05$).

Overall, the brain-wide measurement of tracer influx indicated that glymphatic drainage was different across the various anatomical levels but unaffected by BCAS and in Tg-SwDI mice.

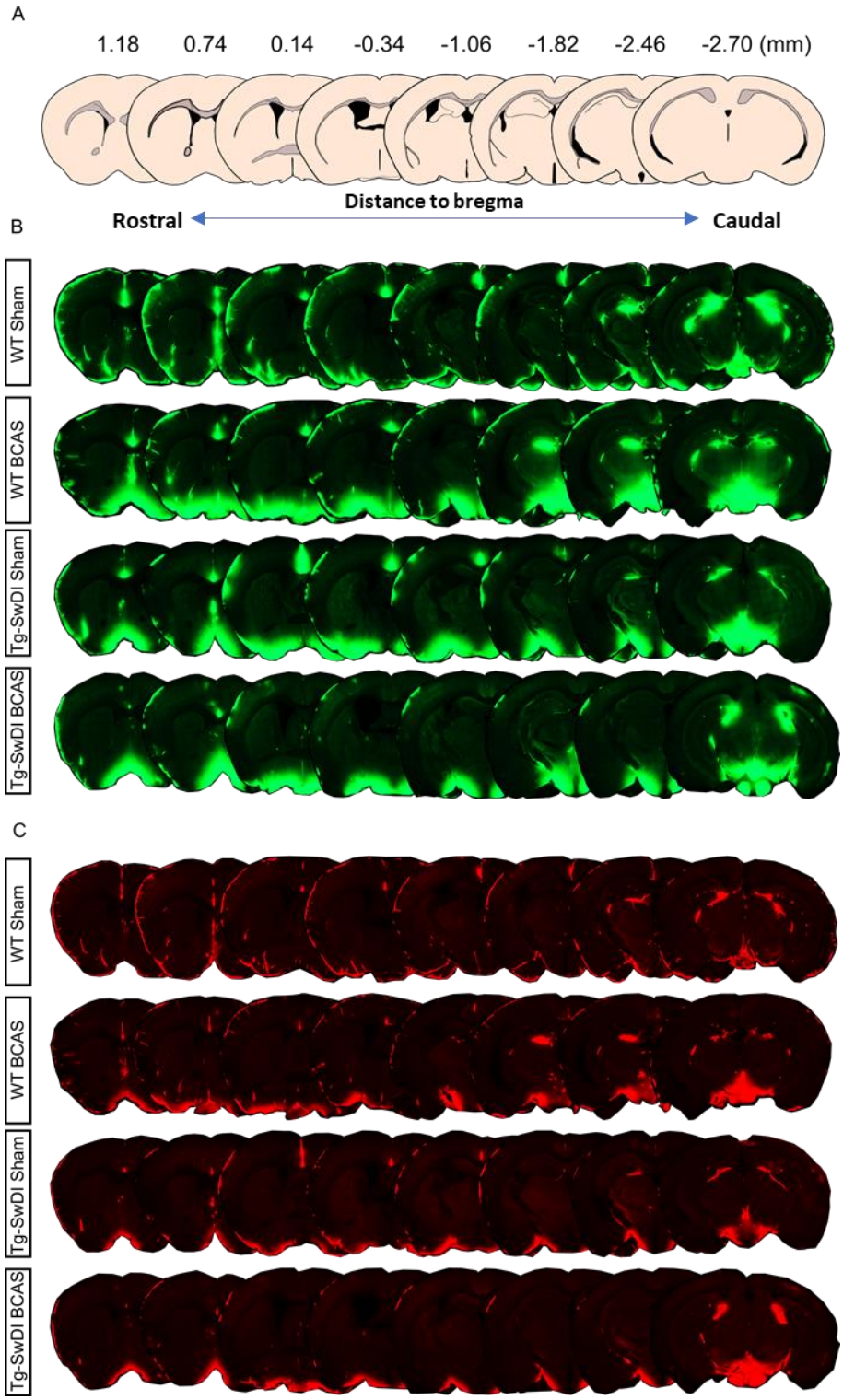

Figure 3-15 Representative images of global tracer influx in wild-type and Tg-SwDI mice and in response to BCAS.

(A) Schematic diagrams for 8 sequential levels (1.18, 0.74, 0.14, -0.34, -1.06, -1.82, -2.46 and -2.70 mm to bregma) of chosen. Representative images for whole-brain scanned fluorescent images: (B) fluorescein labelled 3 kDa soluble lysine fixable dextran D-3 (green) and (C) Alexa Fluor 594 ovalbumin conjugate OA-45 (Red).

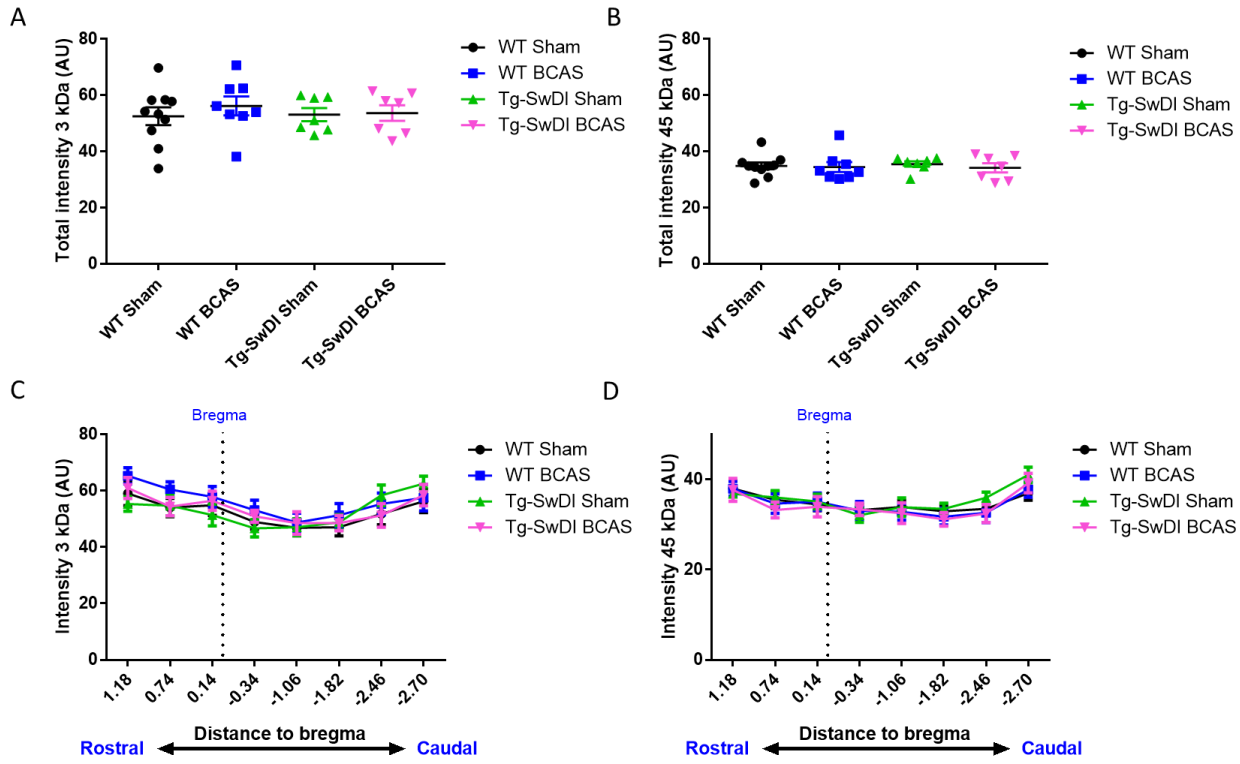

Figure 3-16 Global tracer influx in wild-type and Tg-SwDI mice and in response to chronic cerebral hypoperfusion.

(A and B) Total fluorescent intensity measures of whole-brain sections measuring D-3 (A) and OA-45 (B), respectively. (C and D) Fluorescent intensity measures of global brain sections at each level. Data are presented as mean ± SEM, n=10 WT sham, n=8 WT BCAS, n=7 Tg-SwDI sham, n=7 Tg-SwDI BCAS.

5.6 Regional CSF tracer influx is altered post-BCAS in wild-type and Tg-SwDI mice

To further investigate whether BCAS influences CSF glymphatic influx, *ex vivo* images of the CSF tracer influx in the dorsolateral cortex (DL CTX) and hippocampus (CA1-DG molecular layer) on the D-3 tracer were measured.

CSF glymphatic influx was first measured in the region of the dorsolateral cortex, which shows tracer distributed along the middle cerebral artery (MCA) and its branches (Figure 3-12 and Figure 3-17A and B). There was a significant main effect of BCAS on the

glymphatic influx that was reduced in the dorsolateral area of D-3 ($F_{(1, 27)}$ =4.8, p=0.037) (Figure 3-17B). There was no statistically significant interaction between genotype and BCAS surgery (p>0.05) or main effect of genotype (p=0.064). Post-hoc analysis showed a significant reduction in the WT BCAS compared to sham animals (p<0.05).

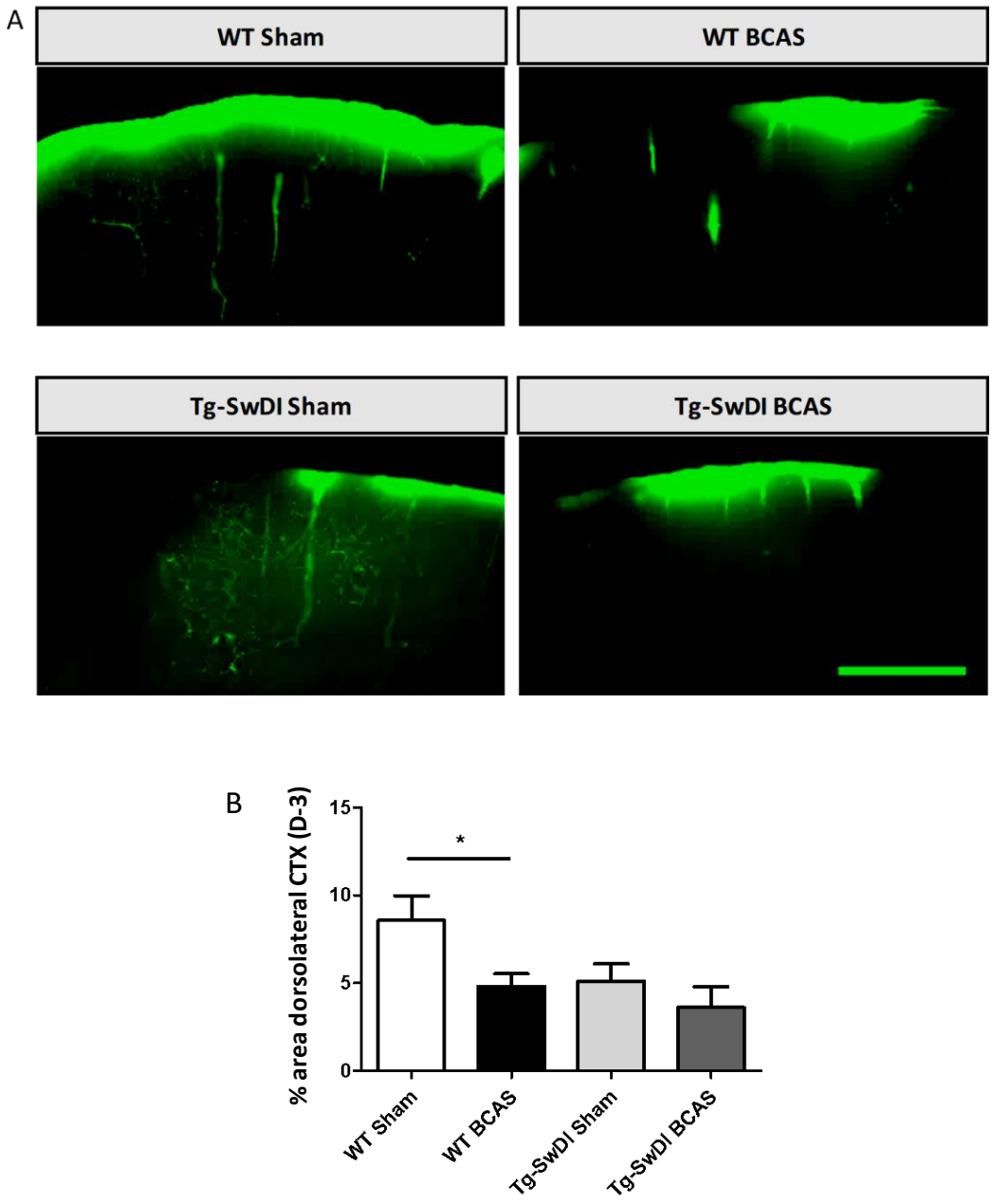

Figure 3-17 Assessment of glymphatic function in the cerebral cortex (dorsolateral cortex) showing altered CSF influx in the BCAS and Tg-SwDI mice.

*(A) Representative images of tracer influx in the dorsolateral cortex (DL CTX). (B) Ex vivo imaging of fluorescent density of the Dextran-3 kDa (D-3) tracer was measured at the hippocampal level. Data are presented as mean ± SEM, n=10 WT sham, n=8 WT BCAS, n=7 Tg-SwDI sham, n=7 Tg-SwDI BCAS, * indicates p<0.05. Scale bar=500 µm.*

The CSF tracer influx in the hippocampal subregion was further measured: CA1-DG molecular layer. A significant main effect of surgery ($F_{(1, 28)}$ =7.5, p=0.011), but no significant

interaction (p>0.05) or main effect of genotype (p>0.05) were found. Post-hoc tests showed a significant reduction between wild-type sham and BCAS mice (p=0.005) (Figure 3-18).

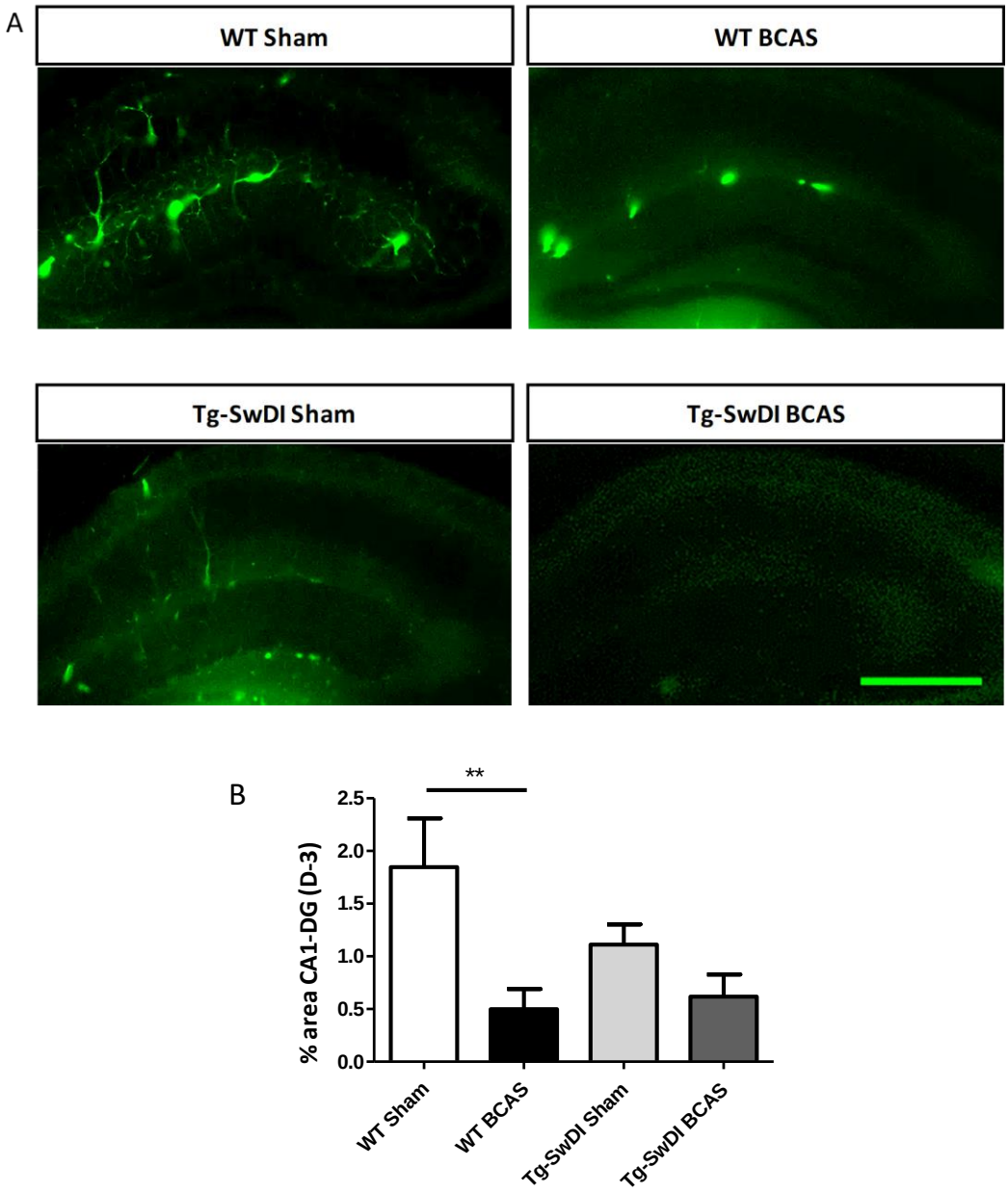

Figure 3-18 Assessment of glymphatic function in the cerebral cortex (dorsolateral cortex) showing altered CSF influx in the BCAS and Tg-SwDI mice.

*(A) Representative images of the glymphatic influx in the hippocampal CA1 dentate gyrus molecular layer (CA1-DG) and schematic image of the selected region of interests (ROIs) for the CA1-DG molecular regions. (B) Ex vivo imaging of fluorescent density of the Dextran-3 kDa (D-3) tracer was measured at the hippocampal level. Data are presented as mean ± SEM and n=10 WT sham, n=8 WT BCAS, n=7 Tg-SwDI sham, n=7 Tg-SwDI BCAS, ** indicates p<0.01. Scale bar=500 µm.*

6. Discussion

These first studies support the original hypothesis that BCAS causes cognitive impairment via reduced cerebral perfusion and impaired glymphatic function. However, contrary to the hypothesis, there was no exacerbation of these effects in Tg-SwDI mice. To begin with, the CBF was measured using laser speckle imaging and supported by MR ASL, to provide comprehensive information at multiple timescales and brain regions. In contrast to the hypothesis, the resting CBF (rCBF) in the cortex and hippocampus were found to be significantly reduced after BCAS, but there was no evidence that suggested amyloid alone could exacerbate this or interact with carotid stenosis. This finding is consistent within the cortical region measured by both laser speckle imaging and MR ASL. In the hypothalamus, there was no significant reduction in CBF either caused by BCAS or amyloid, which is contrary to my hypothesis. A slight increase of CBF after BCAS in the wild-type mice was observed suggesting that vascular remodelling might occur due to the long-term exposure to the insufficient blood supply. Barnes maze revealed significantly impaired visual-spatial learning and memory in mice following 3 months of BCAS. Amyloid did not exacerbate impaired learning and memory until in reversal tests that showed Tg-SwDI mice failed to learn the tests in the reversal trials and poorly performed in the reversal 72 hours probe suggesting impaired long-term memory by amyloid.

6.1 Bilateral common carotid artery stenosis (BCAS) showed sustained effects on cerebral perfusion with potential vascular remodelling

At the outset of the study, sustained reductions in cortical CBF was confirmed by laser speckle imaging at 24h, 1 and 3 months post-BCAS. This set of data added new information demonstrating the blood flow changes over a longer term of carotid stenosis. It is consistent with previous reports from our group and others that BCAS induced a reduction of CBF at approximate 30% at 1 month post-BCAS (Shibata et al., 2004, McQueen et al., 2014). Further, BCAS induced reductions in cortical CBF in both WT and Tg-SwDI mice, but

amyloid did not worsen the hypoperfusion effect at the 3 month time point (10-12 months old). This is not in agreement with another study using laser speckle imaging assessing younger wild-type and Tg-SwDI mice that indicated Aβ deposition was able to accelerate compromised blood perfusion following 3 months of BCAS (Okamoto et al., 2012).

In BCAS models and other models relevant to VCI, CBF has been predominantly assessed using Laser Doppler probes or Laser Doppler Flowmetry. Although this is useful to measure cortical CBF over extended periods, it lacks the spatial resolution of other imaging approaches. CBF can also be evaluated using MR arterial spin labelling (ASL), positron emission tomography (PET) and single photon emission computed tomography (SPECT). Among these methods, ASL is advantageous in assessing CBF due to its non-invasive feature that can be easily transferred to clinical applications. Also, the ability to measure regional alterations in CBF is relevant to VCI in which pathological alterations occur predominantly subcortically.

In the present study following 3 months of BCAS surgery, CBF assessed by MR ASL was found to be reduced to approximately 60% of baseline in wild-type mice and slightly lower in Tg-SwDI mice (50% of baseline) post-BCAS in both cortical and hippocampal regions post-BCAS. To date, there have been no studies that have assessed the longer-term effect of BCAS on rCBF using MR ASL imaging. Instead, a previous study by Hattori et al. (Hattori et al., 2016), using ASL in the BCAS model, demonstrated a substantial decrease of CBF at approximate 50% of the baseline between day 1 to 14 following BCAS, with gradual recovery to 70% of the baseline until 28 days of surgery. In the current study, the progression of CBF changes was not measured, and thus it is not clear if there was a similar recovery in CBF in the first few weeks. Instead I was only able to show CBF at 3 month post-BCAS. The studies above using laser speckle imaging to measure cortical CBF would suggest that CBF is partially restored up to 28 days post-BCAS, but then in the subsequent period this is further reduced. In contrast to the original hypothesis, rCBF was not further impaired in Tg-SwDI mice post-BCAS.

In addition, in the present study using ASL, it was also determined that in the hypothalamus, rCBF was not reduced post-BCAS in WT mice that showed similar values to sham mice although there was a modest reduction of CBF in Tg-SwDI mice post-BCAS. The hypothalamus receives CBF supplied via multiple arteries originating from internal carotid artery (e.g. middle cerebral artery and anterior cerebral artery), which contrasts to the hippocampus and cortex, which receive CBF via the middle cerebral artery or posterior cerebral artery, respectively (Xiong et al., 2017). Post-BCAS there may be compensation of blood flow to the hypothalamus from other parts of the circulation, e.g. collaterals, supporting the possibility of a vascular remodelling mechanism after the long-term exposure to insufficient blood supply from the narrowed carotid arteries. Notably this ability to compensate may be impaired in Tg-SwDI mice.

6.2 BCAS caused an impaired cognitive function

In the behavioural trials, evaluation of cognitive function revealed impaired visuo-spatial learning induced by BCAS surgery in both WT and Tg-SwDI mice. However, this was not further exacerbated in the presence of amyloid pathology. BCAS and amyloid did not result in impaired long-term spatial memory in acquisition phase. In the reversal test, increased challenge revealed no significant effect of BCAS on spatial learning, but Tg-SwDI mice failed to learn the task irrespective of BCAS potentially due to the presence of amyloid pathology.

Chronic cerebral hypoperfusion has been suggested to cause cognitive decline, such as impaired learning and memory and advance the risk of Alzheimer's disease and vascular dementia. In a recent study, (Holland et al., 2015) showed the following 6 months of hypoperfusion impaired spatial working memory in BCAS mice measured using radial arm maze. Moreover, impaired spatial reference learning and memory were identified in the water maze. Here a significant effect of hypoperfusion on escape latency between sham and BCAS mice was seen. In the probe trials, the sham group spent more time than by chance (>25%) in the correct quadrant, in contrast to BCAS mice that did not. The Barnes maze is a

similar behavioural test to water maze and radial arm maze but does not include a strong aversive stimulus or food deprivation as reinforcement. Therefore, the Barnes maze applied in the present study provided weak aversive stimulation, only aiming to increase the motivation of experimental mice and eliminate the stress-induced confounds. The present data coincide with the findings from (Holland et al., 2015) that BCAS results in impaired spatial learning and memory and also extend our knowledge of the effect induced by amyloid pathology. Also, my data documented behavioural deficits at 3 months post-BCAS, which occurs earlier than 6 months that is reported by (Holland et al., 2015), although amyloid pathology did not exacerbate cognitive decline induced by hypoperfusion. In another study, comprehensive behavioural tests were performed to evaluate cognitive function in mice after 5~6 months of BCAS and significantly impaired reference, and working memory was detected using Barnes maze and radial arm maze respectively (Nishio et al., 2010). Another earlier study demonstrated impaired working memory at 30 days following BCAS surgery which was attributable to damaged frontal-subcortical circuits (Shibata et al., 2007). In this shorter-term (30 days) study, there was no marked cortical or hippocampal alterations that might explain preferential damage to the working memory but not the reference memory. By contrast, in a longer-term study (5-6 months for the behavioural test; 8 months for histological assessment), pathological changes including hippocampal atrophy and cell deaths were documented in addition to white matter damage at 8 months after BCAS. These are correlated with both impaired working and reference memory (Nishio et al., 2010). My present behavioural and pathological results showed impaired spatial learning and long-term spatial memory following 3 months of BCAS, with vascular lesions documented mainly in the regions of the cortex, hippocampus, white matter, and thalamus. This present study fits in the intermediate time course of previous investigations, suggesting that the brain regions studied are involved in the progression of spatial learning and memory impairment.

6.3 Compromised glymphatic function after BCAS

The mechanistic link between BCAS and VCI has primarily been attributed to the post-BCAS cerebral perfusion deficits initiating hypoxia-induced white matter pathology and degenerative changes to the glial-vascular unit (Holland et al., 2015). My new data indicates that BCAS can also lead to impaired CSF influx along the glymphatic pathway. In the first instance, tracers were injected into the cisterna magna and were able to be observed surrounding cerebral arteries e.g. middle cerebral artery (MCA) within the perivascular space (Figure 3-12 and Figure 3-13) consistent with previous observations showing that CSF influx moves along the periarterial components into deeper brain regions (Iliff et al., 2012). It has been shown by *in vivo* two-photon imaging that intracisternal CSF tracer travels along with the perivascular component surrounding pial surface (Iliff et al., 2012, Xie et al., 2013). Using this approach, we were able to measure the regional distribution of tracers post-BCAS. Following 3 months of carotid stenosis, the impaired glymphatic function was determined in cortical and deep hippocampal regions suggesting that prolonged disruption to the vascular system may lead to enduring suppression of CSF influx to the brain.

CSF glymphatic influx has also shown to be impaired in other models relevant to cerebral vascular disease. In a rodent model of multiple infarcts, caused by intra-arterial injection of cholesterol crystals via the internal carotid artery, transient suppression of CSF influx was determined (Wang et al., 2017). However, in this study, the glymphatic function was restored within 2 weeks. In other models, a sustained or progressive impairment of glymphatic function has been shown, such as with ageing and in models relevant to AD. For example, in APP/PS1 mice, a model relevant to AD, both glymphatic periarterial influx and amyloid β (Aβ) clearance have been found impaired, with glymphatic failure occurring before significant Aβ accumulation (Peng et al., 2016). Malfunction of the glymphatic pathway has also been shown to be related to a build-up of amyloid, Aβ protein, in the vasculature (Kress et al., 2014). Consistent with this, in the present study, microvascular amyloid as studied in the Tg-SwDI model was related to the impaired glymphatic influx. However, this impairment was not

further altered with stenosis. The reason for this is not clear but maybe in part due to the already prominent impairment of glymphatic function caused by the microvascular amyloid load.

Cerebrovascular pulsatility is a critical driving force facilitating CSF flow into and through brain parenchyma (Iliff et al., 2013b, Mestre et al., 2018b). In work using two-photon imaging assessing vessel pulsation after carotid stenosis, there was evidence showing an impaired pulsation is a potential mechanism. In a parallel study, conducted with other researchers in the group (see Appendix) using intravital imaging, we found that arterial pulsation was specifically impaired and pulsation of other vessels within the vascular network unaltered post-BCAS. Previously, it has been reported that 30 minutes unilateral ligation of the internal carotid artery leads to significantly reduced pulsatility in the penetrating artery with impaired paravascular influx (Iliff et al., 2013b). Collectively, the data suggest altered arterial pulsatility is associated with a reduction in CSF influx post-BCAS (Iliff et al., 2013b).

6.4 Conclusion

In summary, the findings in this chapter provide evidence linking carotid stenosis with cognitive impairment and demonstrate that whilst cerebral perfusion is reduced and sustained over several months, there may additionally be an impairment to glymphatic function that is emerging as having a significant role in the pathogenesis of VCI. This new data adds credence to a growing body of human studies that have challenged the view that cerebral hypoperfusion post-carotid stenosis is the predominant contributor to VCI. It strongly suggests alternate or additional mechanisms need to be considered (Shi et al., 2018, Aribisala et al., 2014a, Wardlaw et al., 2017, Alhusaini et al., 2018). Furthermore, the efficient cellular communications within the brain cells, in particular the neurovascular unit is essential for maintaining tissue health and normal functioning. What happens to the efficient communication within NVU is extremely important to elucidate the underlying mechanism by which BCAS causes cognitive deficits. Building on the work presented in this chapter, the

next studies sought to explore neurovascular coupling and degenerative changes in both WT and Tg-SwDI mice post-BCAS.

Chapter 4. Long-term effects of bilateral common carotid artery stenosis and amyloid-β (Aβ) on neurovascular function and degenerative changes

1. Introduction

The studies outlined in Chapter 3 provide evidence that BCAS causes cognitive impairment via mechanisms involving reduced cerebral perfusion and impaired glymphatic function. Emerging evidence from epidemiology, imaging, clinical, and animal models suggest chronic cerebral hypoperfusion is associated with impaired haemodynamic abnormalities (Liu and Zhang, 2012, Ihara et al., 2014, Sarti et al., 2002). In the brain, the neurovascular unit facilitates dynamic changes in blood flow in response to changes in the neural activity, which is known as the process called neurovascular coupling.

Neurovascular coupling ensures that the brain receives a proportionally matched blood perfusion in response to local neural activity. However, mounting evidence has suggested that neurovascular coupling may be impaired either in ageing or neurological disorders such as Vascular dementia and Alzheimer's disease (Kisler et al., 2017, Shin et al., 2007). It is postulated that impaired blood flow responses to neural activity, as a result of mis-coordinated activity of the neurovascular unit, may cause a mismatch between neural activity and delivery of energy substrates to meet sufficiently adequate metabolic demands (Kisler et al., 2017). Whether neurovascular coupling is altered following chronic cerebral hypoperfusion and whether these effects interact with microvascular Aβ accumulation are still unclear. In addition to the functional changes of cerebral blood vessels, neurodegenerative changes following BCAS is also suggested to be associated with cognitive dysfunction (Iadecola, 2013).

VCI is commonly attributed to brain ischaemic or haemorrhagic injuries such as microinfarcts or microbleeds (Dichgans and Leys, 2017). These vascular related lesions can occur as a

direct consequence of vascular pathology with profound alterations to the neurovascular unit and the normal physiology of neurovascular coupling. Evidence from our group has demonstrated the gliovascular alterations, including microinfarcts, fibrinoid necrosis, white matter disruption and widespread reactive gliosis induced by BCAS (Holland et al., 2015). Also, previous studies such as the NUN study has highlighted that the presence of amyloid lowers the threshold for precipitation of dementia in vascular disease (Snowdon et al., 1997). Thus, whether the presence of microvascular amyloid could affect the degenerative process in response to BCAS requires urgent investigation. The BCAS model in Tg-SwDI mice affords a unique opportunity to study mechanisms related to VCI and the development of dementia. Furthermore, the perivascular or glymphatic clearance of soluble Aβ has been gaining interest since the failure of Aβ clearance is recognised as a critical mechanism related to CVD and AD, leading to cognitive decline. It was shown in the previous chapter that glymphatic function was altered in the cerebral cortex and hippocampus in response to bilateral common carotid stenosis, whether the failure of clearance via glymphatic pathway could result in Aβ accumulation in the microvasculature remains to be determined. The neurodegenerative changes, including vascular related lesions, astrogliosis and the microvascular amyloid post-BCAS will be assessed in this chapter.

2. Hypothesis

BCAS leads to cognitive impairment by impairing vascular function leading to degenerative changes and that these effects will be exacerbated in the presence of microvascular amyloid.

3. Study aims

The present study aimed to assess neurovascular coupling, vascular related lesions, and astrogliosis following 3 months of BCAS, and to determine whether these are exacerbated in the presence of vascular Aβ. Second to this, the study also aimed to determine if BCAS promotes Aβ accumulation.

4. Materials and methods

4.1 Animals

Male heterozygous Tg-SwDI mice and wild-type C57Bl/6J littermates were subjected to BCAS or sham surgeries. A group of mice from cohort 1 (n=42) (Tg-SwDI and wild-type littermates at 7-9 months old of age) were used in experiments for the investigation of neurovascular coupling, vascular related lesions and amyloid. The second cohort of mice (total number=33, Tg-SwDI mice at 5-7 months and wild-type C57Bl/6J at 4-5 months old of age) were prepared to determine the astrogliosis following surgery (cohort 2). Mice were randomly assigned to all the studies. All data were collected and analysed by experimenters that were blind to surgery types, genotype and treatments. In cohort 1, 1 mouse in Tg-SwDI BCAS was culled due to the severe bleeding during the surgery. 4 mice in Tg-SwDI and 2 mice WT groups were culled due to the poor recovery following BCAS surgery. Therefore, these mice were excluded from the study. Final group size for cohort 1: n=8 WT sham, n=10 WT BCAS, n=6 Tg-SwDI sham, n=10 Tg-SwDI BCAS. In cohort 2, n=10 WT sham, n=8 WT BCAS, n=7 Tg-SwDI sham, n=8 Tg-SwDI BCAS.

4.2 BCAS surgery

Mice were anaesthetised under isoflurane in oxygen-enriched airflow. BCAS surgery was performed using microcoils (0.18mm internal diameter) to both common carotid arteries that modestly reduces cerebral blood flow (<30%) to induce luminal narrowing, and methods have been described in previous studies (Shibata et al., 2004, Coltman et al., 2011, Holland et al., 2011a, Reimer et al., 2011b). An interval of 30 minutes was given between the placement of coils to minimise the acute CBF changes caused by the placement of microcoils. Sham-operated animals underwent the identical procedure except for the application of microcoils to both arteries.

4.3 *In vivo* whisker stimulation and neurovascular coupling

In vivo whisker stimulation was performed on mice anaesthetised by intraperitoneal injection with α-chloralose (50 mg/kg) and urethane (750 mg/kg) to preserve physiological vascular responses. Repeated whisker stimulation was used to evoke neurovascular coupling in the barrel cortex. Whiskers on the right side were trimmed at approximate 1 cm for stimulation and were cut on the left to avoid any unwanted disturbances. Mice were positioned on the stereotaxic frame with their head fixed into position. Oxygen airflow was supplied, and the rectal temperature was monitored and maintained at around 37 ºC. Laser speckle imager (moorFLPI-2, Moor Instruments, UK) was set up according to the methods described in the previous section. Stable cortical blood flow in the barrel cortex was recorded for 2 minutes as the baseline recording. During stimulation, the whiskers were deflected by rapid back-and-forth movements using an electric stimulator for 30 seconds to evoke the neuronal activity in the contralateral barrel cortex. CBF was set to return to baseline before the next stimulation. Three successful recordings were recorded for data processing. Raw images from laser speckle imaging were analysed using moorFLPI2 Review software (v4.0). The mean response amplitude was collected and calculated as the result of the percentage increase from baseline.

4.4 Perfusion fixation

Mice were perfused with 30 ml PBS then whole brains were fixed in 4% paraformaldehyde (PFA) in PBS for 24 hours and either transferred into 30% sucrose solution for 72 hours followed by snap freezing in dry ice-cooled isopentane then stored in -80 ºC freezer, or cut by vibratome and stored in -20 ºC freezer.

4.5 Haematoxylin and eosin (H&E) and Perl's Prussian blue staining

Brain slices at 12 µm thickness were obtained at the stereotactic level of (0.86 mm, 0.14 mm, -0.46 mm, -1.34 mm, -1.70 mm and -2.30 mm to Bregma). To determine the vascular

related lesions, such as microinfarcts and microbleeds, sections were stained with H&E and Perl's Prussian blue using methods described in the previous chapter (Chapter 2) to visualise the presence of ischaemic and haemorrhagic tissue damage. Ischaemic lesions were confirmed under a light microscope using H&E staining, and haemorrhagic lesions were confirmed using Perl's staining.

4.6 Quantification of amyloid burden

Immunohistochemistry was performed to determine the burden of amyloid in the cerebral cortex. 12 µm thick cryostat sections at the level of -1.82 mm to Bregma were stained following the immunostaining protocol introduced in Chapter 2. Tissues were double labelled with antibodies of amyloid (6E10) and collagen 4 (COL4) and labelled with secondary antibodies Alexa Fluor 546 and Alexa Fluor 488 for 6E10 and COL4, respectively. Raw images were obtained using a laser scanning confocal microscope (ZEISS LSM 710, Germany) then analysed using ImageJ JACoP plugin.

4.7 Analysis of astrogliosis

Immunostained 100 µm vibratome sections were analysed using a slide scanner (ZEISS Axio Scan.Z1). Astrogliosis was assessed by measuring the percentage of stained area occupied by GFAP staining, using auto thresholding (triangle method). All measurements were carried out using ImageJ (v1.46, NIH, Bethesda, MD, USA).

4.8 Statistical analysis

Neurovascular coupling and astrogliosis were analysed using two-way ANOVA with Bonferroni's multiple comparisons. Mann-Whitney U test was used to compare the amyloid burden and blood vessel density. Difference in proportions test was performed to compare the vascular related lesions. Statistical analysis was performed using IBM SPSS Statistics 22.

5. Results

5.1 Neurovascular coupling is significantly impaired in both WT and Tg-SwDI mice at 3 months following BCAS surgery

In the previous studies, CBF was measured post-BCAS and determined to be reduced in the long-term in both WT and Tg-SwDI mice with no difference between these groups. Although CBF may not be different, neurovascular coupling, (i.e. the CBF response to neural stimulation) as has been shown in studies of other VCI models may be differentially altered. To investigate whether long-term BCAS (3 months) causes alterations in neurovascular coupling, CBF was measured in the barrel cortex at baseline and then changes in CBF in response to whisker stimulation was measured. Responses of cortical blood vessels to whisker stimulation were recorded and quantified as the mean percentage increase from the baseline (Figure 4-1). There was a significant effect of BCAS surgery ($F_{(3, 34)} = 16.61$, $p<0.001$), whereby impaired neurovascular coupling was observed in the BCAS mice from both WT and Tg-SwDI mice. However, there was no significant effect of genotype in these mice ($p>0.05$). Post-hoc tests showed significantly impaired neurovascular coupling in WT ($p<0.05$) and Tg-SwDI groups ($p<0.01$) compared to their sham counterparts, respectively (Figure 4-1).

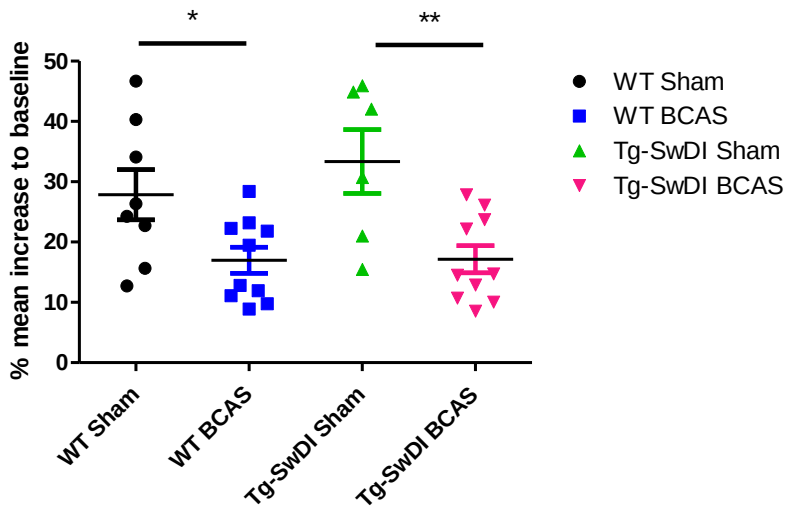

Figure 4-1 BCAS results in impaired neurovascular coupling at 3 months after BCAS surgery.

*Neurovascular coupling was assessed using laser speckle contrast imaging with whisker stimulation at 3 months of BCAS surgery. Significant effect of the surgery was found in both WT and Tg-SwDI mice. No effect of genotype was observed. Post-hoc analysis showed significantly impaired neurovascular coupling in WT and Tg-SwDI group compared to the sham animals, respectively. Data presented as mean ± SEM, n=8 WT sham, n= 10 WT BCAS, n= 6 Tg-SwDI sham, n=10 Tg-SwDI BCAS, * indicates p<0.05 and ** indicates p<0.01.*

5.2 Degenerative changes: vascular related lesions were found in the WT and Tg-SwDI mice after BCAS surgery

Building on the findings that neurovascular coupling was impaired in both WT and Tg-SwDI mice, the impact of BCAS on degenerative changes in the brain was assessed. Chronic cerebral hypoperfusion produced by BCAS has been previously shown to increase the microinfarct area in the Tg-SwDI mice. The present study aimed to use H&E staining to determine the presence of ischaemic lesions (microinfarcts) and Perl's Prussian blue staining to determine the burden of haemorrhagic stroke lesions (microbleeds).

In none of the sham-operated mice were vascular related lesions detected (0 out of 8 in WT sham and 0 out of 6 in Tg-SwDI sham). Further investigation at stereotactic levels (0.86 mm, 0.14 mm, -0.46 mm, -1.34 mm, -1.70 mm and -2.30 mm to Bregma) revealed that 4 out of 10 WT BCAS and 6 out 10 Tg-SwDI BCAS mice were found microinfarcts and microbleeds

lesions. Difference in proportion test showed that mice in the Tg-SwDI BCAS group did not demonstrate a significantly higher proportion of mice with vascular related lesions compared to WT BCAS mice (p=0.371) (Table 4-1). Representative images of ischaemic lesions in the cortex (Figure 4-2A), white matter lesions (Figure 4-2B and D), neuronal damage in the hippocampus CA1 (Figure 4-2C and E) and subcortical lesion (Figure 4-2F) are shown. Subcortical haemorrhagic lesions were predominantly found in the thalamus (Figure 4-2G, I and H).

Table 4-1 Vascular related lesions are found in both WT and Tg-SwDI mice post-BCAS.

	Normal	Vascular related lesions
WT BCAS	6	4
Tg-SwDI BCAS	4	6

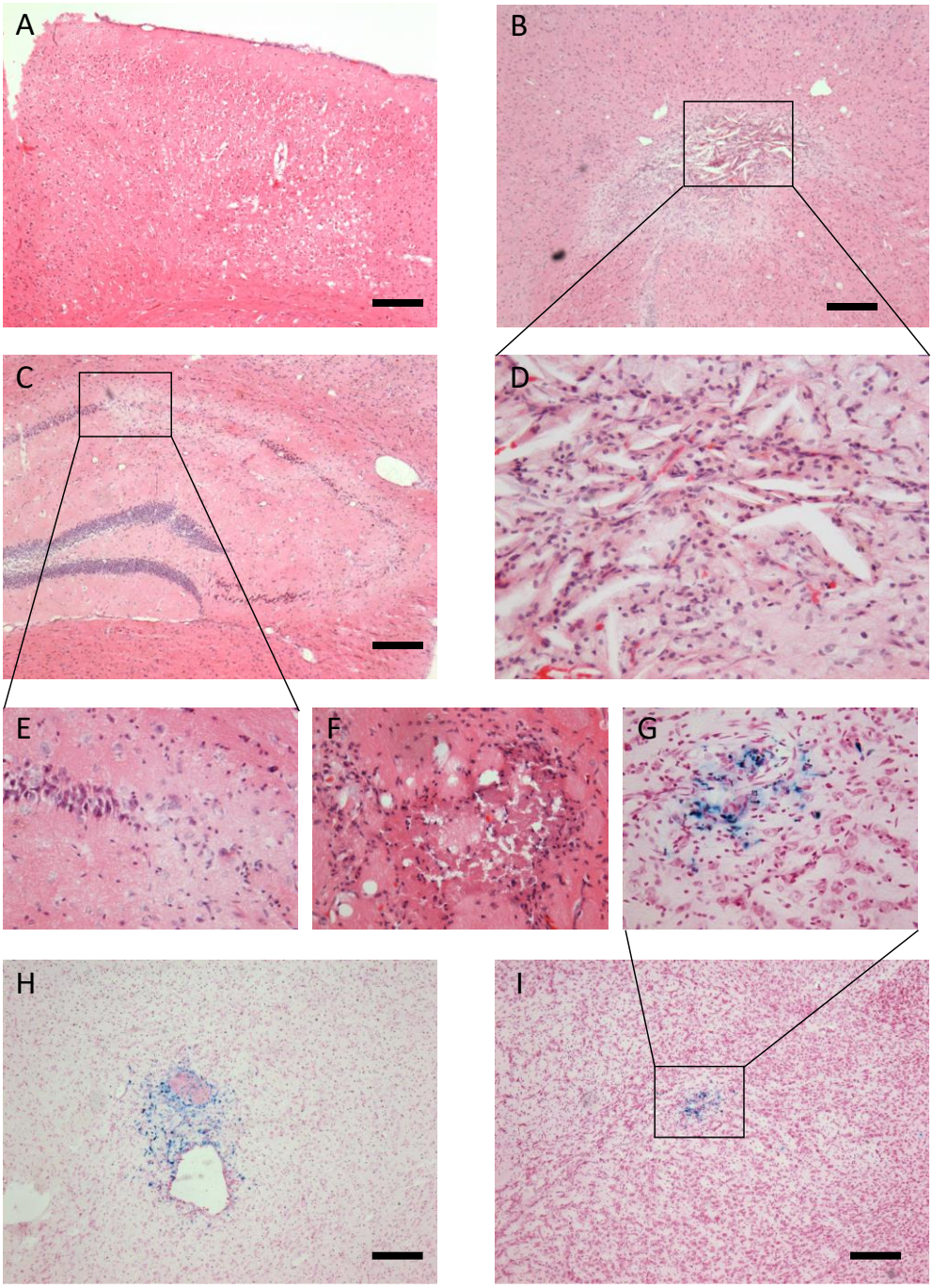

Figure 4-2 Representative images of vascular related lesions in multiple brain regions.

Images of ischaemic lesions were taken from regions of the cortex (A), corpus callosum (B and D), hippocampus (C and E), subcortex (F). Perl's positive staining for haemorrhagic lesion is surrounding a big vessel (H) and subcortical region (G and I). Scale bar = 200 μm.

5.3 Increased astrogliosis following bilateral common carotid stenosis (BCAS)

To discern the mechanisms by which BCAS and microvascular amyloid may impact on the glymphatic function, the extent of astrogliosis was further studied since astrocytes and their end-feet have been shown to alter glymphatic function (Iliff et al., 2012). GFAP immunostaining was undertaken to investigate the extent of reactive gliosis post-BCAS and in Tg-SwDI mice (Figure 4-3A and B). There was a significant effect of BCAS surgery ($F_{(1, 27)}$ =0.3, p=0.01) but no effect of genotype (p>0.05) and interaction (p>0.05) on the extent of astrogliosis in the dorsolateral cortex. Post-hoc tests showed a significant increase of astrogliosis between wild-type sham and BCAS mice (p=0.021).

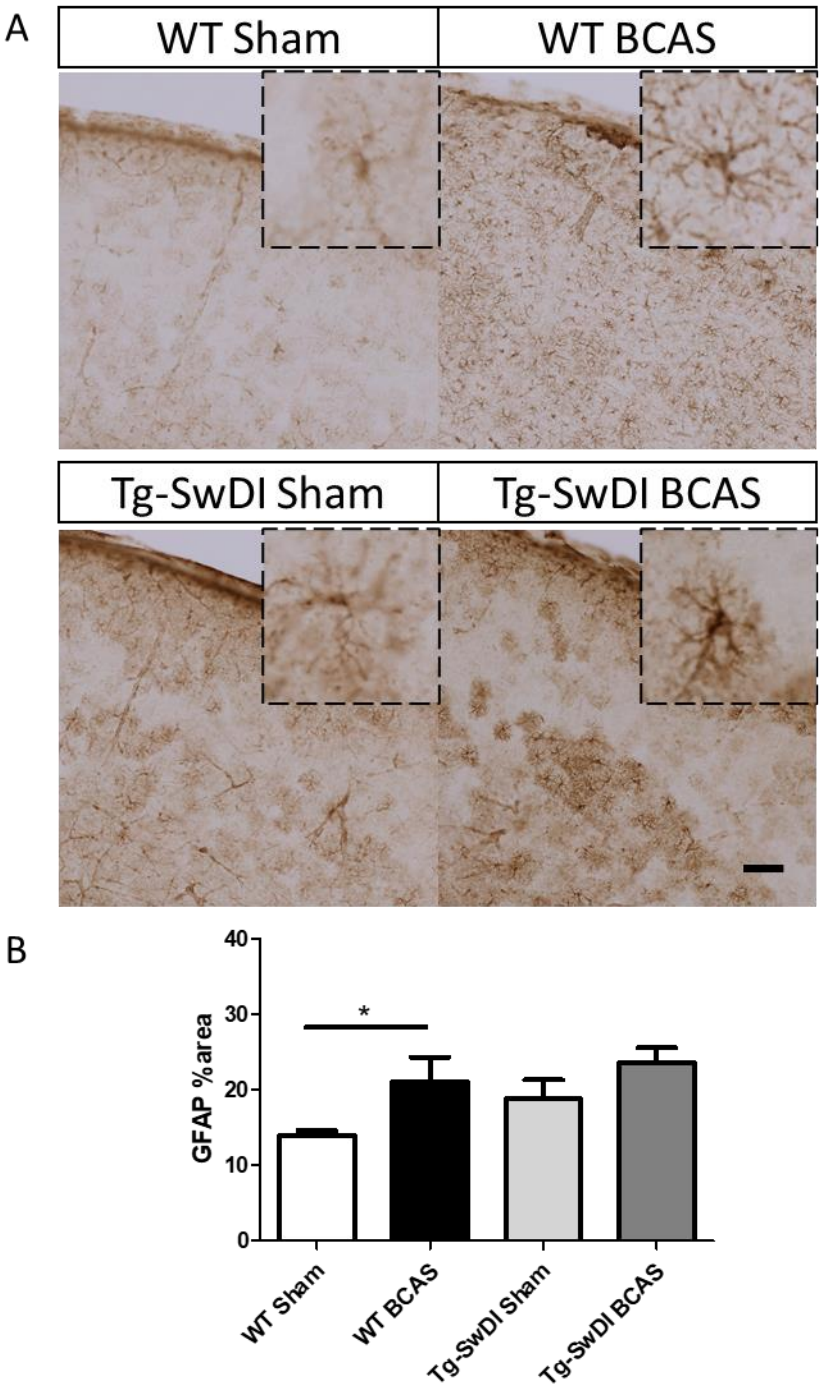

Figure 4-3 GFAP staining was used to assess the degree of astrogliosis in the dorsal lateral cortex.

*(A) Representative images of GFAP staining in the dorsal lateral (DL CTX). (B) BCAS caused increased astrogliosis, and there was no effect on amyloid or interaction. Data are presented as mean ± SEM and analysed by two-way ANOVA with post-hoc Bonferroni procedure, n=10 WT sham, n= 7 WT BCAS, n= 7 Tg-SwDI sham, n=7 Tg-SwDI BCAS, * indicates p<0.05. Scale bar=100 µm.*

The hippocampal CA1-DG molecular layer was further analysed (Figure 4-4A and B). There was a significant effect of genotype ($F_{(1, 28)}$ =0.457, p=0.002) but no effect of BCAS (p>0.05) and interactions (p>0.05) on astrogliosis. Post-hoc tests showed a significant increase between WT BCAS and Tg-SwDI BCAS mice (p=0.009) and a slightly increased astrogliosis between the WT sham and Tg-SwDI mice (p=0.061).

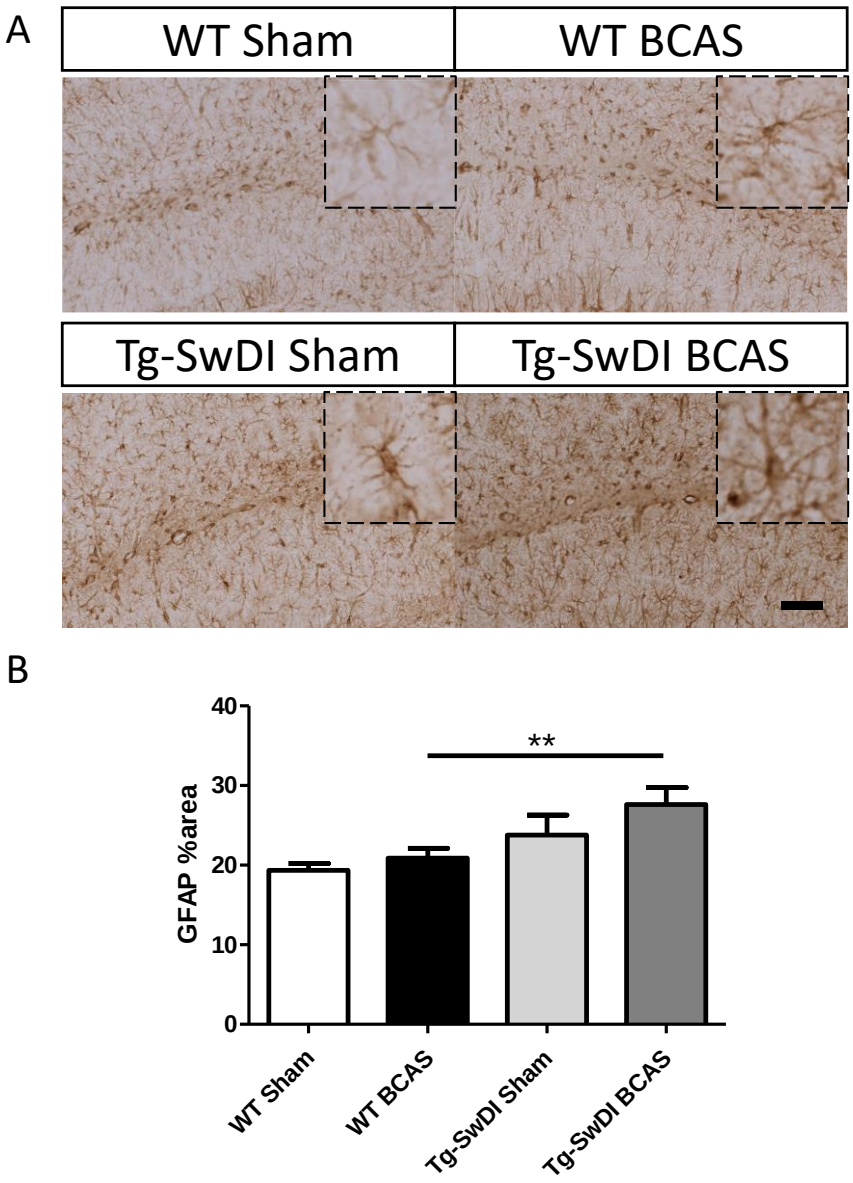

Figure 4-4 GFAP staining was used to assess the degree of astrogliosis in hippocampal CA1-DG molecular layer.

*(A) Representative images of GFAP staining in the hippocampus CA1-DG molecular layer. (B) In the hippocampus, amyloid showed main effect but not BCAS, with increased astrogliosis in the Tg-SwDI mice after carotid stenosis. Data are presented as mean ± SEM, n=10 WT sham, n= 8 WT BCAS, n= 7 Tg-SwDI sham, n=7 Tg-SwDI BCAS, ** indicates p<0.01. Scale bar=100 µm.*

5.4 BCAS leads to increased amyloid burden in the cortical cerebral vasculature

To date, all data suggests that Tg-SwDI mice respond similarly to BCAS than WT mice with comparable rCBF reductions, cognitive alterations and neurovascular alterations. This was contrary to the original hypothesis particularly given that Tg-SwDI mice are reported to have increased microvascular amyloid (Davis et al., 2004). Thus, given that previous studies have shown BCAS can alter amyloid accumulation the next study also sought to determine amyloid levels post-BCAS and compare to sham.

There is no evidence of amyloid accumulation in WT sham or BCAS mice. To investigate the potential changes of amyloid burden following 3 months of BCAS, Aβ (6E10) load was evaluated in the cortex and co-labelled with collagen 4 (COL4) (a marker of the basement membrane of blood vessels) to enable the assessment of microvascular amyloid in our Tg-SwDI mouse model (Figure 4-5A). A significant increase in the total amount of amyloid in the cortex was determined post-stenosis (Figure 4-5B) ($p<0.05$). Additionally, a significant increase in vascular amyloid was determined post-stenosis ($p<0.05$) (Figure 4-5C). Since basement membrane has been shown as pathways for the clearance of Aβ, we further evaluated the collagen 4 levels and did not find significant changes in the mice with 3 months carotid stenosis ($p>0.05$) (Figure 4-5D).

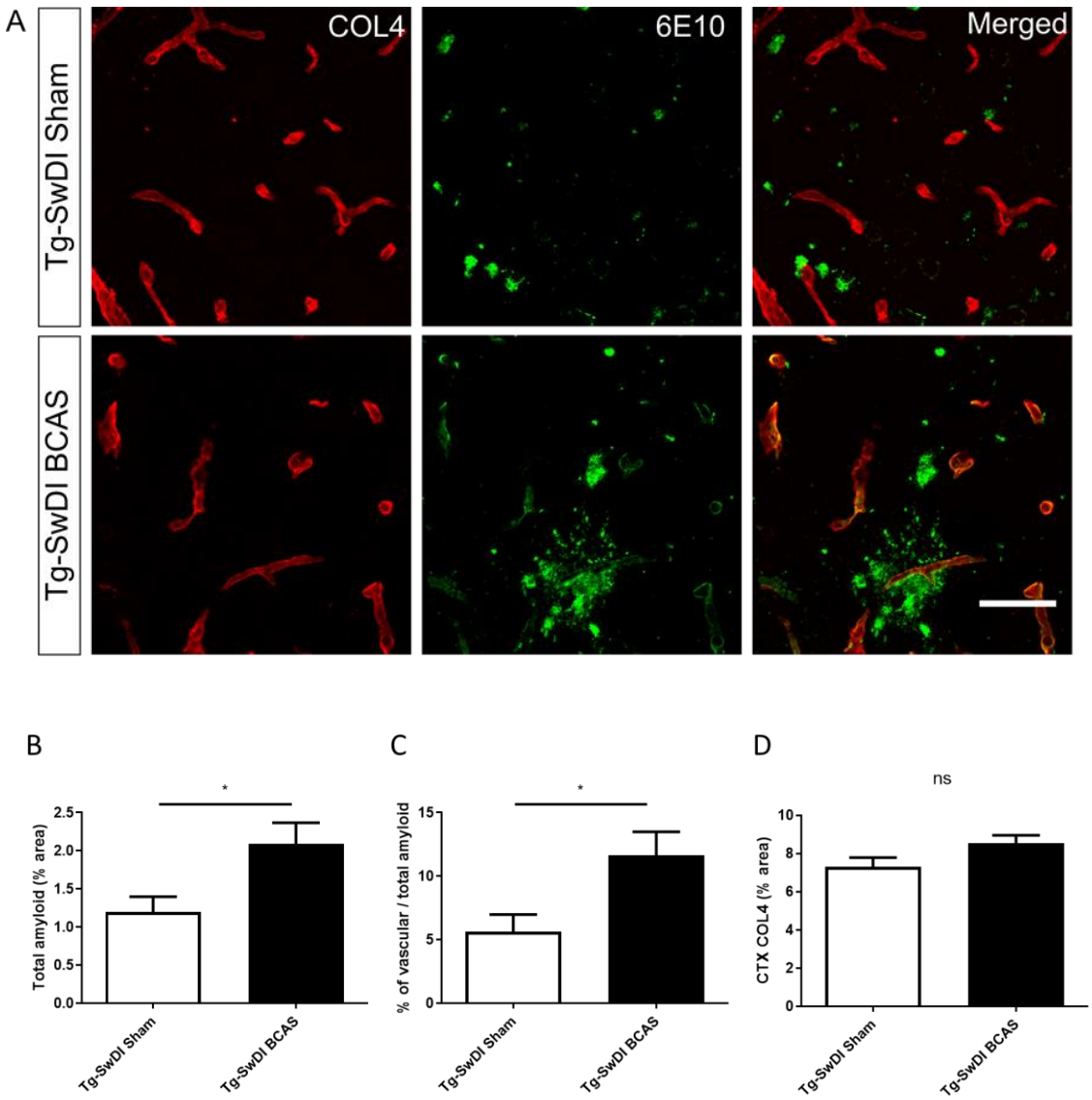

Figure 4-5 Increased amyloid load in the superficial cortex.

*Representative images of amyloid (green) colocalised to the vasculature (red) in the Tg-SwDI sham and BCAS mice (A). Total amyloid was analysed using % area of positive 6E10 staining. Increased total amyloid was found in the superficial cortical area (~250 µm from the pial surface) (B). The percentage of vascular amyloid in total amyloid was analysed using JACoP plugin (ImageJ). Amyloid that was colocalised with COL4 positive staining was considered as vascular amyloid. A increased vascular amyloid load (percentage of vascular amyloid in total amyloid) was found in the same area (C). No alterations of the density of vascular basement membranes (as measured by COL4 immunostaining) were found (D). n=6 Tg-SwDI sham and n=9 Tg-SwDI BCAS, * indicates $p<0.05$ and ns indicates not significant. Scale bar=50 µm.*

6. Discussion

The present study demonstrated that BCAS impaired neurovascular coupling and promoted degenerative changes and second to this provided evidence that BCAS could promote amyloid accumulation in the cerebral microvasculature. In contrast to the hypothesis, neurovascular coupling was found to be impaired solely by the BCAS effect with no further exacerbation by the presence of microvascular amyloid. Neurodegenerative changes including white matter lesions, microinfarcts and microbleeds were observed following BCAS, and found to be promoted in the Tg-SwDI mice.

Widespread reactive astrocytes are a key feature observed in BCAS models and associated with hypoxia-induced neurodegenerative changes contributing to cognitive impairment. To further elucidate the potential mechanisms underlying the structural and functional changes in the neurovascular unit and observed glymphatic dysfunction in response to BCAS, the extent of astrogliosis was assessed. However, the extent of astrogliosis did not always reflect the impaired glymphatic function in different regions: in the cortex following post-BCAS, there was pronounced astrogliosis whereas in the hippocampus astrogliosis was unaltered post-BCAS and instead increased in Tg-SwDI mice. Lastly, the investigation of amyloid load demonstrated that both total amyloid deposition and microvascular amyloid accumulation were increased in the cerebral cortex in response to the BCAS.

6.1 Bilateral common carotid artery stenosis (BCAS) impairs neurovascular coupling

The bilateral common carotid artery stenosis (BCAS) model in mouse has been described as the optimal model to replicate chronic cerebral hypoperfusion. Previous studies as outlined in this thesis (Chapter 3) using laser speckle contrast imaging and ASL indicates that cerebral perfusion is markedly reduced and sustained throughout the three months. However, this level of reduced perfusion may still be sufficient to meet the metabolic demands of tissue in both WT and Tg-SwDI mice. To explore this further, neurovascular

coupling was investigated since sustained reduced perfusion may be insufficient to meet the metabolic demands of tissue. In the present study, BCAS caused a marked impairment in neurovascular coupling in both WT and Tg-SwDI mice to levels of approximately 18% that of baseline. Although no previous studies have specifically measured the neurovascular coupling in response to BCAS using whisker stimulation method. In another relevant model, resting CBF and neurovascular coupling were measured in mice subjected to unilateral common carotid artery occlusion (UCCAO) (Nishino et al., 2016). The percentage changes of CBF response after whisker stimulation in the ipsilateral hemisphere to UCCAO side were significantly decreased at 7 (6.9 ± 2.8%), 14 (6.8 ± 2.3%) and 28 days (4.9 ± 2.4%) following surgery.

In contrast to initial predictions, neurovascular coupling was not further impaired in Tg-SwDI mice post-BCAS compared to WT BCAS mice. To date, there have been no other studies that have measured neurovascular coupling *in vivo* in the Tg-SwDI mice post-BCAS. However neurovascular coupling, independent of BCAS has been reported in Tg-SwDI mice exhibiting impaired responses to whisker stimulation at 3 months, prior to the onset of cerebrovascular amyloid deposition (Park et al., 2014). A recent study from our group investigated the effect of ageing on neurovascular coupling, cellular components within the neurovascular unit and whether these effects would be exacerbated in the presence of amyloid in Tg-SwDI mice (Duncombe et al., 2017b). Impaired neurovascular coupling was detected with advancing age starting at 12 months and notably, similar to the present study, amyloid did not exacerbate these effects. The impaired NVU coupling correlated closely with a loss of astrocytic end feet contacts with vessels and a prominent microglial response.

Although cellular components of the NVU were not measured in the current study, loss of NVU integrity likely underpins this. Previous work by our group has shown a gradual disintegration of the glial-vascular unit post-BCAS with loss of astrocytic end feet contacts and a prominent microglial response (Holland et al., 2015). The reasons for the differences between these studies is not clear. Park et al. have attributed this impaired neurovascular

coupling in such an early stage to the presence of soluble amyloid. Different imaging techniques (e.g. laser doppler vs laser speckle imaging, and cranial window vs intact skull) may also influence the detection of CBF changes produced by whisker stimulation. Future investigations on the direct effect of variable amyloid species on the neurovascular coupling remain required.

Indirect evidence of neurovascular unit changes and remodelling have been shown. Evidence from another group investigating the impact of BCAS in another Alzheimer's disease transgenic mouse model (APP23) demonstrated a major impact of BCAS on the neurovascular unit (Shang et al., 2016). In this study, post-BCAS APP23 mice showed significantly enhanced AD pathology, including cerebrovascular remodelling and restored neuropathological abnormalities by galantamine treatment (Shang et al., 2016). BCAS was induced by surgically placed ameroid constrictors (a device similar to microcoils but gradually narrowing the vessel) on bilateral common carotid arteries rather than using micro coils (as used in this thesis) and in relatively younger mice (4 months old at the time of surgery) and at 2 and 8 months following surgery respectively. Instead of using *in vivo* imaging technique, they used *in vitro* BDNF/TrkB double staining method to examine the neurovascular coupling and found no significant changes at 2 months but significant reductions in the neurovascular unit at 8 months in the subcortical regions including CA1, thalamus and polymorph layer of the dentate gyrus. By contrast, the present study provides the novel evidence of the neurovascular coupling changes following BCAS in a mouse model exhibiting microvascular amyloid.

6.2 Chronic cerebral hypoperfusion induced neurodegenerative pathology

BCAS models usually exhibit a well-described white matter pathology (Coltman et al., 2011). However, our group has reported an increase in subcortical vascular lesions in the longer-term post BCAS in WT mice (Holland et al. 2015). Similarly, in the present study, vascular related lesions were identified in WT (40%) and Tg-SwDI (60%) mice subjected to BCAS

surgery and none were found in sham groups. There was no significant difference between the proportions of WT and Tg-SwDI mice subjected to BCAS ($p>0.05$) suggesting amyloid pathology did not exacerbate vascular related neurodegeneration after BCAS induced cerebral hypoperfusion.

Our group first identified gliovascular alterations after 6 months of BCAS including a marked increase in haemorrhage, fibrinoid necrosis and blood-brain barrier (BBB) breakdown with minimal vascular lesions after 1 month of hypoperfusion and these ischaemic and haemorrhagic lesions were confirmed using T2-weighted MRI scans (Holland et al., 2015). After 6 months of hypoperfusion, 60% of BCAS mice demonstrated ischaemic lesions including cortical infarcts, or areas of hyperintensity, which were located in the region supplied by the middle cerebral artery. 35% of BCAS mice were detected with small focal subcortical infarcts in the thalamus with fewer lesions in hypothalamus and striatum. The haemorrhagic lesions were most intense after 6 months of hypoperfusion which 75% of BCAS mice showed lesions in subcortical regions, particularly thalamic nuclei. In comparison, in the present study, after 3 months hypoperfusion, vascular lesions were mostly identified in the cortex and subcortical regions such as corpus callosum, hippocampus and thalamus, with remarkable vascular pathology including fibrinoid necrosis, microinfarcts and microbleeds. The present study also showed less ischaemic and haemorrhagic lesions compared with 6 months of BCAS surgery, but a higher proportion of ischaemic lesions and a marked increase of haemorrhagic lesions were found compared with 1-month hypoperfusion that has minimal lesion load. The co-occurrence of ischaemic and haemorrhagic lesions at 3 months of hypoperfusion, which is absent in 1 month, indicates the progressive vascular pathology that coincides with previous data and provides additional evidence between the time course of 6 months. The underlying mechanism for the increased pathological burden in Tg-SwDI mice may indicate the potential interactions between vascular and amyloid load leading to neurodegenerative changes, which have been reported in the human data such as NUN study (Snowdon et al., 1997).

6.3 BCAS increases the accumulation of microvascular amyloid

The increased amyloid load, including both total amyloid and in the cerebral vasculature in the Tg-SwDI mice with BCAS, suggested an impaired balance between the production and clearance of the Aβ might occur. Although it was not assessed in the current study, Tg-SwDI hypoperfused mice have demonstrated altered amyloid peptide pools with accelerated microinfarcts compared to the hypoperfused WT mice (Salvadores et al., 2017). Following 1 month of BCAS, increased soluble Aβ (Aβ40/42) was determined with elevated APP and APP proteolytic products. At the stage of 3 months, an increase in insoluble Aβ40/42 was detected in both parenchyma and vasculature. Microinfarct load was significantly increased in the Tg-SwDI as compared with wild-type mice and further exacerbated by hypoperfusion at 1 and 3 months. Also, the number of Tg-SwDI hypoperfused mice with haemorrhages was increased compared with hypoperfused wild-type mice. These findings suggest increased Aβ production occurred following hypoperfusion contributing neurodegenerative process.

In the current study, increased Aβ accumulation was evident and impairment in the glymphatic function was determined in the previous chapter. This provides additional evidence that following long-term cerebral hypoperfusion, alterations in both Aβ production and glymphatic clearance have been produced contributing to the accumulation of Aβ. In accordance with the present results, previous studies have demonstrated that cerebral hypoperfusion accelerates cerebral amyloid angiopathy and promotes cortical microinfarcts (Okamoto et al., 2012). In the first set of post-mortem analysis, CAA severity was detected as the only predictor among all the investigated factors including age, disease, senile plaques, neurofibrillary tangles, CAA, atherosclerosis as well as white matter damage that is associated with the cortical microinfarcts. This finding was further supported by a parallel study in Tg-SwDI mice following BCAS, showing exacerbated deposition of leptomeningeal Aβ with developing microinfarcts in the cerebral cortex. By contrast, without the effect of hypoperfusion, Tg-SwDI mice did not exhibit microinfarcts with fewer Aβ detected in the leptomeningeal vessels. This result may be explained by the fact that microvascular function

was impaired due to the perivascular accumulation of Aβ following hypoperfusion, which was not measured in the study. Okamoto et al. also suggested an implication of this is the possibility that the perivascular drainage pathway was impaired, forming a vicious cycle of vascular Aβ deposition. Overall, the findings reported here shed new light on the accumulation of microvascular Aβ post-hypoperfusion, which was due to impaired microvascular function as a result of BCAS rather Aβ alone. These results also add to the rapidly expanding field of impairment in the glymphatic function following damaged neurovascular integrity is a potential mechanism responsible for the increased Aβ accumulation in the cortical microvasculature.

6.4 Conclusions

The studies within this chapter provide further support that BCAS has damaging effects on the brain, causing not only impaired neurovascular function, degenerative changes but can also lead to a build-up of amyloid. These findings have provided a more in-depth insight into the role of cerebral hypoperfusion and microvascular amyloid in the progression of VCI. It may also help to highlight that cerebral hypoperfusion is the major contributor impacting neurovascular function; however, the amyloid in the microvasculature promotes the degenerative changes. Unfortunately, the study was not able to include data from human studies with perfusion deficits, and Aβ detected in the early stage of VCI. Further investigation to understand the underlying mechanisms leading to the relevant pathophysiological changes following cerebral hypoperfusion is required. Functional magnetic resonance imaging (fMRI), the blood oxygenation level-dependent (BOLD) contrast has become more frequently used in clinical settings, as well as animal studies, to map brain activation and may be a useful tool to detect the longitudinal changes of amyloid deposition in the human brain. The following studies will focus on NADPH oxidase, which has been associated with vascular damage and CAA formation, which may contribute to the pathogenesis of cognitive impairment following BCAS (Salvadores et al., 2017).

Chapter 5. The effect of an NADPH oxidase inhibitor in Tg-SwDI mice following carotid stenosis

1. Introduction

The previous studies outlined in this thesis have shown that BCAS caused reduced cerebral hypoperfusion, impaired NVU coupling and cognitive deficits. In Tg-SwDI mice, BCAS was found to promote the accumulation of amyloid as well as promote degenerative lesions. Although the mechanisms remain ill-defined previous work has shown that excessive production of reactive oxygen species (ROS), which causes increased oxidative stress in the central nervous system may contribute to degenerative processes and amyloid accumulation (Kanamaru et al., 2015, Salvadores et al., 2017).

Oxidative stress is the result of imbalance in levels of antioxidants and ROS production, contributing to the damage to endothelial, glial and neuronal cells in the brain and neurovascular dysregulation (Freeman and Keller, 2012, von Bernhardi et al., 2015, Ma et al., 2017a, Park et al., 2007). There are several enzymes and metabolic processes that can produce ROS, a family of enzymes called the NADPH oxidase (NOX), which is expressed in multiple cell types in the CNS, including endothelial cells. NOX has recently emerged as a primary source of ROS in neurodegenerative diseases (Ma et al., 2017a). Recent evidence suggests NOX-derived ROS mediating vascular amyloidosis is associated with impaired cerebral vascular dysfunction. Importantly, data from our group has demonstrated that BCAS causes increased levels of soluble amyloid, which is associated with increased NOX2 levels (Figure 5-1) (Salvadores et al., 2017). Furthermore, apocynin, a natural source NOX inhibitor, has been shown to ameliorate cerebral vascular reactivity in aged mice developing vascular amyloid (Han et al., 2015). Supported by the close link between NOX activity and cerebral vascular function in the Tg2576 transgenic lines expressing vascular amyloidosis, the present study focuses on the effect of NOX inhibitor on the previously described cognitive impairment caused by chronic cerebral hypoperfusion in the Tg-SwDI mice.

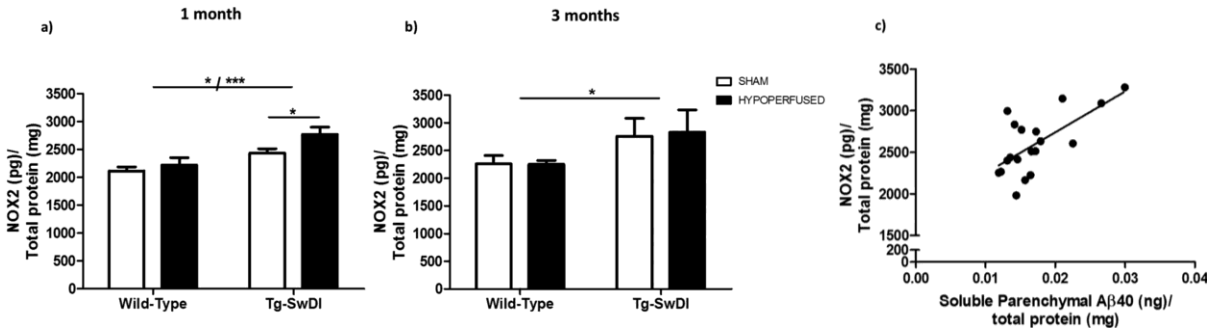

Figure 5-1 Increased NOX2 level in Tg-SwDI mice, which was exacerbated by BCAS induced chronic cerebral hypoperfusion.

*Using a setting similar to studies in this thesis, WT and Tg-SwDI mice were subjected to sham or BCAS surgery at the outset of the study, NOX2 levels were quantified in protein extracts from brain homogenates using ELISA following after 1 (a) and 3 (b) months of hypoperfusion. (c) There was a positive correlation between NOX2 levels and soluble parenchymal Aβ40 levels. * indicates p<0.05 and *** indicates p<0.001. Data presented from a previous study in our group (Salvadores et al., 2017).*

2. Hypothesis

This current study tests the hypothesis that increased NOX levels post-BCAS mediates impaired vascular function and pathological alterations leading to impaired cognitive function.

3. Aims

This study sought to assess whether a NOX inhibitor apocynin would improve cortical blood flow, neurovascular coupling, development of vascular lesions and cognitive performance in Tg-SwDI mice subjected to BCAS.

4. Materials and methods

4.1 Animals

Male heterozygous Tg-SwDI mice (n=41) at approximate 9 months of age were used at the outset for *in vivo* experiments including CBF measurement, neurovascular coupling,

behavioural tests and histology assessments. Mice were group held in standard cages with access to bedding, diet, drinking water, and nestles under 12 h dark/light cycles. The Tg-SwDI mice are expressing human amyloid precursor protein (APP) in the microvasculature (Davis et al., 2004). At the outset, mice were randomly assigned to all the studies. All data were collected and analysed by experimenters that were blind to surgery types and treatment methods. Final group numbers included for analysis are n=6 sham vehicle, n=6 sham apocynin, n=10 BCAS vehicle and n=9 BCAS apocynin (Figure 5-2).

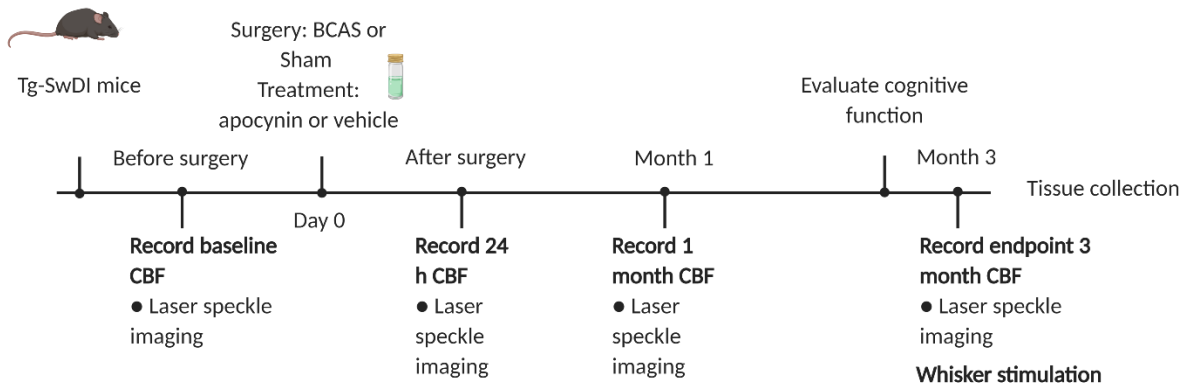

Figure 5-2 Summary for the use of animals in the experiments.

A summary to demonstrate the use of animals in the experiments of this chapter. Tg-SwDI mice were given apocynin/vehicle treatment immediately after BCAS/sham surgeries. These mice were used for in vivo experiments to measure CBF changes over a period of 3 months. Barnes maze was performed to evaluate cognitive function at about 3 months. CBF and vascular function were measured at 3 months following treatment then tissue was collected for histological examination.

4.2 BCAS surgery

Tg-SwDI mice received surgery at 9 months of their age. Details of surgical methods were described in the Chapter 2. In brief, Tg-SwDI mice were anaesthetised under isoflurane in oxygen-enriched airflow then subjected to BCAS or sham surgery. 5 mice were culled from BCAS vehicle group (1 mouse was culled without recovery due to serious bleeding during surgery, 4 mice were culled due to the poor recovery) and 3 were culled in BCAS apocynin

group. 1 mouse was found seizure and dead in sham apocynin group. Therefore, these mice were excluded from *in vivo* study.

4.3 Administration of NOX inhibitor apocynin

Following BCAS surgery, mice were immediately fed with either apocynin or vehicle in their drinking water for 12 weeks at a dose of 30 mg/kg/day. Apocynin stock was freshly made using commercially obtained compound (Sigma, UK). A working solution was defrosted with light protection before the administration. Apocynin and vehicle were changed three times per week with a maximal duration less than three days to keep the freshness. The consumption of apocynin and water were monitored throughout the study.

4.4 *In vivo* laser speckle contrast imaging

In vivo laser speckle imaging was performed to measure the cortical CBF level. Repeated cortical CBF data were collected at baseline before the surgery, 24h, 1 month and 3 months post-surgery. After each measurement, the surgical incision was sutured, and mice were recovered at the end of each imaging session except the endpoint experiment. Details see Methods section (Chapter 2).

4.5 Assessment of spatial learning and memory using Barnes maze

Barnes Maze was used to assess the spatial learning and memory ability at about 3 months following BCAS or sham surgery. At the outset, the velocity was taken as a control measurement to decide whether the motor function was altered by drug treatment and surgery. Several parameters were included in the final analysis of behavioural tests, including escape latency and % time spent in quadrants. Barnes maze was recorded using a camera connected with a tracking software ANY-maze v 4.99 (San Diego, California). Details were described in method chapter (Chapter 2).

4.6 Perfusion fixation

Mice were perfused with 30 ml PBS then whole brains were fixed in 4% paraformaldehyde (PFA) in PBS for 24 hours and transferred into 30% sucrose solution for 72 hours followed by snap freezing in dry ice-cooled isopentane then stored in a -80 ºC freezer.

4.7 Haematoxylin and eosin (H&E) and Perl's Prussian blue staining

Brain tissue slices at 12 µm thickness were obtained at the stereotactic level of 0.86 mm, 0.14 mm, -0.46 mm, -1.34 mm, -1.70 mm and -2.30 mm to Bregma. To determine the vascular related lesions, such as microinfarcts and microbleeds, sections were stained with H&E and Perl's Prussian blue using methods described in the previous Chapter 2 to visualise the presence of ischaemic and haemorrhagic tissue damage. Ischaemic lesions were confirmed under the microscope using H&E staining and haemorrhagic lesions were confirmed using Perl's staining.

4.8 Quantification of amyloid burden

Immunohistochemistry was performed to determine the burden of amyloid in the cerebral cortex. 12 µm thick cryostat sections at the level -1.82 mm to Bregma were stained following the immunostaining protocol introduced in Chapter 2. Subsequently, tissues were double labelled with antibodies of amyloid (6E10) and collagen 4 (COL4). Sections were labelled with secondary antibody Alexa Fluor 546 and Alexa Fluor 488 for 6E10 and COL4, respectively. Raw images were obtained using a laser scanning confocal microscope (ZEISS LSM 710, Germany) then analysed using ImageJ JACoP plugin.

4.9 Statistical analysis

Details of statistical analysis were summarised in Chapter 2. Cortical CBF from laser speckle imaging and Barnes maze spatial learning were carried out by repeated measures ANOVA followed by Bonferroni's multiple comparisons. Barnes maze probe tests were analysed by

two-way ANOVA followed by Bonferroni's multiple comparison test. Difference in proportions test was performed to compare the proportions of vascular related lesions. Amyloid burden and vessel density were compared using Mann-Whitney U test. One sample t-test was used to compare the performance of each group with the chance. Statistical analysis was performed using IBM SPSS Statistics 22.

5. Results:

5.1 NADPH oxidase inhibitor improved CBF following 3 months of carotid stenosis

To investigate the effect of apocynin on cortical CBF, laser speckle contrast imaging was applied to a subset of Tg-SwDI mice at approximate 9 months old to determine cortical blood perfusion levels at baseline, 24 hours, 1 month and 3 months post-BCAS surgery. The data were quantified as percentage changes from baseline blood flow at each point following surgery. Significant effects of time ($F_{(2.0, 65.2)} = 13.9$, $p<0.001$) and surgery ($F_{(1, 32)} = 41.8$, $p<0.001$) were observed. However, no overall effect of apocynin treatment ($F_{(1, 32)} = 0.1$, $p>0.05$) was detected (Figure 5-3). A significant interaction between time and surgery ($F_{(2.0, 65.2)} = 9.4$, $p<0.001$) was detected. Further post-hoc tests revealed significantly reduced CBF between sham and BCAS mice at 24 hours ($p<0.001$), 1 month ($p<0.001$), and 3 months ($p<0.001$) by giving vehicle treatment following surgery. Meanwhile, in apocynin treated mice, there was a significant difference in cortical blood flow at 24 hours ($p<0.05$) and 1 month ($p<0.05$) between sham and BCAS mice. However, no significant difference was detected at 3 months ($p=0.67$). This data indicates that apocynin restored reduced blood flow after 3 months of treatment (Figure 5-4).

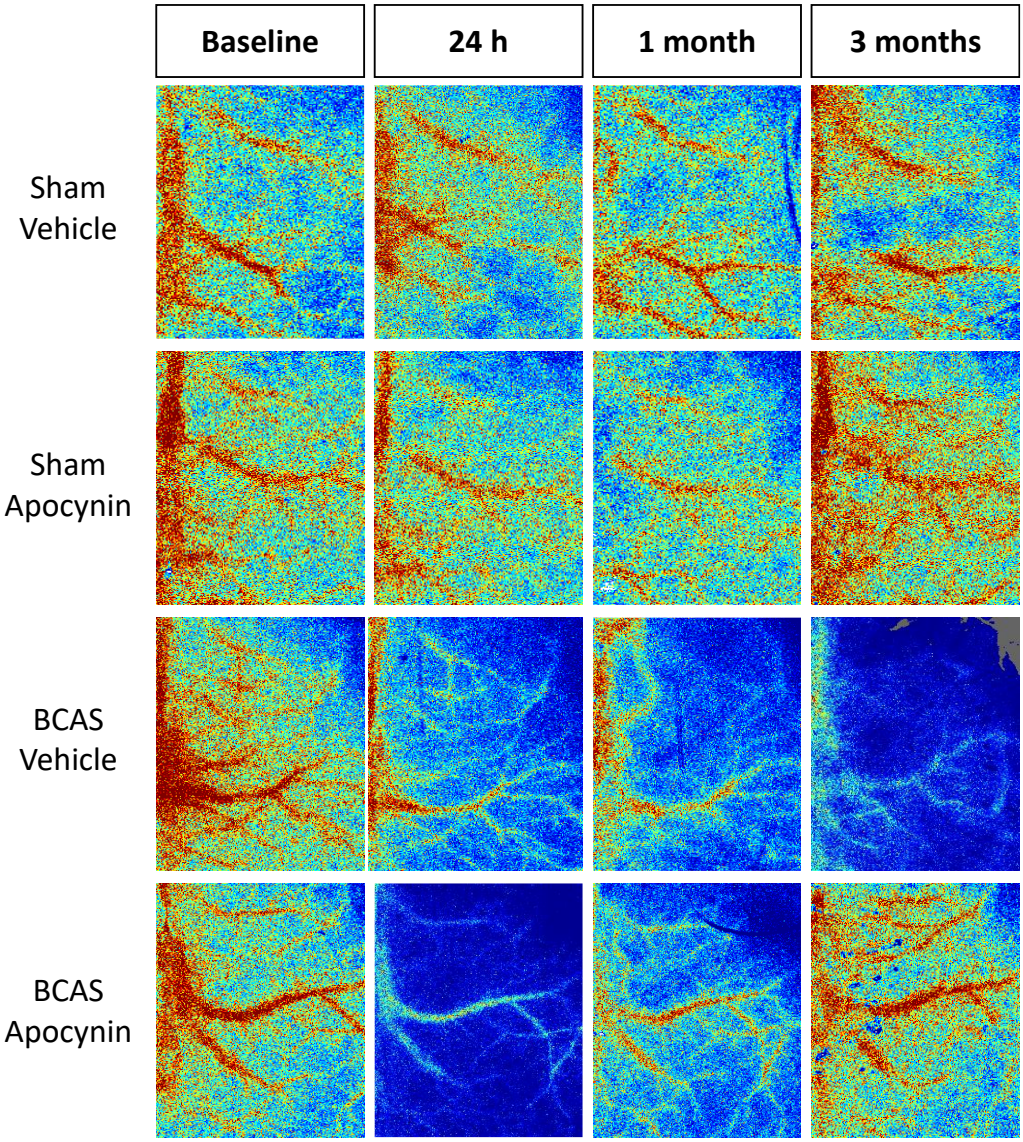

Figure 5-3 Representative images of cortical CBF measured by laser speckle imaging.

Tg-SwDI mice were given treatment for a period of 3 months after BCAS or sham surgeries. The cortical CBF levels were measured by laser speckle imaging. Representative images were taken at 24 hours before BCAS or sham surgeries (baseline), each animal was then imaged at 24 hours, 1 month and 3 months after surgeries.

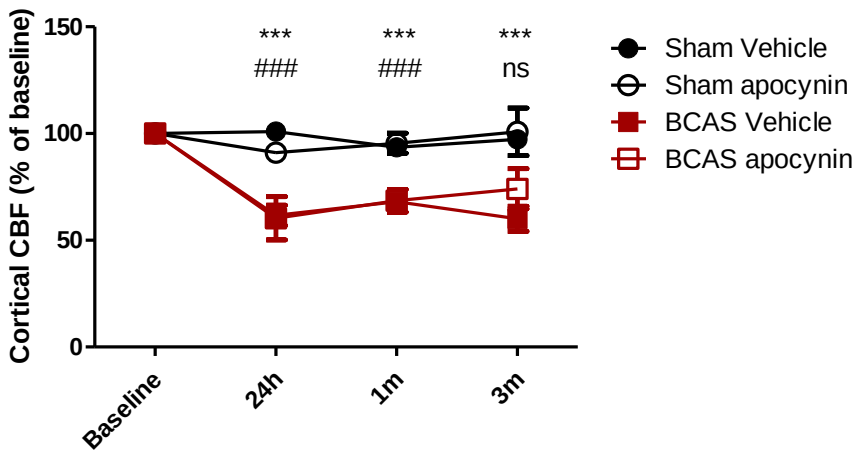

Figure 5-4 Improved cortical blood flow following 3 months of apocynin treatment in Tg-SwDI mice.

*BCAS showed a significant effect on CBF over 3 months. Further post-hoc analysis revealed significantly reduced CBF between sham and BCAS mice at 24 hours, 1 month and 3 months compared to mice given vehicle treatment following surgery, respectively. Meanwhile, in apocynin treated mice, there were significant differences in cortical blood flow at both 24 hours and 1 month following surgery between the sham and BCAS animals. Notably, at the end of 3 months, recovery of CBF from the BCAS apocynin group after 3 months of treatment can be found; n=4 sham vehicle, n=3 sham apocynin, n=4 BCAS vehicle, n= 5 BCAS apocynin. *** and ### indicate p<0.001, respectively. Data presented as Mean ± SEM.*

5.2 Apocynin restored neurovascular uncoupling following 3 months of cerebral hypoperfusion

In order to determine whether apocynin affects neurovascular coupling, the cortical vascular function was assessed using whisker stimulation at 3 months following BCAS (Figure 5-5). A significant interaction between BCAS surgery and apocynin treatment ($F_{(1, 26)}$ =1.9, $p<0.05$) was found after 3 months of BCAS/treatment. In vehicle treated mice, there was a significant difference between sham and BCAS mice ($p<0.05$) confirming the impaired neurovascular coupling following BCAS surgery. However, there was no significant difference between sham and BCAS Tg-SwDI mice in the apocynin treated group ($p>0.05$), which indicates improved neurovascular coupling in the BCAS mice after 3 months of apocynin treatment. Besides, in the mice that received BCAS surgery, apocynin treated mice demonstrated significantly stronger responses compared to those received vehicle treatment ($p<0.05$),

supporting the finding that apocynin restored impaired neurovascular coupling after 3 months treatment (Figure 5-6).

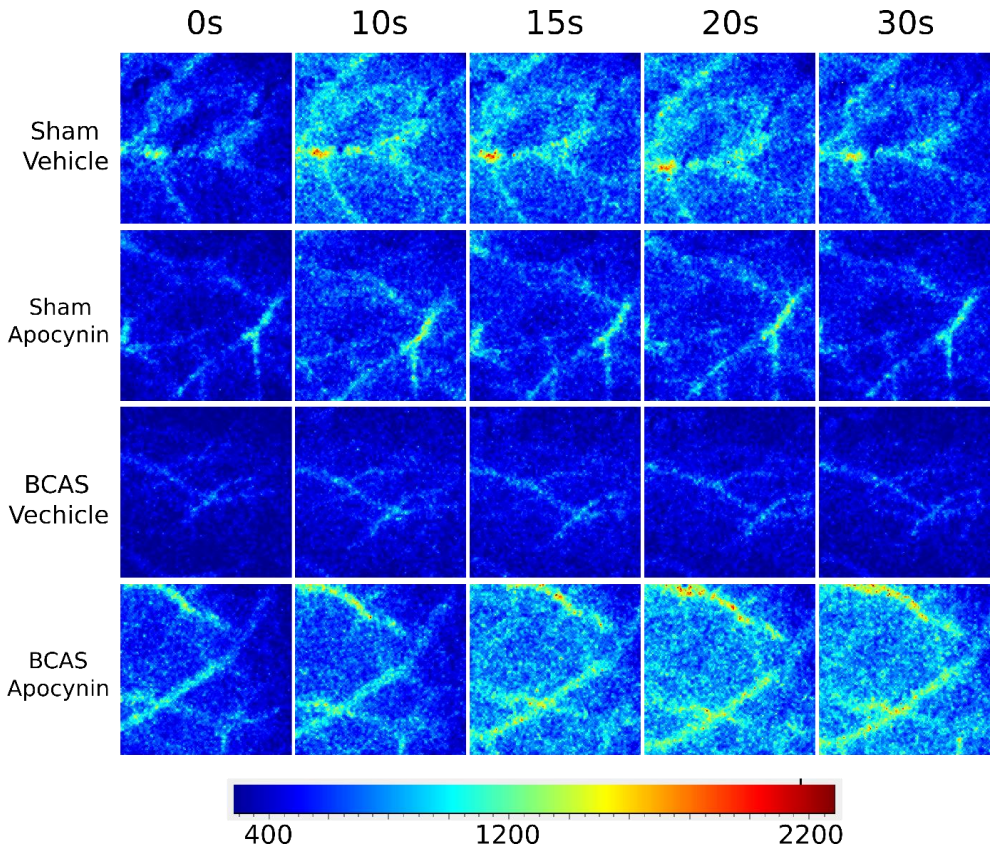

Figure 5-5 Representative images of CBF changes in the barrel cortex during whisker stimulation.

Vascular function was assessed by whisker stimulation in Tg-SwDI mice at about 12 months old. Representative images were showing the time-lapse changes of CBF from 0 s to 30 s of stimulation in the barrel cortex.

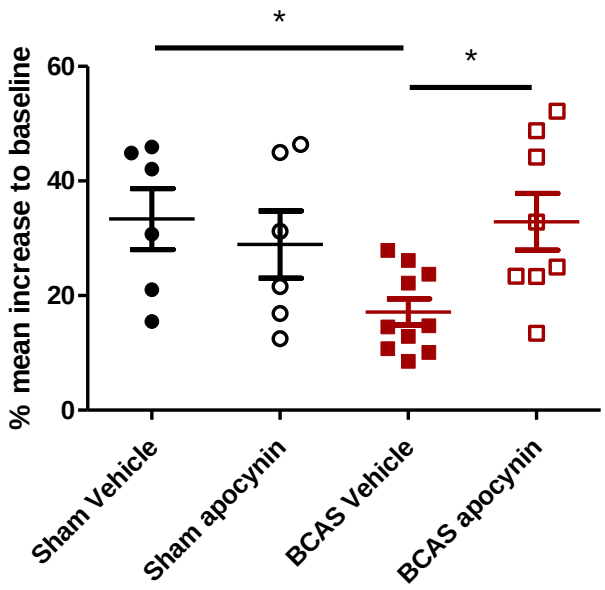

Figure 5-6 Apocynin restored vascular function following carotid stenosis.

*BCAS vehicle group showed an inadequate response, but the mice received 3 months of apocynin treatment showed robust response during the stimulation. There was a significant interaction between BCAS surgery and treatment in the mice treated with apocynin following surgery. In the vehicle treated mice, there was a significant difference between sham and BCAS mice, confirming the impaired neurovascular coupling following BCAS surgery. However, there was no significant difference between sham and BCAS mice treated with apocynin, suggesting restored vascular function in the BCAS mice after apocynin treatment. BCAS mice with apocynin treatment demonstrated significantly higher vascular responses compared to vehicle treated group, supporting the finding that apocynin restored impaired neurovascular coupling after 3 months of treatment; n=6 sham vehicle, n=6 sham apocynin, n=10 BCAS vehicle, n=8 BCAS apocynin. * indicates $p<0.05$. Data presented as Mean ± SEM.*

5.3 Vascular related pathology was not ameliorated by apocynin treatment

In the previous studies (Chapter 4), it was shown that BCAS promoted the development of vascular lesions in Tg-SwDI mice. In order to determine whether inhibiting NOX activity could provide any beneficial effect on the development of vascular pathology, the number of animals that presented evident microinfarcts and microbleeds was counted through 6 selected brain levels. H&E and Perl's Prussian blue staining were used to identify ischaemic

and haemorrhagic lesions, respectively (Figure 5-7). 6 out of 10 mice from the vehicle treated group (60%) and 3 out of 9 mice (33%) from the apocynin treated group showed vascular related lesions (Table 5-1). However, there was no significant difference between the proportions of these groups ($p>0.05$). Thus, apocynin treatment did not influence the development of neurodegenerative pathology of mice with vascular related lesions.

Table 5-1 Comparison of vascular related lesions between vehicle and apocynin treated Tg-SwDI BCAS mice.

	Normal	Vascular related lesions
BCAS Vehicle	4	6
BCAS Apocynin	6	3

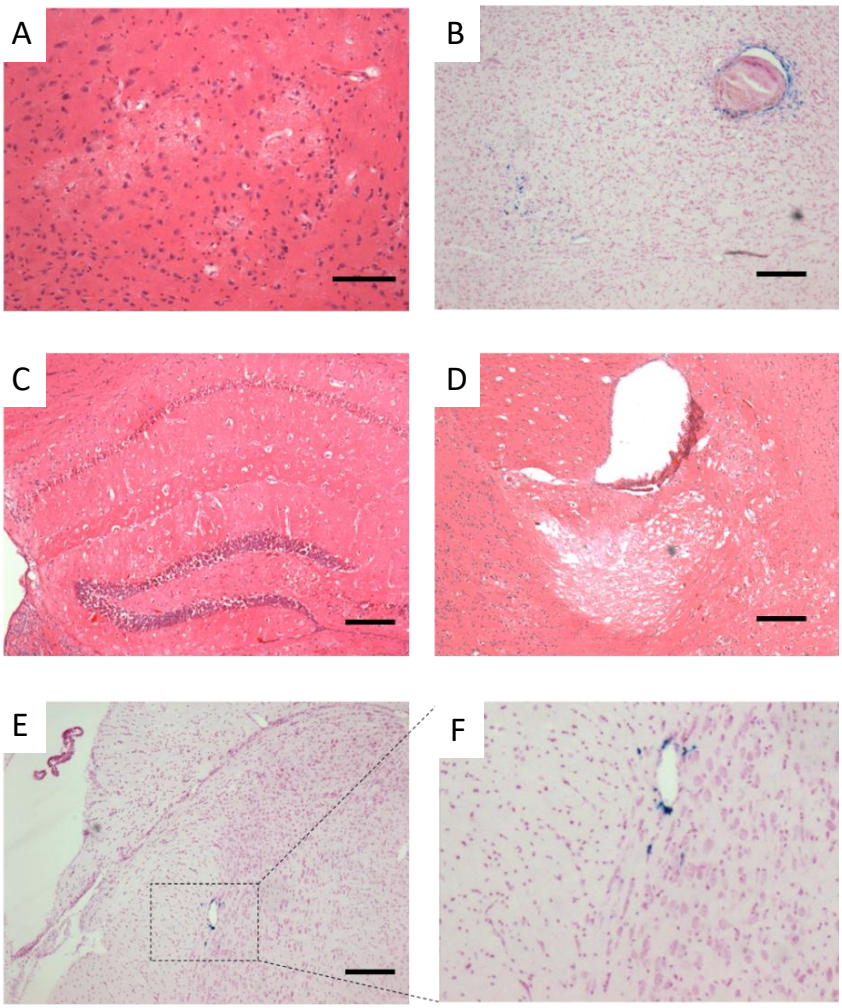

Figure 5-7 Apocynin treatment did not ameliorate vascular related lesions induced by carotid stenosis.

The effect of apocynin on the development of vascular related pathology has been examined by counting the frequency of mice with vascular lesions. H&E (A-F) staining shows hypoxia-induced microinfarcts in the cerebral cortex (A) and microbleeds in deep cortical region (B). Comprehensive neuronal damage in the hippocampal brain regions (C). Ischaemic lesions in the fimbria (below the lateral ventricle) (D). Perl's Prussian blue staining shows haemorrhagic lesions in the medial amygdala region (E and F). Scale bar in B=100 µm, C-F= 200 µm.

5.4 The amyloid burden in the cerebral cortex was not reduced after apocynin treatment

In previous studies described in this thesis (Chapter 4), it was shown that BCAS promoted the accumulation of Aβ. Other work from our lab indicated increased soluble Aβ was associated with increased NOX2 levels (Salvadores et al., 2017). The effect of NOX inhibition on the vascular amyloid, parenchymal amyloid and total amyloid load was

measured after 3 months of apocynin treatment in the BCAS groups. The amyloid burden was investigated in the cerebral cortex in which it was shown apocynin partially restored CBF and vascular function (Figure 5-8A). When comparing the total amyloid load, there was no significant difference between vehicle treated, and apocynin treated mice after BCAS surgery ($p>0.05$) (Figure 5-8B). There was no significant difference when comparing the burden of cortical vascular amyloid (percentage of total amyloid that is vascular type) in the vehicle, and apocynin treated mice ($p>0.05$) (Figure 5-8C). When further comparing the amyloid load distributed in the parenchyma, there was no significant difference of the parenchymal amyloid load in the cerebral cortex ($p>0.05$) (Figure 5-8D). Because COL4 has been reported to play a pivotal role in the clearance of amyloid, the percentage area of COL4 distribution in the cerebral cortex was measured, but there was no significant difference between vehicle and apocynin treated groups (Figure 5-8E).

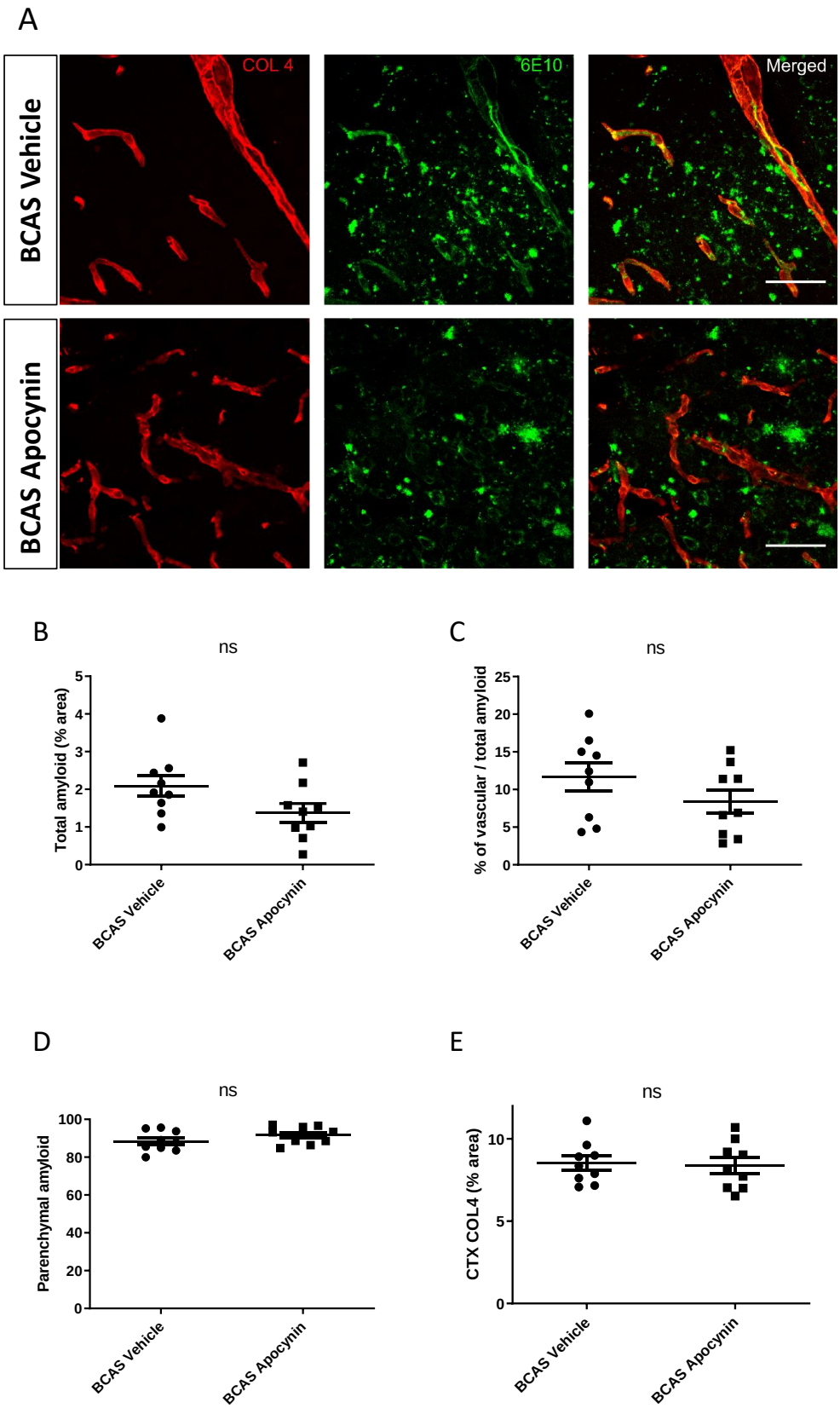

Figure 5-8 Amyloid burden was unaltered after the treatment of apocynin following 3 months of BCAS.

The cortical amyloid load was assessed by double labelling of COL4 and 6E10 in Tg-SwDI mice. (A) Representative images for BCAS Vehicle (top panel) and apocynin treated group (bottom panel). The COL4 and 6E10 markers showed the localisation of Aβ with microvasculature in the cerebral cortex. (B) Total amyloid was analysed using % area of positive 6E10 staining. The comparison of total amyloid level in vehicle and apocynin treated mice following carotid stenosis. There were no significant changes in total amyloid load after apocynin treatment. (C) Amyloid that was colocalised with COL4 positive staining was considered as vascular amyloid. The percentage of vascular amyloid in total amyloid was analysed using JACoP plugin (ImageJ). There was no alteration of vascular amyloid load (percentage of total amyloid that is vascular type) between the two groups. (D) The parenchymal amyloid load was calculated by the subtraction of the vascular amyloid by total amyloid. No significant difference in parenchymal amyloid load was observed when comparing vehicle, and apocynin treated mice following BCAS surgery. (E) As COL4 is involved in the build-up of amyloid in the vessel walls, the COL4 density was compared between two groups showing no significant difference. n=9 per group, ns indicates not significant. Mann-Whitney U test was performed to compare the difference between two groups. Scale bar=50 μm.

5.5 Apocynin did not rescue cognitive dysfunction caused by 3-month of BCAS

Previously, BCAS has been shown to lead to cognitive deficits. To determine whether apocynin treatment has any beneficial effects on the impaired cognitive function, a Barnes maze task was used to assess visuo-spatial learning and memory. At the outset of analysis, velocity was compared between groups to investigate whether the motor function was altered by drug treatment and surgery. Both drug treatment and surgery did not have a significant effect on the velocity suggesting that there were no changes in motor ability due to these two factors ($p>0.05$, respectively) (Figure 5-9). Escape latency was used to evaluate learning ability of experimental animals. There was a significant effect of time ($F_{(5,135)} =26.0$, $p<0.001$) showing decreased escape latency with increasing training days, and surgery ($F_{(1, 27)} =11.2$, $p<0.05$) showing that BCAS Vehicle mice took longer to complete the task than their sham-operated counterparts. However, no significant effect of apocynin treatment could be detected ($p>0.05$) (Figure 5-9). To investigate the effect of apocynin on long-term memory, a 72 hours probe test was performed. All groups spent significantly

longer time than by chance (Sham vehicle 58.2 ± 24.4%, BCAS vehicle 50.7 ± 30.3%, Sham apocynin 60.5 ± 33.5%) except BCAS apocynin treated mice (39.5 ± 36.4, $p>0.05$). There were no significant effects of apocynin and surgery on the duration spent on the target quadrant (Figure 5-9).

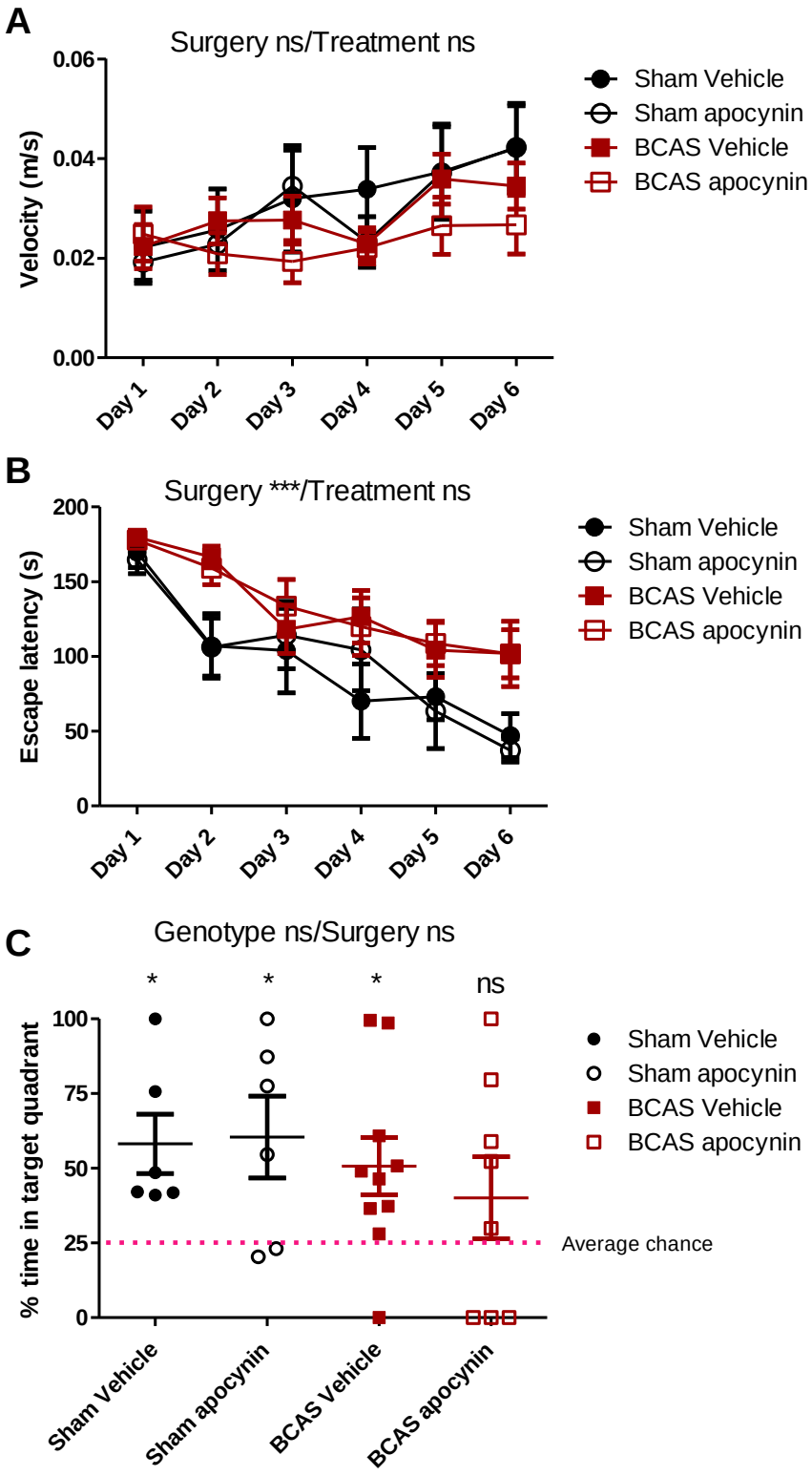

Figure 5-9 Apocynin did not protect spatial learning and memory in the acquisition training and probe trial.

Mice were assessed using Barnes maze to evaluate the visuo-spatial learning and memory function. Motor ability was assessed to determine whether there were any differences in velocity due to surgery or drug treatment. (A)

*No effect of surgery and drug treatment on the motor ability between groups were detected. (B) Spatial learning ability was assessed by comparing escape latency. There was a significant effect of time showing decreased escape latency over time, and surgery showing BCAS mice spent more prolonged time to complete the task escape the maze than their sham-operated counterparts. However, there was no significant effect of apocynin treatment can be detected. (C) Long-term memory was determined using a 72 hours probe test. All groups spent significantly longer time than by chance except BCAS apocynin treated mice (39.53 ± 36.42, p>0.05); * indicates p<0.05 and ns indicates not significant (p>0.05). n=6 sham vehicle, n=6 sham apocynin, n=10 BCAS vehicle, n=8 BCAS apocynin. There were no significant effects of treatment and BCAS on time spent on the target quadrant.*

5.5.1 Reversal test

The Barnes maze task can also be used to probe cognitive flexibility. In the reversal task, there were no significant effects of time, surgery, and apocynin treatment on the escape latency when comparing between groups, which suggests mice from all groups failed to learn the new location and apocynin did not help to improve the visuo-spatial learning when the task was enhanced (Figure 5-10). In the 72 hours reversal probe test, mice from all four groups spent time lower than chance (Sham vehicle 20.36 ± 15.50, BCAS vehicle 26.79 ± 16.79, Sham apocynin 20.46 ± 26.14, BCAS apocynin: 15.79 ± 117.46) (Figure 5-10). In summary, apocynin did not restore the impaired visuo-spatial learning and memory at 3 months following BCAS surgery (Figure 5-10).

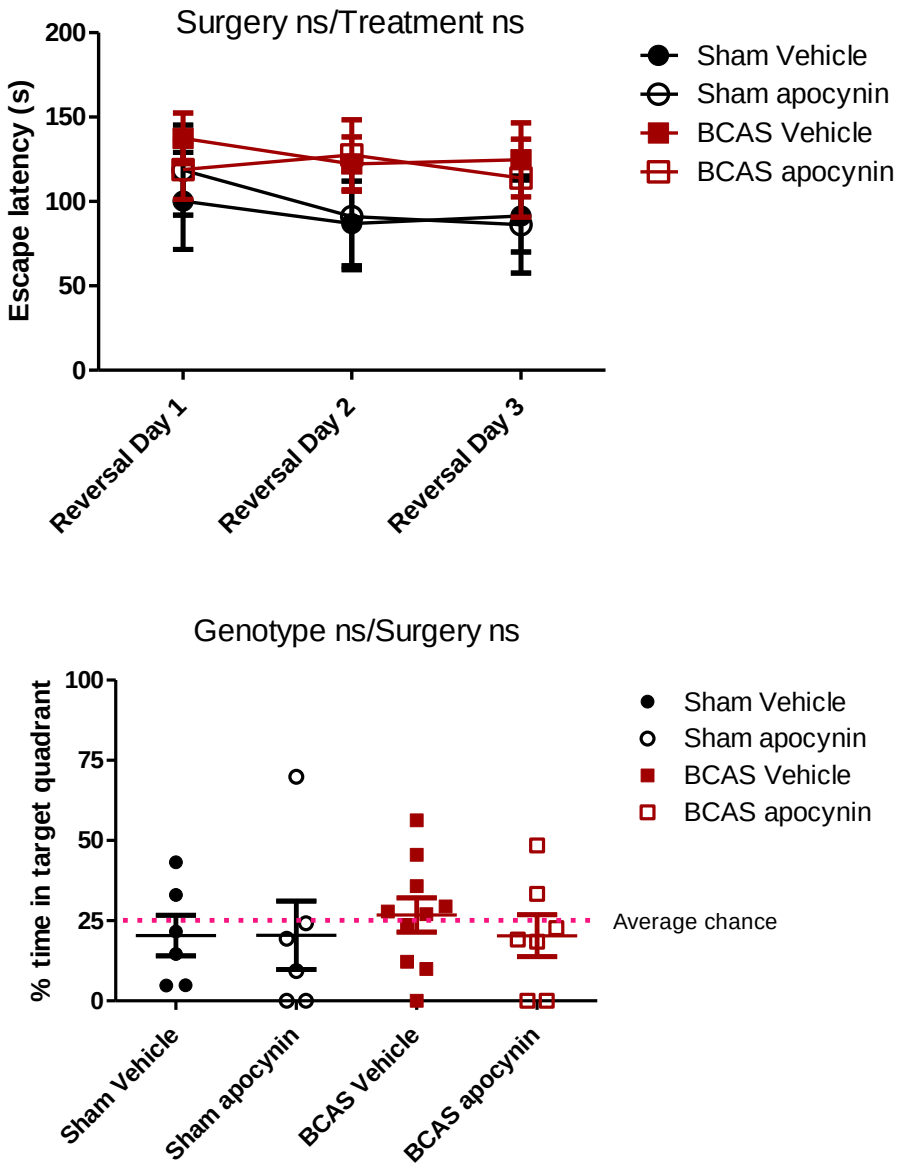

Figure 5-10 Apocynin did not improve spatial learning and memory in the reversal acquisition and probe trial.

In the reversal task, there were no significant effects of time, surgery, and apocynin treatment on the escape latency when comparing between groups, which suggested mice from all groups failed to learn the new location and apocynin did not help to improve the visuo-spatial learning when the task was enhanced. In the 72 hours reversal probe test, mice from all four groups spent time lower than by chance; ns indicates not significant (p>0.05). n=6 sham vehicle, n=6 sham apocynin, n=10 BCAS vehicle, n=7 BCAS apocynin. In summary, apocynin did not restore the impaired visuo-spatial learning and memory at 3 months following BCAS surgery.

6. Discussion

Several reports have shown that NADPH oxidase is a potential target contributing to the pathogenesis of cognitive impairment (Park et al., 2008, Choi et al., 2014, Toyama et al., 2014, Han et al., 2015). However, these studies demonstrated that whilst apocynin treatment had a beneficial effect on the neurovascular function, it was unable to restore the BCAS-induced degenerative changes and impaired cognitive function.

6.1 NADPH oxidase inhibitor impacts on the CBF and vascular function

Prior evidence has suggested NOX2 is the primary source of reactive oxygen species (ROS) in several conditions including hypertension, hypercholesterolaemia, diabetes and ageing, and so they are significant producers of oxidative stress leading to endothelial dysfunction and vascular inflammation (Drummond et al., 2011). Among the NOX isoforms, NOX2 has been the most widely studied in cerebral vascular diseases such as focal ischaemia and stroke. The use of pharmacological inhibitors of NADPH oxidase (NOX) to defeat oxidative stress and its cerebral perfusion deficits has been supported by the previous evidence (Yao et al., 2017, Han et al., 2015). When apocynin (1.5 mM) was fed in drinking water for 10-12 weeks, the responses of a live pial vessel to vascular smooth muscle cell-dependent vasodilators and constrictor and endothelial cell-dependent vasodilator were restored in aged Tg2576 mice through the mechanism of reducing oxidative stress (Han et al., 2015). Since cerebral hypoperfusion has been reported as the earliest alteration before the onset of dementia symptoms and shown to have a vital role in the progression of Alzheimer's disease, including the accumulation of amyloid pathology in the cerebral vasculature (Salvadores et al., 2017). In the present study, to elucidate the effect of NADPH oxidase inhibitor on the vascular function following chronic cerebral hypoperfusion and its interactions with amyloid pathology, Tg-SwDI mice subjected to BCAS were given apocynin in drinking water for 3 months. The dose of apocynin (1.5 mM) was selected from previous studies in which mice were treated with apocynin in drinking water (Han et al., 2015).

Notably, it was shown that there were significantly higher perfusion responses after whisker stimulation in apocynin treated BCAS mice compared to vehicle treated group, indicating a restored vascular function by apocynin. Our finding is in line with Han and colleagues who reported a protective effect of apocynin on cerebral vascular dysfunction in aged Tg2576 mice (Han et al., 2015).

In another study on NOX2-null mice, angiotensin II (Ang II) was shown to have a detrimental effect on neurovascular coupling, evoking an impaired CBF response to the neural activity via a mechanism involving NOX mediated reactive oxygen species (Kazama et al., 2004). These effects were blocked after the administration of ROS scavenger Mn(III)tetrakis (4-benzoic acid) porphyrin and by the NOX inhibitor apocynin. Furthermore, Ang II significantly increased mean arterial pressure in the neocortex and the immediate superfusion of ROS scavenger restored the neurovascular coupling that was impaired by increased arterial pressure.

Hypertension has been suggested as a major vascular risk factor contributing to the vascular dysfunction leading to the development of vascular cognitive impairment. It has also been suggested that ROS, the main product of NADPH oxidase, is a crucial factor influencing vascular function during hypertension. Our present study has provided additional evidence that following BCAS induced cerebral vascular dysfunction, blocking the NADPH oxidase can be a potential strategy to restore damaged cerebral vascular responses. These studies provide important evidence that oxidative stress may play a common role in vascular disease. Notably, targeting the NOX-derived ROS using the pharmacological NOX inhibitor apocynin can restore vascular function after damage to the cerebral vascular system. The deletion of NOX2 in aged Tg2576 mice has also been linked to rescue cerebrovascular dysfunction, which was in line with the effect of NADPH oxidase inhibitor MnTBAP that counteracted the neurovascular dysfunction in aged Tg2576 mice (Park et al., 2008).

However, ROS are potent signalling molecules that are involved in both physiological and pathological cellular functions. ROS has been shown to increase the CBF via endothelium-

dependent vasodilators (Niwa et al., 2001a, Rosenblum, 1987) and to disrupt the cerebrovascular regulation in conditions including ageing and Alzheimer's disease (Iadecola, 2004). In the previous study, CBF was shown to be increased by the exogenous NADPH through NADPH oxidase-dependent and independent mechanisms (Park et al., 2004b). When CBF was measured using laser Doppler imaging, the CBF increase was attenuated by a free radical scavenger MnTBAP but not by the H_2O_2 scavenger catalase. The CBF increase was also attenuated by NOX inhibitor (gp91ds-tat) and by the nitric oxide synthase inhibitor *N*ω-nitro-L-arginine. There was also an attenuated increase in CBF by NADPH in the gp91-null mice supporting the involvement of NOX. In the present study, an increase of cortical blood flow after feeding 3 months of apocynin was observed, suggesting a long-term beneficial effect that inhibition of NADPH oxidase ameliorates CBF following BCAS. Our result does not support the data that the NOX inhibitor attenuated CBF after cerebral vascular insults.

6.2 NADPH oxidase inhibitor did not improve cerebrovascular pathology

Several studies have described NOX isoforms in the cerebral vasculature, suggestive that inhibition of the ROS-producing NADPH oxidases activity may benefit cerebrovascular disease (Chrissobolis and Faraci, 2008, De Silva and Miller, 2016). Moreover, evidence revealed that the expression of NOX in multiple cell types in the brain as the primary sources of ROS involved in ischaemic brain injury. It has been reported by Walder et al. that the infarct volume was significantly reduced in mice lacking functional type 2 NADPH oxidase (NOX2), suggesting NOX2 is a key mediator in the pathogenesis of ischaemia-reperfusion injury in the CNS (Walder et al., 1997). NOX2 has been shown accounting for the oxidative stress that contributes to the vascular related stroke lesions in focal and global stroke models (De Silva et al., 2011, Brait et al., 2010). More importantly, targeting NOX2-derived superoxide by apocynin was shown to be neuroprotective that led to reduced infarct volume, indicating its promising effect on ischaemic brain injury (Chen et al., 2009, Tang et al., 2008, Jackman et al., 2009). These studies have provided numerous evidence that apocynin has a

protective role on experimental stroke models. In a study using transient middle cerebral artery occlusion (tMCAO) model, apocynin was given intravenously at different doses and shown to reduce the volume of infarcts, cerebral haemorrhage and neurological function (Tang et al., 2008). Moreover, in another study looking at the effect of apocynin in BCAS model after a short-term of surgery, they reported improved outcomes of white matter lesions, reduced haemorrhagic lesions as well as astrocytes activation after apocynin treatment (Toyama et al., 2014). In the present study, apocynin did not rescue vascular related lesions such as microinfarcts and haemorrhages following 3 months of treatment. Current data supports the finding that apocynin has a protective effect on the vascular function but not the coexisting pathological changes in the microvasculature.

In previous literature, a dose-dependent effect of apocynin has been indicated. A wide range of doses might be associated with different treatment outcomes. Various results suggest that the daily administration of apocynin in drinking water at different doses (30, 150 and 300 mg/kg) in a mouse model of amyotrophic lateral sclerosis (ALS) led to an improved survival rate with increasing doses of apocynin (Harraz et al., 2008). By contrast, an apocynin dose below 5 mg/kg was considered ineffective to provide a protective effect against neurodegenerative changes (Ferreira et al., 2013). It is worth noting that in my study 5 mice from the vehicle treated group were culled due to the severe damage or poor recovery after the BCAS surgery compared to the apocynin treated group. A higher dose of apocynin at 3.75 or 5 mg/kg was shown to increase the brain haemorrhage compared to 2.5 mg/kg that reduced infarct volume. A narrow dose range has therefore been suggested when acutely applying the selective NOX inhibitor apocynin in experimental stroke models (Tang et al., 2008).

Apocynin has also been shown to reduce the cerebral infarct volume in pre-treatment and absent in post-treatment. In another study, apocynin was applied 0.5 h prior to the ischaemia induced by MCAO. As a result, infarct volume, neurological impairment and mortality were improved by the pre-treatment. By contrast, treatment given 1 h post MCAO did not have a

protective effect. My data provide evidence that long-term administration of apocynin could not protect the brain against cerebral infarcts caused by lasting hypoperfusion. Although most of the studies support the protective role of apocynin on the brain post-ischaemic injuries, it is suspected that in aged animals after MCAO, there is an increased mortality rate and failure to restore functional outcome, infarct size, BBB integrity have been observed (Jackman et al., 2009). In the current study, there was also an unexpected vascular lesion in the sham apocynin treated group suggesting a risk of worsened vascular related pathological outcome may happen when treating against ischaemic injuries especially in aged animals involving vascular amyloidosis. In summary, apocynin is so far the most selective inhibitor for NOX and is thought to effectively block the activation of the enzyme by preventing translocation of p47*phox*. However, the data from the current study suggest apocynin was not able to ameliorate vascular related lesions following chronic cerebral hypoperfusion in the model expressing microvascular amyloid.

6.3 NADPH oxidase inhibitor and amyloid accumulation

Vascular oxidative stress has been shown to play a causal role in vascular amyloid-induced cerebrovascular dysfunction, accumulation of microvascular amyloid and related brain haemorrhagic injuries (Han et al., 2015). Amyloid accumulation in the cerebral vasculature is one of the pathological hallmarks of AD and is recognised as a strong risk factor for cerebral ischaemic lesion, intracerebral haemorrhage and cognitive impairment. Recently, Han and colleagues provided evidence that NADPH oxidase-derived ROS is the key mediator of vascular amyloid-induced cerebral vascular deficits. In their study, apocynin was applied to reduce oxidative stress leading to a reduction in vascular amyloid accumulation and related vasomotor impairment (Han et al., 2015). Besides, apocynin also reduced ApoE levels, with no significant effect on the levels of Aβ40 and Aβ42 nor the Aβ40/Aβ42 ratios in the cerebral cortex and CSF.

The exact role of oxidative stress in the development of Aβ accumulation in the parenchyma and cerebral vasculature is not fully understood. In my study, the combination of BCAS with Tg-SwDI mice allowed me to investigate the effect of a NOX inhibitor on the microvascular amyloid load in response to chronic cerebral hypoperfusion. The data suggests no significant effect of apocynin on the amyloid load in the microvasculature, parenchyma and total amyloid in the cerebral cortex. This is in line with past literature that apocynin treatment was not sufficient to alter the amyloid load in aged Tg2576 mice (Park et al., 2008). Mice overexpressing the Swedish mutation of the APP (Tg2576) crossed with mice deficient in the NOX2 subtype of NADPH oxidase have been studied to determine the role of NOX2 in the formation of vascular amyloid (Park et al., 2008). Park et al. showed the deletion of NOX2 in aged Tg2576 mice did not develop oxidative stress, neurovascular dysfunction and cognitive deficits, which were independent of brain plaque load and Aβ levels. Given the fact that amyloid levels are determined by the production and clearance of Aβ in the brain, although the apocynin improved vascular function and reduced perfusion, the effect of apocynin treatment might not be enough to reverse the damage caused by a combined effect of BCAS and amyloid toxicity. In the current study, the level amyloid species was not investigated to test the effect of apocynin on the Aβ peptide pools that have been reported to be affected in Tg-SwDI model following BCAS (Salvadores et al., 2017).

Another consideration regarding the ineffectiveness of apocynin against amyloid accumulation is its role in the glymphatic pathway. In the previous study (Chapter 3 and 4), an impairment in glymphatic function was observed following BCAS, and this was postulated to accelerate the Aβ accumulation in the cerebral microvasculature. It is still unclear whether NOX playing a role in the glymphatic pathway, since it is a common target associated with vascular dysfunction and neurogenerative changes.

6.4 NADPH oxidase inhibitor impacts on the cognitive function

Oxidative stress is one of the factors contributing to the pathogenesis of dementia, such as AD and VaD. Moreover, administration of antioxidants has been reported to ameliorate cognitive impairment in animal models of vascular cognitive impairment (VCI). Histidine, a precursor of histamine with properties in antioxidant, anti-apoptosis, and against excitotoxicity, shows neuroprotective effects that alleviate cognitive impairment caused by chronic cerebral hypoperfusion (Song et al., 2018). Similarly, polyphenol antioxidants have been reported to reduce cognitive decline and superoxide levels following chronic cerebral hypoperfusion (Xu et al., 2010). A recent study focused more specifically on the inhibition of NOX2 in animal models of VCI has shown neuroprotective effects of apocynin against motor and spatial memory deficits following transient global cerebral ischaemia (Shen et al., 2011). Other pharmaceutical methods targeting the NOX2's subunit Rac1-GTPase also reduces oxidative stress and reference memory deficit following global cerebral ischaemia (Zhang et al., 2009) (Raz et al., 2010). Furthermore, in another investigation on the CCH induced by bilateral occlusion of the common carotid arteries (2VO), apocynin, as well as adeno-associated virus (AAV) mediated NOX1 knockdown, reduced memory impairment, superoxide generation and hippocampal neuronal death (Choi et al., 2014). In the present study, apocynin did not show a beneficial effect in reducing the cognitive impairment induced by BCAS. In the acquisition training tests, regardless of apocynin treatment, BCAS mice took relatively longer time to escape compared to the sham groups, indicating a more powerful effect of BCAS over the apocynin on the spatial learning ability in the Tg-SwDI mice. This is further evident even after the difficulty is increased in the reversal training tests. In the 72 h probe tests that evaluate the long-term memory function, the apocynin treated BCAS group shows a lower chance staying in the target quadrant compared to the vehicle treated group with both sham groups performed nicely above the chance. Furthermore, the BCAS mice that received apocynin treatment also presented a higher number of mice that spent no time

in the target quadrant (3/8 in 72 h and 2/8 in reversal 72 h probe test) suggesting no beneficial effect of apocynin on the long-term memory after a period of hypoperfusion effect.

6.5 Conclusions

Vascular cognitive impairment (VCI) refers to the full spectrum of disorders associated with cerebrovascular disease (CVD). Vascular dementia is a severe form of VCI and is the second most prevalent cause of age-related cognitive impairment and dementia after Alzheimer's disease (AD). There is mounting evidence that management of vascular risk factors may assist in preventing dementia including AD (Dichgans and Leys, 2017). Recent advances have suggested the role of oxidative stress in the pathogenesis of CVD and AD that shows a promising effect by targeting NADPH oxidase to reduce the pathological changes leading to cognitive deficits. Therefore, in the present study, we focused on an AD model that expresses an average level of amyloid in the cerebral vasculature and combine the long-term cerebral hypoperfusion with building a more clinically relevant model and tested a range of effects following antioxidant treatment. This set of data suggested that the NOX inhibitor apocynin provided powerful effects to restore cortical perfusion as well as vascular function. However, apocynin was not able to affect the amyloid load and reduce ultimately improve cognitive performance. These data have provided novel evidence in a well-established preclinical VCI model and challenging the view that targeting NADPH oxidases is an effective therapeutic strategy to treat VCI.

Despite the fact that the amyloid accumulation was investigated in the current study, the exact changes in the soluble and insoluble species of Aβ is still unclear. Since Tg-SwDI mice do not express high-level oligomeric amyloid, a further study looking at the biochemical changes following the treatment of apocynin in this model will provide useful information. Furthermore, due to the lack of available inhibitor that targets the specific NOX isoforms. The current study was unable to selectively block the NOX2 enzyme among others. Future work targeting the NOX2 specific isoforms using transgene model (e.g. NOX2 knockout or

overexpressing model) or developing more selective pharmacological compounds may be useful to provide additional evidence.

Chapter 6. General discussion

The findings in this thesis present novel evidence of how carotid stenosis damages the cerebral microcirculation and structure, contributing to the pathogenesis of cognitive impairment. Specifically, long-term bilateral common carotid stenosis causes chronic cerebral hypoperfusion as a primary outcome and impaired glymphatic function, which is likely to contribute to the accumulation of Aβ in the microvasculature. Additionally, carotid stenosis causes sustained cerebral hypoperfusion and leads to secondary outcomes including impaired neurovascular coupling, neurodegenerative changes and cognitive deficits. However, despite evidence supporting a basis for targeting NADPH oxidase, there was an only modest beneficial effect of the NOX inhibitor on neurovascular function.

Collectively, this thesis provides evidence that following the carotid stenosis, while reducing cerebral perfusion, it may also affect the glymphatic drainage pathway, leading to cognitive impairment. These new data add credence to a growing body of human studies that have challenged the theory that hypoperfusion is the major contributor leading to VCI, and instead alternate or additional mechanisms need to be considered (Shi et al., 2018, Aribisala et al., 2014a, Wardlaw et al., 2017, Alhusaini et al., 2018). The treatment with non-selective NOX inhibitor successfully restored blood perfusion and vascular function with no ultimate improvement in cognitive function, suggesting a limited role in targeting NOX to restore the full pathological processes in VCI. Thus, further studies using more specific method targeting post-carotid stenosis events will help to understand the proposed mechanisms and provide a therapeutic strategy.

1. Limitations

The studies are limited by the lack of CAA models that is ethically available for studying a long-term effect of carotid stenosis on Aβ deposition. In my thesis, I have used a heterozygous Tg-SwDI mouse model that predominantly expresses microvascular Aβ. The results from behavioural tests revealed that vascular amyloid alone was unlikely to cause

cognitive impairment. This is not in agreement with the previous study that conducted behavioural tests on homozygous Tg-SwDI mice (Xu et al., 2007). A consideration of using heterozygous Tg-SwDI model was due to a high mortality risk of performing BCAS surgery on homozygous Tg-SwDI mice and it was not practical to observe combined BCAS and Aβ effects over a period of three months. Further, accumulation of the peptide Aβ and tau protein in brains are thought to both initiates the pathological process of AD. Being limited to AD model in this thesis, it was not possible to assess the impact of BCAS on the accumulation of tau protein in the brains. Further studies using different AD models need to be carried out in order to validate how carotid stenosis influences other forms of Aβ and tau protein and whether there would be interactions in the pathophysiological processes leading to cognitive impairment.

Another limitation of my thesis is that the glymphatic drainage pathway was primarily investigated as it was hypothesized to accelerate the Aβ accumulation in the cerebral microvasculature. However, other clearance mechanisms might be also involved in the accumulation of Aβ and affected by BCAS. The role of BBB transport is important for maintaining the homeostasis of Aβ in the brain. Evidence also suggests that vascular-mediated pathophysiology can lead to BBB dysfunction that is associated with the accumulation of molecules such as Aβ within the brain parenchyma (Zlokovic, 2011). Whether BCAS has any impact on receptors mediating Aβ across BBB, such as the receptor for advanced glycation end products (RAGE) and low-density lipoprotein receptor-related protein 1 (LRP1), is largely unknown. This would be a fruitful area for further work studying BBB changes following BCAS and its contribution to the formation of CAA. More information on these vascular-mediated clearance pathways (i.e. BBB and glymphatic pathway) would help us to establish a greater understanding of the mechanisms that lead to VCI.

2. Future directions

Future investigations on the role of the glymphatic system in the pathogenesis of vascular cognitive impairment and dementia is an encouraging field. As described previously, the glymphatic system is a drainage pathway depending on the cerebral vascular network and its cellular components in the brain. In cerebral vascular diseases, it is reasonable to postulate that the homeostasis and the integrity of the cerebral vascular system are disrupted, and therefore impaired glymphatic system fails to remove the waste out of the brain, which may lead to a vicious circle. Given the fact that the accumulation of Aβ in the brain is a common finding in elderly people with VaD and AD, the present studies highlighted the link between vascular disturbances and the Aβ accumulation in the vasculature. Specifically, carotid stenosis is the initiator that influences brain haemodynamics in the blood vessels as well as the glymphatic pathway in the perivascular regions. Therefore, longitudinal studies of the population with carotid stenosis would help to detect the development or changes in the patients exposed to such risk factors across the life span.

The glymphatic system has been proposed to have three functional stages: the CSF glymphatic influx, CSF and interstitial fluid (ISF) exchange and the final efflux stage. The current studies are focused on the CSF glymphatic influx, which is the process most relevant to the cerebral vascular system and the CAA model. Future work is needed to confirm whether altered glymphatic function in response to carotid stenosis/cerebral hypoperfusion also applies in the patients diagnosed with AD or VaD. The glymphatic system has been visualised in animal studies using a variety of approaches including *ex vivo* microscopy and *in vivo* imaging such as two-photon microscopy and MRI. However, visualising glymphatic system in human is an emerging field, and progress has been made to achieve a non-invasive or minimally invasive method. Novel techniques such as contrast-enhanced MR imaging may provide *in vivo* information of access to all brain subregions. By injecting contrast agents into the CSF, the MRI imaging can visualise glymphatic flow in a 3-

dimension and real-time manner. It also enables the quantification of glymphatic function in both experiments and clinical settings (Iliff et al., 2013a, Ringstad et al., 2018).

The outflow routes of CSF in neurological disorders are still poorly documented. However, recent studies have reported a variety of efflux pathways in rodents. These outflow sites include perineural sheaths surrounding cranial and spinal nerves (Ma et al., 2017b, Johnston et al., 2004a), dura lymphatic vessels (Louveau et al., 2015), skull (Cai et al., 2019, Ahn et al., 2019) and arachnoid granulations (Pollay, 2010). Whether carotid stenosis affects these post-glymphatic outflow pathway is unclear, and its interrelation with cerebral hypoperfusion and soluble Aβ require further investigation.

Besides, in response to cerebral hypoperfusion, Aβ accumulation is associated with increased NOX2 that contributes to cerebral vascular dysfunction and the development of vascular related lesions (Salvadores et al., 2017). In the current studies, apocynin treatment did not improve the vascular pathology and the cognitive function but demonstrated strong effect ameliorating vascular function. Therefore, future studies using NOX2 specific inhibitors that can block the individual isoforms within the NOX2 complex is urgently demanded. Novel NOX2 specific inhibitors CPP11G and CPP11H demonstrated beneficial effects ameliorating TNFα-induced ROS and neuroinflammation and shown to improve vascular function and hind-limb blood flow (Li et al., 2019). These studies support the therapeutic value of NOX2 inhibition in periphery inflammatory disease. However, more evidence is still needed to confirm whether these compounds are suitable for the use in the scenario of neurological disorders (e.g. BBB permeability) and safety-related issues. The observed improvement in blood perfusion and neurovascular coupling indicates apocynin still has beneficial effects on the neuro-glial-vascular network. Further studies regarding its role on CSF movement and neuronal and glial cells would be worthwhile.

References

AHN, J. H., CHO, H., KIM, J. H., KIM, S. H., HAM, J. S., PARK, I., SUH, S. H., HONG, S. P., SONG, J. H., HONG, Y. K., JEONG, Y., PARK, S. H. & KOH, G. Y. 2019. Meningeal lymphatic vessels at the skull base drain cerebrospinal fluid. *Nature,* 572**,** 62-66.

ALHUSAINI, S., KARAMA, S., NGUYEN, T. V., THIEL, A., BERNHARDT, B. C., COX, S. R., CORLEY, J., TAYLOR, A., EVANS, A. C., STAR, J. M., BASTIN, M. E., WARDLAW, J. M., DEARY, I. J. & DUCHARME, S. 2018. Association between carotid atheroma and cerebral cortex structure at age 73 years. *Ann Neurol,* 84**,** 576-587.

ALOSCO, M. L., BRICKMAN, A. M., SPITZNAGEL, M. B., GARCIA, S. L., NARKHEDE, A., GRIFFITH, E. Y., RAZ, N., COHEN, R., SWEET, L. H., COLBERT, L. H., JOSEPHSON, R., HUGHES, J., ROSNECK, J. & GUNSTAD, J. 2013. Cerebral perfusion is associated with white matter hyperintensities in older adults with heart failure. *Congest Heart Fail,* 19**,** E29-34.

ALSOP, D. C., DAI, W., GROSSMAN, M. & DETRE, J. A. 2010. Arterial spin labeling blood flow MRI: its role in the early characterization of Alzheimer's disease. *J Alzheimers Dis,* 20**,** 871-80.

ANSARI, M. A. & SCHEFF, S. W. 2011. NADPH-oxidase activation and cognition in Alzheimer disease progression. *Free Radic Biol Med,* 51**,** 171-8.

ANSTEY, K. J., VON SANDEN, C., SALIM, A. & O'KEARNEY, R. 2007. Smoking as a risk factor for dementia and cognitive decline: a meta-analysis of prospective studies. *Am J Epidemiol,* 166**,** 367-78.

ARIBISALA, B. S., MORRIS, Z., EADIE, E., THOMAS, A., GOW, A., VALDES HERNANDEZ, M. C., ROYLE, N. A., BASTIN, M. E., STARR, J., DEARY, I. J. & WARDLAW, J. M. 2014a. Blood pressure, internal carotid artery flow parameters, and age-related white matter hyperintensities. *Hypertension,* 63**,** 1011-8.

ARIBISALA, B. S., WISEMAN, S., MORRIS, Z., VALDES-HERNANDEZ, M. C., ROYLE, N. A., MANIEGA, S. M., GOW, A. J., CORLEY, J., BASTIN, M. E., STARR, J., DEARY, I. J. & WARDLAW, J. M. 2014b. Circulating inflammatory markers are associated with magnetic resonance imaging-visible perivascular spaces but not directly with white matter hyperintensities. *Stroke,* 45**,** 605-7.

ARIES, M. J., ELTING, J. W., DE KEYSER, J., KREMER, B. P. & VROOMEN, P. C. 2010. Cerebral autoregulation in stroke: a review of transcranial Doppler studies. *Stroke,* 41**,** 2697-704.

ARNTZEN, K. A., SCHIRMER, H., JOHNSEN, S. H., WILSGAARD, T. & MATHIESEN, E. B. 2012. Carotid atherosclerosis predicts lower cognitive test results: a 7-year follow-up study of 4,371 stroke-free subjects - the Tromso study. *Cerebrovasc Dis,* 33**,** 159-65.

ARVANITAKIS, Z., CAPUANO, A. W., LEURGANS, S. E., BENNETT, D. A. & SCHNEIDER, J. A. 2016. Relation of cerebral vessel disease to Alzheimer's disease dementia and cognitive function in elderly people: a cross-sectional study. *Lancet Neurol,* 15**,** 934-943.

ASGARI, M., DE ZELICOURT, D. & KURTCUOGLU, V. 2016. Glymphatic solute transport does not require bulk flow. *Sci Rep,* 6**,** 38635.

ATTEMS, J., JELLINGER, K., THAL, D. R. & VAN NOSTRAND, W. 2011. Review: sporadic cerebral amyloid angiopathy. *Neuropathol Appl Neurobiol,* 37**,** 75-93.

AURIEL, E. & GREENBERG, S. M. 2012. The pathophysiology and clinical presentation of cerebral amyloid angiopathy. *Curr Atheroscler Rep,* 14**,** 343-50.

AYER, R. E. & ZHANG, J. H. 2008. Oxidative stress in subarachnoid haemorrhage: significance in acute brain injury and vasospasm. *Acta Neurochir Suppl,* 104**,** 33-41.

BALESTRINI, S., PEROZZI, C., ALTAMURA, C., VERNIERI, F., LUZZI, S., BARTOLINI, M., PROVINCIALI, L. & SILVESTRINI, M. 2013. Severe carotid stenosis and impaired cerebral hemodynamics can influence cognitive deterioration. *Neurology,* 80**,** 2145-50.

BALLERIO, R., GIANAZZA, E., MUSSONI, L., MILLER, I., GELOSA, P., GUERRINI, U., EBERINI, I., GEMEINER, M., BELCREDITO, S., TREMOLI, E. & SIRONI, L. 2007. Gender differences in endothelial function and inflammatory markers along the occurrence of pathological events in stroke-prone rats. *Exp Mol Pathol,* 82**,** 33-41.

BARKER, R., ASHBY, E. L., WELLINGTON, D., BARROW, V. M., PALMER, J. C., KEHOE, P. G., ESIRI, M. M. & LOVE, S. 2014. Pathophysiology of white matter perfusion in Alzheimer's disease and vascular dementia. *Brain,* 137**,** 1524-32.

BARNHAM, K. J., MASTERS, C. L. & BUSH, A. I. 2004. Neurodegenerative diseases and oxidative stress. *Nat Rev Drug Discov,* 3**,** 205-14.

BARONE, F. C., KNUDSEN, D. J., NELSON, A. H., FEUERSTEIN, G. Z. & WILLETTE, R. N. 1993. Mouse strain differences in susceptibility to cerebral ischemia are related to cerebral vascular anatomy. *J Cereb Blood Flow Metab,* 13**,** 683-92.

BATEMAN, R. J., XIONG, C., BENZINGER, T. L., FAGAN, A. M., GOATE, A., FOX, N. C., MARCUS, D. S., CAIRNS, N. J., XIE, X., BLAZEY, T. M., HOLTZMAN, D. M., SANTACRUZ, A., BUCKLES, V., OLIVER, A., MOULDER, K., AISEN, P. S., GHETTI, B., KLUNK, W. E., MCDADE, E., MARTINS, R. N., MASTERS, C. L., MAYEUX, R., RINGMAN, J. M., ROSSOR, M. N., SCHOFIELD, P. R., SPERLING, R. A., SALLOWAY, S., MORRIS, J. C. & DOMINANTLY INHERITED ALZHEIMER, N. 2012. Clinical and biomarker changes in dominantly inherited Alzheimer's disease. *N Engl J Med,* 367**,** 795-804.

BELANGER, M., ALLAMAN, I. & MAGISTRETTI, P. J. 2011. Brain energy metabolism: focus on astrocyte-neuron metabolic cooperation. *Cell Metab,* 14**,** 724-38.

BOUVY, W. H., ZWANENBURG, J. J. M., REININK, R., WISSE, L. E. M., LUIJTEN, P. R., KAPPELLE, L. J., GEERLINGS, M. I., BIESSELS, G. J. & UTRECHT VASCULAR COGNITIVE IMPAIRMENT STUDY, G. 2016. Perivascular spaces on 7 Tesla brain MRI are related to markers of small vessel disease but not to age or cardiovascular risk factors. *J Cereb Blood Flow Metab,* 36**,** 1708-1717.

BRAIT, V. H., JACKMAN, K. A., WALDUCK, A. K., SELEMIDIS, S., DIEP, H., MAST, A. E., GUIDA, E., BROUGHTON, B. R., DRUMMOND, G. R. & SOBEY, C. G. 2010. Mechanisms contributing to cerebral infarct size after stroke: gender, reperfusion, T lymphocytes, and Nox2-derived superoxide. *J Cereb Blood Flow Metab,* 30**,** 1306-17.

BRANDES, R. P. 2003. Role of NADPH oxidases in the control of vascular gene expression. *Antioxid Redox Signal,* 5**,** 803-11.

BRUCE-KELLER, A. J., GUPTA, S., PARRINO, T. E., KNIGHT, A. G., EBENEZER, P. J., WEIDNER, A. M., LEVINE, H., 3RD, KELLER, J. N. & MARKESBERY, W. R. 2010. NOX activity is increased in mild cognitive impairment. *Antioxid Redox Signal,* 12**,** 1371-82.

BRUNDEL, M., DE BRESSER, J., VAN DILLEN, J. J., KAPPELLE, L. J. & BIESSELS, G. J. 2012. Cerebral microinfarcts: a systematic review of neuropathological studies. *J Cereb Blood Flow Metab,* 32**,** 425-36.

BU, G. 2009. Apolipoprotein E and its receptors in Alzheimer's disease: pathways, pathogenesis and therapy. *Nat Rev Neurosci,* 10**,** 333-44.

BUCUR, B. & MADDEN, D. J. 2010. Effects of adult age and blood pressure on executive function and speed of processing. *Exp Aging Res,* 36**,** 153-68.

CAI, R., PAN, C., GHASEMIGHARAGOZ, A., TODOROV, M. I., FORSTERA, B., ZHAO, S., BHATIA, H. S., PARRA-DAMAS, A., MROWKA, L., THEODOROU, D., REMPFLER, M., XAVIER, A. L. R., KRESS, B. T., BENAKIS, C., STEINKE, H., LIEBSCHER, S., BECHMANN, I., LIESZ, A., MENZE, B., KERSCHENSTEINER, M., NEDERGAARD, M. & ERTURK, A. 2019. Panoptic imaging of transparent mice reveals whole-body neuronal projections and skull-meninges connections. *Nat Neurosci,* 22**,** 317-327.

CALHOUN, M. E., BURGERMEISTER, P., PHINNEY, A. L., STALDER, M., TOLNAY, M., WIEDERHOLD, K. H., ABRAMOWSKI, D., STURCHLER-PIERRAT, C., SOMMER, B., STAUFENBIEL, M. & JUCKER, M. 1999. Neuronal overexpression of mutant amyloid precursor protein results in prominent deposition of cerebrovascular amyloid. *Proc Natl Acad Sci U S A,* 96**,** 14088-93.

CHAO, L. L., BUCKLEY, S. T., KORNAK, J., SCHUFF, N., MADISON, C., YAFFE, K., MILLER, B. L., KRAMER, J. H. & WEINER, M. W. 2010. ASL perfusion MRI predicts cognitive decline and conversion from MCI to dementia. *Alzheimer Dis Assoc Disord,* 24**,** 19-27.

CHARIDIMOU, A., BOULOUIS, G., GUROL, M. E., AYATA, C., BACSKAI, B. J., FROSCH, M. P., VISWANATHAN, A. & GREENBERG, S. M. 2017. Emerging concepts in sporadic cerebral amyloid angiopathy. *Brain,* 140**,** 1829-1850.

CHARIDIMOU, A., GANG, Q. & WERRING, D. J. 2012. Sporadic cerebral amyloid angiopathy revisited: recent insights into pathophysiology and clinical spectrum. *J Neurol Neurosurg Psychiatry,* 83**,** 124-37.

CHARIDIMOU, A., MEEGAHAGE, R., FOX, Z., PEETERS, A., VANDERMEEREN, Y., LALOUX, P., BARON, J. C., JAGER, H. R. & WERRING, D. J. 2013. Enlarged perivascular spaces as a marker of underlying arteriopathy in intracerebral haemorrhage: a multicentre MRI cohort study. *J Neurol Neurosurg Psychiatry,* 84**,** 624-9.

CHEN, H., SONG, Y. S. & CHAN, P. H. 2009. Inhibition of NADPH oxidase is neuroprotective after ischemia-reperfusion. *J Cereb Blood Flow Metab,* 29**,** 1262-72.

CHEN, W., SONG, X., ZHANG, Y. & ALZHEIMER'S DISEASE NEUROIMAGING, I. 2011. Assessment of the Virchow-Robin Spaces in Alzheimer disease, mild cognitive impairment, and normal aging, using high-field MR imaging. *AJNR Am J Neuroradiol,* 32**,** 1490-5.

CHENG, H. L., LIN, C. J., SOONG, B. W., WANG, P. N., CHANG, F. C., WU, Y. T., CHOU, K. H., LIN, C. P., TU, P. C. & LEE, I. H. 2012. Impairments in cognitive function and brain connectivity in severe asymptomatic carotid stenosis. *Stroke,* 43**,** 2567-73.

CHOI, D. H., KIM, J. H., LEE, K. H., KIM, H. Y., KIM, Y. S., CHOI, W. S. & LEE, J. 2015. Role of neuronal NADPH oxidase 1 in the peri-infarct regions after stroke. *PLoS One,* 10**,** e0116814.

CHOI, D. H., LEE, K. H., KIM, J. H., SEO, J. H., KIM, H. Y., SHIN, C. Y., HAN, J. S., HAN, S. H., KIM, Y. S. & LEE, J. 2014. NADPH oxidase 1, a novel molecular source of ROS in hippocampal neuronal death in vascular dementia. *Antioxid Redox Signal,* 21**,** 533-50.

CHOW, N., BELL, R. D., DEANE, R., STREB, J. W., CHEN, J., BROOKS, A., VAN NOSTRAND, W., MIANO, J. M. & ZLOKOVIC, B. V. 2007. Serum response factor and myocardin mediate arterial hypercontractility and cerebral blood flow dysregulation in Alzheimer's phenotype. *Proc Natl Acad Sci U S A,* 104**,** 823-8.

CHRISSOBOLIS, S., BANFI, B., SOBEY, C. G. & FARACI, F. M. 2012. Role of Nox isoforms in angiotensin II-induced oxidative stress and endothelial dysfunction in brain. *J Appl Physiol (1985),* 113**,** 184-91.

CHRISSOBOLIS, S. & FARACI, F. M. 2008. The role of oxidative stress and NADPH oxidase in cerebrovascular disease. *Trends Mol Med,* 14**,** 495-502.

CHUNG, Y. A., O, J. H., KIM, J. Y., KIM, K. J. & AHN, K. J. 2009. Hypoperfusion and ischemia in cerebral amyloid angiopathy documented by 99mTc-ECD brain perfusion SPECT. *J Nucl Med,* 50**,** 1969-74.

CIPOLLA, M. J. 2007. Cerebrovascular function in pregnancy and eclampsia. *Hypertension,* 50**,** 14-24.

CIPOLLA, M. J., SMITH, J., KOHLMEYER, M. M. & GODFREY, J. A. 2009. SKCa and IKCa Channels, myogenic tone, and vasodilator responses in middle cerebral arteries and parenchymal arterioles: effect of ischemia and reperfusion. *Stroke,* 40**,** 1451-7.

CLAASSEN, J. A. & ZHANG, R. 2011. Cerebral autoregulation in Alzheimer's disease. *J Cereb Blood Flow Metab,* 31**,** 1572-7.

COLTMAN, R., SPAIN, A., TSENKINA, Y., FOWLER, J. H., SMITH, J., SCULLION, G., ALLERHAND, M., SCOTT, F., KALARIA, R. N., IHARA, M., DAUMAS, S., DEARY, I. J., WOOD, E., MCCULLOCH, J. & HORSBURGH, K. 2011. Selective white matter pathology induces a specific impairment in spatial working memory. *Neurobiol Aging,* 32**,** 2324 e7-12.

DAVIS, J., XU, F., DEANE, R., ROMANOV, G., PREVITI, M. L., ZEIGLER, K., ZLOKOVIC, B. V. & VAN NOSTRAND, W. E. 2004. Early-onset and robust cerebral microvascular

accumulation of amyloid beta-protein in transgenic mice expressing low levels of a vasculotropic Dutch/Iowa mutant form of amyloid beta-protein precursor. *J Biol Chem,* 279**,** 20296-306.

DE HEUS, R. A. A., DE JONG, D. L. K., SANDERS, M. L., VAN SPIJKER, G. J., OUDEGEEST-SANDER, M. H., HOPMAN, M. T., LAWLOR, B. A., OLDE RIKKERT, M. G. M. & CLAASSEN, J. 2018. Dynamic Regulation of Cerebral Blood Flow in Patients With Alzheimer Disease. *Hypertension,* 72**,** 139-150.

DE JONG, G. I., DE VOS, R. A., STEUR, E. N. & LUITEN, P. G. 1997. Cerebrovascular hypoperfusion: a risk factor for Alzheimer's disease? Animal model and postmortem human studies. *Ann N Y Acad Sci,* 826**,** 56-74.

DE LA TORRE, J. C. 2000a. Cerebral hypoperfusion, capillary degeneration, and development of Alzheimer disease. *Alzheimer Dis Assoc Disord,* 14 Suppl 1**,** S72-81.

DE LA TORRE, J. C. 2000b. Critically attained threshold of cerebral hypoperfusion: can it cause Alzheimer's disease? *Ann N Y Acad Sci,* 903**,** 424-36.

DE LA TORRE, J. C. 2000c. Impaired cerebromicrovascular perfusion. Summary of evidence in support of its causality in Alzheimer's disease. *Ann N Y Acad Sci,* 924**,** 136-52.

DE LA TORRE, J. C. 2012a. Cardiovascular risk factors promote brain hypoperfusion leading to cognitive decline and dementia. *Cardiovasc Psychiatry Neurol,* 2012**,** 367516.

DE LA TORRE, J. C. 2012b. Cerebral Hemodynamics and Vascular Risk Factors: Setting the Stage for Alzheimer's Disease. *Journal of Alzheimers Disease,* 32**,** 553-567.

DE SILVA, T. M., BRAIT, V. H., DRUMMOND, G. R., SOBEY, C. G. & MILLER, A. A. 2011. Nox2 oxidase activity accounts for the oxidative stress and vasomotor dysfunction in mouse cerebral arteries following ischemic stroke. *PLoS One,* 6**,** e28393.

DE SILVA, T. M. & FARACI, F. M. 2012. Effects of angiotensin II on the cerebral circulation: role of oxidative stress. *Front Physiol,* 3**,** 484.

DE SILVA, T. M. & MILLER, A. A. 2016. Cerebral Small Vessel Disease: Targeting Oxidative Stress as a Novel Therapeutic Strategy? *Frontiers in Pharmacology,* 7.

DICHGANS, M. & LEYS, D. 2017. Vascular Cognitive Impairment. *Circ Res,* 120**,** 573-591.

DIETRICH, H. H., XIANG, C., HAN, B. H., ZIPFEL, G. J. & HOLTZMAN, D. M. 2010. Soluble amyloid-beta, effect on cerebral arteriolar regulation and vascular cells. *Mol Neurodegener,* 5**,** 15.

DING, J., SIGURETHSSON, S., JONSSON, P. V., EIRIKSDOTTIR, G., CHARIDIMOU, A., LOPEZ, O. L., VAN BUCHEM, M. A., GUETHNASON, V. & LAUNER, L. J. 2017. Large Perivascular Spaces Visible on Magnetic Resonance Imaging, Cerebral Small Vessel Disease Progression, and Risk of Dementia: The Age, Gene/Environment Susceptibility-Reykjavik Study. *JAMA Neurol,* 74**,** 1105-1112.

DOUBAL, F. N., MACLULLICH, A. M., FERGUSON, K. J., DENNIS, M. S. & WARDLAW, J. M. 2010. Enlarged perivascular spaces on MRI are a feature of cerebral small vessel disease. *Stroke,* 41**,** 450-4.

DOYLE, K. P., FATHALI, N., SIDDIQUI, M. R. & BUCKWALTER, M. S. 2012. Distal hypoxic stroke: a new mouse model of stroke with high throughput, low variability and a quantifiable functional deficit. *J Neurosci Methods,* 207**,** 31-40.

DRUMMOND, G. R., SELEMIDIS, S., GRIENDLING, K. K. & SOBEY, C. G. 2011. Combating oxidative stress in vascular disease: NADPH oxidases as therapeutic targets. *Nature Reviews Drug Discovery,* 10**,** 453-471.

DUNCOMBE, J., KITAMURA, A., HASE, Y., IHARA, M., KALARIA, R. N. & HORSBURGH, K. 2017a. Chronic cerebral hypoperfusion: a key mechanism leading to vascular cognitive impairment and dementia. Closing the translational gap between rodent models and human vascular cognitive impairment and dementia. *Clin Sci (Lond),* 131**,** 2451-2468.

DUNCOMBE, J., LENNEN, R. J., JANSEN, M. A., MARSHALL, I., WARDLAW, J. M. & HORSBURGH, K. 2017b. Ageing causes prominent neurovascular dysfunction associated with loss of astrocytic contacts and gliosis. *Neuropathol Appl Neurobiol,* 43**,** 477-491.

DWORAKOWSKI, R., ANILKUMAR, N., ZHANG, M. & SHAH, A. M. 2006. Redox signalling involving NADPH oxidase-derived reactive oxygen species. *Biochem Soc Trans,* 34**,** 960-4.

DWYER, R., SKROBOT, O. A., DWYER, J., MUNAFO, M. & KEHOE, P. G. 2013. Using Alzgene-Like Approaches to Investigate Susceptibility Genes for Vascular Cognitive Impairment. *Journal of Alzheimers Disease,* 34**,** 145-154.

EIDE, P. K., VATNEHOL, S. A. S., EMBLEM, K. E. & RINGSTAD, G. 2018. Magnetic resonance imaging provides evidence of glymphatic drainage from human brain to cervical lymph nodes. *Sci Rep,* 8**,** 7194.

ESIRI, M. M., NAGY, Z., SMITH, M. Z., BARNETSON, L. & SMITH, A. D. 1999. Cerebrovascular disease and threshold for dementia in the early stages of Alzheimer's disease. *Lancet,* 354**,** 919-20.

FANTINI, S., SASSAROLI, A., TGAVALEKOS, K. T. & KORNBLUTH, J. 2016. Cerebral blood flow and autoregulation: current measurement techniques and prospects for noninvasive optical methods. *Neurophotonics,* 3**,** 031411.

FARKAS, E., DONKA, G., DE VOS, R. A., MIHALY, A., BARI, F. & LUITEN, P. G. 2004. Experimental cerebral hypoperfusion induces white matter injury and microglial activation in the rat brain. *Acta Neuropathol,* 108**,** 57-64.

FERREIRA, A. P., RODRIGUES, F. S., DELLA-PACE, I. D., MOTA, B. C., OLIVEIRA, S. M., VELHO GEWEHR CDE, C., BOBINSKI, F., DE OLIVEIRA, C. V., BRUM, J. S., OLIVEIRA, M. S., FURIAN, A. F., DE BARROS, C. S., FERREIRA, J., SANTOS, A. R., FIGHERA, M. R. & ROYES, L. F. 2013. The effect of NADPH-oxidase inhibitor apocynin on cognitive impairment induced by moderate lateral fluid percussion injury: role of inflammatory and oxidative brain damage. *Neurochem Int,* 63**,** 583-93.

FLICKER, L. 2010. Cardiovascular risk factors, cerebrovascular disease burden, and healthy brain aging. *Clin Geriatr Med,* 26**,** 17-27.

FOWLER, J. H., MCQUEEN, J., HOLLAND, P. R., MANSO, Y., MARANGONI, M., SCOTT, F., CHISHOLM, E., SCANNEVIN, R. H., HARDINGHAM, G. E. & HORSBURGH, K. 2017. Dimethyl fumarate improves white matter function following severe hypoperfusion: Involvement of microglia/macrophages and inflammatory mediators. *J Cereb Blood Flow Metab***,** 271678X17713105.

FREEMAN, L. R. & KELLER, J. N. 2012. Oxidative stress and cerebral endothelial cells: regulation of the blood-brain-barrier and antioxidant based interventions. *Biochim Biophys Acta,* 1822**,** 822-9.

GABEREL, T., GAKUBA, C., GOULAY, R., MARTINEZ DE LIZARRONDO, S., HANOUZ, J. L., EMERY, E., TOUZE, E., VIVIEN, D. & GAUBERTI, M. 2014. Impaired glymphatic perfusion after strokes revealed by contrast-enhanced MRI: a new target for fibrinolysis? *Stroke,* 45**,** 3092-6.

GIAU, V. V., BAGYINSZKY, E., YOUN, Y. C., AN, S. S. A. & KIM, S. Y. 2019. Genetic Factors of Cerebral Small Vessel Disease and Their Potential Clinical Outcome. *Int J Mol Sci,* 20.

GILL, P. S. & WILCOX, C. S. 2006. NADPH oxidases in the kidney. *Antioxid Redox Signal,* 8**,** 1597-607.

GORELICK, P. B. 1997. Status of risk factors for dementia associated with stroke. *Stroke,* 28**,** 459-63.

GORELICK, P. B. 2004. Risk factors for vascular dementia and Alzheimer disease. *Stroke,* 35**,** 2620-2.

GORELICK, P. B., SCUTERI, A., BLACK, S. E., DECARLI, C., GREENBERG, S. M., IADECOLA, C., LAUNER, L. J., LAURENT, S., LOPEZ, O. L., NYENHUIS, D., PETERSEN, R. C., SCHNEIDER, J. A., TZOURIO, C., ARNETT, D. K., BENNETT, D. A., CHUI, H. C., HIGASHIDA, R. T., LINDQUIST, R., NILSSON, P. M., ROMAN, G. C., SELLKE, F. W., SESHADRI, S., AMERICAN HEART ASSOCIATION STROKE COUNCIL, C. O. E., PREVENTION, C. O. C. N. C. O. C. R., INTERVENTION, COUNCIL ON CARDIOVASCULAR, S. & ANESTHESIA 2011. Vascular contributions

to cognitive impairment and dementia: a statement for healthcare professionals from the american heart association/american stroke association. *Stroke,* 42**,** 2672-713.
GOTTESMAN, R. F., SCHNEIDER, A. L., ZHOU, Y., CORESH, J., GREEN, E., GUPTA, N., KNOPMAN, D. S., MINTZ, A., RAHMIM, A., SHARRETT, A. R., WAGENKNECHT, L. E., WONG, D. F. & MOSLEY, T. H. 2017. Association Between Midlife Vascular Risk Factors and Estimated Brain Amyloid Deposition. *JAMA,* 317**,** 1443-1450.
GREGG, N. M., KIM, A. E., GUROL, M. E., LOPEZ, O. L., AIZENSTEIN, H. J., PRICE, J. C., MATHIS, C. A., JAMES, J. A., SNITZ, B. E., COHEN, A. D., KAMBOH, M. I., MINHAS, D., WEISSFELD, L. A., TAMBURO, E. L. & KLUNK, W. E. 2015. Incidental Cerebral Microbleeds and Cerebral Blood Flow in Elderly Individuals. *JAMA Neurol,* 72**,** 1021-8.
GUPTA, A. & IADECOLA, C. 2015. Impaired Abeta clearance: a potential link between atherosclerosis and Alzheimer's disease. *Front Aging Neurosci,* 7**,** 115.
HACHINSKI, V. & MUNOZ, D. G. 1997. Cerebrovascular pathology in Alzheimer's disease: cause, effect or epiphenomenon? *Ann N Y Acad Sci,* 826**,** 1-6.
HAFFNER, C., MALIK, R. & DICHGANS, M. 2016. Genetic factors in cerebral small vessel disease and their impact on stroke and dementia. *J Cereb Blood Flow Metab,* 36**,** 158-71.
HAGLUND, M., PASSANT, U., SJOBECK, M., GHEBREMEDHIN, E. & ENGLUND, E. 2006. Cerebral amyloid angiopathy and cortical microinfarcts as putative substrates of vascular dementia. *Int J Geriatr Psychiatry,* 21**,** 681-7.
HAJJAR, I., QUACH, L., YANG, F., CHAVES, P. H., NEWMAN, A. B., MUKAMAL, K., LONGSTRETH, W., JR., INZITARI, M. & LIPSITZ, L. A. 2011. Hypertension, white matter hyperintensities, and concurrent impairments in mobility, cognition, and mood: the Cardiovascular Health Study. *Circulation,* 123**,** 858-65.
HAN, B. H., ZHOU, M. L., JOHNSON, A. W., SINGH, I., LIAO, F., VELLIMANA, A. K., NELSON, J. W., MILNER, E., CIRRITO, J. R., BASAK, J., YOO, M., DIETRICH, H. H., HOLTZMAN, D. M. & ZIPFEL, G. J. 2015. Contribution of reactive oxygen species to cerebral amyloid angiopathy, vasomotor dysfunction, and microhemorrhage in aged Tg2576 mice. *Proc Natl Acad Sci U S A,* 112**,** E881-90.
HARRAZ, M. M., MARDEN, J. J., ZHOU, W., ZHANG, Y., WILLIAMS, A., SHAROV, V. S., NELSON, K., LUO, M., PAULSON, H., SCHONEICH, C. & ENGELHARDT, J. F. 2008. SOD1 mutations disrupt redox-sensitive Rac regulation of NADPH oxidase in a familial ALS model. *J Clin Invest,* 118**,** 659-70.
HATTORI, Y., ENMI, J., IGUCHI, S., SAITO, S., YAMAMOTO, Y., NAGATSUKA, K., IIDA, H. & IHARA, M. 2016. Substantial Reduction of Parenchymal Cerebral Blood Flow in Mice with Bilateral Common Carotid Artery Stenosis. *Sci Rep,* 6**,** 32179.
HERZIG, M. C., VAN NOSTRAND, W. E. & JUCKER, M. 2006. Mechanism of cerebral beta-amyloid angiopathy: murine and cellular models. *Brain Pathol,* 16**,** 40-54.
HOLLAND, C. M., SMITH, E. E., CSAPO, I., GUROL, M. E., BRYLKA, D. A., KILLIANY, R. J., BLACKER, D., ALBERT, M. S., GUTTMANN, C. R. & GREENBERG, S. M. 2008. Spatial distribution of white-matter hyperintensities in Alzheimer disease, cerebral amyloid angiopathy, and healthy aging. *Stroke,* 39**,** 1127-33.
HOLLAND, P. R., BASTIN, M. E., JANSEN, M. A., MERRIFIELD, G. D., COLTMAN, R. B., SCOTT, F., NOWERS, H., KHALLOUT, K., MARSHALL, I., WARDLAW, J. M., DEARY, I. J., MCCULLOCH, J. & HORSBURGH, K. 2011a. MRI is a sensitive marker of subtle white matter pathology in hypoperfused mice. *Neurobiology of Aging,* 32.
HOLLAND, P. R., BASTIN, M. E., JANSEN, M. A., MERRIFIELD, G. D., COLTMAN, R. B., SCOTT, F., NOWERS, H., KHALLOUT, K., MARSHALL, I., WARDLAW, J. M., DEARY, I. J., MCCULLOCH, J. & HORSBURGH, K. 2011b. MRI is a sensitive marker of subtle white matter pathology in hypoperfused mice. *Neurobiol Aging,* 32**,** 2325 e1-6.
HOLLAND, P. R., SEARCY, J. L., SALVADORES, N., SCULLION, G., CHEN, G., LAWSON, G., SCOTT, F., BASTIN, M. E., IHARA, M., KALARIA, R., WOOD, E. R., SMITH, C., WARDLAW, J. M. & HORSBURGH, K. 2015. Gliovascular disruption and cognitive

deficits in a mouse model with features of small vessel disease. *J Cereb Blood Flow Metab*.
HOWARTH, C. 2014. The contribution of astrocytes to the regulation of cerebral blood flow. *Front Neurosci,* 8**,** 103.
HSIAO, K., CHAPMAN, P., NILSEN, S., ECKMAN, C., HARIGAYA, Y., YOUNKIN, S., YANG, F. & COLE, G. 1996. Correlative memory deficits, Abeta elevation, and amyloid plaques in transgenic mice. *Science,* 274**,** 99-102.
HUANG, K. L., LIN, K. J., HO, M. Y., CHANG, Y. J., CHANG, C. H., WEY, S. P., HSIEH, C. J., YEN, T. C., HSIAO, I. T. & LEE, T. H. 2012. Amyloid deposition after cerebral hypoperfusion: Evidenced on [F-18]AV-45 positron emission tomography. *Journal of the Neurological Sciences,* 319**,** 124-129.
HUGHES, T. M., KULLER, L. H., BARINAS-MITCHELL, E. J., MCDADE, E. M., KLUNK, W. E., COHEN, A. D., MATHIS, C. A., DEKOSKY, S. T., PRICE, J. C. & LOPEZ, O. L. 2014. Arterial stiffness and beta-amyloid progression in nondemented elderly adults. *JAMA Neurol,* 71**,** 562-8.
IADECOLA, C. 2004. Neurovascular regulation in the normal brain and in Alzheimer's disease. *Nat Rev Neurosci,* 5**,** 347-60.
IADECOLA, C. 2013. The pathobiology of vascular dementia. *Neuron,* 80**,** 844-66.
IADECOLA, C. 2017. The Neurovascular Unit Coming of Age: A Journey through Neurovascular Coupling in Health and Disease. *Neuron,* 96**,** 17-42.
IADECOLA, C. & NEDERGAARD, M. 2007. Glial regulation of the cerebral microvasculature. *Nat Neurosci,* 10**,** 1369-76.
IADECOLA, C., YAFFE, K., BILLER, J., BRATZKE, L. C., FARACI, F. M., GORELICK, P. B., GULATI, M., KAMEL, H., KNOPMAN, D. S., LAUNER, L. J., SACZYNSKI, J. S., SESHADRI, S., ZEKI AL HAZZOURI, A., AMERICAN HEART ASSOCIATION COUNCIL ON, H., COUNCIL ON CLINICAL, C., COUNCIL ON CARDIOVASCULAR DISEASE IN THE, Y., COUNCIL ON, C., STROKE, N., COUNCIL ON QUALITY OF, C., OUTCOMES, R. & STROKE, C. 2016. Impact of Hypertension on Cognitive Function: A Scientific Statement From the American Heart Association. *Hypertension,* 68**,** e67-e94.
IADECOLA, C., ZHANG, F., NIWA, K., ECKMAN, C., TURNER, S. K., FISCHER, E., YOUNKIN, S., BORCHELT, D. R., HSIAO, K. K. & CARLSON, G. A. 1999. SOD1 rescues cerebral endothelial dysfunction in mice overexpressing amyloid precursor protein. *Nat Neurosci,* 2**,** 157-61.
IHARA, M., TAGUCHI, A., MAKI, T., WASHIDA, K. & TOMIMOTO, H. 2014. A mouse model of chronic cerebral hypoperfusion characterizing features of vascular cognitive impairment. *Methods Mol Biol,* 1135**,** 95-102.
IHARA, M. & TOMIMOTO, H. 2011. Lessons from a mouse model characterizing features of vascular cognitive impairment with white matter changes. *J Aging Res,* 2011**,** 978761.
ILIFF, J. J., LEE, H., YU, M., FENG, T., LOGAN, J., NEDERGAARD, M. & BENVENISTE, H. 2013a. Brain-wide pathway for waste clearance captured by contrast-enhanced MRI. *J Clin Invest,* 123**,** 1299-309.
ILIFF, J. J. & NEDERGAARD, M. 2013. Is there a cerebral lymphatic system? *Stroke,* 44**,** S93-5.
ILIFF, J. J., WANG, M., LIAO, Y., PLOGG, B. A., PENG, W., GUNDERSEN, G. A., BENVENISTE, H., VATES, G. E., DEANE, R., GOLDMAN, S. A., NAGELHUS, E. A. & NEDERGAARD, M. 2012. A paravascular pathway facilitates CSF flow through the brain parenchyma and the clearance of interstitial solutes, including amyloid beta. *Sci Transl Med,* 4**,** 147ra111.
ILIFF, J. J., WANG, M., ZEPPENFELD, D. M., VENKATARAMAN, A., PLOG, B. A., LIAO, Y., DEANE, R. & NEDERGAARD, M. 2013b. Cerebral arterial pulsation drives paravascular CSF-interstitial fluid exchange in the murine brain. *J Neurosci,* 33**,** 18190-9.
ITURRIA-MEDINA, Y., SOTERO, R. C., TOUSSAINT, P. J., MATEOS-PEREZ, J. M., EVANS, A. C. & ALZHEIMER'S DISEASE NEUROIMAGING, I. 2016. Early role of vascular

dysregulation on late-onset Alzheimer's disease based on multifactorial data-driven analysis. *Nat Commun,* 7**,** 11934.
JACKMAN, K. A., MILLER, A. A., DE SILVA, T. M., CRACK, P. J., DRUMMOND, G. R. & SOBEY, C. G. 2009. Reduction of cerebral infarct volume by apocynin requires pretreatment and is absent in Nox2-deficient mice. *Br J Pharmacol,* 156**,** 680-8.
JACOBSEN, J. S., WU, C. C., REDWINE, J. M., COMERY, T. A., ARIAS, R., BOWLBY, M., MARTONE, R., MORRISON, J. H., PANGALOS, M. N., REINHART, P. H. & BLOOM, F. E. 2006. Early-onset behavioral and synaptic deficits in a mouse model of Alzheimer's disease. *Proc Natl Acad Sci U S A,* 103**,** 5161-6.
JELLINGER, K. A. 2013. Pathology and pathogenesis of vascular cognitive impairment-a critical update. *Front Aging Neurosci,* 5**,** 17.
JESSEN, N. A., MUNK, A. S., LUNDGAARD, I. & NEDERGAARD, M. 2015. The Glymphatic System: A Beginner's Guide. *Neurochem Res,* 40**,** 2583-99.
JOHNSTON, M., ZAKHAROV, A., PAPAICONOMOU, C., SALMASI, G. & ARMSTRONG, D. 2004a. Evidence of connections between cerebrospinal fluid and nasal lymphatic vessels in humans, non-human primates and other mammalian species. *Cerebrospinal Fluid Res,* 1**,** 2.
JOHNSTON, S. C., O'MEARA, E. S., MANOLIO, T. A., LEFKOWITZ, D., O'LEARY, D. H., GOLDSTEIN, S., CARLSON, M. C., FRIED, L. P. & LONGSTRETH, W. T., JR. 2004b. Cognitive impairment and decline are associated with carotid artery disease in patients without clinically evident cerebrovascular disease. *Ann Intern Med,* 140**,** 237-47.
KAHLES, T., LUEDIKE, P., ENDRES, M., GALLA, H. J., STEINMETZ, H., BUSSE, R., NEUMANN-HAEFELIN, T. & BRANDES, R. P. 2007. NADPH oxidase plays a central role in blood-brain barrier damage in experimental stroke. *Stroke,* 38**,** 3000-6.
KALARIA, R. N., AKINYEMI, R. & IHARA, M. 2016. Stroke injury, cognitive impairment and vascular dementia. *Biochim Biophys Acta,* 1862**,** 915-25.
KANAMARU, T., KAMIMURA, N., YOKOTA, T., IUCHI, K., NISHIMAKI, K., TAKAMI, S., AKASHIBA, H., SHITAKA, Y., KATSURA, K., KIMURA, K. & OHTA, S. 2015. Oxidative stress accelerates amyloid deposition and memory impairment in a double-transgenic mouse model of Alzheimer's disease. *Neurosci Lett,* 587**,** 126-31.
KAZAMA, K., ANRATHER, J., ZHOU, P., GIROUARD, H., FRYS, K., MILNER, T. A. & IADECOLA, C. 2004. Angiotensin II impairs neurovascular coupling in neocortex through NADPH oxidase-derived radicals. *Circ Res,* 95**,** 1019-26.
KELLEY, E. E., KHOO, N. K., HUNDLEY, N. J., MALIK, U. Z., FREEMAN, B. A. & TARPEY, M. M. 2010. Hydrogen peroxide is the major oxidant product of xanthine oxidase. *Free Radic Biol Med,* 48**,** 493-8.
KIM, S., TOKUYAMA, M., HOSOI, M. & YAMAMOTO, K. 1992. Adrenal and circulating renin-angiotensin system in stroke-prone hypertensive rats. *Hypertension,* 20**,** 280-91.
KIMBROUGH, I. F., ROBEL, S., ROBERSON, E. D. & SONTHEIMER, H. 2015. Vascular amyloidosis impairs the gliovascular unit in a mouse model of Alzheimer's disease. *Brain,* 138**,** 3716-33.
KISLER, K., NELSON, A. R., MONTAGNE, A. & ZLOKOVIC, B. V. 2017. Cerebral blood flow regulation and neurovascular dysfunction in Alzheimer disease. *Nat Rev Neurosci,* 18**,** 419-434.
KITAGAWA, K., MATSUMOTO, M., YANG, G., MABUCHI, T., YAGITA, Y., HORI, M. & YANAGIHARA, T. 1998. Cerebral ischemia after bilateral carotid artery occlusion and intraluminal suture occlusion in mice: evaluation of the patency of the posterior communicating artery. *J Cereb Blood Flow Metab,* 18**,** 570-9.
KITAGUCHI, H., TOMIMOTO, H., IHARA, M., SHIBATA, M., UEMURA, K., KALARIA, R. N., KIHARA, T., ASADA-UTSUGI, M., KINOSHITA, A. & TAKAHASHI, R. 2009. Chronic cerebral hypoperfusion accelerates amyloid beta deposition in APPSwInd transgenic mice. *Brain Res,* 1294**,** 202-10.
KITAMURA, A., MANSO, Y., DUNCOMBE, J., SEARCY, J., KOUDELKA, J., BINNIE, M., WEBSTER, S., LENNEN, R., JANSEN, M., MARSHALL, I., IHARA, M., KALARIA, R. N. & HORSBURGH, K. 2017. Long-term cilostazol treatment reduces gliovascular

damage and memory impairment in a mouse model of chronic cerebral hypoperfusion. *Sci Rep,* 7**,** 4299.
KLEINSCHNITZ, C., GRUND, H., WINGLER, K., ARMITAGE, M. E., JONES, E., MITTAL, M., BARIT, D., SCHWARZ, T., GEIS, C., KRAFT, P., BARTHEL, K., SCHUHMANN, M. K., HERRMANN, A. M., MEUTH, S. G., STOLL, G., MEURER, S., SCHREWE, A., BECKER, L., GAILUS-DURNER, V., FUCHS, H., KLOPSTOCK, T., DE ANGELIS, M. H., JANDELEIT-DAHM, K., SHAH, A. M., WEISSMANN, N. & SCHMIDT, H. H. 2010. Post-stroke inhibition of induced NADPH oxidase type 4 prevents oxidative stress and neurodegeneration. *PLoS Biol,* 8.
KNOPMAN, D., BOLAND, L. L., MOSLEY, T., HOWARD, G., LIAO, D., SZKLO, M., MCGOVERN, P., FOLSOM, A. R. & ATHEROSCLEROSIS RISK IN COMMUNITIES STUDY, I. 2001. Cardiovascular risk factors and cognitive decline in middle-aged adults. *Neurology,* 56**,** 42-8.
KOBER, F., DUHAMEL, G. & COZZONE, P. J. 2008. Experimental comparison of four FAIR arterial spin labeling techniques for quantification of mouse cerebral blood flow at 4.7 T. *NMR Biomed,* 21**,** 781-92.
KRESS, B. T., ILIFF, J. J., XIA, M., WANG, M., WEI, H. S., ZEPPENFELD, D., XIE, L., KANG, H., XU, Q., LIEW, J. A., PLOG, B. A., DING, F., DEANE, R. & NEDERGAARD, M. 2014. Impairment of paravascular clearance pathways in the aging brain. *Ann Neurol,* 76**,** 845-61.
KWEE, R. M. & KWEE, T. C. 2007. Virchow-Robin spaces at MR imaging. *Radiographics,* 27**,** 1071-86.
LANDI, D., MAGGIO, P., LUPOI, D., PALAZZO, P., ALTAMURA, C., FALATO, E., ALTAVILLA, R., VOLLARO, S., CONIGLIO, A. D., TIBUZZI, F., PASSARELLI, F., SILVESTRINI, M., PASQUALETTI, P. & VERNIERI, F. 2015. Cortical ischemic lesion burden measured by DIR is related to carotid artery disease severity. *Cerebrovasc Dis,* 39**,** 23-30.
LASSEN, N. A. 1959. Cerebral blood flow and oxygen consumption in man. *Physiol Rev,* 39**,** 183-238.
LAUNER, L. J., HUGHES, T. M. & WHITE, L. R. 2011. Microinfarcts, brain atrophy, and cognitive function: the Honolulu Asia Aging Study Autopsy Study. *Ann Neurol,* 70**,** 774-80.
LEVY, E., CARMAN, M. D., FERNANDEZ-MADRID, I. J., POWER, M. D., LIEBERBURG, I., VAN DUINEN, S. G., BOTS, G. T., LUYENDIJK, W. & FRANGIONE, B. 1990. Mutation of the Alzheimer's disease amyloid gene in hereditary cerebral hemorrhage, Dutch type. *Science,* 248**,** 1124-6.
LEYS, D., HENON, H., MACKOWIAK-CORDOLIANI, M. A. & PASQUIER, F. 2005. Poststroke dementia. *Lancet Neurol,* 4**,** 752-9.
LI, J., WANG, Y. J., ZHANG, M., XU, Z. Q., GAO, C. Y., FANG, C. Q., YAN, J. C., ZHOU, H. D. & GRP, C. A. S. 2011. Vascular risk factors promote conversion from mild cognitive impairment to Alzheimer disease. *Neurology,* 76**,** 1485-1491.
LI, Y., CIFUENTES-PAGANO, E., DEVALLANCE, E. R., DE JESUS, D. S., SAHOO, S., MEIJLES, D. N., KOES, D., CAMACHO, C. J., ROSS, M., ST CROIX, C. & PAGANO, P. J. 2019. NADPH oxidase 2 inhibitors CPP11G and CPP11H attenuate endothelial cell inflammation & vessel dysfunction and restore mouse hind-limb flow. *Redox Biol,* 22**,** 101143.
LIU, H. & ZHANG, J. 2012. Cerebral hypoperfusion and cognitive impairment: the pathogenic role of vascular oxidative stress. *Int J Neurosci,* 122**,** 494-9.
LOBO, A., LAUNER, L. J., FRATIGLIONI, L., ANDERSEN, K., DI CARLO, A., BRETELER, M. M., COPELAND, J. R., DARTIGUES, J. F., JAGGER, C., MARTINEZ-LAGE, J., SOININEN, H. & HOFMAN, A. 2000. Prevalence of dementia and major subtypes in Europe: A collaborative study of population-based cohorts. Neurologic Diseases in the Elderly Research Group. *Neurology,* 54**,** S4-9.
LOUVEAU, A., SMIRNOV, I., KEYES, T. J., ECCLES, J. D., ROUHANI, S. J., PESKE, J. D., DERECKI, N. C., CASTLE, D., MANDELL, J. W., LEE, K. S., HARRIS, T. H. & KIPNIS,

J. 2015. Structural and functional features of central nervous system lymphatic vessels. *Nature,* 523**,** 337-41.
LUCHSINGER, J. A., TANG, M. X., STERN, Y., SHEA, S. & MAYEUX, R. 2001. Diabetes mellitus and risk of Alzheimer's disease and dementia with stroke in a multiethnic cohort. *Am J Epidemiol,* 154**,** 635-41.
MA, M. W., WANG, J., ZHANG, Q., WANG, R., DHANDAPANI, K. M., VADLAMUDI, R. K. & BRANN, D. W. 2017a. NADPH oxidase in brain injury and neurodegenerative disorders. *Mol Neurodegener,* 12**,** 7.
MA, Q. L., INEICHEN, B. V., DETMAR, M. & PROULX, S. T. 2017b. Outflow of cerebrospinal fluid is predominantly through lymphatic vessels and is reduced in aged mice. *Nature Communications,* 8.
MATSUNO, K., YAMADA, H., IWATA, K., JIN, D., KATSUYAMA, M., MATSUKI, M., TAKAI, S., YAMANISHI, K., MIYAZAKI, M., MATSUBARA, H. & YABE-NISHIMURA, C. 2005. Nox1 is involved in angiotensin II-mediated hypertension: a study in Nox1-deficient mice. *Circulation,* 112**,** 2677-85.
MCCOLL, B. W., CARSWELL, H. V., MCCULLOCH, J. & HORSBURGH, K. 2004. Extension of cerebral hypoperfusion and ischaemic pathology beyond MCA territory after intraluminal filament occlusion in C57Bl/6J mice. *Brain Res,* 997**,** 15-23.
MCQUEEN, J., REIMER, M. M., HOLLAND, P. R., MANSO, Y., MCLAUGHLIN, M., FOWLER, J. H. & HORSBURGH, K. 2014. Restoration of Oligodendrocyte Pools in a Mouse Model of Chronic Cerebral Hypoperfusion. *Plos One,* 9.
MEDINA, M. & AVILA, J. 2014. New perspectives on the role of tau in Alzheimer's disease. Implications for therapy. *Biochem Pharmacol,* 88**,** 540-7.
MESTRE, H., HABLITZ, L. M., XAVIER, A. L., FENG, W., ZOU, W., PU, T., MONAI, H., MURLIDHARAN, G., CASTELLANOS RIVERA, R. M., SIMON, M. J., PIKE, M. M., PLA, V., DU, T., KRESS, B. T., WANG, X., PLOG, B. A., THRANE, A. S., LUNDGAARD, I., ABE, Y., YASUI, M., THOMAS, J. H., XIAO, M., HIRASE, H., ASOKAN, A., ILIFF, J. J. & NEDERGAARD, M. 2018a. Aquaporin-4-dependent glymphatic solute transport in the rodent brain. *Elife,* 7.
MESTRE, H., KOSTRIKOV, S., MEHTA, R. I. & NEDERGAARD, M. 2017. Perivascular spaces, glymphatic dysfunction, and small vessel disease. *Clin Sci (Lond),* 131**,** 2257-2274.
MESTRE, H., TITHOF, J., DU, T., SONG, W., PENG, W. G., SWEENEY, A. M., OLYEDA, G., THOMAS, J. H., NEDERGAARD, M. & KELLEY, D. H. 2018b. Flow of cerebrospinal fluid is driven by arterial pulsations and is reduced in hypertension. *Nature Communications,* 9.
MIAO, J., XU, F., DAVIS, J., OTTE-HOLLER, I., VERBEEK, M. M. & VAN NOSTRAND, W. E. 2005. Cerebral microvascular amyloid beta protein deposition induces vascular degeneration and neuroinflammation in transgenic mice expressing human vasculotropic mutant amyloid beta precursor protein. *Am J Pathol,* 167**,** 505-15.
MIYAMOTO, N., TANAKA, R., SHIMURA, H., WATANABE, T., MORI, H., ONODERA, M., MOCHIZUKI, H., HATTORI, N. & URABE, T. 2010. Phosphodiesterase III inhibition promotes differentiation and survival of oligodendrocyte progenitors and enhances regeneration of ischemic white matter lesions in the adult mammalian brain. *J Cereb Blood Flow Metab,* 30**,** 299-310.
NAGEL, S., GENIUS, J., HEILAND, S., HORSTMANN, S., GARDNER, H. & WAGNER, S. 2007. Diphenyleneiodonium and dimethylsulfoxide for treatment of reperfusion injury in cerebral ischemia of the rat. *Brain Res,* 1132**,** 210-7.
NAGEL, S., HADLEY, G., PFLEGER, K., GROND-GINSBACH, C., BUCHAN, A. M., WAGNER, S. & PAPADAKIS, M. 2012. Suppression of the inflammatory response by diphenyleneiodonium after transient focal cerebral ischemia. *J Neurochem,* 123 Suppl 2**,** 98-107.
NAKAJI, K., IHARA, M., TAKAHASHI, C., ITOHARA, S., NODA, M., TAKAHASHI, R. & TOMIMOTO, H. 2006. Matrix metalloproteinase-2 plays a critical role in the

pathogenesis of white matter lesions after chronic cerebral hypoperfusion in rodents. *Stroke,* 37**,** 2816-23.
NICOLAKAKIS, N. & HAMEL, E. 2011. Neurovascular function in Alzheimer's disease patients and experimental models. *J Cereb Blood Flow Metab,* 31**,** 1354-70.
NISHINO, A., TAJIMA, Y., TAKUWA, H., MASAMOTO, K., TANIGUCHI, J., WAKIZAKA, H., KOKURYO, D., URUSHIHATA, T., AOKI, I., KANNO, I., TOMITA, Y., SUZUKI, N., IKOMA, Y. & ITO, H. 2016. Long-term effects of cerebral hypoperfusion on neural density and function using misery perfusion animal model. *Sci Rep,* 6**,** 25072.
NISHIO, K., IHARA, M., YAMASAKI, N., KALARIA, R. N., MAKI, T., FUJITA, Y., ITO, H., OISHI, N., FUKUYAMA, H., MIYAKAWA, T., TAKAHASHI, R. & TOMIMOTO, H. 2010. A mouse model characterizing features of vascular dementia with hippocampal atrophy. *Stroke,* 41**,** 1278-84.
NIWA, K., HAENSEL, C., ROSS, M. E. & IADECOLA, C. 2001a. Cyclooxygenase-1 participates in selected vasodilator responses of the cerebral circulation. *Circ Res,* 88**,** 600-8.
NIWA, K., KAZAMA, K., YOUNKIN, L., YOUNKIN, S. G., CARLSON, G. A. & IADECOLA, C. 2002a. Cerebrovascular autoregulation is profoundly impaired in mice overexpressing amyloid precursor protein. *Am J Physiol Heart Circ Physiol,* 283**,** H315-23.
NIWA, K., KAZAMA, K., YOUNKIN, S. G., CARLSON, G. A. & IADECOLA, C. 2002b. Alterations in cerebral blood flow and glucose utilization in mice overexpressing the amyloid precursor protein. *Neurobiol Dis,* 9**,** 61-8.
NIWA, K., PORTER, V. A., KAZAMA, K., CORNFIELD, D., CARLSON, G. A. & IADECOLA, C. 2001b. A beta-peptides enhance vasoconstriction in cerebral circulation. *Am J Physiol Heart Circ Physiol,* 281**,** H2417-24.
NIWA, K., YOUNKIN, L., EBELING, C., TURNER, S. K., WESTAWAY, D., YOUNKIN, S., ASHE, K. H., CARLSON, G. A. & IADECOLA, C. 2000. Abeta 1-40-related reduction in functional hyperemia in mouse neocortex during somatosensory activation. *Proc Natl Acad Sci U S A,* 97**,** 9735-40.
OKAMOTO, Y., YAMAMOTO, T., KALARIA, R. N., SENZAKI, H., MAKI, T., HASE, Y., KITAMURA, A., WASHIDA, K., YAMADA, M., ITO, H., TOMIMOTO, H., TAKAHASHI, R. & IHARA, M. 2012. Cerebral hypoperfusion accelerates cerebral amyloid angiopathy and promotes cortical microinfarcts. *Acta Neuropathol,* 123**,** 381-94.
OSOL, G., BREKKE, J. F., MCELROY-YAGGY, K. & GOKINA, N. I. 2002. Myogenic tone, reactivity, and forced dilatation: a three-phase model of in vitro arterial myogenic behavior. *Am J Physiol Heart Circ Physiol,* 283**,** H2260-7.
PANDAY, A., SAHOO, M. K., OSORIO, D. & BATRA, S. 2015. NADPH oxidases: an overview from structure to innate immunity-associated pathologies. *Cell Mol Immunol,* 12**,** 5-23.
PANZA, F., LOZUPONE, M., LOGROSCINO, G. & IMBIMBO, B. P. 2019. A critical appraisal of amyloid-beta-targeting therapies for Alzheimer disease. *Nat Rev Neurol,* 15**,** 73-88.
PARIS, D., TOWN, T., MORI, T., PARKER, T. A., HUMPHREY, J. & MULLAN, M. 2000. Soluble beta-amyloid peptides mediate vasoactivity via activation of a pro-inflammatory pathway. *Neurobiol Aging,* 21**,** 183-97.
PARK, L., ANRATHER, J., FORSTER, C., KAZAMA, K., CARLSON, G. A. & IADECOLA, C. 2004a. Abeta-induced vascular oxidative stress and attenuation of functional hyperemia in mouse somatosensory cortex. *J Cereb Blood Flow Metab,* 24**,** 334-42.
PARK, L., ANRATHER, J., GIROUARD, H., ZHOU, P. & IADECOLA, C. 2007. Nox2-derived reactive oxygen species mediate neurovascular dysregulation in the aging mouse brain. *J Cereb Blood Flow Metab,* 27**,** 1908-18.
PARK, L., ANRATHER, J., ZHOU, P., FRYS, K., WANG, G. & IADECOLA, C. 2004b. Exogenous NADPH increases cerebral blood flow through NADPH oxidase-dependent and -independent mechanisms. *Arterioscler Thromb Vasc Biol,* 24**,** 1860-5.
PARK, L., KOIZUMI, K., EL JAMAL, S., ZHOU, P., PREVITI, M. L., VAN NOSTRAND, W. E., CARLSON, G. & IADECOLA, C. 2014. Age-dependent neurovascular dysfunction and damage in a mouse model of cerebral amyloid angiopathy. *Stroke,* 45**,** 1815-21.

PARK, L., ZHOU, P., PITSTICK, R., CAPONE, C., ANRATHER, J., NORRIS, E. H., YOUNKIN, L., YOUNKIN, S., CARLSON, G., MCEWEN, B. S. & IADECOLA, C. 2008. Nox2-derived radicals contribute to neurovascular and behavioral dysfunction in mice overexpressing the amyloid precursor protein. *Proc Natl Acad Sci U S A,* 105**,** 1347-52.

PEILA, R., RODRIGUEZ, B. L., LAUNER, L. J. & HONOLULU-ASIA AGING, S. 2002. Type 2 diabetes, APOE gene, and the risk for dementia and related pathologies: The Honolulu-Asia Aging Study. *Diabetes,* 51**,** 1256-62.

PENDLEBURY, S. T. & ROTHWELL, P. M. 2009. Prevalence, incidence, and factors associated with pre-stroke and post-stroke dementia: a systematic review and meta-analysis. *The Lancet Neurology,* 8**,** 1006-1018.

PENG, W., ACHARIYAR, T. M., LI, B., LIAO, Y., MESTRE, H., HITOMI, E., REGAN, S., KASPER, T., PENG, S., DING, F., BENVENISTE, H., NEDERGAARD, M. & DEANE, R. 2016. Suppression of glymphatic fluid transport in a mouse model of Alzheimer's disease. *Neurobiol Dis,* 93**,** 215-25.

PETERS, A., SCHWEIGER, U., PELLERIN, L., HUBOLD, C., OLTMANNS, K. M., CONRAD, M., SCHULTES, B., BORN, J. & FEHM, H. L. 2004. The selfish brain: competition for energy resources. *Neurosci Biobehav Rev,* 28**,** 143-80.

PLOG, B. A., DASHNAW, M. L., HITOMI, E., PENG, W., LIAO, Y., LOU, N., DEANE, R. & NEDERGAARD, M. 2015. Biomarkers of traumatic injury are transported from brain to blood via the glymphatic system. *J Neurosci,* 35**,** 518-26.

POLLAY, M. 2010. The function and structure of the cerebrospinal fluid outflow system. *Cerebrospinal Fluid Res,* 7**,** 9.

POPA-WAGNER, A., BUGA, A. M., POPESCU, B. & MURESANU, D. 2015. Vascular cognitive impairment, dementia, aging and energy demand. A vicious cycle. *Journal of Neural Transmission,* 122**,** 47-54.

PORASUPHATANA, S., TSAI, P. & ROSEN, G. M. 2003. The generation of free radicals by nitric oxide synthase. *Comp Biochem Physiol C Toxicol Pharmacol,* 134**,** 281-9.

POTTER, G. M., CHAPPELL, F. M., MORRIS, Z. & WARDLAW, J. M. 2015a. Cerebral perivascular spaces visible on magnetic resonance imaging: development of a qualitative rating scale and its observer reliability. *Cerebrovasc Dis,* 39**,** 224-31.

POTTER, G. M., DOUBAL, F. N., JACKSON, C. A., CHAPPELL, F. M., SUDLOW, C. L., DENNIS, M. S. & WARDLAW, J. M. 2015b. Enlarged perivascular spaces and cerebral small vessel disease. *Int J Stroke,* 10**,** 376-81.

PRINCE, E. A. & AHN, S. H. 2013. Basic vascular neuroanatomy of the brain and spine: what the general interventional radiologist needs to know. *Semin Intervent Radiol,* 30**,** 234-9.

RAJAGOPALAN, S., KURZ, S., MUNZEL, T., TARPEY, M., FREEMAN, B. A., GRIENDLING, K. K. & HARRISON, D. G. 1996. Angiotensin II-mediated hypertension in the rat increases vascular superoxide production via membrane NADH/NADPH oxidase activation. Contribution to alterations of vasomotor tone. *J Clin Invest,* 97**,** 1916-23.

RAJANI, R. M., QUICK, S., RUIGROK, S. R., GRAHAM, D., HARRIS, S. E., VERHAAREN, B. F. J., FORNAGE, M., SESHADRI, S., ATANUR, S. S., DOMINICZAK, A. F., SMITH, C., WARDLAW, J. M. & WILLIAMS, A. 2018. Reversal of endothelial dysfunction reduces white matter vulnerability in cerebral small vessel disease in rats. *Sci Transl Med,* 10.

RAZ, L., ZHANG, Q. G., ZHOU, C. F., HAN, D., GULATI, P., YANG, L. C., YANG, F., WANG, R. M. & BRANN, D. W. 2010. Role of Rac1 GTPase in NADPH oxidase activation and cognitive impairment following cerebral ischemia in the rat. *PLoS One,* 5**,** e12606.

REIMER, M. M., MCQUEEN, J., SEARCY, L., SCULLION, G., ZONTA, B., DESMAZIERES, A., HOLLAND, P. R., SMITH, J., GLIDDON, C., WOOD, E. R., HERZYK, P., BROPHY, P. J., MCCULLOCH, J. & HORSBURGH, K. 2011a. Rapid disruption of axon-glial integrity in response to mild cerebral hypoperfusion. *J Neurosci,* 31**,** 18185-94.

REIMER, M. M., MCQUEEN, J., SEARCY, L., SCULLION, G., ZONTA, B., DESMAZIERES, A., HOLLAND, P. R., SMITH, J., GLIDDON, C., WOOD, E. R., HERZYK, P., BROPHY,

P. J., MCCULLOCH, J. & HORSBURGH, K. 2011b. Rapid Disruption of Axon-Glial Integrity in Response to Mild Cerebral Hypoperfusion. *Journal of Neuroscience,* 31**,** 18185-18194.

REMACLE, J., RAES, M., TOUSSAINT, O., RENARD, P. & RAO, G. 1995. Low levels of reactive oxygen species as modulators of cell function. *Mutat Res,* 316**,** 103-22.

RENNELS, M. L., BLAUMANIS, O. R. & GRADY, P. A. 1990. Rapid solute transport throughout the brain via paravascular fluid pathways. *Adv Neurol,* 52**,** 431-9.

RENNELS, M. L., GREGORY, T. F., BLAUMANIS, O. R., FUJIMOTO, K. & GRADY, P. A. 1985. Evidence for a 'paravascular' fluid circulation in the mammalian central nervous system, provided by the rapid distribution of tracer protein throughout the brain from the subarachnoid space. *Brain Res,* 326**,** 47-63.

RIBA-LLENA, I., JIMENEZ-BALADO, J., CASTANE, X., GIRONA, A., LOPEZ-RUEDA, A., MUNDET, X., JARCA, C. I., ALVAREZ-SABIN, J., MONTANER, J. & DELGADO, P. 2018. Arterial Stiffness Is Associated With Basal Ganglia Enlarged Perivascular Spaces and Cerebral Small Vessel Disease Load. *Stroke,* 49**,** 1279-1281.

RINGSTAD, G., VALNES, L. M., DALE, A. M., PRIPP, A. H., VATNEHOL, S. S., EMBLEM, K. E., MARDAL, K. A. & EIDE, P. K. 2018. Brain-wide glymphatic enhancement and clearance in humans assessed with MRI. *JCI Insight,* 3.

RINGSTAD, G., VATNEHOL, S. A. S. & EIDE, P. K. 2017. Glymphatic MRI in idiopathic normal pressure hydrocephalus. *Brain,* 140**,** 2691-2705.

ROBERTS, J. M., MANISKAS, M. E. & BIX, G. J. 2018. Bilateral carotid artery stenosis causes unexpected early changes in brain extracellular matrix and blood-brain barrier integrity in mice. *PLoS One,* 13**,** e0195765.

ROMERO, J. R., BEISER, A., SESHADRI, S., BENJAMIN, E. J., POLAK, J. F., VASAN, R. S., AU, R., DECARLI, C. & WOLF, P. A. 2009. Carotid artery atherosclerosis, MRI indices of brain ischemia, aging, and cognitive impairment: the Framingham study. *Stroke,* 40**,** 1590-6.

ROSENBLUM, W. I. 1987. Hydroxyl radical mediates the endothelium-dependent relaxation produced by bradykinin in mouse cerebral arterioles. *Circ Res,* 61**,** 601-3.

ROZEMULLER, A. J., VAN GOOL, W. A. & EIKELENBOOM, P. 2005. The neuroinflammatory response in plaques and amyloid angiopathy in Alzheimer's disease: therapeutic implications. *Curr Drug Targets CNS Neurol Disord,* 4**,** 223-33.

RUITENBERG, A., DEN HEIJER, T., BAKKER, S. L., VAN SWIETEN, J. C., KOUDSTAAL, P. J., HOFMAN, A. & BRETELER, M. M. 2005. Cerebral hypoperfusion and clinical onset of dementia: the Rotterdam Study. *Ann Neurol,* 57**,** 789-94.

SACZYNSKI, J. S., JONSDOTTIR, M. K., GARCIA, M. E., JONSSON, P. V., PEILA, R., EIRIKSDOTTIR, G., OLAFSDOTTIR, E., HARRIS, T. B., GUDNASON, V. & LAUNER, L. J. 2008. Cognitive impairment: an increasingly important complication of type 2 diabetes: the age, gene/environment susceptibility--Reykjavik study. *Am J Epidemiol,* 168**,** 1132-9.

SAHATHEVAN, R., BRODTMANN, A. & DONNAN, G. A. 2012. Dementia, stroke, and vascular risk factors; a review. *Int J Stroke,* 7**,** 61-73.

SALVADORES, N., SEARCY, J. L., HOLLAND, P. R. & HORSBURGH, K. 2017. Chronic cerebral hypoperfusion alters amyloid-beta peptide pools leading to cerebral amyloid angiopathy, microinfarcts and haemorrhages in Tg-SwDI mice. *Clin Sci (Lond),* 131**,** 2109-2123.

SARTI, C., PANTONI, L., BARTOLINI, L. & INZITARI, D. 2002. Cognitive impairment and chronic cerebral hypoperfusion: what can be learned from experimental models. *J Neurol Sci,* 203-204**,** 263-6.

SCHIEBER, M. & CHANDEL, N. S. 2014. ROS function in redox signaling and oxidative stress. *Curr Biol,* 24**,** R453-62.

SCHNEIDER, J. A., ARVANITAKIS, Z., BANG, W. & BENNETT, D. A. 2007. Mixed brain pathologies account for most dementia cases in community-dwelling older persons. *Neurology,* 69**,** 2197-204.

SCHUFF, N., MATSUMOTO, S., KMIECIK, J., STUDHOLME, C., DU, A., EZEKIEL, F., MILLER, B. L., KRAMER, J. H., JAGUST, W. J., CHUI, H. C. & WEINER, M. W. 2009. Cerebral blood flow in ischemic vascular dementia and Alzheimer's disease, measured by arterial spin-labeling magnetic resonance imaging. *Alzheimers Dement,* 5**,** 454-62.

SERRANO-POZO, A., FROSCH, M. P., MASLIAH, E. & HYMAN, B. T. 2011. Neuropathological Alterations in Alzheimer Disease. *Cold Spring Harbor Perspectives in Medicine,* 1.

SHANG, J., YAMASHITA, T., ZHAI, Y., NAKANO, Y., MORIHARA, R., FUKUI, Y., HISHIKAWA, N., OHTA, Y. & ABE, K. 2016. Strong Impact of Chronic Cerebral Hypoperfusion on Neurovascular Unit, Cerebrovascular Remodeling, and Neurovascular Trophic Coupling in Alzheimer's Disease Model Mouse. *J Alzheimers Dis,* 52**,** 113-26.

SHEN, J., BAI, X. Y., QIN, Y., JIN, W. W., ZHOU, J. Y., ZHOU, J. P., YAN, Y. G., WANG, Q., BRUCE, I. C., CHEN, J. H. & XIA, Q. 2011. Interrupted reperfusion reduces the activation of NADPH oxidase after cerebral I/R injury. *Free Radic Biol Med,* 50**,** 1780-6.

SHI, Y., THRIPPLETON, M. J., BLAIR, G. W., DICKIE, D. A., MARSHALL, I., HAMILTON, I., DOUBAL, F. N., CHAPPELL, F. & WARDLAW, J. M. 2018. Small vessel disease is associated with altered cerebrovascular pulsatility but not resting cerebral blood flow. *J Cereb Blood Flow Metab***,** 271678X18803956.

SHI, Y. & WARDLAW, J. M. 2016. Update on cerebral small vessel disease: a dynamic whole-brain disease. *Stroke Vasc Neurol,* 1**,** 83-92.

SHIBATA, M., OHTANI, R., IHARA, M. & TOMIMOTO, H. 2004. White matter lesions and glial activation in a novel mouse model of chronic cerebral hypoperfusion. *Stroke,* 35**,** 2598-603.

SHIBATA, M., YAMASAKI, N., MIYAKAWA, T., KALARIA, R. N., FUJITA, Y., OHTANI, R., IHARA, M., TAKAHASHI, R. & TOMIMOTO, H. 2007. Selective impairment of working memory in a mouse model of chronic cerebral hypoperfusion. *Stroke,* 38**,** 2826-32.

SHIN, H. K., JONES, P. B., GARCIA-ALLOZA, M., BORRELLI, L., GREENBERG, S. M., BACSKAI, B. J., FROSCH, M. P., HYMAN, B. T., MOSKOWITZ, M. A. & AYATA, C. 2007. Age-dependent cerebrovascular dysfunction in a transgenic mouse model of cerebral amyloid angiopathy. *Brain,* 130**,** 2310-9.

SHOKRI-KOJORI, E., WANG, G. J., WIERS, C. E., DEMIRAL, S. B., GUO, M., KIM, S. W., LINDGREN, E., RAMIREZ, V., ZEHRA, A., FREEMAN, C., MILLER, G., MANZA, P., SRIVASTAVA, T., DE SANTI, S., TOMASI, D., BENVENISTE, H. & VOLKOW, N. D. 2018. beta-Amyloid accumulation in the human brain after one night of sleep deprivation. *Proc Natl Acad Sci U S A*.

SIMARD, D., OLESEN, J., PAULSON, O. B., LASSEN, N. A. & SKINHOJ, E. 1971. Regional cerebral blood flow and its regulation in dementia. *Brain,* 94**,** 273-88.

SIMONYI, A., SERFOZO, P., LEHMIDI, T. M., CUI, J., GU, Z., LUBAHN, D. B., SUN, A. Y. & SUN, G. Y. 2012. The neuroprotective effects of apocynin. *Front Biosci (Elite Ed),* 4**,** 2183-93.

SKROBOT, O. A., ATTEMS, J., ESIRI, M., HORTOBAGYI, T., IRONSIDE, J. W., KALARIA, R. N., KING, A., LAMMIE, G. A., MANN, D., NEAL, J., BEN-SHLOMO, Y., KEHOE, P. G. & LOVE, S. 2016. Vascular cognitive impairment neuropathology guidelines (VCING): the contribution of cerebrovascular pathology to cognitive impairment. *Brain,* 139**,** 2957-2969.

SKROBOT, O. A., O'BRIEN, J., BLACK, S., CHEN, C., DECARLI, C., ERKINJUNTTI, T., FORD, G. A., KALARIA, R. N., PANTONI, L., PASQUIER, F., ROMAN, G. C., WALLIN, A., SACHDEV, P., SKOOG, I., GROUP, V., BEN-SHLOMO, Y., PASSMORE, A. P., LOVE, S. & KEHOE, P. G. 2017. The Vascular Impairment of Cognition Classification Consensus Study. *Alzheimers Dement,* 13**,** 624-633.

SMITH, A. J., YAO, X., DIX, J. A., JIN, B. J. & VERKMAN, A. S. 2017. Test of the 'glymphatic' hypothesis demonstrates diffusive and aquaporin-4-independent solute transport in rodent brain parenchyma. *Elife,* 6.

SNOWDON, D. A., GREINER, L. H., MORTIMER, J. A., RILEY, K. P., GREINER, P. A. & MARKESBERY, W. R. 1997. Brain infarction and the clinical expression of Alzheimer disease. The Nun Study. *JAMA,* 277**,** 813-7.

SOARES, L. M., SCHIAVON, A. P., MILANI, H. & DE OLIVEIRA, R. M. 2013. Cognitive impairment and persistent anxiety-related responses following bilateral common carotid artery occlusion in mice. *Behav Brain Res,* 249**,** 28-37.

SONG, J., YANG, L., NAN, D., HE, Q., WAN, Y. & GUO, H. 2018. Histidine Alleviates Impairments Induced by Chronic Cerebral Hypoperfusion in Mice. *Front Physiol,* 9**,** 662.

SOONTORNNIYOMKIJ, V., LYNCH, M. D., MERMASH, S., POMAKIAN, J., BADKOOBEHI, H., CLARE, R. & VINTERS, H. V. 2010. Cerebral microinfarcts associated with severe cerebral beta-amyloid angiopathy. *Brain Pathol,* 20**,** 459-67.

STARKOV, A. A. 2008. The role of mitochondria in reactive oxygen species metabolism and signaling. *Ann N Y Acad Sci,* 1147**,** 37-52.

STURCHLER-PIERRAT, C., ABRAMOWSKI, D., DUKE, M., WIEDERHOLD, K. H., MISTL, C., ROTHACHER, S., LEDERMANN, B., BURKI, K., FREY, P., PAGANETTI, P. A., WARIDEL, C., CALHOUN, M. E., JUCKER, M., PROBST, A., STAUFENBIEL, M. & SOMMER, B. 1997. Two amyloid precursor protein transgenic mouse models with Alzheimer disease-like pathology. *Proc Natl Acad Sci U S A,* 94**,** 13287-92.

SURACE, M. J. & BLOCK, M. L. 2012. Targeting microglia-mediated neurotoxicity: the potential of NOX2 inhibitors. *Cell Mol Life Sci,* 69**,** 2409-27.

TAKEDA, S., SATO, N., TAKEUCHI, D., KURINAMI, H., SHINOHARA, M., NIISATO, K., KANO, M., OGIHARA, T., RAKUGI, H. & MORISHITA, R. 2009. Angiotensin receptor blocker prevented beta-amyloid-induced cognitive impairment associated with recovery of neurovascular coupling. *Hypertension,* 54**,** 1345-52.

TANG, X. N., CAIRNS, B., CAIRNS, N. & YENARI, M. A. 2008. Apocynin improves outcome in experimental stroke with a narrow dose range. *Neuroscience,* 154**,** 556-62.

TANG, X. N., CAIRNS, B., KIM, J. Y. & YENARI, M. A. 2012. NADPH oxidase in stroke and cerebrovascular disease. *Neurol Res,* 34**,** 338-45.

TARANTINI, S., FULOP, G. A., KISS, T., FARKAS, E., ZOLEI-SZENASI, D., GALVAN, V., TOTH, P., CSISZAR, A., UNGVARI, Z. & YABLUCHANSKIY, A. 2017. Demonstration of impaired neurovascular coupling responses in TG2576 mouse model of Alzheimer's disease using functional laser speckle contrast imaging. *Geroscience,* 39**,** 465-473.

TARASOFF-CONWAY, J. M., CARARE, R. O., OSORIO, R. S., GLODZIK, L., BUTLER, T., FIEREMANS, E., AXEL, L., RUSINEK, H., NICHOLSON, C., ZLOKOVIC, B. V., FRANGIONE, B., BLENNOW, K., MENARD, J., ZETTERBERG, H., WISNIEWSKI, T. & DE LEON, M. J. 2015. Clearance systems in the brain-implications for Alzheimer disease. *Nat Rev Neurol,* 11**,** 457-70.

TER LAAN, M., VAN DIJK, J. M., ELTING, J. W., STAAL, M. J. & ABSALOM, A. R. 2013. Sympathetic regulation of cerebral blood flow in humans: a review. *Br J Anaesth,* 111**,** 361-7.

THOMAS, T., THOMAS, G., MCLENDON, C., SUTTON, T. & MULLAN, M. 1996. beta-Amyloid-mediated vasoactivity and vascular endothelial damage. *Nature,* 380**,** 168-71.

THOMSEN, M. S., ROUTHE, L. J. & MOOS, T. 2017. The vascular basement membrane in the healthy and pathological brain. *J Cereb Blood Flow Metab***,** 271678X17722436.

TOYAMA, K., KOIBUCHI, N., UEKAWA, K., HASEGAWA, Y., KATAOKA, K., KATAYAMA, T., SUETA, D., MA, M. J., NAKAGAWA, T., YASUDA, O., TOMIMOTO, H., ICHIJO, H., OGAWA, H. & KIM-MITSUYAMA, S. 2014. Apoptosis signal-regulating kinase 1 is a novel target molecule for cognitive impairment induced by chronic cerebral hypoperfusion. *Arterioscler Thromb Vasc Biol,* 34**,** 616-25.

VAN DEN BOOM, R., BORNEBROEK, M., BEHLOUL, F., VAN DEN BERG-HUYSMANS, A. A., HAAN, J. & VAN BUCHEM, M. A. 2005. Microbleeds in hereditary cerebral hemorrhage with amyloidosis-Dutch type. *Neurology,* 64**,** 1288-9.

VAN DEN BRINK, H., ZWIERS, A., SWITZER, A. R., CHARLTON, A., MCCREARY, C. R., GOODYEAR, B. G., FRAYNE, R., BIESSELS, G. J. & SMITH, E. E. 2018. Cortical

Microinfarcts on 3T Magnetic Resonance Imaging in Cerebral Amyloid Angiopathy. *Stroke,* 49**,** 1899-1905.
VAN VELUW, S. J., ZWANENBURG, J. J., ENGELEN-LEE, J., SPLIET, W. G., HENDRIKSE, J., LUIJTEN, P. R. & BIESSELS, G. J. 2013. In vivo detection of cerebral cortical microinfarcts with high-resolution 7T MRI. *J Cereb Blood Flow Metab,* 33**,** 322-9.
VENKAT, P., CHOPP, M. & CHEN, J. 2015. Models and mechanisms of vascular dementia. *Exp Neurol*.
VERMEER, S. E., PRINS, N. D., DEN HEIJER, T., HOFMAN, A., KOUDSTAAL, P. J. & BRETELER, M. M. 2003. Silent brain infarcts and the risk of dementia and cognitive decline. *N Engl J Med,* 348**,** 1215-22.
VON BERNHARDI, R., EUGENIN-VON BERNHARDI, L. & EUGENIN, J. 2015. Microglial cell dysregulation in brain aging and neurodegeneration. *Front Aging Neurosci,* 7**,** 124.
WAKITA, H., TOMIMOTO, H., AKIGUCHI, I. & KIMURA, J. 1994. Glial activation and white matter changes in the rat brain induced by chronic cerebral hypoperfusion: an immunohistochemical study. *Acta Neuropathol,* 87**,** 484-92.
WALDER, C. E., GREEN, S. P., DARBONNE, W. C., MATHIAS, J., RAE, J., DINAUER, M. C., CURNUTTE, J. T. & THOMAS, G. R. 1997. Ischemic stroke injury is reduced in mice lacking a functional NADPH oxidase. *Stroke,* 28**,** 2252-8.
WANG, M., DING, F., DENG, S., GUO, X., WANG, W., ILIFF, J. J. & NEDERGAARD, M. 2017. Focal Solute Trapping and Global Glymphatic Pathway Impairment in a Murine Model of Multiple Microinfarcts. *J Neurosci,* 37**,** 2870-2877.
WARDLAW, J. M., ALLERHAND, M., EADIE, E., THOMAS, A., CORLEY, J., PATTIE, A., TAYLOR, A., SHENKIN, S. D., COX, S., GOW, A., STARR, J. M. & DEARY, I. J. 2017. Carotid disease at age 73 and cognitive change from age 70 to 76 years: A longitudinal cohort study. *J Cereb Blood Flow Metab,* 37**,** 3042-3052.
WARDLAW, J. M., SMITH, E. E., BIESSELS, G. J., CORDONNIER, C., FAZEKAS, F., FRAYNE, R., LINDLEY, R. I., O'BRIEN, J. T., BARKHOF, F., BENAVENTE, O. R., BLACK, S. E., BRAYNE, C., BRETELER, M., CHABRIAT, H., DECARLI, C., DE LEEUW, F. E., DOUBAL, F., DUERING, M., FOX, N. C., GREENBERG, S., HACHINSKI, V., KILIMANN, I., MOK, V., OOSTENBRUGGE, R., PANTONI, L., SPECK, O., STEPHAN, B. C., TEIPEL, S., VISWANATHAN, A., WERRING, D., CHEN, C., SMITH, C., VAN BUCHEM, M., NORRVING, B., GORELICK, P. B., DICHGANS, M. & NEUROIMAGING, S. T. F. R. V. C. O. 2013. Neuroimaging standards for research into small vessel disease and its contribution to ageing and neurodegeneration. *Lancet Neurol,* 12**,** 822-38.
WELLER, R. O., MASSEY, A., NEWMAN, T. A., HUTCHINGS, M., KUO, Y. M. & ROHER, A. E. 1998. Cerebral amyloid angiopathy: amyloid beta accumulates in putative interstitial fluid drainage pathways in Alzheimer's disease. *Am J Pathol,* 153**,** 725-33.
WIERENGA, C. E., HAYS, C. C. & ZLATAR, Z. Z. 2014. Cerebral blood flow measured by arterial spin labeling MRI as a preclinical marker of Alzheimer's disease. *J Alzheimers Dis,* 42 Suppl 4**,** S411-9.
WINN, H. R., MORII, S. & BERNE, R. M. 1985. The role of adenosine in autoregulation of cerebral blood flow. *Ann Biomed Eng,* 13**,** 321-8.
WOLF, R. L. & DETRE, J. A. 2007. Clinical neuroimaging using arterial spin-labeled perfusion magnetic resonance imaging. *Neurotherapeutics,* 4**,** 346-59.
WOLTERS, F. J., ZONNEVELD, H. I., HOFMAN, A., VAN DER LUGT, A., KOUDSTAAL, P. J., VERNOOIJ, M. W., IKRAM, M. A. & HEART-BRAIN CONNECTION COLLABORATIVE RESEARCH, G. 2017. Cerebral Perfusion and the Risk of Dementia: A Population-Based Study. *Circulation,* 136**,** 719-728.
WORTMANN, M. 2012. Dementia: a global health priority - highlights from an ADI and World Health Organization report. *Alzheimers Res Ther,* 4**,** 40.
XIE, L., KANG, H., XU, Q., CHEN, M. J., LIAO, Y., THIYAGARAJAN, M., O'DONNELL, J., CHRISTENSEN, D. J., NICHOLSON, C., ILIFF, J. J., TAKANO, T., DEANE, R. & NEDERGAARD, M. 2013. Sleep drives metabolite clearance from the adult brain. *Science,* 342**,** 373-7.

XIONG, B., LI, A., LOU, Y., CHEN, S., LONG, B., PENG, J., YANG, Z., XU, T., YANG, X., LI, X., JIANG, T., LUO, Q. & GONG, H. 2017. Precise Cerebral Vascular Atlas in Stereotaxic Coordinates of Whole Mouse Brain. *Front Neuroanat,* 11**,** 128.

XU, F., GRANDE, A. M., ROBINSON, J. K., PREVITI, M. L., VASEK, M., DAVIS, J. & VAN NOSTRAND, W. E. 2007. Early-onset subicular microvascular amyloid and neuroinflammation correlate with behavioral deficits in vasculotropic mutant amyloid beta-protein precursor transgenic mice. *Neuroscience,* 146**,** 98-107.

XU, Y., ZHANG, J. J., XIONG, L., ZHANG, L., SUN, D. & LIU, H. 2010. Green tea polyphenols inhibit cognitive impairment induced by chronic cerebral hypoperfusion via modulating oxidative stress. *J Nutr Biochem,* 21**,** 741-8.

XU, Z., XIAO, N., CHEN, Y., HUANG, H., MARSHALL, C., GAO, J., CAI, Z., WU, T., HU, G. & XIAO, M. 2015. Deletion of aquaporin-4 in APP/PS1 mice exacerbates brain Abeta accumulation and memory deficits. *Mol Neurodegener,* 10**,** 58.

YAMORI, Y. 1991. Overview: studies on spontaneous hypertension-development from animal models toward man. *Clin Exp Hypertens A,* 13**,** 631-44.

YANG, S.-H. & LIU, R. 2017. Cerebral autoregulation. *Primer on cerebrovascular diseases.* Elsevier.

YAO, H., AGO, T., KITAZONO, T. & NABIKA, T. 2017. NADPH Oxidase-Related Pathophysiology in Experimental Models of Stroke. *Int J Mol Sci,* 18.

YOSHIOKA, H., NIIZUMA, K., KATSU, M., OKAMI, N., SAKATA, H., KIM, G. S., NARASIMHAN, P. & CHAN, P. H. 2011. NADPH oxidase mediates striatal neuronal injury after transient global cerebral ischemia. *J Cereb Blood Flow Metab,* 31**,** 868-80.

YOSHIZAKI, K., ADACHI, K., KATAOKA, S., WATANABE, A., TABIRA, T., TAKAHASHI, K. & WAKITA, H. 2008. Chronic cerebral hypoperfusion induced by right unilateral common carotid artery occlusion causes delayed white matter lesions and cognitive impairment in adult mice. *Exp Neurol,* 210**,** 585-91.

YU, J., WEIWER, M., LINHARDT, R. J. & DORDICK, J. S. 2008. The role of the methoxyphenol apocynin, a vascular NADPH oxidase inhibitor, as a chemopreventative agent in the potential treatment of cardiovascular diseases. *Curr Vasc Pharmacol,* 6**,** 204-17.

ZHANG, Q. G., WANG, R., HAN, D., DONG, Y. & BRANN, D. W. 2009. Role of Rac1 GTPase in JNK signaling and delayed neuronal cell death following global cerebral ischemia. *Brain Res,* 1265**,** 138-47.

ZLOKOVIC, B. V. 2005. Neurovascular mechanisms of Alzheimer's neurodegeneration. *Trends Neurosci,* 28**,** 202-8.

ZLOKOVIC, B. V. 2011. Neurovascular pathways to neurodegeneration in Alzheimer's disease and other disorders. *Nat Rev Neurosci,* 12**,** 723-38.

Appendix

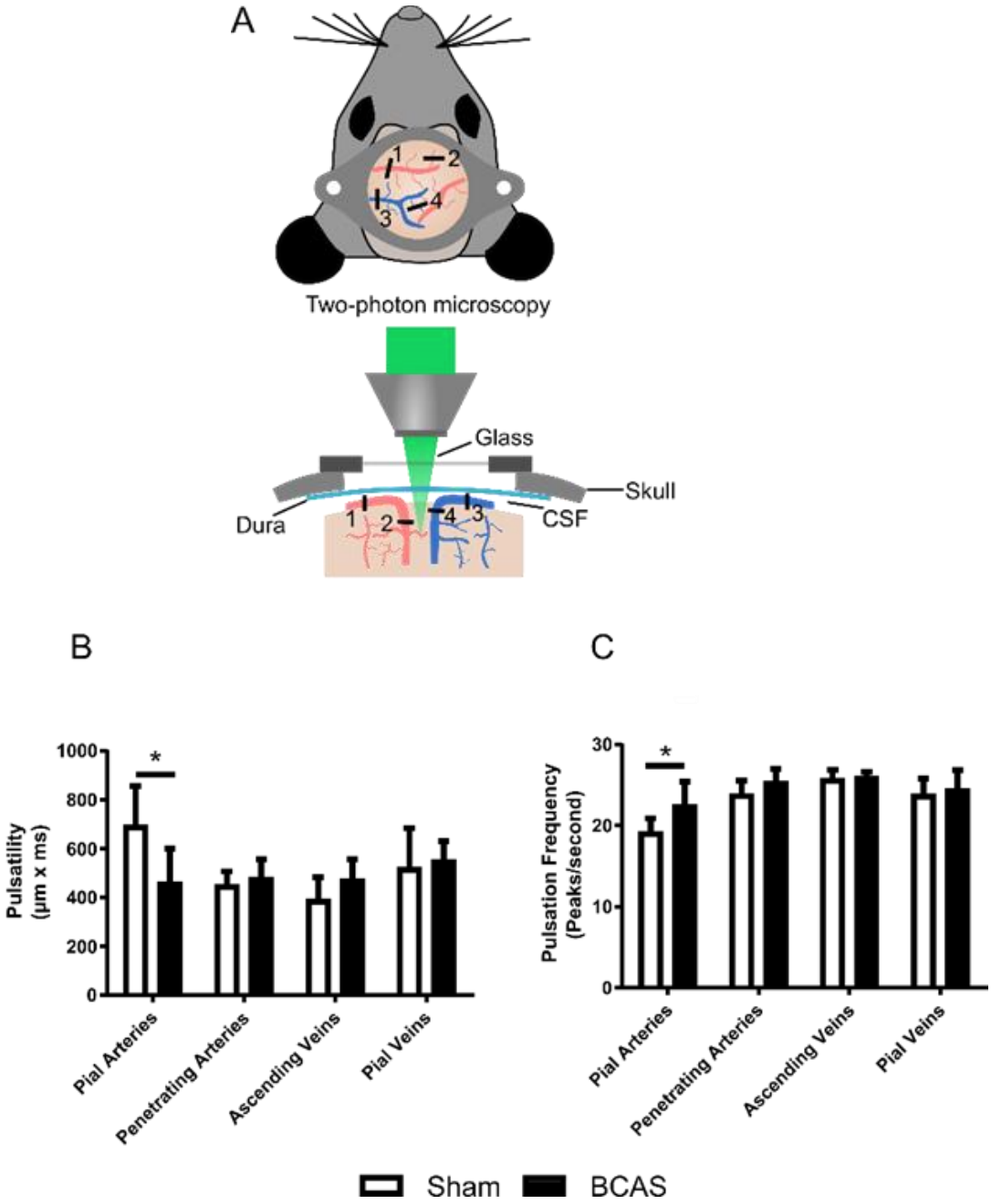

Pial artery pulsatility is reduced post-BCAS.

***(A)** Two-photon microscopy was used to assess vessel pulsation in sham and post-BCAS WT mice. Four categories of blood vessels were investigated: 1. Pial arteries; 2. Penetrating arteries; 3. Ascending veins; 4. Pial veins. (**B**) Significantly decreased pulsatility was found in pial arteries but not in other vessels in the mice post-BCAS. (**C**) There was a significant increase of frequency in the corresponding pial arteries but*

not in other vessels in the mice post-BCAS. Data are presented as mean ± SEM, n=6-7 per group. Data provided by Dr Juraj Koudelka and Joshua Beverley.